Chapter - E

ROCK MECHANICS &
GEOTECHNICAL APPLICATIONS

KAYA MEKANİĞİ &
JEOTEKNİK UYGULAMALAR

Effect of the Stress State on Waterjet Performance in Rock Slotting

R. Ciccu, B. Grosso
Department of Civil and Environmental Engineering and Architecture, University of Cagliari, Italy

A. Bortolussi
Institute of Environmental Geology and Geo-engineering, National Research Council of Italy, Cagliari

ABSTRACT The economic benefit resulting from the application of waterjet technology in underground and surface quarrying of dimension stone chiefly depends on slotting rate. The performance achievable in the field is connected with the operating features of the machine, the characteristics of the material and the tensional state of the rock massif. In order to assess the influence of the state of stress of the massif on the slotting rate, tests with oscillating nozzle have been carried out on samples subjected to a static load, either in the direction of the compressive force or perpendicular to it. Results are illustrated and discussed and conclusions are drawn regarding the effect of the tensional state of the rock on material removal rate.

1 FOREWORD

Surface quarrying is the most widespread method for extracting dimension stones. This is mainly due to the relatively low depth of the deposits and to the difficulties in the application of traditional technologies in an underground environment. On the other side, in developed countries, new constraints are continuously imposed to surface activities by the environmental legislation. The solutions aimed at mitigating the impact on the environment during the production activity and the land reclamation required at the end of the quarrying, introduce negative issues in the overall economic balance of the industrial enterprise. Considering that quarrying consumes land surface, landscape, and, clearly, the natural resource, it must be conducted with the maximum achievable efficiency. It means that efforts have to be directed to minimize the negative effects on the environment and to improve the recovery of the geologic resource (Agus et al. 1997).

To these concerns underground quarrying appear to be better suited to the modern trend. In fact it minimizes the consumption of land, reduces the impact on the landscape and requires few and cheap interventions for the final land reclamation.

Underground quarrying is widely diffused in the marble extraction industry (Fornaro et al. 1992) while it is rarely adopted for granite extraction. This fact is mainly due to the cutting technologies used in the two cases: the diamond wire and the rock-cutter for marble extraction, drilling and explosive splitting for granite. While marble cutting technologies are suited for an underground environment and have been adopted with few modifications, those for granite can hardly be used underground. In the last decades two technologies have been developed that can make feasible granite underground quarrying: diamond wire and waterjet slotting.

Diamond wire needs the support of another technology, due to its inherent limitations. To this end, waterjet would match very well the wire saw, playing a role

similar to that of rock-cutter in marble quarries.

Therefore a suitable combination of these two technologies appears to be the most interesting solution for quarrying.

2 UNDERGROUND QUARRYING

The underground granite quarrying method here proposed makes use of a combination of diamond wire and waterjet technologies.

A waterjet equipment used for tunnel excavation in a Japanese granite quarry is shown in Figure 1.

Figure 1. Tunnel excavation in a Japanese quarry by means of waterjet slotting equipment

The access underground would consist of a large gateway tunnel, from which production activity can be developed. For each advance step of tunnel excavation a pilot hole is first drilled perpendicular to the face, from which a slot can be started. The waterjet lance, bearing the oscillating nozzle directed towards the rock to be excavated, is traversed forth and back parallel to the pilot hole and after each cycle it is periodically moved sideways by incremental steps, thus extending progressively the rectangular area slotted until reaching the opposite end of the slot (Figure 2). From the first one all subsequent slots can be started following a convenient order.

Once all the waterjet slots are completed, individual blocks can be extracted by cutting the back hidden face with diamond wire (Figure 3).

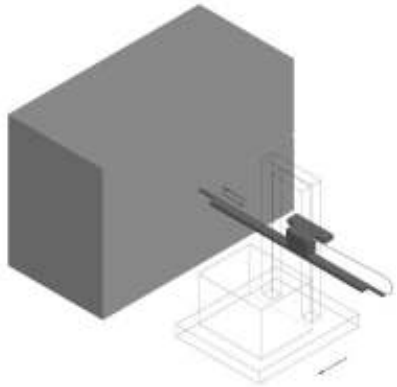

Figure 2. Scheme of tunnel excavation in underground granite quarry using waterjet and diamond wire. First phase: Waterjet slotting at the face. Slot depth: 3m

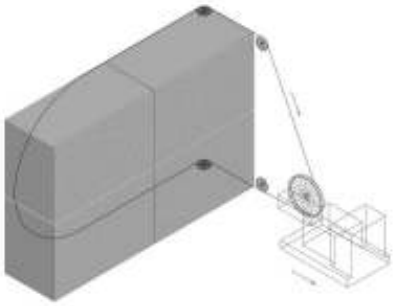

Figure 3. Scheme of tunnel excavation in underground granite quarry using waterjet and diamond wire. Second phase. Diamond wire sawing of the rear face in two stages of slicing. Block width: 1.5 m

In the case of flat orebodies, blocks will be extracted by room-and-pillar method according to a well-planned layout, whereas in the case of steeply dipping formations rock will be excavated by levels that are worked out individually with a downwards sequence, leaving large chambers some tens of meters high.

Regarding bench geometry, two configurations can be adopted:

A - High bench, where the vertical extent of the face varies from 6 to 18 m, according

to cases. Commercial blocks, whose size ranges from 4 to 12 m^3, are produced with a sequence of cascade subdivisions. A primary block, up to 2,000 m^3 in size, is first isolated from the hillside and then split into secondary blocks (slices), about 100 - 200 m^3 big and 1.5 to 3 m wide, that in turn are toppled to the floor. Production of final blocks takes place by means of suitably directed cuts across the thickness of each slice, aimed at separating the valuable stone from the defective material to be dumped as a quarry waste. This variant is applied whenever a selection is needed. Quarry recovery typically varies from 20 to 60%.

B - Low bench, where face height is smaller than 3 m. Commercial blocks are individually extracted right from the bench, their size being of the order of 10 m^3 with a very narrow range of variability. Recovery can be considerably large. This variant should be preferred if selection is not needed (rock exempt from flaws and little fractured).

3 INFLUENCE OF THE STRESS ON THE WATERJET PERFORMANCE

Many industrial experiences demonstrate that the slotting rate achievable on a given rock, with fixed operational parameters (waterjet pressure and nozzle diameter, lance traverse velocity, nozzle oscillation frequency) depends on the state of stress acting in the rock mass being cut (Ciccu 1993, Ciccu and Flamminghi 1996).

Aimed at finding the relation between the rock's state of stress and the slotting rate an experimental research has been started at the DICAAR waterjet laboratory.

3.1 Experimental Set-up

The experimental set-up consisted of:

- a Hammelmann High Pressure plunger pump (power at the engine flywheel: about 300 kW; maximum flowrate: 54 l/min at 250 MPa);
- a waterjet lance provided with an oscillating nozzle (top frequency: 20 Hz; maximum traverse velocity: 15 m/min);
- a block carrier platform (minimum advance step: 1 mm/cycle);
- a programmable control unit;
- a specially designed uniaxial compression cell provided with a hydraulic jack capable of imparting a load of up to 100 t to the sample.

Tests have been carried out under the following experimental conditions:

- pressure: 100, 160 and 200 MPa
- nozzle diameter: 0.96 mm
- oscillation frequency: 20 Hz
- sweeping angle: 22° on each side
- advance per stroke [mm] and traverse speed [m/min]: variable

3.2 Material

Cubic samples of granite quarried in Sardinia, whose main characteristics are given in Table 1, have being used.

Table 1. Physical and mechanical properties of the Rosa Beta granite

Properties	Meas. Value
Bulk specific gravity [kg/m^3]	2,588
Absorption coefficient [%]	4.85
Porosity [%]	0.63
Compressive strength [MPa]	1,920
Flexural strength	156
Impact test (Height of fall) [cm]	68
P-wave velocity [m/s]	5,626

3.3 Testing Procedure

Four series of tests have been carried out with variable setting of pressure and traverse velocity, at constant nozzle diameter, oscillation frequency and sweeping angle.
Each series was conceived for putting into evidence the effect of stressing in relation to the cutting direction. The first series was aimed at disclosing the variation of volume removal due to a compressive load applied in the central part (shadowed area) of a

parallelepiped shaped sample, perpendicular to the cutting plane, as shown in Figure 4.

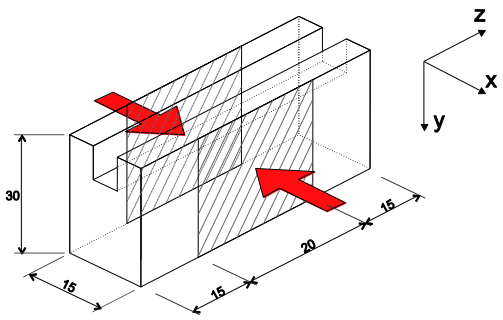

Figure 4. Experimental conditions for the first series of test

Three tests have been made at variable jet pressure (200, 160 and 100 MPa), under a load of 50 t.

Since the effect of stressing is enhanced near the pressure threshold of the rock, the further three series of tests have all been carried out at 100 MPa. It was also decided to maintain the advance per cycle constant (2 mm) and to find the peak cutting rate by varying the traverse velocity.

The purpose of the second series was to put into evidence the effect of a static load parallel to the cutting plane, as shown in Figure 5.

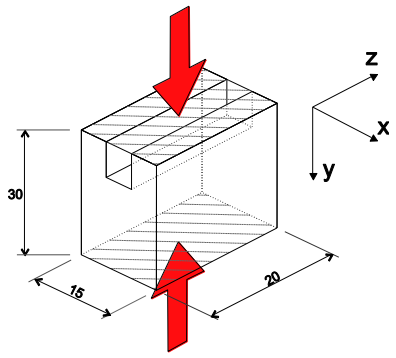

Figure 5. Experimental conditions for the second series of test

The slot was made nearer to one of the free faces of the sample in order to show the effect of load unbalance, producing a differential stress at the slot sides.

The necessary clearance for the traversing lance was obtained by opening a 6 cm deep slot before imparting the load. The variation in cutting rate with depth of slot was then determined.

The third series of tests was carried out subjecting the sample to an evenly distributed lateral compression (25 and 50 t): the effect of stress on cutting performance was assessed by measuring the maximum slot depth down to which predetermined levels of cutting rate could be maintained.

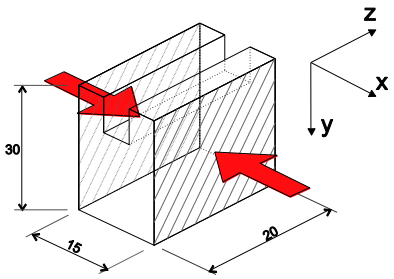

Figure 6. Experimental conditions for the third series of test

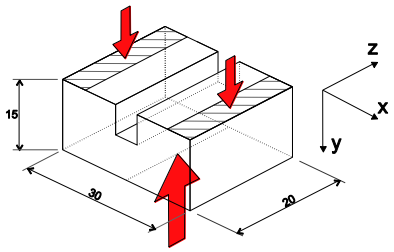

Figure 7. Experimental conditions for the fourth series of test

Loading conditions are shown in Figure 6. Finally, the alleged favorable effect of tensile stress on cutting rate was investigated by applying a flexural load as illustrated in Figure 7.

Stress distribution in the neighbors of the slot bottom was assessed using the three-dimensional FLAC code. The study was carried out on suitable cross sections of the cubic samples used for the experiments, at variable slot depth.

Samples have been spatially oriented as follows:

Z-direction = axis of the slot

Y-direction = depth of the slot

X-direction = perpendicular to the slot plane

Therefore the jet is always traversed in the Z-direction and the cross sections are taken parallel to the X-Y plane.

3.4 Results

3.4.1 Preliminary investigation

Results obtained with the first series of tests are summarized by the curves of Figure 8 giving the relative variation in volume removal per unit length of slot for the different cross sections of the sample.

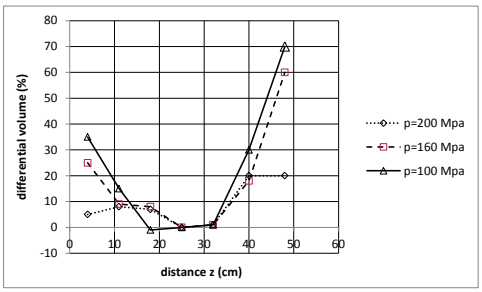

Figure 8. Variation in volume removal along the Z-direction

From the comparison of these curves it clearly appears that:

- volume removal is considerably lower in the central part of the sample where compression is higher;
- average slotting velocity at 100 MPa resulted to be 0.45 m^2/h, lower than that obtained in the case of unloaded samples (0.63 m^2/h); this performance is approached at both extremes of the sample where stress is gradually reduced;
- the variation in volume removal is much more evident in the case of 100 MPa pumping pressure, as expected.

3.4.2 Compression parallel to cutting plane

Under a constant load of 25 t, it was found that cutting rate decreased to 0.48 m^2/h after deepening the initial slot by further 10 cm and to 0.39 m^2/h after additional 15 cm, compared to 0.63 m^2/h achieved on the unloaded reference sample.

It was also observed that slot walls were very smooth and that the bottom showed an unusual section characterized by a marked excavation at the corner corresponding to the thicker leg between the slot and the lateral free face of the sample.

3.4.3 Compression perpendicular to cutting plane

Results confirm the indication of the first series of tests, as shown in Table 3 giving the maximum slot depth achievable with predetermined levels of cutting rate as a function of compressive load.

Table 3. Depth of slot as a function of compressive load at different cutting rates.

Load [t]	Cutt. rate [m^2/h]	Depth [mm]	
		Marg.	Abs.
25	0.45	25	25
	0.36	10	35
	0.30	>25	>60
50	0.45	15	15
	0.36	10	25
	0.30	25	60

It is clear that, as the slot is deepened, the resisting area is progressively reduced, entailing a corresponding increase in compressive stress. This explains the decrease in cutting rate at depth.

Moreover, the higher the external load, the shallower the slot that can be excavated with a given cutting rate, roughly with a reverse-proportion trend.

The negative influence of compressive stress on jet performance appears demonstrated.

3.4.4 Flexural load

By applying a force of 5 t at the central line between two flat 5 cm wide bearings, cutting rate increased from 0.63 to 0.69 m^2/h over 34 mm depth. On doubling that force, cutting rate jumped to 0.84 m^2/h over further 30 mm, then the sample split apart.

The explanation of this outcome is trivial: jet performance is greatly enhanced if the rock at the bottom of the slot is subjected to tensile stress, whereby preexisting and newly induced cracks are better propagated, producing a faster rock disintegration (Erdman – Jesnitzer 1980).

Cutting rate appears to be very well correlated with σ_x as shown in Figure 9 where the results of all tests are reported.

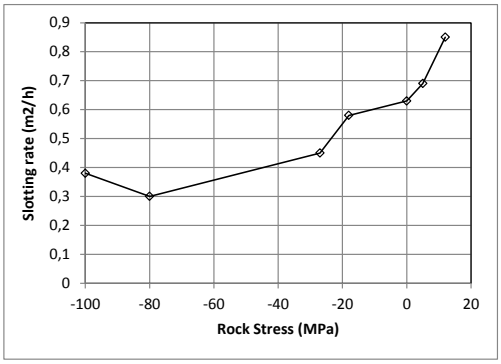

Figure 9. Cutting rate versus maximum σ_x stress component at the central point of the slot bottom

4 CONCLUSIONS

At the present state of the art, the most promising prospects concerning the application of waterjet in granite quarries are for:

- bench opening slot (replacing flamejet) and horizontal underhand cut (replacing explosive splitting) in the case of surface quarrying according to the conventional high-bench method;
- as an alternative, L-shaped horizontal and vertical slots, up to 3.5 m deep, on the side face of the bench, (diamond wire can then be encompassed along the exposed perimeter, with no need for preliminary drilling, for the subsequent slicing operation);
- all face cuts (no substitute technologies are at hand) in the case of tunnel excavation;
- perimetrical slice delimitation in the case of development of large underground chambers according to the high bench method.

The association of waterjet with diamond wire offers a very interesting solution for mechanized quarrying, since both are able to work in a completely automated fashion.

The importance of stressing conditions of the rock must be emphasized.

In fact, rock slotting with waterjet is very sensitive to the stress at the slot bottom normal to the cut plane.

The considerable influence of stressing state on waterjet performance in rock slotting with high velocity waterjet have been demonstrated by the results of the described experimental research.

In particular cutting rate increases if the rock near the slot bottom is subjected to tensile stress whereas it deteriorates in presence of compressive stress.

Therefore in quarrying operations suitable cutting sequences should be devised in order to generate a stress pattern characterized by prevailing traction in the slotting region.

When crossing a strongly compressed rock, jet pressure should be increased for winning the tough-to-cut material, whereas hydraulic energy is better exploited using a lower pressure, higher flow rate jet when crossing tensile areas (Summer 1987, Agus et al. 1991, Agus et al. 1993).

5 REFERENCES

Agus M., Bortolussi A., Ciccu R., 1997 “Aspetti ambientali legati allo sviluppo tecnologico nel settore estrattivo del granito.” *Atti del IX Congresso Nazionale dei Geologi,* pp. 118-124 Roma, Italia.

Fornaro M., Mancini R., Pelizza S., Stragiotti L.. 1992 “Underground production of marble in Italy: technology, economy and environmental constraints”, *Proceedings of XV World Mining Congress,* pp 573-582, Madrid.

Ciccu R., Fiamminghi A.. 1996. Quarrying granite underground is now feasible with waterjet, paper, *13th Int. Conf. on Jet Cutting Technology*, Cagliari, Italy.

Erdmann-Jesnitzer F., Louis H. and Wiedemeier J.. 1980. "Rock Excavation with High Speed Water Jets. A view on drilling and cutting results of rock materials in relation to their fracture mechanical behaviour", *Proc. 5th Int. Symp. on Jet Cutting Technology*, pp 229-236, Hanover, Germany.

Summers D.A. AIME 1987. "Water jet cutting related to jet and rock properties", *Proc. 14th Symp. on Rock Mechanics, pp. 569-588, Pennsylvania State University*.

Agus M., Bortolussi A., Ciccu R., Manca P.P. and Massacci G.. 1991."Granite cutting with water jets", *Int. J. of Waterjet Techn.* Vol. 1, N. 2, , pp. 73-83

Agus M., Bortolussi A., Ciccu R., Kim W.M. and Manca P.P.:The influence of rock properties on waterjet performance, Proc. 7th American Waterjet Technology Conference, pp 427-442, Seattle, 1993.

Modeling Aspects of Block Toppling in Rock Slopes

L. Cláudia Pereira, M. Sabino Lana, F. Costa Melo, P. F. Trindade Lopes
Federal University of Ouro Preto,Ouro Preto, Brazil

ABSTRACT Sliding failure mechanisms are well-known by the geotechnical community and their use in engineering practice is very common. It is not the situation for failure mechanisms involving toppling. Despite the widespread occurrence of block toppling in rock slopes, methods currently available to study the phenomenon are not used regularly in engineering practice.

Many analytical approaches have been developed to study block toppling. However, it is necessary to make over-simplifications concerning the geometry of the discontinuities and the slope which are difficult to achieve in the field. Numerical models to study block toppling are also not trivial. An adequate numerical model to represent the failure mechanism should be capable of representing the discontinuities.

In this paper analytical and numerical methods to study block toppling are discussed. Advantages and limitations of the various methods are presented. Both continuous and discontinuous numerical methods are used.

1 INTRODUCTION

Block toppling is a very common failure mechanism in rock slopes. It occurs in a variety of rock types and conditions. Discontinuity patterns that lead to block toppling are very general. High or small discontinuity persistence and spacing are possible configurations in block toppling.

Toppling failure is due to forces that cause block rotation, column flexure or both. Blocks or columns are created by the intersection of discontinuity sets. Three main types of toppling are described by Goodman & Bray (1976): flexure toppling, block toppling and block-flexure toppling. They are showed in Figure 1.

In flexural toppling the flexure of well-developed, steeply dipping discontinuities occurs. According to Wyllie & Mah (2004), flexural toppling occurs in typical geological conditions. It may occur, for instance, in thinly bedded shale and slate, in which orthogonal joints are not well developed. In Brazil common occurrences of flexural toppling were found in phyllites, where foliation joints are the dominant discontinuities.

According to Goodman & Bray (1976), conditions for the start of flexural toppling involve interlayer slip, which liberates the columns to bend in flexure.

Block toppling occurs in the presence of two discontinuity sets; one dipping steeply into the face and another with orthogonal joints cutting the former set.

According to Wyllie & Mah (2004), the short blocks at the slope toe are pushed forward by the loads from the overturning blocks behind, allowing further toppling to develop higher up the slope.

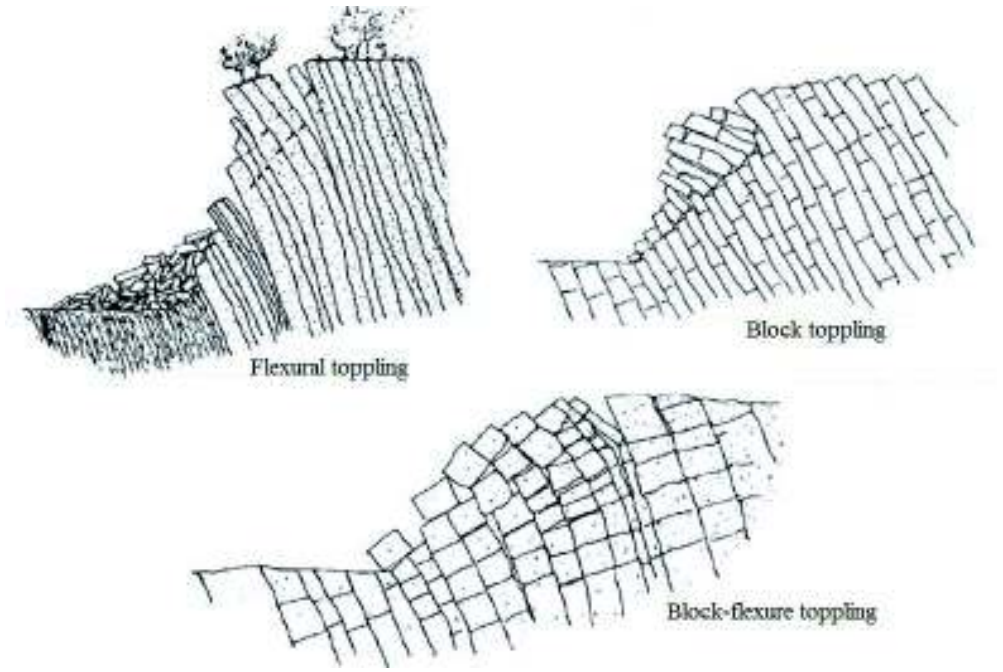

Figure 1: Types of toppling, Goodman & Bray (1976)

A failure basal surface is developed in toppling. In flexure toppling this basal surface tends to be planar. In block toppling this basal surface tends to be a stepped surface rising from one cross joint to the next.

In block-flexure toppling, flexure along pseudo-continuous columns occurs. These columns are divided by many cross joints. Instead of flexure along columns the failure is due to their toppling because of the movements along the cross joints.

2 BLOCK TOPPLING KINEMATICS

Discontinuity sets involved in toppling should be identified as well as their position in relation to the slope face. Hemispherical projection methods and field observations are used to identify block geometry. In addition, discontinuity spacing should be measured in order to define block height and width.

Kinematic conditions for block toppling and sliding are defined in Figure 2, for gravitational loading. Block toppling occurs when the moment of the sliding force is greater than the moment of the normal force to the block base, see Figure 2 (a). This condition is represented by:

$$\frac{\Delta x}{y} < \tan \psi_p \qquad (1)$$

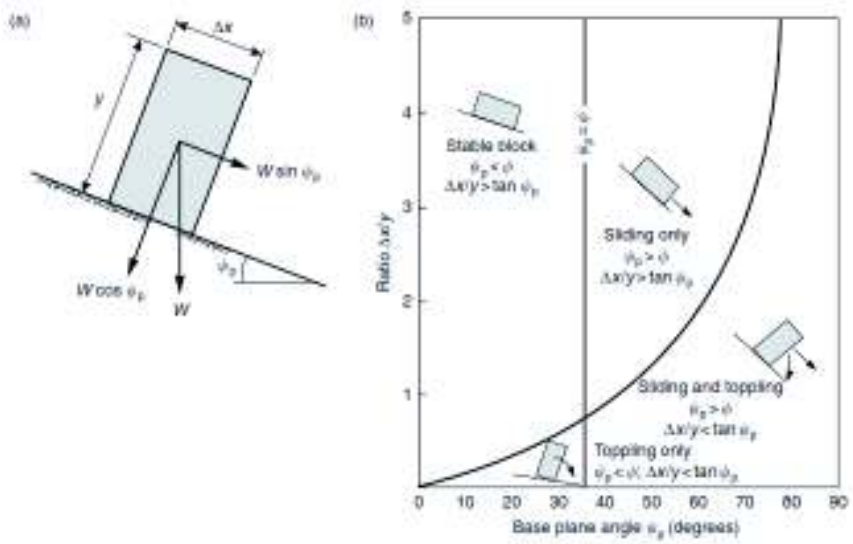

Figure 2: Kinematic condition for block toppling: (a) block in an inclined plane; (b) conditions for sliding and toppling, Wyllie & Mah (2004).

Block sliding occurs when the base plane angle is greater than its friction angle.

Both sliding and toppling kinematic conditions apply to null cohesion discontinuities.

In Figure 2(b) kinematic conditions for toppling and sliding of blocks are shown, as a function of width to height of blocks and the base plane angle.

3 STABILITY ANALYSIS OF BLOCK TOPPLING

3.1 Limit Equilibrium Methods

Limit equilibrium methods involves the use of analytical solutions. The rock masses or rock blocks are rigid bodies and their movement occurs along a basal failure surface. Equilibrium of forces and moments are considered in limit equilibrium analysis of block toppling.

In classical solutions force and moment equilibrium equations are solved for each block, starting at the uppermost block. The block can be stable, toppling or sliding, depending on block dimensions, sliding strength and external forces. Goodman & Bray (1976) were the first authors to propose a limit equilibrium solution for block toppling. Their model is shown in Figure 3. The base of the toppling blocks is a stepped surface with an overall dip ψ_b. There is no suggestion to determine the dip of this basal surface but it has a great influence on the stability of slope. One possible simplification is to consider the basal surface planar instead of stepped but the problem of this dip angle remains undetermined.

Bobet (1999) proposed another solution for limit equilibrium analysis of block toppling, where block thickness is small comparing to block height. The relation between slope height and block thickness was called slenderness ratio. The problem can be solved considering that the rock mass behaves as a continuous medium. The method proposed by Bobet (1999) eliminates the need of knowing the detailed geometry of blocks, as it is the case in the method of Goodman & Bray (1976).

Sagaseta et. al. (2001) extended Bobet model to incorporate a basal failure surface not necessarily normal to discontinuity set prone to toppling. Their model is valid for a slenderness ratio greater than 20.

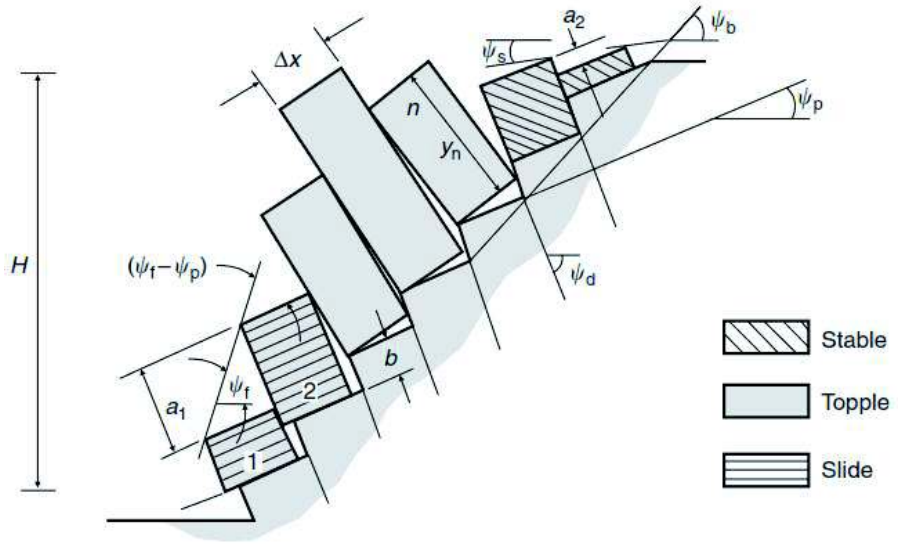

Figure 3: Limit equilibrium model for analysis of block toppling on a stepped base, according to Goodman & Bray (1976).

Liu et. al. (2008) have also presented a solution of block toppling for continuous rocks mass, based on the proposals of Bobet (1999) and Sagaseta et. al. (2009). In another paper, Liu et. al. (2009) presented a solution for block toppling applied to discontinuous rock masses.

3.2 Numerical Methods

Numerical analyses are the most flexible methods to solve stability problems. They allow the solution of equilibrium equations and the use of many different constitutive relations, considering the material deformations. The rock mass can be a continuous or discontinuous medium. A comprehensive discussion of numerical methods and their application in engineering practice can be found in Jing & Hudson (2002).

Numerical modeling of block toppling requires discontinuity representation in the model. Continuous methods which permit the explicit representation of the discontinuities can be used, as the finite element method implemented in the two-dimensional software Phase2, of Rocscience Inc. (2005). These methods can be useful to determine the collapse onset or the larger displacements that cause rock blocks separation. Nevertheless, complex mechanisms involving rotation or breakout of blocks cannot be modeled by continuous approaches.

Discontinuous methods, as the discrete element method, are alternatives to continuous approach. The rock mass is represented as an assembly of discrete blocks which interact through contact forces. Blocks can be rigid or deformable.

The Universal Distinct Element Code (UDEC), which is a software based on the distinct element method, can be used to model block toppling. It is adequate to model problems with large displacements or deformations. Two dimensional and three dimensional versions are available.

Model behavior in UDEC is numerically modeled by an algorithm of the type timestep, where timestep size is limited by the hypothesis that velocities and accelerations are constant in a timestep or a cycle. Collapse will generate an unbalanced force in the system. The number of cycles

and the values could be established by the user to monitor the failure process. In Figure 4, the modeling of a collapse situation in block toppling is showed. By monitoring the number of cycles, Nichol et. al. (2002) could represent the failure process.

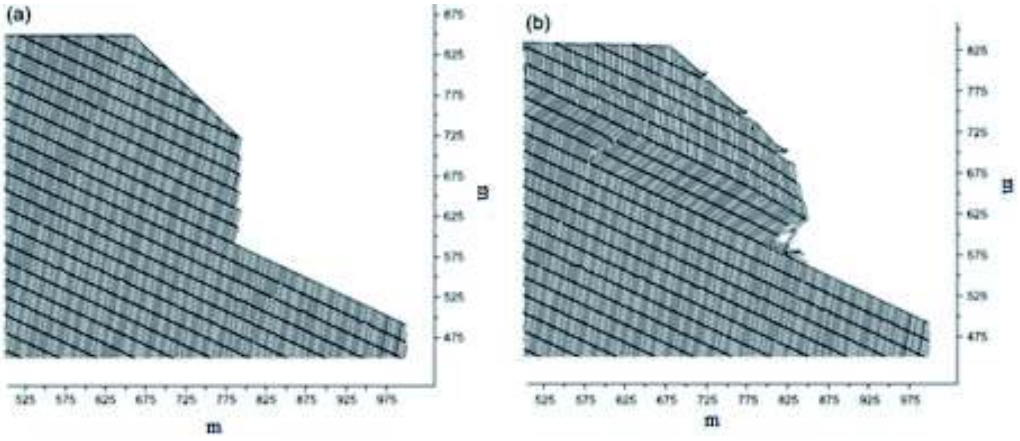

Figure 4: Block displacements in block toppling modeled by UDEC: (a) after 20,000 cycles; (b) after 40,000 cycles (Nichol et. al., 2002)

4 CASE STUDIES

4.1 Toppling of a Single Block

A simple case of block toppling is illustrated in Figure 5. It is a single block in an urban slope in Ouro Preto, Brazil. The rock mass is a schist.

The hemispherical projection of the discontinuities and the slope face can be seen in Figure 6. Two failure mechanisms are possible in this figure; sliding through 3m or toppling through 1m. Discontinuity 1m is the foliation and it dips into the slope face, see Figure 5. Discontinuity 2m forms the lateral release surfaces of the block.

Figure 5: Toppling block in the slope at Vila Aparecida neighborhood.

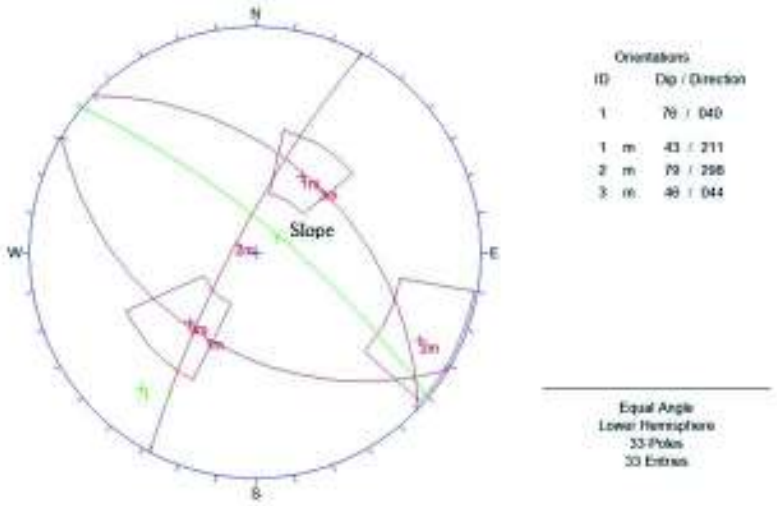

Figure 6: Discontinuity sets and the slope at Vila Aparecida neighborhood (Dips 5.0).

Basal surface is formed by discontinuity 3m, whose average spacing is equal to 0.36m, the block height. Average spacing of discontinuity 1m is 0.24m, the block width. Friction angle of basal discontinuity is equal to 35°. According to Figure 2 the block can toppling and sliding.

4.2 Toppling of a Set of Blocks

Two approaches were used to study block toppling involving many blocks; numerical methods and analytical methods. For numerical methods continuous and

discontinuous approaches were employed. Phase2 and UDEC programs were used.

The analytical approach used in this work was the limit equilibrium method proposed by Liu et. al. (2009) for discontinuous rock a) masses. The database is typical of a quartzite slope of a roadway from Ouro Preto to Belo Horizonte, Brazil.

4.2.1 Numerical methods

The following data was used for the models:
Slope: height of 25.8m and dip face angle of 80°.
Rock mass: Young modulus: 200,000MPa, Poisson ratio: 0.2
Unit weight: 0.024MN/m^3
Frictionangle: 43.6°, Cohesion: 2.45MPa
Discontinuity properties:
Dip of toppling discontinuity: 45°, into the slope face; Spacing: 4.8m
Dip of basal discontinuity: 28°; Spacing: 1.2m
Friction angle of discontinuities: 24°, Cohesion: 0
Normal stiffness coefficient: 40MPa/m
Shear stiffness coefficient: 0,4MPa/m
In situ stress:
Gravitational field stress with horizontal stresses calculated as a poisson ratio function.

Results from Phase2 showed collapse due to discontinuity movements. Basal failure surface can be deduced from model displacements, as indicated in Figure 7. Beyond the basal failure surface, displacements are close to zero. Basal surface dip angle is 47° and its height is 25.563m. The direction of displacement vectors in the model shows a tendency to sliding failure.

In Figure 8 the deformed contours of discontinuities shows a tendency to block toppling. Both failure modes are possible but observations in the field showed block toppling is the dominant mechanism.

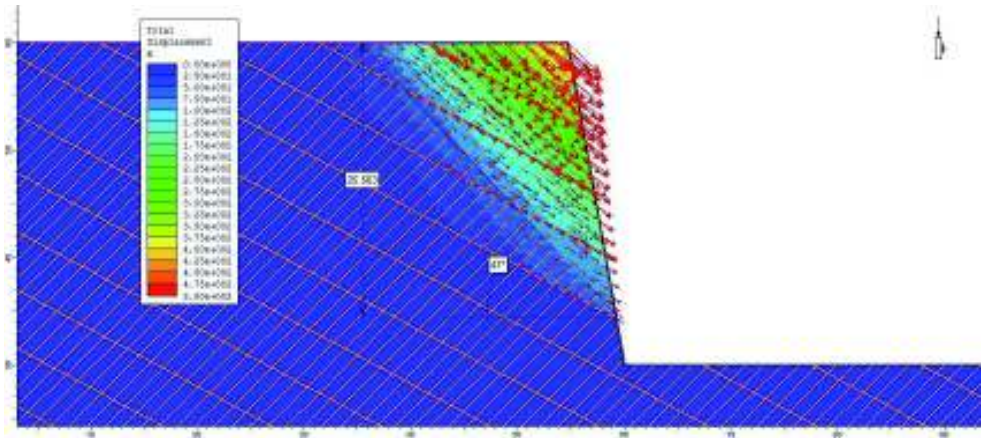

Figure 7: Total displacement and displacement vectors (Phase2, v.8.0).

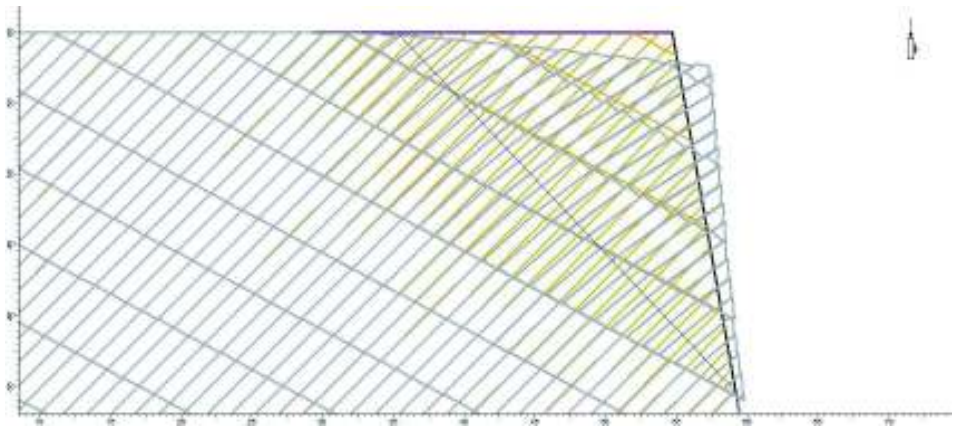

Figure 8: Deformed contours of discontinuities (Phase2, v.8.0).

In UDEC the model presented serious problems. The execution was not successful due to small dimensions of blocks. It was decided to execute the model with larger discontinuity spacing. A multiplier factor of 100 was applied to discontinuity spacing. Despite the fact the discontinuity spacing is completely out of range, the same proportions were kept considering block sizes in the model. Different values of displacements are expected but the direction of the displacement vectors tends to be the same of the original model.

Results from UDEC are shown in Figure 9. Displacement vectors indicate a tendency to sliding failure mode. The model has not converged; which means its collapse, the same result found in Phase2.

The results are very similar to those found in Phase2 in terms of total displacement and displacement vectors. The basal failure surface is noticeable in the model, as it was in Phase2.

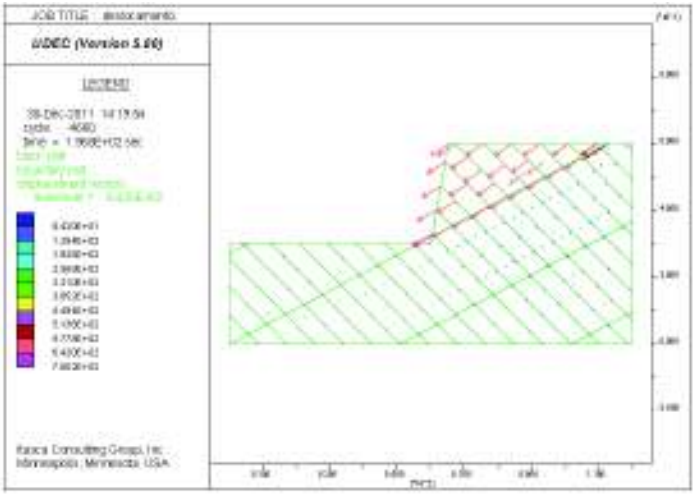

Figure 9: Total displacements and displacement vectors (UDEC, v.5.0)

4.2.2 Analytical methods

The analytical method proposed by Liu et. al. (2009) was applied. The same geometrical conditions of the computational models were assumed. The position of the basal failure surface found in computational models was assumed for the limit equilibrium model. It was considered a good indication of the position of this surface as it is quite arbitrary in limit equilibrium methods.

The following data was used in the model:
Model height: $H = 25.563m$
Block thickness: $t = 1.2m$
Unit weight: $\gamma = 24kN/m^3$
Angle of the normal line to toppling discontinuity and the x axis: $\beta = 45°$
Dip angle of basal discontinuity: $\beta_b = 28°$
Dip slope angle: $\beta_s = 80°$
Angle of the natural ground and the x axis: $\beta_g = 0$
Dip angle of basal failure surface: $\theta = 47°$
Friction angle of discontinuities: $\phi = 24°$

The geometry of the limit equilibrium model is shown in Figure 10.

The transition for toppling to sliding failure in the model of Liu et. al. (2009) occurs when the following equation is verified:

$$f_i = \frac{W_i \sin\beta_b - [W_i' + (\psi_{i-1})N_{i-1}](\cos\beta_{br} + \tan\phi_d \sin\beta_{br})}{\{W_i \cos\beta_b - [W_i' + (\psi_{i-1} - 1)N_{i-1}](\tan\phi_d \cos\beta_{br} - \sin\beta_{br})\}\tan\phi_b} \geq 1 \qquad (2)$$

where:

W_i is the weight of block i

$$W_i' = \frac{1}{2}\gamma t^2\{\sin\beta[\chi + (m-i)A_g] - \cos\beta - \sin\beta\tan\beta_{br}\} \qquad (i < m)$$

$$W_i' = \frac{1}{2}\gamma t^2 \frac{[\chi - (i-m)A_s]\{\sin\beta[\chi - (i-m)A_s + \tan\beta_{br}] - \cos\beta\}}{\chi - (i-m)A_s - tan\beta_{sr} + \tan\beta_{br}} \qquad (i \geq m)$$

χ is the slenderness ratio

$m = int\left\{\frac{1}{A_g\tan\beta} - \frac{\cos\beta_{sr}}{\sin\beta_s}\frac{A_s}{A_g}\frac{H}{t} - \frac{\tan\beta_{br}}{A_g} + 1\right\}$, m is the crest block number

$A_g = \tan\beta_{gr} - \tan\theta_r$

$A_s = \tan\beta_{sr} - \tan\theta_r$

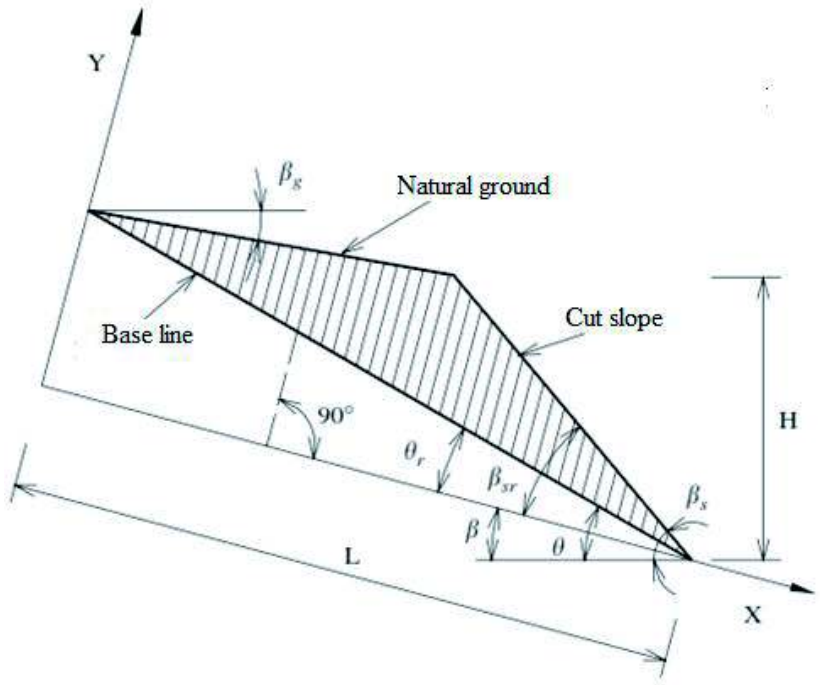

Figure 10: Limit equilibrium model for block toppling (Liu et. al., 2008).

The results of the analytical model are showed in Table 1. The number of the crest block is 10. Stable blocks are not considered in this model. Therefore, toppling starts with block number 1.

Slenderness ratio is equal to 11.79. Liu et. al. recommend the use of discontinuous model for slenderness ratios smaller than 15.

All blocks in the model belong to toppling set, according to equation (2). Blocks whose number is equal or greater than 20 must be disregarded as the values of f_i are less than zero. As a result there are 19 toppling blocks in the system.

The support force to keep the system stable can be calculated, based on the equilibrium equations. If this force is greater than zero, the system is unstable. For a null support force the system is in the point of equilibrium limit and for negative support forces the system is stable.

The support force in the model is approximately 39KN. This force means the entire system is unstable. The collapse of the system also happened in all computational models.

Table 1: Results of the analytical model (adapted from Liu et. al., 2009)

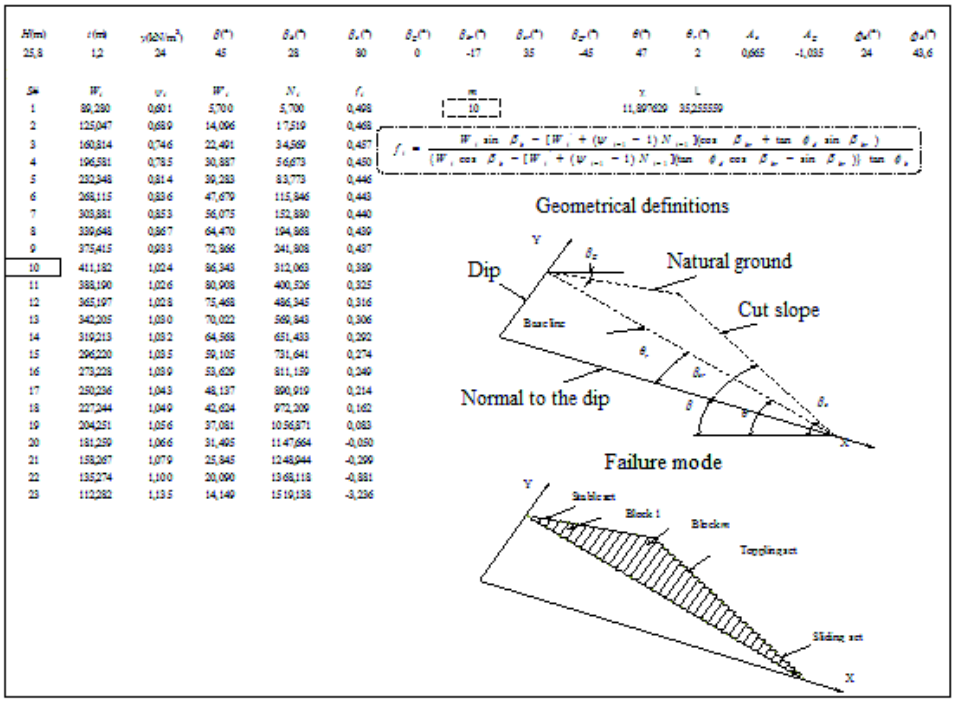

5 CONCLUSIONS

Although block toppling is a common failure mode in rock slopes, the available methods for its stability analysis need to be improved. They have not yet incorporated to engineering practice because of over simplifications and the need to assume arbitrary hypotheses.

One of the arbitrary assumptions concerns to the position of basal failure surface in limit equilibrium analysis. In this paper a suggestion to determine this surface is presented, based on the results of computational models. It seems to be an interesting suggestion. On the other hand analytical results become dependent on the availability of numerical methods.

The models used in this paper lead to similar results in terms of collapse of the entire system. Although computational and analytical methods are quite different in their assumptions, they seem to confirm the analysis. The authors recommend the use of other models of block toppling to judge the apparent similarity of the methods.

The improvement of analytical methods would be a good contribution to the study of block toppling in engineering practice. Computational methods present difficulties which must be overcome, especially the limitations related to block sizes.

REFERENCES

Bobet, A., 1999. Analytical solutions for toppling failure, *Int. J. Rock Mech. Min. Sci.*, 36, pp. 971-980.

Goodman, R. E. & Bray, J. W., (Boulder, CO: American Society of Civil Engineers.), 1976. Toppling of rock slopes, *Proceedings of the specialty conference rock engineering for foundations and slopes*, pp. 201-234.

Jing I. & Hudson, J. A., 2002. Numerical methods in rock mechanics, *Int. J. Rock Mech. Min. Sci.*, 39, pp. 409-427.

Itasca Consulting Group, Inc., 2004. UDEC version 5.0, Minneapolis.

Liu, C. H., Jaksa, M. B. & Meyers, A. G., 2008. Improved analytical solution for toppling stability analysis of rock slopes, *Int. J. Rock Mech. Min. Sci.*, 45, 8, pp. 1361-1372.

Liu, C. H., Jaksa, M. B. & Meyers, A. G., 2009. A transfer coefficient method for rock slope toppling, *Can. Geotech. J.*, 46, pp. 1-9.

Nichol, S. L., Hungr., O. & Evans, S. G., 2002. Large-scale and ductile toppling of rock slopes, *Can. Geotech. J.*, 39, pp. 773-788.

Rocscience Inc., 1998. Dips version 5.0 – Graphical and Statistical Analysis of Orientation Data. www.rocscience.com, Toronto, Ontario, Canada.

Rocscience Inc., 2008, Phase^{2}Version 7.0 - Finite Element Analysis for Excavations and Slopes. www.rocscience.com, Toronto, Ontario, Canada.

Rocscience Inc., 2005. Phase2 v.8.0 – Two dimensional finite element slope stability analysis.

Sagaseta. C., Sánchez, J. M., Cañizal, J., 2001. A general analytical solution for the required anchor force in rock slopes with toppling failure, *Int. J. Rock Mech. Min. Sci.*, 38, pp. 421-435.

Wyllie, D. C. & Mah, C. W., 2004. *Rock slope engineering: civil and mining*, Institution of Mining and Metllurgy, Spon Press, London, 431p.

Jeopolimerlerin Macun Dolgunun Dayanım ve İşlenebilirlik Özelliklerine Etkisi

The Effect of Geopolimers on the Strength and Workability Characteristics of Paste Backfill

F. Cihangir, B. Erçıkdı, A. Kesimal, H. Deveci
Karadeniz Teknik Üniversitesi Maden Mühendisliği Bölümü, Trabzon
Y. Akyol, S. Ocak, M. Kurtuluş
Maden Mühendisi, *Trabzon*

ÖZET Macun dolguda jeopolimer esaslı bağlayıcıların kullanılabilirliği, dolguya kazandıracağı mekanik ve durabilite özelliklerinin yanında işlenebilirlik özelliklerine de bağlıdır. Bu çalışmada sülfürce zengin normal ve şlamı uzaklaştırılmış maden tesis atıklarından aktifleştirilmiş yüksek fırın cürufu esaslı jeopolimerler ve normal portland çimentosu kullanılarak numuneler hazırlanmıştır. Hazırlanan taze macun dolgu malzemelerinin kıvam (işlenebilirlik) özellikleri ve kür işlemine tabi tutulan numunelerin de 28 günlük dayanım sonuçları araştırılmıştır. Jeopolimer bağlayıcılar ile hazırlanan macun dolgu numunelerinin tamamının 28 günlük kür süresindeki 1 MPa'lık eşik dayanım değerini sağladığı görülmüştür. Ancak, normal Portland çimentosu ile sadece şlamı uzaklaştırılmış atıktan hazırlanan numuneler eşik dayanım değerini sağlamıştır. Normal Portland çimentosu içeren macun dolgu malzemelerinde iki saatlik süre içinde %1 ila %6 oranında işlenebilirlik kaybı görülürken, jeopolimer içeren macun dolgu malzemelerinin kıvamında azalma izlenmiştir. Dolayısıyla, jeopolimerlerin macun dolgu mekanik özelliklerinin yanında, dolgu malzemelerinin işlenebilirlik özelliklerini de iyileştirdiği sonucu elde edilmiştir.

ABSTRACT The utilization of geopolimer based binders in paste backfill depends on the workability characteristics in addition to the mechanical and durability properties. In this study, fresh paste backfill materials were prepared with geopolimer binders (alkali activated blast-furnace slag) and normal Portland cement from sulphide-rich tailings of normal mill tailings and de-slimed tailings. Afterwards, the consistency (workability) properties of fresh backfill samples and the strength values were tested at 28 days curing time. Paste backfill samples prepared with geopolimers were seen to give the value of the threshold strength of 1 Mpa at 28-days curing time. However, only the samples prepared with ordinary Portland cement from de-slimed tailings were observed to maintain the value of the threshold strength. A workability loss of 1.0 to 6.0 percent was obtained in fresh paste backfill materials prepared with normal Portland cement in two-hours period. On the other hand, geopolimers were followed to decrease the consistency of fresh paste backfill materials. Therefore, geopolimers were seen to increase not only the mechanical properties of the paste backfill material, but they improved the workability characteristics, also.

1 GİRİŞ

Macun dolgu; cevher zenginleştirme işlemleri sonrası ortaya çıkan maden tesis atıkları, amaca bağlı olarak % 3-9 oranında bağlayıcı madde ve su karışımından oluşan, %70-85 oranında nihai katı oranında ve uygun kıvamda (7.0-8.5 slamp) bir malzemedir. Dolgu bileşenlerinden her biri, macun dolgunun kısa ve uzun dönemdeki dayanımını, durabilitesini, nakliyesini ve boşluklara yerleştirilmesi gibi işlenebilirlik özelliklerini önemli derecede etkilemektedir. Macun dolguda genellikle normal Portland çimentosu ve mineral katkılı Portland kompoze çimentolar kullanılmaktadır. Son yıllarda, puzolanik mineral katkı maddelerinin alkali aktivasyon teknikleri ile aktifleştirilerek çimento yerine kullanımı giderek yaygınlaşmaktadır. Macun dolguda normal Portland çimentosuna (CEM I 42.5R) alternatif olarak alkali aktive yüksek fırın cüruflarının (jeopolimer bağlayıcılar) kullanılması durumunda, asit, sülfat, vb. etkiler ile kimyasal korozyonlara karşı daha dayanıklı ve daha yüksek dayanıma sahip dolgu üretilebilmektedir (Cihangir, 2011).

Jeopolimer çimentoların kullanımı eski Mısırlılar'dan günümüze kadar ulaşmasına ragmen, günümüzde yeni bir teknoloji olarak düşünülmektedir. Özellikleri az bilindiğinden ve yaygın kullanılmadığından ticari olarak sınırlı kullanıma sahiptir. Davidovits (1979), eski Romalıların ve Mısırlıların günümüze dek ulaşan yapıtlarını doğal taşlardan değil, jeopolimer çimentolar kullanarak inşa ettiklerini belirtmiştir. Mısır piramitlerinin; kireçtaşı kumu, NaOH, Na_2CO_3 ve su kullanılarak yerinde inşa edildiklerini, yaptığı mineralojik, kimyasal, yapısal ve dokusal araştırmalarına bağlı olarak kanıtlamış ve rapor etmiştir (Torgal vd., 2008).

Jeopolimer çimentolar; yüksek fırın cürufu ve uçucu kül gibi alimünyum ve silikatça zengin puzolanik malzemelerin alkali kimyasallarla muamele edilmesiyle elde edilirler. Jeopolimer çimentolar atık veya yan sanayi ürünlerinden üretildiklerinden ve bağlayıcı olarak ekstra bir kullanıma sahip olduğundan, oldukça avantajlıdırlar. Bununla birlikte, çimento ile kıyaslandığında sıfır sera gazı emisyonu, ekstra pişirme enerjisi ve doğal mineral kaynaklarının kullanımını gerektirmemesi gibi yönlerinden dolayı oldukça çevrecidirler (Ehrenberg, 2005). Jeopolimerler; madencilikte, inşaat sektöründe, atık yönetimi ve özel beton uygulamalarında kullanılabilmektedir. Jeopolimer çimentoların, madencilikte yeraltı dolgu uygulamalarında aşırı tuzlu su ortamlarında dahi çimentolu ürünlerle kıyaslandığında daha düşük maliyetlerde 5 kata kadar daha yüksek dayanım sonuçları ürettiği belirtilmektedir (Drechsler, 2006). Macun dolguya yönelik yüksek sülfat içeren maden tesis atıklarının kullanıldığı agresif ortamlarda dahi (DIN 4030), jeopolimerlerin çimento içeren dolgu örneklerine kıyasla daha duraylı ve 5 kata kadar yüksek dayanım sonuçlarının elde edildiği görülmüştür (Cihangir vd., 2012).

Macun dolguda dayanım ve durabilitenin yanında önemli diğer bir husus ise dolgu malzemesinin pompa-boru sistemi ile yeraltına taşınması ve yeraltındaki cevheri alınmış boşluklara yerleştirilmesidir. Dolgu malzemesi 6 ila 15 dakika arasında, macun dolgu tesisine olan uzaklığa bağlı olarak yeraltında doldurulacağı nihai boşluğa ulaşmaktadır. Taşınma esnasında macun dolgu malzemesinin kıvamında herhangi bir değişiklik olmaması ve başlangıç kıvamını koruması; pompa basıncı ve enerji maliyetlerinin yanında, borularda tıkanma ve aşırı sürtünmeden dolayı aşınma problemlerinin engellenmesi ve tamir-bakım meliyetleri açısından büyük önem arz etmektedir (Hewitt vd., 2009).

Macun dolgunun yeraltına taşınma esnasındaki reolojik özelliklerine yönelik literatürde çok az çalışmaya rastlanmıştır. Ayrıca şlamı uzaklaştırılmış tesis atıklarından hazırlanan macun dolgu özelliklerine yönelik de literatürde sınırlı sayıda çalışma bulunmaktadır (Kesimal vd., 2003; Erçıkdı vd., 2003).

İnşaat sektöründe jeopolimer bağlayıcılar kullanıldığında taze numunelerde işlenebilirlik kayıpları meydana gelmektedir.

Bu yüzden özel kimyasal ve ultra ince mineral katkı maddelerine başvurulmaktadır (Collins ve Sanjayan, 1998; Torgal vd., 2011). Macun dolguda jeopolimer bağlayıcıların beton malzemelerine benzer şekilde işlenebilirik kayıplarına neden olup olmayacağının ortaya konulması, bu bağlayıcıların macun dolguda teknik olarak kullanılıp kullanılamayacağının belirlenmesi açısından büyük önem taşımaktadır.

Bu çalışmada; normal Portland çimento ve jeopolimer bağlayıcılar ile sülfür içeriği yüksek normal atıklardan ve bu atıkların siklonlanması ile ince miktarının uzaklaştırılmasından elde edilen biraz daha iri boyuta sahip cevher zenginleştirme tesis atıklarından hazırlanan macun dolgu malzemelerinin kıvam özellikleri araştırılmıştır. Bu kapsamda normal Portland çimento ve iki farklı jeopolimer (alkali aktive yüksek fırın cürufu) bağlayıcı malzeme kullanılarak hazırlanan taze macun dolgu malzemelerinin ilk iki saatteki reolojik davranışları araştırılmıştır. Macun dolguda dolgu malzemesinin işlenebilirlik özelliklerine yönelik literatürde sınırlı sayıda çalışma bulunmaktadır (Yin vd., 2012). Dolayısıyla bu çalışmanın, hem normal Portland çimento ile hem de jeopolimer bağlayıcılar kullanılarak hazırlanan macun dolgu malzemesinin pompa-boru sistemi ile taşınması ve yerleşmesi esnasında geçen süredeki reolojik özelliklerinin belirlenmesinin uygulamada ve literatüre katkılar sağlayacağı düşünülmektedir.

1.1 Macun Dolgunun Yeraltına Nakliyesi

Macun dolgu malzemesi macun dolgu tesisinde hazırlanmaktadır. Macun dolgu tesisleri, yaklaşık olarak ağırlıkça ortalama %75-85 katı oranında, 12-200 m^3/sa kapasitede ve 5-13 MPa pompa basıncında dolgu malzemesi üretme ve nakliye kapasitelerinde tasarlanabilir (Paterson, 2011; Erçıkdı vd., 2012). Ağırlıkça yaklaşık %30 katı içeren tesis atıkları öncelikle 4" çapında borularla macun dolgu tesisine gönderilmektedir. Atıklar ilk olarak değişik çaplardaki tiknerlerde koyulaştırılmakta ve buradan depolama tankına nakledilmektedir. Depolama tankında homojenleştirilen atıklar vakumlu disk filtreler kullanılarak susuzlaştırılmaktadır. Bu işlem sonucu oluşan filtre kekinin katı içeriği ağırlıkça %80-86'dır. Burada susuzlandırmanın temel amaçları; tesise su geri beslemesini sağlamak, dolgu için gerekli uygun, işlenebilir karışım malzemesini sağlamak ve dolgu bünyesinde yer alabilecek suyun kimyasal açıdan maksimum kontrolünü ($SO_4^=$ içeriği vs.) sağlamaktır.

Daha sonra filtre kekine kondisyoner tankında su ve mikserde bağlayıcı ilave edilerek homojen bir şekilde karıştırılmakta, hazırlanan karışım 5" çapındaki borular ve pompalar vasıtasıyla yeraltı üretim boşluklarına nakledilmektedir (Şekil 1).

Şekil 1. Macun dolgunun yeraltı boşluğuna nakliyesi (Yılmaz, 2003)

Macun dolgu malzemesi pratikte 7.0-8.5 inç slampta yer altına basılmaktadır. Ancak dolgu malzemesinin yer altı boşluklarına 6-10 inç slampta basılabileceği belirtilmektedir (Erçıkdı vd., 2012). Macun dolgu malzemesinin kıvamı, yeraltında yerleştirileceği boşluğa nakliyatı açısından büyük öneme sahiptir.

Macun dolguda 20 μm altı malzeme miktarı, dolgu malzemesinin su tutma yeteneği açısından önemlidir. Macun dolgu malzemesi, kuru ağırlıkça en az %15 oranında 20 μm altı ince tane içerdiğinden kolloidal bir yapıya sahiptir (Brackebusch, 1994). Böylelikle; dolgu malzemesinin kıvamını bir müddet koruması ve boru sistemi ile yer altına kolay bir şekilde taşınması mümkün olmaktadır.

1.2 Bağlayıcı İçeren Malzemelerde İşlenebilirlik Testi

Çimento içeren taze beton, harç vb. malzemelerin özellikleri; karışım anından en son yerleştirileceği yere kadarki zaman aralığında malzemelerin kıvamı, akışkanlıkları, taşınabilirlikleri, pompalanabilirlikleri, sıkıştırılabilirlikleri, yerleştirilebilirlikleri gibi özellikler belirlenir. Bu özellikler, bağlayıcı içeren taze malzemelerin işlenmesinde ekipman seçimi ve konsolidasyon gibi özellikleri etkilediğinden büyük önem arz eder. İşlenebilirlik ise taze beton gibi malzemelere yönelik yukarıda sayılan bütün parametreleri yaklaşık olarak temsil eden bir kavram olmakla birlikte herhangi bir segregasyona izin vermeden beton vb. malzemelerin yerine yerleştirilmesi ve sıkıştırılmasına kadar gerekli işlerin bütünü olarak belirtilebilir. İşlenebilirlik ölçümlerine yönelik önerilen en yaygın test yöntemleri *i)* slamp testi *ii)* vebe testi *iii)* kompaksiyon testi ve *iv)* akış testi şeklinde sıralanabilir (Shi vd., 2006).

Bağlayıcı içeren taze harç ve beton malzemelerinde işlenebilirlik özellikleri pratikte genel olarak slamp testleri ile ölçülmektedir. Macun dolguda da taze dolgu malzemesinin başlangıç slamp seviyesi ölçülmektedir. Malzemenin slampı su ile ayarlandığından, fazla su kıvamın azalmasına neden olurken, diğer taraftan dolgunun kolloidal yapısından dolayı su tutması nedeniyle boşluk miktarı artmaktadır. Dolayısıyla macun dolguda kısa ve uzun dönemde dayanım problemleri meydana gelmektedir. Bu yüzden macun dolguda kıvamın optimum seviyede olması istenmektedir.

Slamp ölçümünde standart kesik koninin (12 inç yüksekliğe sahip) içine taze dolgu malzemesi 3 kademede hava alma ve sıkılama işlemleri ile doldurulur. Daha sonra kesik koninin üst yüzeyi düzeltilir. Koni iki tarafındaki tutma kulplarından tutularak yukarı doğru sabit ve kontrollü bir şekilde çekilir. Böylece kesik koninin içindeki malzemenin serbest bırakılarak düşürülmesi sağlanır. Malzemenin başlangıç seviyesinden olan düşme seviyesi ölçülerek macun dolgu malzemesinin slampı bulunur (Şekil 2).

Şekil 2. Macun dolgu kıvamının slamp testi ile ölçülmesi

2 DENEYSEL ÇALIŞMALAR

Bu çalışmada; bir maden işletmesine ait sülfür içeriği yüksek normal atık ve bu atıktan hidrosiklon ile ince malzemenin bir kısmının uzaklaştırılmasıyla elde edilen atık olmak üzere iki farklı atık kullanılmıştır. Bu atıklardan aktifleştirilmiş yüksek fırın cürufu içeren jeoplimerler ve normal Portland çimentosu kullanılarak hazırlanan taze macun dolgu numunelerinde, atık ve bağlayıcı özelliklerinin dolgu malzemesinin dayanım ve reolojik özelliklerine etkileri araştırılmıştır. Bu amaçla hazırlanan macun dolgu numunelerinin macun dolguda kullanılabilirliklerine yönelik eşik süre olan 28 günlük kür süresinde dayanımları ve ilk iki saatlik süredeki işlenebilirlik özellikleri araştırılmıştır.

Deneysel çalışmalarda kullanılan atık malzemeler Rize'nin Çayeli ilçesinde Madenköy'de bulunan Çayeli Bakır İşletmeleri'nden temin edilmiştir. Bağlayıcı olarak bir çimento fabrikasından normal Portland çimentosu temin edilmiştir. Ayrıca jeopolimer bağlayıcılar için bir demir çelik fabrikasından yüksek fırın cürufu temin edilmiştir. Yüksek fırın cürufunun aktifleştirilmesinde kullanılmak üzere sıvı sodyum silikat (LSS-$Na_2O{\cdot}2SiO_2$) ve granüle sodyum hidroksit (NaOH) olmak üzere iki farklı aktivatör temin edilmiştir.

2.1 Malzemelerin Karakterizasyonu

2.1.1 Atık Malzeme

Deneysel çalışmalarda kullanılan atık malzeme flotasyon işlemine tutulmuş bakır cevherinin zenginleştirildiği cevher zenginleştirme tesisinin disk filtre çıkışından alınmıştır. Atık malzemelerin tane boyu dağılımı analizleri, Malvern Mastersizer Hydro 2000 MU marka tane boyu dağılımı ölçüm cihazı ile gerçekleştirilmiştir.

Şekil 3'te normal atık ve şlamı uzaklaştırılmış atık için 20 µm altı malzeme miktarının ağırlıkça sırasıyla %50.99 ve %16.01olduğu görülmektedir. Buna göre normal atık orta boyutlu atık sınıfına girerken, şlamı uzaklaştırılmış atık iri boyutlu atık sınıfına girmiştir (Landriault, 2001; Kesimal vd., 2010). Atık malzemelerin macun dolguda kullanılabilmesi için 20 mikron altı ince malzeme miktarı minimum %15 olması gerektiği göz önüne alındığında, her iki atığın da macun dolguda kullanılabileceği görülmektedir.

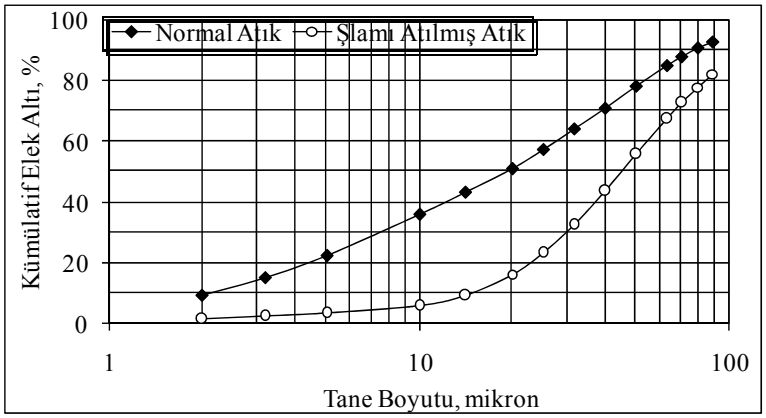

Şekil 3. Atık malzemelerin tane boyut dağılımları

Atık malzemelerin üniformluk katsayıları (C_u) ve eğrilik katsayıları (C_c) göz önüne alındığında atık malzemelerin her ikisinin de iyi bir tane boyut dağılımına sahip oldukları söylenebilir. Bununla birlikte, şlam uzaklaştırma ile elde edilen atığın daha iyi

bir granülometriye sahip olduğu söylenebilir (Landriault, 2001). Atık malzemelerin özgül ağırlıkları (G_s) 100 ml'lik piknometreler kullanılarak ASTM C 128-97 (2002) standartlarına göre elde edilmiştir. Atık malzemelerin özgül yüzey alanları değerlendirildiğinde şlam uzaklaştırma işlemi sonucunda 20 mikron altı malzeme miktarlarına bağlı olarak yüzey alanlarının başlangıç değerine göre %47 oranında azaldığı görülmektedir (Çizelge 1).

Dolgu malzemesinin yeraltı üretim boşluklarına nakliyesi esnasında kıvamını koruması ve arzu edilen akışkanlığa sahip olabilmesi için beli oranda suyu bünyesinde tutması gerekmektedir. Macun dolguda su tutmayı sağlayacak kolloidal yapı için atık malzemedeki 20 μm altı malzeme miktarının ağırlıkça en az %15 olması gerekmektedir. Malzemenin kolloidal özelliklerini belirlemek için standart slamp koni testi ve su tutma-bırakma testleri kullanılmaktadır. Atıkların reolojik özelliklerinin belirlenmesine yönelik öncelikle ASTM C 143'e göre beton standart kesik koni test aleti ile 7.5 inch slampta çimentosuz numuneler hazırlanmıştır. Daha sonra bu numunelerden belirli miktarda numune alınarak 6 saat boyunca numuneden ayrılan su miktarları toplanarak başlangıçtaki su miktarına oranlanmıştır. Reolojik testlerde normal atıkların su tutma kapasitelerinin şlam malzemesi uzaklaştırılmış atıklara kıyasla yaklaşık 12 kat daha yüksek olduğu görülmüştür. Şekil 4'te şlam malzemesi uzaklaştırılan atıklarda 6 saat sonunda daha fazla oranda oturma gerçekleştiği görülmektedir.

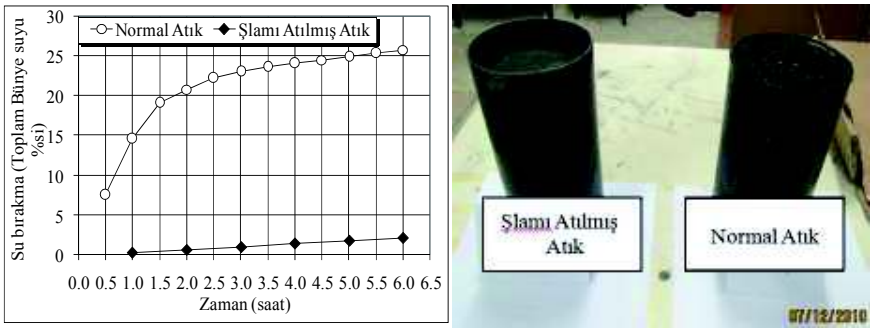

Şekil 4. Atık malzemelerin su tutma-bırakma kapasiteleri

Atık malzemelerin kimyasal analizleri Kanada'da ACME kimyasal analiz laboratuvarlarında gerçekleştirilmiştir. Atık malzemenin kimyasal analizlerinden S^{-2} (Sülfid Kükürdü) içeriklerinin oldukça yüksek olduğu görülmektedir. Ayrıca SiO_2 + Al_2O_3 içerikleri bakımından şlamı uzaklaştırılan atığın yaklaşık %30 oranında daha az kil mineralleri içerdiği görülmüştür. Şlam uzaklaştırma işlemi sonucunda elde edilen atığın pirit içeriğinin başlangıca göre yaklaşık %13 oranında arttığı görülmektedir. Atık malzemelerin bazı kimyasal ve fiziksel özellikleri aşağıda Çizelge 1'de verilmiştir.

2.1.2 Bağlayıcı Malzemeler

Bu çalışmada, kontrol amaçlı olarak macun dolgu malzemelerinin hazırlanmasında normal Portland çimentosu kullanılmıştır. Normal çimentoya alternatif bağlayıcı olarak kullanılan yüksek fırın cürufu Kardemir demir çelik fabrikasından temin edilmiştir.

Bağlayıcı maddelerin kimyasal ve mineralojik analizleri Çizelge 2'de ve fiziksel özellikleri Çizelge 3'te verilmiştir. Çizelge 2'den normal Portland çimentosunun CaO yüzdesinin çok yüksek olduğu (%65,0) ve dolayısıyla sülfür içeriği yüksek atıklardan hazırlanacak macun dolguda asit ve sülfat etkilerine karşı dayanıksız olabileceği söylenebilir.

Çizelge 1. Atık malzemelerin bazı fiziksel ve kimyasal özellikleri

Kimyasal bileşim	Normal Atık (%)	Şlamı Uzaklaştırılmış Atık (%)
SiO_2	13.16	10.43
Al_2O_3	4.81	2.46
Fe_2O_3	48.41	53.93
MgO	1.13	0.91
CaO	1.83	1.28
Na_2O	0.19	0.18
K_2O	0.64	0.23
TiO_2	0.08	0.07
P_2O_5	0.02	0.02
MnO	0.06	0.05
Cr_2O_3	0.01	<0.01
$BaSO_4$	2.54	2.02
Kızdırma kaybı	26.9	28.2
Sülfür içeriği (S^{-2})	37.4	42.23
Pirit içeriği (FeS_2)	70.13	79.19
Fiziksel özellikler		
Özgül ağırlık	4.09	4.32
Özgül yüzey alanı (cm^2/g)	3662	1956
Eğrilik çapı (C_c)	0.96	1.08
Üniformluk katsayısı (C_u)	13.33	3.62

Çizelge 2. Bağlayıcı maddelerin kimyasal ve mineralojik özellikleri

Kimyasal	Normal Portland Çimentosu (%)	Yüksek Fırın Cürufu (%)
SiO_2	21.88	39,75
Al_2O_3	4.74	10,91
Fe_2O_3	2.90	0,80
CaO	65.00	38,02
MgO	1.40	5,92
TiO_2	0.19	0,51
Cr_2O_3	0.01	0,01
Na_2O	0.39	0,32
K_2O	0.75	1,19
MnO	0.12	1,54
P_2O_5	0.06	<0.01
Serbest Kireç	1.04	-
Kızdırma	2.5	0,20
SO_3	2.67	1,62
Reaktif SiO_2	-	39,1
Baziklik	-	1,03
Mineralojik bileşim	(%)	
C_3S	50,42	
C_2S	27,76	
C_3A	7,66	
C_4AF	8,83	

Çizelge 3. Bağlayıcı maddelerin fiziksel özellikleri

Fiziksel Özellikler	Normal Portland Çimentosu	Yüksek Fırın Cürufu
Özgül ağırlık	3,07	2,89
Özgül yüzey (cm^2/g)	4120	4600
45 µm elek bakiyesi (%)	2,17	4,15
32 µm elek bakiyesi (%)	7,48	9,6

Bağlayıcı malzemelerin özgül ağırlıkları (G_s) 100 ml'lik piknometreler kullanılarak ASTM C 128-97 (2002) standartlarına göre elde edilmiştir. Malzemelerin özgül yüzey alanları ise blain (incelik) testleri ile belirlenmiştir. Bağlayıcı malzemelerin kimyasal analizleri de Kanada'da bulunan ACME laboratuvarlarında gerçekleştirilmiştir.

Yüksek fırın cüruflarının aktifleştirilmesinde modül oranı 2.0 (ağırlıkça SiO_2/Na_2O oranı; $M_S=SiO_2/Na_2O$) olan sıvı sodyum silikat (LSS: $Na_2O.2SiO_2$) ve %99,5 saflıkta granüle sodyum hidroksit (NaOH) kullanılmıştır. LSS, Ege Kimyasalları Ltd. Şti.'den ve NaOH, Merck Kimyasalları'ndan temin edilmiştir. Aktifleştirme çalışmalarında modül oranı NaOH kullanılarak yapılmıştır. Deneysel çalışmalarda NaOH granülleri önce suda çözülmüş, daha sonra atık malzeme, yüksek fırın cürufu ve sudan oluşan karışım ortamına ilave edilmiştir.

2.2 Macun Dolgu Malzemelerinin Hazırlanması

Macun dolgu malzemeleri, tesis atıkları, karışım suyu, aktivatörler ve bağlayıcı malzemelerin, 20,8 litre kapasiteli bir mikserde (Univex SRMF20 Stand Model) karıştırılarak homojenleştirilmesiyle hazırlanmıştır. Karıştırma işlemi 105 devir/dk'lık dönme hızında 7 dakika süreyle yapılmıştır. Macun dolgu malzemelerinin başlangıç slampları yaklaşık 7.5 inç (190 mm) slamp olarak hazırlanmıştır.

Macun dolgu numuneleri %6.5 bağlayıcı oranında hazırlanmıştır. Bağlayıcı oranı, dolgu dizaynında toplam katı miktarının (bağlayıcı+atık) ağırlıkça %'sidir. Jeopolimer bağlayıcılarda bağlayıcı faz (her bir farklı dizayn için kullanılan malzemeleri kapsayacak şekilde); cüruf, sodyum silikatın bileşenleri olan sodyum oksit (Na_2O) ve silisyum dioksit (SiO_2) ile sodyum hidroksit kombinasyonlarından oluşmaktadır. Normal Portland çimento için bağlayıcı faz ise, belirli bir dizayn için dolgu bünyesindeki toplam katının ağırlıkça %'sidir. Dolgu dizaynlarında jeopolimer ve Normal Portland çimento bağlayıcı fazları ağırlıkça eşittir (Cihangir, 2011). İki farklı atık için macun dolgu malzemeleri normal Portland çimentosu, sıvı sodyum silikat+NaOH+yüksek fırın cürufu ve NaOH+yüksek fırın cürufu olmak üzere üçer farklı dizaynda hazırlanmıştır. Normal Portland çimento içeren macun dolgu malzemeleri kontrol amaçlı olarak kullanılmıştır.

2.3 Dayanım Testleri

6 farklı bileşime ait macun dolgu malzemelerinden 10 cm x 20 cm boyutlarında üçer adet dolgu numunesi hazırlanmıştır. Numunelerin dayanım testleri, 28 günlük kür süresi sonunda, yükleme kapasitesi 50 kN olan bilgisayar kontrollü tek eksenli basınç ve deformasyon ölçer ünitesinde 0.5 mm/dk yükleme hızında ASTM C 39 standardına uygun olarak gerçekleştirilmiştir. Elde edilen tek eksenli basınç dayanımlarının ortalamaları alınarak her numune grubunun ortalama dayanımı hesaplanmıştır. Atık ve bağlayıcı malzemelerin kombinasyonlarından oluşan macun dolgu numunelerinin dolgu olarak kullanılabilirliklerine yönelik eşik değer olarak 1.0 MPa'lık dayanım değeri esas alınmıştır (Cihangir, 2011).

2.4 İşlenebilirlik Testleri

Hazırlanan 6 farklı bileşime ait macun dolgu malzemelerinin 0-30-60-90 ve 120. dakikalarda ayrı ayrı slampları alınmıştır. Her malzeme, slamp ölçümü alındıktan

hemen sonra tekrar ilgili slamp alma sürelerine kadar mikserde karıştırma işlemine tabi tutulmuştur.

3 BULGULAR VE İRDELEME

Jeopolimer bağlayıcılar ve normal Portland çimentosu ile hazırlanan macun dolgu numunelerinin dayanım sonuçları Şekil 5'te verilmiştir. Jeopolimer bağlayıcılarla hazırlanan numuneler her iki atık türünde de 28 günlük kür süresi sonunda 1 MPa'lık eşik dayanım değerini sağlamıştır. Normal Portland çimentosu ile sadece şlamı uzaklaştırılmış atıktan hazırlanan macun dolgu numunelerinin eşik dayanım değerini sağladığı görülmüştür. İri boyutlu atıkların kullanılması durumunda, normal atıklardan hazırlanan dolgu numunelerine kıyasla daha yüksek dayanım değerlerinin elde edildiği belirtilmektedir (Kesimal vd., 2003; Fall vd., 2005; Erçıkdı vd., 2013).

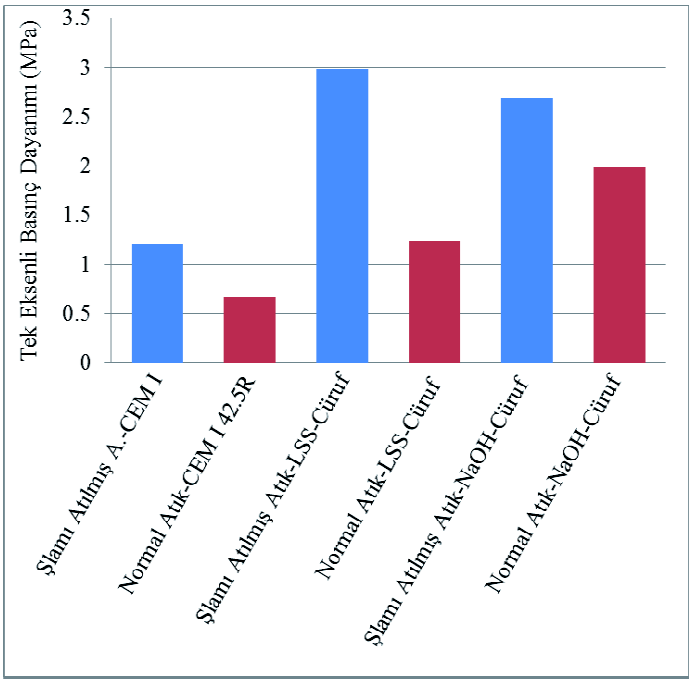

Şekil 5. Macun dolgu malzemelerinin dayanım seviyeleri

Normal atık, normal Portland çimento ve jeopolimer bağlayıcılar ile hazırlanan taze macun dolgu malzemelerinin ilk iki saat boyunca slamp seviyeleri ise Şekil 6'da verilmiştir.

Normal atık ile çimento kullanılarak hazırlanan macun dolgu malzemelerinde zamana bağlı olarak çok az (%1.3) işlenebilirlik kaybı olduğu görülmüştür. Fakat bu işlenebilirlik kaybının macun dolgunun taşınabilirlik özelliğini etkilemeyeceği görülmektedir.

Jeopolimer bağlayıcılar ile hazırlanan macun dolgu malzemelerinde ise herhangi bir işlenebilirlik kaybının yaşanmadığı, aksine işlenebilirliklerinde bir artma olduğu görülmektedir. LSS-yüksek fırın cürufu kullanılarak hazırlanan malzemelerin 2 saat sonundaki slamp seviyesi yaklaşık 229 mm (9.0 inç) olmuştur. Dolayısıyla jeopolimerlerin macun dolguda bağlayıcı olarak kullanılması durumunda macun dolgu malzemelerinin taşınması ve yeraltındaki üretim boşluklarına yerleşmelerinin normal

çimentoya göre biraz daha kolay olabileceği söylenebilir. Aşağıda Şekil 7'de LSS-cüruf içeren macun dolgu malzemesinin 0-2 saat arasındaki slamp seviyeleri görülmektedir.

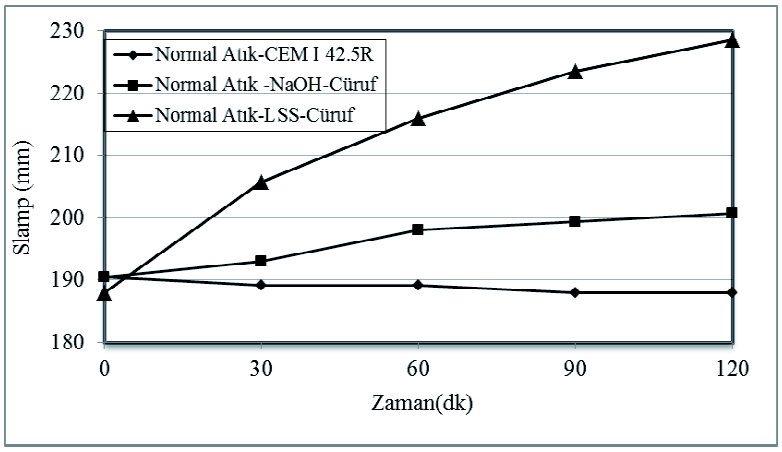

Şekil 6. Normal atıktan hazırlanan macun dolgu malzemelerinin slamp seviyeleri

Şekil 7. LSS-cüruf ile hazırlanan macun dolgu malzemesinin 0-2 saatlik kıvamları

Şlamı uzaklaştırılmış atık ile hazırlanan macun dolgu malzemelerinin slamp seviyeleri ise Şekil 8'de özetlenmiştir. Normal atıkla hazırlanan macun dolgu malzemesinin kıvamına benzer şekilde, şlam malzemesi uzaklaştırılmış atıktan hazırlanan macun dolgu malzemelerinde de benzer kıvam özellikleri elde edilmiştir. Normal Portland çimentosu ile hazırlanan macun dolgu numunelerinin işlenebilirliklerinde başlangıca göre yaklaşık %6'lık (slamp 7.5 inç'ten 7.05 inç\17.91 mm'ye düşme) bir

kayıp olmuştur. Ancak bu durumun, benzer özelliklere sahip macun dolgu malzemelerinin nakliyesinde problem oluşturmayacağı düşünülmektedir.

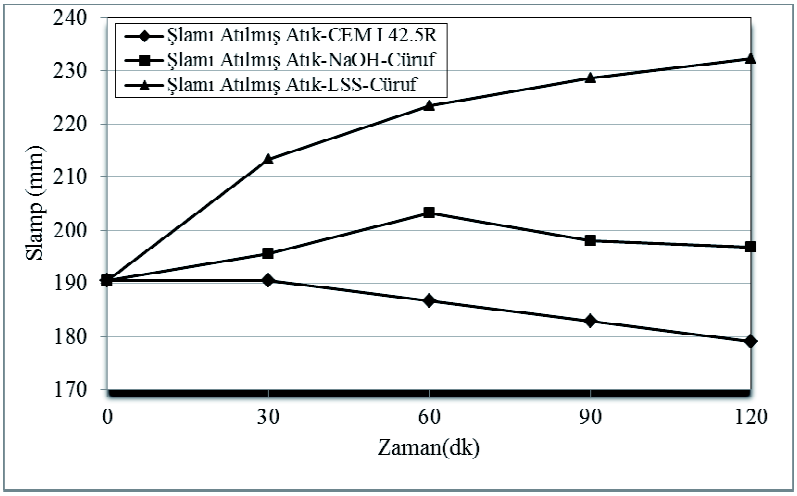

Şekil 8. Şlamı uzaklaştırılmış atıktan hazırlanan dolgu malzemelerinin slamp seviyeleri

Aktifleştirilmiş yüksek fırın cürufu + NaOH ile hazırlanan numunelerin ilk 60 dakika boyunca kıvamı azalmış, bu süreden sonra ise artmıştır. Ancak, iki saat sonundaki slamp seviyesi başlangıç slamp seviyesinin üzerindedir. LSS-cüruf içeren malzeme ise en düşük kıvama yani en yüksek işlenebilirlik özelliğine sahiptir.

Cihangir 2011, aktifleştirilmiş yüksek fırın cürufu içeren bağlayıcılarda hidratasyon esnasında, çimentodan farklı olarak, cüruf taneciklerinin başlangıçta çözünerek öncelikle jelimsi bir yapı oluştuğunu, asıl sertleşme işleminin ise çözünme işlemi tamamlandıktan sonra başladığını belirtmiştir. Macun dolguda çimento ve jeopolimer bağlayıcıların işlenebilirliklerinin normal taze beton/harç malzemesi örneklerine göre farklı davranış sergilemesinin; *i*) macun dolguda su/bağlayıcı oranının normal beton örneklerine göre daha yüksek olması; *ii*) suyun macun dolgu bünyesinde çok uzun süreler boyunca tutulması ve *iii*) jeopolimer bağlayıcıların sulu ortamlarda (macun dolgu için) farklı hidratasyon mekanizmasına sahip olmasından kaynaklanabileceği düşünülmektedir.

Beton örneklerinde aynı kimyasal aktivatörlerle (LSS, NaOH) hazırlanan taze beton/harç numunelerinden, macun dolguda elde edilen sonuçlara zıt sonuçlar elde edilmiştir (Collins ve Sanjayan, 1999; Atiş vd., 2009). Belirtilen çalışmalarda LSS ve NaOH içeren jeopolimer çimentolarla hazırlanan taze beton örneklerinde ilk 1 saat içerisinde önemli derecede işlenebilirlik kayıpları (slamp kaybı) görülmüştür.

İşlenebilirlik değerlerinin beton ve macun dolgu sistemlerinde farklı özellik sergilemesinin, bu iki sistemin birbirinden farklı olmasından ve sistemlerin farklı çalışmasından kaynaklandığı söylenebilir (Benzaazoua vd., 2004).

4 SONUÇLAR

Bu çalışmada normal ve şlamı uzaklaştırılmış atık ile hazırlanan macun dolgu malzemelerinde bağlayıcı olarak kullanılan normal Portland çimento ve jeopolimer bağlayıcıların dayanım ve işlenebilirlik özellikleri araştırılmıştır.

Bu atıklardan normal Portland çimentosu kullanılarak hazırlanan macun dolgu malzemelerinde zamana bağlı olarak düşük

oranlarda (%1-6) işlenebilirlik kaybı görülmüştür.

Jeopolimer bağlayıcılar ile hazırlanan macun dolgu malzemelerinde ise işlenebilirlik kaybı görülmemiş, aksine jeopolimer bağlayıcıların macun dolgu malzemelerinin işlenebilirliklerini ilk saatlerde artırdığı görülmüştür. Sıvı sodyum silikat ile hazırlanan macun dolgu malzemelerinin NaOH ile hazırlanan malzemelerin işlenebilirliklerinden daha iyi olduğu görülmüştür.

Jeopolimer bağlayıcılar ile hazırlanan macun dolgu malzemelerinin işlenebilirliklerinin artmasının, bu tür bağlayıcılarda başlangıçta hemen hidratasyonun gerçekleşmemesi, bağlayıcı cüruf tanelerinin başlangıçta çözünerek matrix içerisinde jelimsi yapıya dönüşmesinden kaynaklandığı düşünülmektedir.

Teşekkür

Yazarlar, TÜBİTAK'a (112M378 no'lu proje), Karadeniz Teknik Üniversitesi Bilimsel Araştırma Projeleri Koordinasyon Birimine (8629 no'lu KTÜ BAP03 araştırma projesi) ve malzeme desteğinden dolayı Çayeli Bakır İşletmeleri'ne teşekkür eder.

KAYNAKLAR

ASTM C 39, 2002. Standard test method for compressive strength of cylindrical concrete specimens, Annual Book of American Standard of Testing Materials Standards, vol. 04.02.

Atiş, C. D, Bilim, C., Çelik, Ö. and Karahan, O., 2009. Influence of Activator on The Strength and Drying Shrinkage of Alkali-Activated Slag Mortar, *Construction and Building Materials*, 23, 1, (s.548-555).

Benzaazoua, M, Fall, M and Belem, T, 2004. A Contributing to Understanding the Hardening Process of Cemented Pastefill, *Minerals Engineering,* 17, 2, (s.141-152).

Brackebusch, F. W.,1994. Basics of Paste Backfill Systems, *Mining Engineering,* 46, 1,(s.1175-1178).

Cihangir, F, 2011. Aktifleştirilmiş Yüksek Fırın Cürufunun Macun Dolguda Bağlayıcı Olarak Kullanılabilirliğinin Araştırılması, *Doktora Tezi,* Karadeniz Teknik Üniversitesi, Fen Bilimleri Enstitüsü, Maden Mühendisliği Anabilim Dalı, Danışman: Prof. Dr. Ayhan KESİMAL, Trabzon, 181 s.

Cihangir, F, Erçıkdı, B, Kesimal, A, Turan, A. and Deveci, H, 2012. Utilisation of alkali-activated blast furnace slag in paste backfill of high-sulphide mill tailings: Effect of binder type and dosage. *Minerals Engineering*, 30, (s.33-43).

Collins, F. and Sanjayan, J. G, 1998. Early Age Strength and Workability of Slag Pastes Activated by NaOH and Na_2CO_3, *Cement and Concrete Research,* Vol. 28 (5) (s.655–664).

Collins, F. and Sanjayan, J. G, 1999. Workability and mechanical properties of alkali activated slag concrete, *Cement and Concrete Research*, 29, (s. 455–458).

Davidovits, J, 1979. Synthesis of New High Temperature Geo-Polymers for Reinforced Plastics/Composites, SPE PACTEC 79 Society of Plastic Engineers, Brookfield Center, (s.151–154).

DIN 4030, 2001. Standard assessment of water, soil, and gases for their aggressiveness to concrete; principles and limiting values. *German Standard*, Construction Materials and Building.

Drechsler, M, 2006. Geopolimers: A new technology for sustainability in mining, construction and hazardous waste industries, Stabilizing Mines, *PB Network 62*, Adelaide, South Australia (http://www.pbworld.com/news_events/publications/network/).

Ehrenberg, A, 2005. Environmental Aspects of Slag Use, Granulated Blast Furnace Slag: Its Advantages with Respect to CO_2 Emissions and Energy Consumption, *Cement and Concrete World,* ISSN 1301-0859, 10-56, (s.36-51).

Erçıkdı, B, Kesimal, A, Yılmaz, E, Deveci, H, 2003. Effect of desliming on thestrength of paste backfill. *Proceedings of the X Balkan Mineral Processing Congress, Mineral Processing in the 21st Century*, Varna, Bulgaria,15-20 June, (s.850-857).

Erçıkdı, B, Cihangir, F, Kesimal, A. ve Deveci, H, 2012. Tesis Atıklarının Yönetiminde Macun Dolgu Teknolojisi, *Madencilik Türkiye Dergisi*, (s.70-76).

Fall, M, Benzaazoua, M. and Ouellet, S, 2005. Experimental Characterization of the Influence of Tailings Fineness and Density on the Quality of Cemented Paste Backfill, *Minerals Engineering*, 18, 1, (s.41–44).

Hewitt, D, Allard, S. and Radziszewski, P, 2009. Pipe lining abrasion testing for paste backfill operations, *Minerals Engineering*, (22), (s.1088–1090).

Kesimal, A, Erçıkdı, B. and Yılmaz, E, 2003. The Effect of Desliming by Sedimentation on Paste Backfill Performance, *Minerals Engineering*, 16, 10, (s.1009-1011).

Kesimal, A, Deveci, H, Alp, İ, Erçıkdı, B. and Cihangir, F, 2010. Optimization of Paste Backfill Performance for Different Ore Types in Cayeli

Copper Mine, Karadeniz Technical University, Mining Engineering Department, *Revolving Fund Project*, Trabzon, Turkey, 36 s.

Landriault, D, 2001. Backfilling in Underground Mining, in: W.A. Hustrulid (Eds.), *Underground Mining Methods Engineering Fundamentals and International Case Studies*, SME, 15 s.

Paterson, A. J. C, 2011. (Editors: Richard Jewell, Andy Fourie).The pipeline transport of high density slurries-A historical review of past mistakes, lessons learned and current Technologies, *Paste 2011, Proceedings of the 14th International seminar on paste and thickened tailings,* Perth, Australia, (s.351-367).,

Torgal F. P, Castro-Gomes J. and Jalali, S, 2008. Alkali-Activated Binders: A Review. Part 2. About Materials and Binders Manufacture, *Construction and Building Materials*, 22, 7, (s. 1315-1322).

Torgal F. P, Moura, D, Ding, Y. and Jalali, S, 2011. Composition, strength and workability of alkali-activated metakaolin based mortars, *Construction and Building Materials,* 25 (8), (s.3732–3745).

Shi, C, Krivenko, P. V. and Roy, D., 2006. Alkali-Activated Cements and Concretes. 1st ed. USA: *Taylor and Francis*, ISBN 10:0-415-70004-3.

Yılmaz, E, 2003. Sülfit İçeren Maden Atıklarından Hazırlanan Çimentolu Macun Dolgu Örneklerinin Dayanım Özelliklerinin İncelenmesi, *Yüksek Lisans Tezi*, Karadeniz Teknik Üniversitesi, Fen Bilimleri Enstitüsü, Trabzon, 92 s.

Yin, S, Wu, A, Hu, K, Wang, Y. and Zhang, Y, 2012. The effect of solid components on the rheological and mechanical properties of cemented paste backfill, *Minerals Engineering*, 35, (s.61–66).

The Importance of an Environmental Monitoring and Geotechnical Control Plan in a Mine

F. J. G. Márquez
PhD Master of Environmental Technology, University of Huelva.
Mining Departament. Industry, Energy and Mining Service. Office in Seville of the Regional Ministry of Economy, Innovation, Science and Employment of Seville. Government of Andalusia

E. M. R. Macías
Professor, Minning area, University of Huelva.
Members of the Research Centre for Sustainable Mining Engineering (C.I.P.I.M.S.)

ABSTRACT The environmental monitoring and geotechnical control plan is a tool for ensuring compliance with the requirements and corrective and protective measures that were established in the proposed operation of the mine.

The environmental monitoring program has control functions. It is a data source, mainly empirical, because it can assess how correct are the predictions made in the Environmental Impact Assessment (EIA). From this information, it is also possible to detect unforeseen changes in the Environmental Impact Study, which should be properly corrected by corrective measures. Thus, the environmental monitoring program is a source for feedback on the results of the EIA.

The geotechnical monitoring program allows the operators to measure surface and depth of deformation of slopes and their evolution.

Therefore, the most important aspect of a monitoring plan is the interpretation of the collected information in order to determine the need of modifying the initial objectives that were established in the project.

1. INTRODUCTION

The Monitoring Plan is to update and revise all elements that provide information about the stability of the areas affected by mining structures (like mines, dumps, etc.), (Fig. 1) and to check the efficiency of mining operations in the short and long term, through the foreknowledge of the stability conditions, the continuous updating of the design and, where appropriate, the implementation of preventive and corrective measures.

Figure 1: Landslide in collapse produced in mine

1.1. Objectives

The objectives of the Monitoring Plan are:

- To carry out a Geotechnical control, which includes both field work and laboratory testing.

- To Review the instrumentation and auscultation (stress and strain control) working at the present moment.

- To developed an integrated data management: Data Storage of auscultation in software for quick viewing.

- To Update the Emergency Plan design based on acquired experience.

1.2. Parameters to Control

The proposed plan allows continuous monitoring of the following operations:

- Geological mapping, lithology, structure and geotechnical excavation progress.

- Measurement of the properties of materials in situ, if necessary.

- Measurement of surface and deep of deformation of slopes and their evolution.

- Evaluation of surface weathering and collapse, either through specific tests or by visual monitoring of their evolution over time.

- Monitoring of the development of pore pressures and total pressures.

1.3. Reading Systems

Monitoring of constructive activities is performed by combining various methods integrated into a comprehensive system of data collection, analysis and corrective decision. Generally, are used simple methods of observation and manual measurement and automatic reading systems, combined with a process of data analysis and decision making in real time.

The monitoring system implemented ultimately depends most on the initial monitoring results.

2. OBTAINING DATA IN A MINE

Records of the slopes of the banks will be done, in order to collect the following information:

- **Geometry and progress of the excavation:** geometric control of the excavation will alert on possible deviations of the project design, both caused by the needs of the excavation itself or due to local instabilities.
- **Geotechnical control of a bank slope:** in order to take proper control over auscultation and recognize the progress of the open-cut mining, geological record will be made of the new excavated fronts, including the observed incidents.
- **Evaluation of the observed instabilities:** type definition of detected instabilities and, in case of observed failures, it will be given a rough estimate of the volume moved.
- **Photo-interpretation of bank slope:** It will be made from digital photographs of slope. It will allow identify areas with different geo-mechanical behavior. On the slopes excavated in rock will be proceed the execution of **geo-mechanical stations**, geo-technically classifying the ground through RMR of Bieniawski and conducting a survey of the discontinuities, obtaining the necessary data for its characterization following the methodology of Barton-Bandis.
- **Mapping or survey of the bank slope:** with all available data from the ground reconnaissance and photographic study will be made an analysis of the excavation front which will reflect at least, the following geotechnical data:

- Lithology and structure of affected formations.
- Tectonic features detected or suspected.
- Levels of alteration of the rock surface.
- Structural discontinuities. They include the features of each familyes, like dip slope and dip slope direction, spacing, continuity, openness, roughness, presence of water and filler (type and thickness). In addition, each of the families will be represented by stereographic projection.
- Areas of soil with a symbol that indicates the type and thickness.

Also be carried out the following activities:

- **Inventory of water points:** all the water points that appear will be catalogued with the open-cut mining.
  - Control of fissures and cracks: a file is made of all those cracks and crevices (Fig. 2) that may arise during the course of the operation, both within the interior of the open-cut mining and in the perimeter of influence (at least 100 m width from coronation).

3. AUSCULTATION

The following sections describe the plan of a mining auscultation.

3.1. Monitor parameters

During the excavation of the mine is necessary to perform the following parameters:

- Environmental parameters.
- Deformations by mean of topographic control, inclinometers and extensometers.
- Changes in pore pressure using piezometers.
- Variations in the total pressure determined by a pressure cells.

Figure 2: Cracks of decompression in header of slope mining

3.1.1. Environmental monitoring

It includes analysis of the evolution of atmospheric factors such, as temperature, humidity, atmospheric pressure, solar radiation and rainfall.

As for the tailings leachates, it is necessary including control the following parameters: flow, pH, conductivity and dissolved solids.

This control will be carried out to verify the existence of leachate through the berm barrier.

3.1.2. Topographic control

3.1.2.1. Topographic milestones

To know the movements generated in aun open-cut mine, as a result of the excavation, and in the dumps, as a result of pouring, are placed on the ground surface topographic milestones so that it is always possible to measure and ensure as far as possible it is not affected by the development of the excavation or pouring.

3.1.2.2. Topographic prisms

In order to obtain real-time moving all topographic prisms installed in an open-cut mine, will be monitored by means a total station.

Except in cases when the device has to be replaced for maintenance, or in moments when there are variations in the coordinates of the guidance bases and, therefore, variation in the coordinates of the measured points, the displacement calculation of the prisms of the edges of the ramp slope and of the open-cut mine access will be made with a period of 15 days regression, taking the mean value of each point for each day.

3.1.2.3. Inclinometers

The biaxial inclinometers are instruments for determining angular displacements of a drilling, by using a torpedo which is slid inside a special casing (inclinometer's pipe).

3.1.2.4. Extensometer

The extensometer probe consists of a steel pipe and is equipped with an inductive type transducer at each of its ends and of a centering device.

However, is considered of great importance to maintain the extensometers projected for the control of the future areas of interaction between different mining works.

3.1.3. Piezometers and total pressure cells

To control the interstitial and total pressure are used piezometers in the mine (Fig. 3), and piezometers and total pressure cells in the dumps.

In the installation of the pressure cells, particular attention must be paid to obtain the greatest possible horizontal, in order to detect the maximum land pressure on the cell and no smaller (variable depending on the inclination of the sensor of the maximum vertical pressure).

Figure 3: Drainage control by piezometers

3.2. Data collection

3.2.1. Verification of the correct operation of the sensors and the frequency

All devices of auscultation must be installed with sufficient time, to enable the initial reading which will be used as a reference to the successive.

Auscultation elements which, for whatever reason, are eliminated must be replaced as soon as possible, in the case that there is no close range instrumentation that can provide the same information.

As for the frequency of reads and based on the gained experience, it follows:

- To establish a reliable zero reading of the new sensors installed, will be done two readings in the first week.
- The frequency of readings will be weekly, during the first quarter, although this may be reduced if the newly installed sensors are not in active work areas and / or should be given the priority to measure to other sensors in justified cases, except in monthly sensors.
- After the first quarter, the frequency of readings will be fortnightly for the next six months, after which the frequency will be monthly. As in the previous case, the frequency may be reduced if the newly installed sensors are not in active work areas and/or should be given the priority to measure to other sensors in justified cases, except in monthly sensors.
- The sensor installed as replacement of an existing and located approximately in the

same position as his predecessor won't be considered as new one. Thus, the frequency of current in the sensor readings will remain inoperative sensor replacement in its place, although it will be necessary to establish a reliable zero reading by two readings within one week from the sensor installation. Those sensors that were already in the monthly reading schedule for the next step in sensor replacement, after the two zero readings taken in the first week will be made within a period not exceeding two weeks from installation.

The frequency of the established readings will be fulfilled as long as the operating conditions, safety and/or weather allow it, in a way that is considered acceptable omission of a reading within each level-up, except monthly sensors.
However, this reading should be performed once when normal functions, safety or weather is recovered.

3.2.2. *Data representation*

As already mentioned, each control point will be an initial reading that serves as a reference for all the other readings. Each team will be calibrated to ensure proper operation.

In the tab of each sensor calibration, appear conversion factors needed to convert the units in which the readings are made in the units of measurement for each case.

3.2.2.1. Environmental parameters

Data about atmospheric factors: temperature (°C), humidity (% RH), atmospheric pressure (mb), solar radiation (W/m2) and rain (l/m2) may be taken weekly and/or monthly. Its results are reflected in tables containing the maximum, minimum and mean and/or graphs showing their evolution over time.

3.2.2.2. Topographic control

3.2.2.2.1. Topographic milestones

Given the limited accuracy of topographic landmarks to the correct interpretation of the speeds provided by these, check that the tendency of displacement is consistent with the kinematics of the movement. In turn, the interpretation of the velocity values will biweekly or monthly basis and always be contrasted with the velocity values given by the inclinometers which are in the same area.

From every auscultation point are presented graphs showing the direction of displacement and the average speed of the last recorded readings.

3.2.2.2.2. Topographic prisms

In each one of the points is performed the initial reading as the baseline for successive readings.

In each of the graphs shown in the ordinate, the displacement value of each of the points expressed in meters, and in the abscissa, the time expressed in days.

For each month graphs are obtained for the monitoring carried out during that period, so that the reflected displacements are not accumulated from the previous month, but reflect only the displacements produced during that time interval.

Furthermore, **Figure 4** shows the displacement vector of each of the prisms. This will check the displacement points whose trend is consistent with the kinematics of the movement and the magnitude of its displacement in meters.

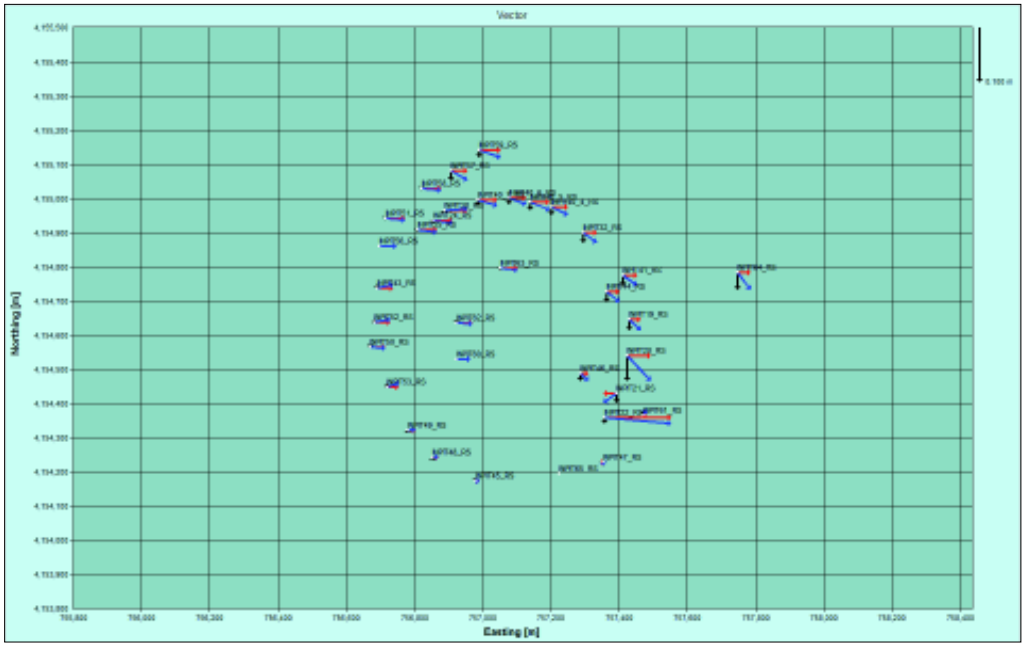

Figure 4: Resultant displacement vector

3.2.2.2.3. Inclinometers

The data can be represented by the type of graph shown in **Figure 5.**

The **graph of cumulative displacements**, because the horizontal scale is exaggerated relative to the vertical, it is very easy to detect the displacements that occur in the cutting or breakage plans.

However, if the cutting plane does not exist and the graph shows an overall inclination or distributed tension, then the interpretation is more complicated. In some cases, the accumulated systematic error may be responsible for the inclinations recorded on the graph.

To avoid the systematic error, are performed **graphics of relative displacements**, wherein each displacement register is subtracted from the previous one, so that each peak that appears in the graph represents a significant movement.

The graphs of displacement can be disordered and difficult to analyze when including a data set too large. Therefore it is better to include in each graphic small size data set.

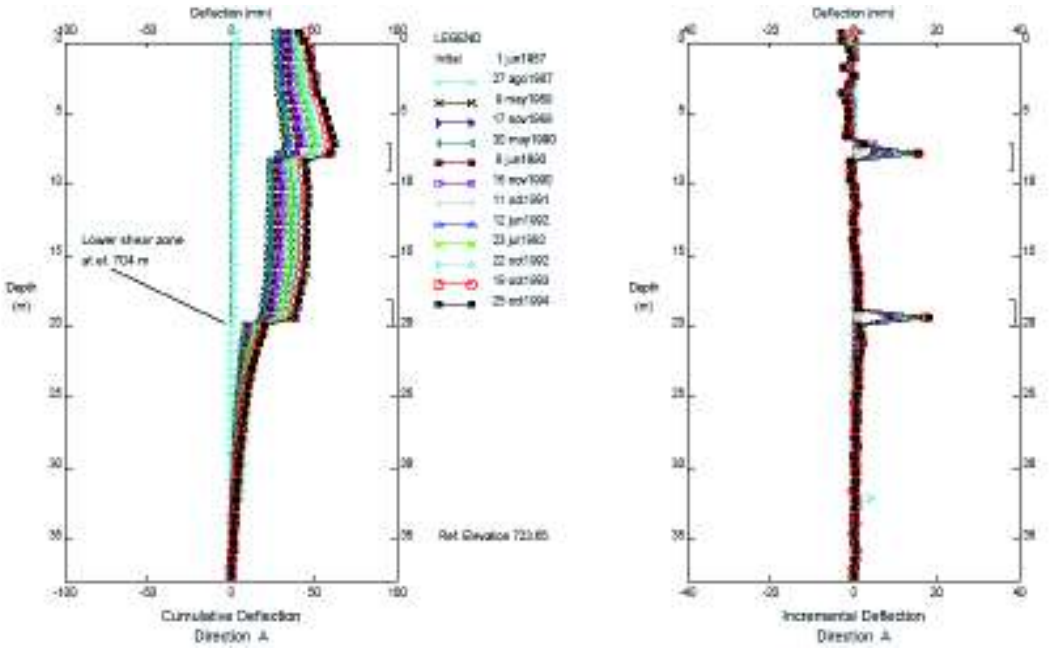

Figure 5: Graphic of cumulative and relative displacement

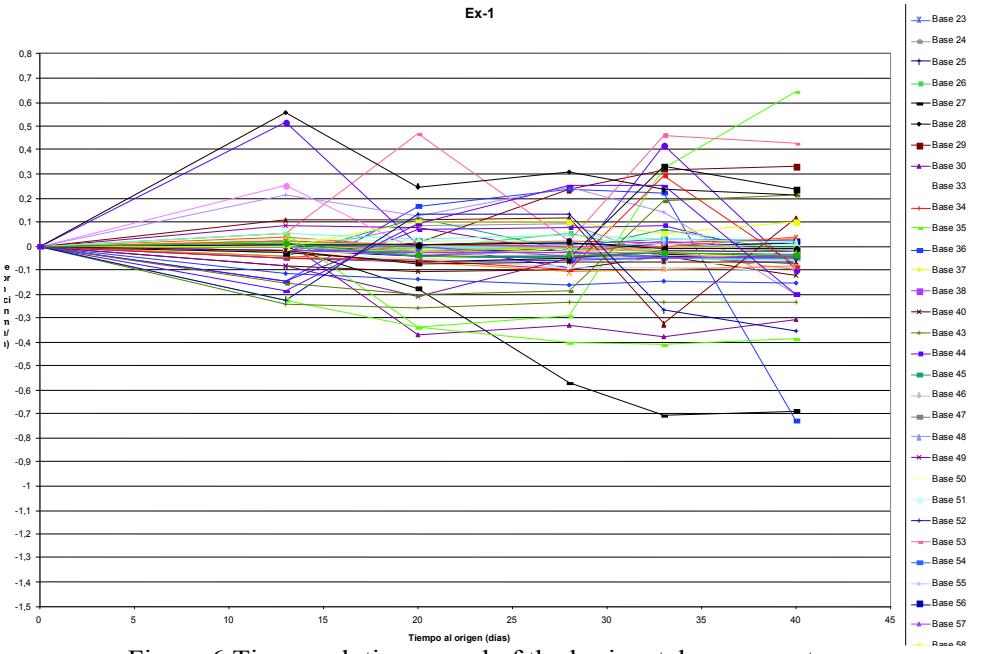

Figure 6:Time evolution record of the horizontal movements.

3.2.2.2.4. Extensometers

The measurement results are represented on a graph that reflects the vertical movements (settlements or swelling) occurring in areas under control.

Occasionally, the graphs present anomaly displacement in certain bases, in case that these anomalies are stabilized returning to its initial position. The following readings are considered that this phenomenon corresponds to a systematic error, usually caused by the operator.

In **Figure 6** shows an example of graphs of the evolution of the horizontal movements in function of time and depth.

If the supposed movement detected in some of the bases does not stabilize, the frequency of the measures in the depths corresponding to these bases will be increased. Furthermore, the behavior of the bases adjacent will be observed to verify that they also present a similar trend. Thus, corroborate that a true vertical movement in the auscultation zone is being detected.

3.2.2.2.5. Piezometers and total pressure cells

As mentioned above, for controlling the pore pressures or interstitial and total pressures in the open-cut mining currently are used piezometers. In the dumps are used piezometers and total pressure cells. The measurement results are shown in graphs that display the evolution of pressure versus time.

4. PREDICTIVE MODEL AND EMERGENCY LEVELS

The predictive model is based on the models, so that the criterion for assigning values to the various emergency levels has been based on the various analysis of sensitivity of model calculations.

Because of the many uncertainties and local variations of geo-mechanical model parameters should be considered convenient to increase at about 10% of deformations values obtained in the calculation model to establish normal deformations values, which will position us on the side of safety.

4.1. Emergency Levels

Once made manifest the existence of predictive models of the behavior of the mine slopes should be given particular attention to forecast what will be the deformations, their speeds and the evolution of pore pressure within the natural terrain of these slopes.

Since the parameters of pore pressure and deformation are easier to monitor, reliably with the instrumentation on the market and in order to evaluate the behavior of the slopes in the open-cut mining, it is proposed monitoring and control of:

- **Deformations.** It has been considered more reliable the speed of deformation than the deformation itself, since the prediction is simpler and provides more information about the state of stability of the slope and of the proximity of the fracture.
- **Pore pressure.** In connection with the pumping of water and with consequent dissipation and the ground decompression generated after excavation.

According to the impact of excessive deformation speed and / or an increase in pore pressure involving the stability of the slopes of the open-cut mining, these increases have been tabulated in three segments. First one involves no stability problems. Second one compromises the long-term stability of the mine and a final compromises the stability of the slopes.

Therefore, for dynamic monitoring of the evolution of the mine slopes are proposed (based on the gained experience) the three emergency levels, defined below:

- **Attention level:** the speed range of the deformation is greater than 1 mm / day and pore pressure deviations occur between 10 to 15% over the forecast.

- **Alert level:** the speed range of deformations is greater than 3 mm / day

and deviations occur between 15 to 25% for the estimated pore pressure.

- **Alarm level:** the speed range of the deformation is greater than 1 cm / day and 25% deviations occur for the estimated pore pressure in the predictive model. In case of activating this alarm level immediate action of stabilization are required.

Each emergency level entail, for their involvement and significance of the structure stability, activities and different measures, which constitute the technical measures protocol.

5. TECHNICAL ACTION PROTOCOLS OF EMERGENCY LEVELS

Below are present the technical action protocols to take for any of emergency levels defined for mining.

The implementing procedures in correspondence with the established emergency levels are different because, as noted, its meaning and involvement in stability is quite different and can be said broadly that, in the first case, there are no stability problems, in the second case, stability may be compromised in the long term and, finally, in the third case, the stability can be compromised in the short term.

Thus, the action protocols are defined in line and proportion to the potential problems that may be generated in the mine.

Specifically action protocols proposed for the three emergency levels are defined as:

- **Level 1 (attention)**

  - Increasing the frequency of the readings, one step backward in the timing of measurement instrumentation in the area where there has been an increase in the rate of deformation or pore pressure. (That is if the measuring monthly will be changed to fortnightly and so on).
  - Visual inspection of the area details where attention has been generated in order to detect cracks, movement signals, etc.
  - Check with the Department of Mines what were the activities developed in the influence area of the zone where the attention has been detected.

- **Level 2 (alert)**

  - Increased frequency of readings, according to the criteria specified in the standard of attention level, with a maximum frequency of two measures per week.
  - Visual inspection according to the same criteria described above.
  - Check with the Department of Mines what were the activities developed in the influence area of the zone where the attention has been detected.
  - Evaluation of the situation from the magnitude of pore pressure and the speed of evolution of the deformation according to the predictive model.
  - Reviewing calculation processes.

- **Level 3 (alarm)**

  - Analysis of the situation, based on the five actions described for the alert level. In this case the frequency of the measures and visual inspection will be daily.
  - Placing additional instrumentation if necessary.
  - Feedback of calculation models used for evaluating the stability of the structure and deformation prediction model and pore pressures.
  - Stoppage, if applicable, of the activity in the area where the alarm has been detected.
  - Introduction of corrective action or reinforcement if necessary.

The transition from one to another lower emergency level must be justified in each case based on measurements made in the action protocol for each emergency level.

In the three defined emergency levels all obtained data is stored on computer so it will be instantly accessible and actionable.

Statistical studies on the collected data sets will allow refining the predictions about the behavior of subsequent control units.

It is necessary to have a system that ensures easy and fast transmission of all data so this can be done without delay. For this will be taken (as optimal solution) transmission to the computer all the information supplied by the inclinometers, topographic landmarks and piezometers, which in the case of the information provided by the prisms leveling is immediate.

6. VERIFICATION OF RESULTS AND CORRECTIVE ACTIONS OF REINFORCEMENT

This section provides an assessment of the most appropriate corrective measures to be implemented after verification of the results for the open-cut mining and dumps.

It will be established a procedure to ensure that all information is absolutely organized in a database.

This information will be compared with the values in the predictive model according to the construction phase in which it is. Discrepancies that can be detected will be identified, discussed and considered, after which action will be taken as deemed appropriate and will be transmitted to the centers of decision makers.

It is essential for the safety of the work that the chain of transmission is rigorously established.

The generated information will be managed by computer equipment capacity and adequate processing speed. Programs and routines will be provided (from conceptual models of each type of control unit) which allow establishing reference values of the measured variables for each alert level.

In order to assess which are the most appropriate remedial actions necessary to implement, define whether the detected instability affects one or more banks. In the first case the adoption of corrective measures is not necessary, since they are in charge of berms which correct these local instabilities. On the contrary, if the generated instability affects more than one bank, it is necessary to evaluate what is the optimal measure to adopt.

The actions to be taken in the case of generated instability that affects several banks of open-cut mining will be:

- **Measures based on the modification of the geometry of the slope;** in order to correct the overturning moment of the resultant of weights. Specifically, it can act on the height and angle of bank, and on the width of the berm.

- **Measures based on the reduction of pore pressures;** this action will take place in case that it is expected that the instability is causing increased pore pressures. It could run pumping wells for drainage of the ground water and reduce the pore pressure, provided they are environmentally authorized.

- **Measures based on the increased resistance of the ground;** this step will be implemented in the case that earlier performances are not effective. You could resort to using mesh reinforcements, bolts and cable anchors. Can also act by building resistant elements, such gabion walls, breakwater (with or without concrete, etc.). At the foot movement. These measures in open-cut mining cannot be viewed as widespread but as specific measures in specific areas.

Any previous reinforcement measures should be supported, as was included in the previous section, by a model calculation that includes a retrospective analysis and quantifying at a later stage the goodness and effectiveness of the proposed measures.

If necessary, design and implement a campaign to survey and take samples of the breaking surface that later will be sent to a laboratory to check the strength of the ground after the breaking.

Once those properties are obtained, by applying a safety factor SF = 1, mentioned retrospective analysis can be made by equilibrium methods set limit and the new geometry of the slopes to ensure stability.

7. REGULAR ISSUE REPORTS

From the information obtained, it may emit three different report types:

- **Fortnightly report:** immediate action will be taken to validate the continuity of the excavation, as long as there have been geotechnical problems during the excavation of the mine, otherwise it will be deleted. Consist mainly in the graphical representation of the latest available data from the instrumentation.
- **Monthly report:** will include graphical analysis comparing the results with the expected values justifying its admissibility or non-admissibility. Also, based on the collected data, it will be created a bank of geological and geotechnical data.
- **Urgent action report:** should be sent no later than 24 hours when something unexpected happen.

8. CONCLUSIONS

The environmental monitoring program and geotechnical control besides having control functions using the different tools mentioned in this article, is an important source of data, mainly empirical, because it can assess how far the predictions made in the EIA (EIA) are correct. From this information, it is also possible to detect unforeseen changes in the Environmental Impact Study, which should be properly corrected by corrective measures. It is considered necessary to carry out mining operations in order to monitor the parameters that affect safety and the environment.

REFERENCES

Law 7/2007, Integrated Environmental Quality, July 9th

Law 22/1973, Mines, July 21st

General Rules for Mining Regime, August 25th, 1978

Basic Rules of Mine Safety - General Regulation, April 2, 1985.

A Solution to Intensive Underground Mine Scheduling at Çayeli Bakır

S. Evcil
Planning Engineer, Inmet Mining Corp., Çayeli Bakır İşletmeleri A.Ş.
F. Kesepara
Senior Planning Engineer, Inmet Mining Corp., Çayeli Bakır İşletmeleri A.Ş.
M. Güreşçi
Technical Services Manager, Inmet Mining Corp., Çayeli Bakır İşletmeleri A.Ş.

ABSTRACT Çayeli Bakır İşletmeleri A.Ş. (ÇBİ) is an underground copper and zinc mine. The mine has to produce from more than 150 different production stopes, associated with around 4,000 meters of waste and ore development. The planning and scheduling becomes even more intense and tedious when the life of mine plan is prepared. In the past, schedules have been prepared manually in Excel spread sheets, which was labor-intensive and time consuming.

ÇBİ has recently utilized a specialized mine scheduling software to manage complex underground scheduling work. This paper will briefly explain ÇBİ's transition to scheduling, how the software was enhanced with the mine's specific needs, and how the year 2013 and the life of mine production was planned and scheduled, for the first time. The paper will cover the steps of scheduling from geology definition to creating scenarios and to publishing results. The specific benefits of this implementation will be discussed.

1 INTRODUCTION

The mine planning is vital for a mine operation and it is a very complex process that integrates several technical disciplines like mine design, rock mechanics and ventilation. It involves mine planners' suggestions and decisions on cut-off estimates, scheduling alternatives and waste removal sequences. The mine planner evaluates a variety of alternates and chooses the best one. Such decisions are updated within time intervals, as the production continues and new information becomes available.

Mine planning is a forward-looking exercise, which provides direction to the operation. Whether being a short term or a long term plan, it reveals how to mine, where and when to mine.

The mine planning workflow constitutes four steps: geological database, geological modeling, mine planning and production scheduling.

The Çayeli underground mine, operated by Çayeli Bakır İşletmeleri A.Ş., is a wholly owned subsidiary of Inmet Mining Corporation. The town of Çayeli is located at 8 km south of the Black Sea coast, at approximately 100 km west of the Georgian border in north-eastern Turkey.

Construction of the mine started in 1992 and the ore production began in 1994. ÇBİ is the largest fully mechanized underground base metal mine in Turkey. The mine extracts about 1.2 million tonnes of ore per annum to produce about 240,000 tonnes of copper and zinc concentrates.

1.1 Geology

The deposit is similar to VMS Kuroko style deposits. The Çayeli orebody is located between hanging wall pyroclastites and

flows and footwall rhyolite. Mineralization, which is typical of a volcanogenic massive sulphide environment, is known over a strike length of 920 m. Massive sulphides form the majority of the ore in the deposit. The ore comprises varying amounts of pyrite, chalcopyrite, and sphalerite with minor amounts of dolomite and barite. The measured resource has a strike length of approximately 600 m, a vertical depth of over 600 m, and varies in thickness from a few meters to 80 m, with a mean of approximately 20 m. The average dip is 65° NNW in the upper part of the deposit and approximately 50° at depth. Below the massive sulphides, there are varying widths of stringer mineralization which can often exceed the cut-off grade due to chalcopyrite veining.

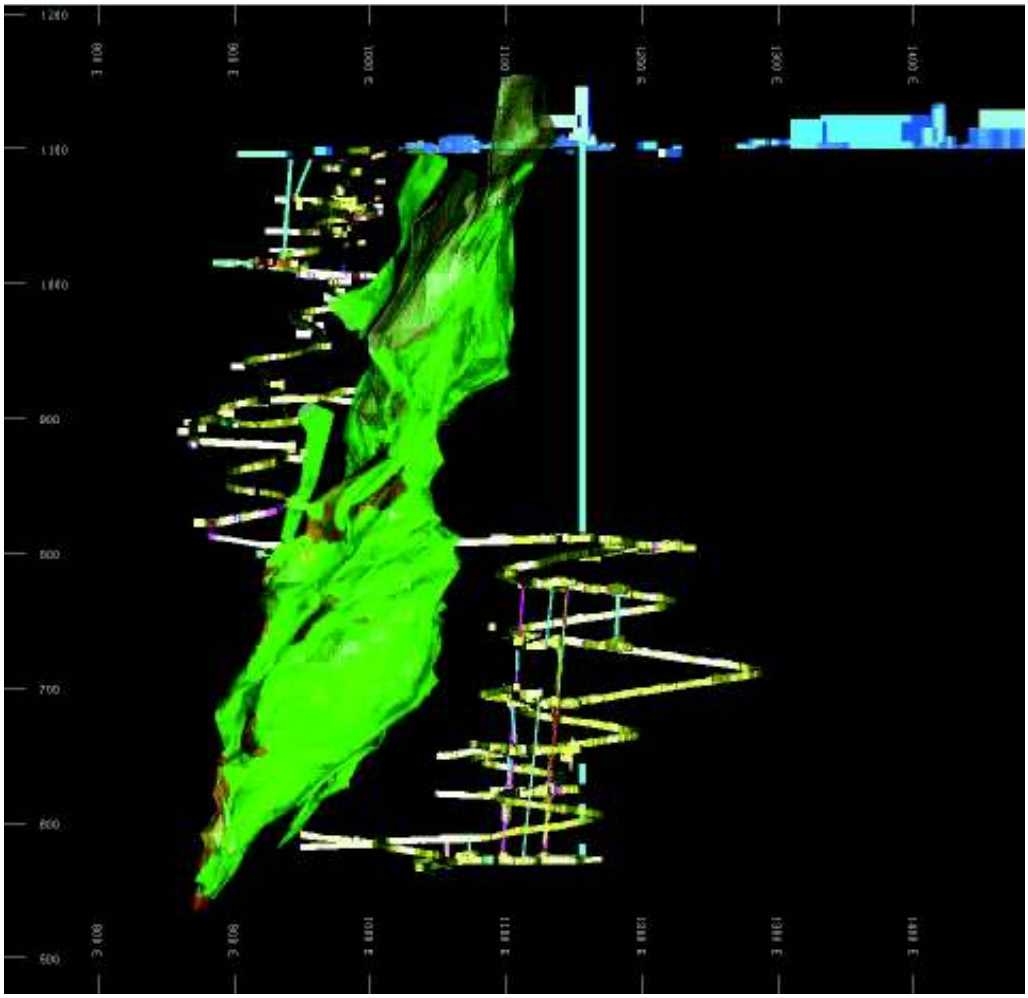

Figure 1. 3D view of the mine infrastructure

1.2 Mining Method

The mine design is based on underground bulk mining methods with the use of delayed backfill to extract the ore in a sequential manner. A single production shaft located on the footwall side of the orebody and a service ramp provide access to the mine, as seen on Figure 1.

The primary mining method for the Çayeli orebody is retreat transverse and longitudinal longhole stoping with paste fill and loose or consolidated waste rock backfill application. The stopes are mined in primary, secondary, and tertiary sequencing. The primary and secondary stopes are mined as transverse and the tertiary as longitudinal stopes.

The main levels are developed off the service ramp along the strike of the orebody at 45-100 m vertical intervals. From the top of the mine down to the 800 level, levels are located on the hanging wall side and, from the 800 level down to the bottom of the mine levels are located on the footwall side of the orebody. The main levels divide the orebody into mining blocks.

Sublevels are developed inside the orebody along the contact with the hanging wall, or in the centre of the orebody in the upper parts of the mine. In the lower parts of the mine, sublevels are developed along the contact with the footwall. The sublevels are part of the stopes. The ore within sublevel drift configurations is recovered after the primary and secondary stopes in a block are mined out and backfilled. Extraction of the ore from the sublevel drifts is called the tertiary stoping and is done in a retreat scenario. The sublevel vertical distance is dictated by the stope height. In the upper parts of the mine, it is 20 m, allowing the development of a 15 m high by 7 m wide stope bench for production drilling. In the lower part of the mine, the sublevels have been developed 15 m apart, allowing the development of a 10 m high by 10 m wide bench for production drilling.

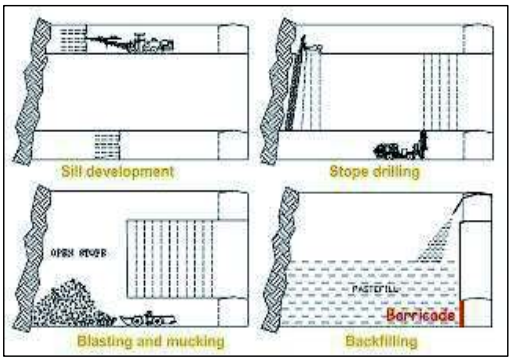

Figure 2. Mining method at ÇBİ

2 MINE PLANNING

All mine production plans at ÇBİ are prepared by the mine planning engineers with the use of the block model updated by the geologists. MineSight is utilized as the design software.

Mine planning at ÇBİ is classified in two groups as long term and short term planning.

2.1 Long Term Planning

These are the plans for periods of minimum 1 year or longer, which are the Life of Mine Plan and the Budget Plan respectively.

2.1.1 Life of Mine Plan

The overall aim of the Life of Mine (LOM) plan at ÇBİ is to determine the best strategy for extracting the available ore reserves.

While preparing the LOM plan, consideration is being given to maintain maximum production rates for as long as possible, by evaluating the mining options for each mining zone and increasing the number of active mining zones at the same time. The thoughts and the strategy for each mining zone are being documented along with the assumptions and key mining physicals for the remainder of mine life.

Milestones are being determined that must be achieved for the LOM plan to be realized with a resolution of half a year. The key risks to accomplish the LOM plan are being defined and a SWOT (Strength-Weakness-

Opportunity-Threat) analyses is being made for each zone. The uncertainties associated with the mining zones are being addressed and a "to do list" is being prepared for them.

Some of the features of the LOM plan at ÇBİ are:

- Tonnes ramp down toward end of mine life but a sharp finish is required.
- Fixed mining sequence for each block is used.
- Waste development scheduling starts after scheduling stopes.
- Look at peaks & troughs in production for each mining area.
- Waste development:
  - Schedule in months.
  - Check waste development meters & number of headings.
- Correlation between production & proportions of backfill types.
- Milestones highlighted for mining areas.
- Check quantity of development on each level.
- Strengths, weaknesses, opportunities and threats are identified for each block.
- Correlation between production & rehab.
- Development (ore & waste), tonnes & grade scheduled.
- Factors used for number of barricades, backfill volumes, & rehab.

2.1.2 Budget Plan

Budget is prepared annually, as part of the LOM plan according to the long term (ore reserves) metal prices.

Grade model is being updated with the most recent diamond drill and drill sludge data before planning is commenced.
Net Smelter Return (NSR) cut of boundary is being used and wire frame is being updated as well for the cut off boundary.

As a general strategy, the maximum possible production from upper blocks are planned at first, and then the remaining required tonnage is provided from the deepest block, the block where capital waste development is still being carried out.

A reliable production rate is being established for each stand-alone mining block or zone consistent with the maximum actual historical production records, and the current situation of the particular block / zone. The past records of tonnage extracted and the number of stopes mined are utilized to predict the achievable production rate.

Monthly target production rate is simply defined by the annual target being divided into 365 days and multiplied with the number of days for each month to get the target tonnes.

A maximum of 30 m is developed from each face per month. This corresponds to around two rounds per week, which is a common cycle time for an ore advance. A cut per week per face is considered for waste development faces.

The average stope cycle time per stope in 2012 without curing of paste was 42 days: 14 days of production and 28 days of barricade & backfill. Therefore the stope cycle time is taken to be around 2 months, taking the curing time of pastefill into account.

Some of the features of the Budget plan at ÇBİ are:

- Dilution & recovery:
  - Historical measurements for stoping blocks are used, and,
  - Different factors are used for primary, secondary, & tertiary stopes.
  - Dilution factor: 5.06% (excluding internal dilution)
  - Recovery factor: 94.22% (permanent ore loss)
- Copper grade reduction factor of 0.95 is used for high risk, high grade stopes.
- NSR value is utilized to determine if low grade ore type can be mined.
- A buffer is being built into schedule through rates:
  - Development rate per heading is 21m/month (up to 30m/month in shorter term schedules).
  - Stope cycle time is 42 days. 2 months allowed in schedule.
- Plan from top of mine down:
  - Upper stopes have higher grade but limited stopes can be mined due to seismic activity.
- Number of stopes per mine area is a schedule limit.
- Run through checks:
  - Tonnes & number of stopes from each mining area against

previous performance. Reasons for steps up or down are being explained.
  - Trucking & hoisting tonnes are being split.
  - Ore type distribution is being presented.
  - Development & stope tonnage split (around 25% & 75% respectively) is calculated.
- Once the Budget is completed, it is communicated with the mine management.
- Risks & opportunities are being highlighted.
- Backfill calculations are being based on historical records.
- Production is being prioritized over waste development.
- Scheduled: tonnes, grade, development meters, backfill volume, & number of barricades.

Budget 2013 was scheduled for the first time with scheduling software MineSched, a product of Gemcom, in the summer of 2012.

All designs of stopes and headings created with MineSight were uploaded to this software. Then, according the constraints and planning strategy, the development & production sequences were created. This paper briefly explains how this is achieved with MineSched.

2.2 Short Term Planning

These are the plans for periods of maximum 1 year or shorter, which are the quarterly forecasts made at the end of the first quarter, second quarter and third quarter of the year, 3-month mine production plans and weekly mine production plans, respectively.

2.2.1 Quarterly Forecasts

Budget is readjusted three times a year to make an achievable schedule:

Forecasts:
- Aim for the budget tonnes/year. If the budget does not seem realistic in the last quarter of the year, last quarter is scheduled less.
- Are extended into January of the following year.
- Focus on production – to catch up to budget.
- Updates (for all longer term schedules):
  - Development from survey updates.
  - Stope status from operations & geotechnical engineers & geologists.

2.2.2 3-Monthly Plans

This schedule contains the mine's monthly plan for execution. The first month of the 3-month schedule is prepared in detail as following:
- Stopes are sequenced by zone.
- Aim is to keep on track with budget & reforecast budget.
- Targeting budget tonnes & grade.
- Number of stopes is considered. This is a production limit.
- Stope cycle time is considered along with predecessor activities.
- High risk stopes are identified.
- Stopes & development are scheduled.
- Plan is discussed with the Mining and Engineering superintendents.
- Geology reviews the ore type.
- Priorities are highlighted for each activity when schedule is presented.
- The following is listed in weeks:
  - Ore headings (tonnes, grade, & some comments)
  - Stopes (tonnes, grade, & some comments)
  - Waste headings (number of cuts)
  - Rehab sites (type of rehab indicated only).
- Sites are also listed for backfill, production drilling, wire-meshing, & diamond drilling.
- Plan updated:
  - Survey plans & AutoCAD
  - Underground measurements & inspections.
- Priorities communicated verbally & via e-mail for some priorities.
- Priorities at this stage focus on achieving short term production targets.

Figure 3 shows a typical monthly plan spread sheet.

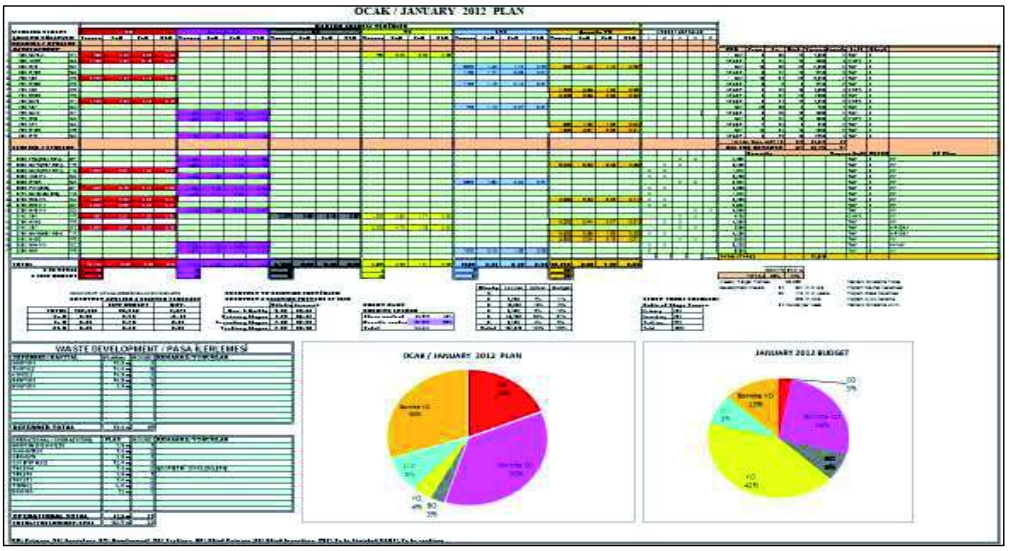

Figure 3. Typical monthly mine production plan

2.2.3 Weekly Plan

Weekly schedules are prepared 4 days in advance of the start of the week:

- 1st month of 3 month schedule is taken into consideration.
- The following is considered when developing the schedule:
  - Balancing haulage methods
  - Achieving physical ore production targets for the week
  - Predecessor activities to bring a stope on line
  - Equipment utilization & availability
  - Labor resources
  - Un-planned events & how to get back on track to achieve targets.
- Next month's stopes can be used to substitute this month's stopes.
- Ore development, stopes, then waste development sites listed in plan.
- Focus is on achieving target production tonnes for the week.
- Weekly grade targets are also considered.

3 MINE SCHEDULING

The mine has to produce from more than 150 different production stopes, associated with around 4,000 meters of waste and ore development, at around 200 different faces each year, due to its extremely poor ground conditions. This requires careful and diligent planning and scheduling practices. The planning and scheduling becomes even more intense and tedious when the life of mine plans are prepared, as 1,200 different stopes and over 16,000 meters of development faces needs to be handled.

In the past, the monthly, quarterly, annual and life of mine plans and schedules have been prepared manually in Excel spreadsheets by the mine planners. Scheduling with such traditional planning method is labor-intensive and time consuming. It relies on individuals and data preparation depends on the skills of the planner. This method does not offer 3D visualization of the schedule; the mine planner cannot visually check for errors and it is difficult to communicate. Furthermore, it requires quite amount of repetitive work when different scheduling options are

needed to be assessed, or a part of the scheduling is needed to be revised.

ÇBİ has recently utilized a specialized mine scheduling software, Gemcom's MineSched, to manage the mine's complex underground scheduling work. This paper will briefly explain ÇBİ's transition to scheduling with MineSched, how the software was enhanced with the mine's specific needs, and how the year 2013 and the life of mine production was planned and scheduled, for the first time. The paper will cover the steps of scheduling from geology definition to creating scenarios and to publishing results. The specific benefits of this implementation will be discussed as well.

3.1 Existing Mine Planning Process Strengths at ÇBİ

The thought processes is generally adequate to create robust schedules:

- Formalized processes through full scheduling cycle.
- 3 month schedule focuses on bringing budget stopes on line. Focus is on stopes not on reaching targets for equipment.
- Priorities are being assigned to certain activities.
- Generally a focus on locations not on equipment.
- Good understanding & communication between mine planning & operations.

3.2 Mine Planning Process Weaknesses Identified at ÇBİ

The following were identified to be the weaknesses of the planning and scheduling system of ÇBİ:

- Communicating schedules: Sequences of events are in mine planners' heads.
- Activity dependences: No activity links thus activity successors & predecessors are unclear. This leads to oversights in scheduling & execution.
- Resourcing & timing: It cannot be known if a schedule is robust or even feasible if not scheduled in an appropriate time resolution.
- Information flow: Transferring of scheduling information from one time frame to the next & meeting the next broader time frame schedule is difficult if information is not presented in an appropriate time resolution.
- Schedule compliance measuring: Compliance to schedule tracking & measuring is difficult if the schedule is not presented in an appropriate time resolution.
- Full 2 week schedule is not discussed in 2 week schedule meeting. Focus is on the current week.
- Compliance to monthly plan is around 65%.
- Budget:
  - Waste development quantity decided by set waste development capacity.
  - Historical waste development rates used for budget rates.

3.3 Improvements Required

The following critical improvements have been identified:

- Stop using lists & start using schedules.
- Use appropriate scheduling software for LOM to 3 month scheduling.
- More human resources in Mine Planning: another full time mine planner.
- Schedule compliance
  - Schedule compliance to be the key performance criteria for the mine with a commitment from top down.
  - Compliance to schedule tracking for all schedule time frames as graphed & discussed in schedule compliance meetings.
  - Mine Captains & managers to be held accountable for schedule compliance.
- Noncompliance: root cause formal identification process.
  - Identify noncompliance due to lack of planning.
- Input from all areas into all mine schedules.
  - One-on-ones to be setup for 3 month schedule & 2 week schedule.
- Activity rates based on future resources & strategic planning to achieve mine targets.
  - Not based on historical rates.

- Year look ahead in addition to the budget.
  - Maintain budget detail for 2 years ahead.
- Budget reforecast:
  - Include a reforecast for the 1st quarter.
- Include bottleneck in schedule.
  - Rehab to be scheduled from at least 3 month schedule through to real time scheduling.
- Track activity buffers.
- Scenario planning using MineSched.
- For 3 month schedule:
  - Include all significant activities including: ore development, waste development, production, production drilling, raise drilling, major fixed plant shutdowns, barricades, backfilling, rehab, major project/services.
  - Schedule should be presented in weeks.
  - Data entered appropriate for weekly resolution.
  - Links between activities. Clear stope dependences.
  - Issue a draft before planning meeting.
  - Split 3 month schedule planning meeting & monthly compliance meeting.
  - Formal commitment to 1st month.
  - Full 3 months to be planned & presented to operations.
- Critical information handover point: 3 month schedule to 2 weekly schedule.
  - Clear communication of 3 month schedule.
- Track & present graphically schedule compliance: for all time frames. Also compare to forecast.
- Reporting of actuals to match schedule formats.

One of the most significant outcomes of this technical forum was to speed up and progress with the mine scheduling tool.

4 SCHEDULING SOFTWARE

It's been started to prepare forecasts 3 times a year and a LOM plan every year starting from 2009, in addition to the monthly plans and the budget. The scheduling works done within a year and the amount of time needed for them are listed below:

- Monthly and 3 months plan – 12 times (12 weeks)
- Quarterly forecasts – 3 times (3 weeks)
- Budget – 1 time (6 weeks)
- LOM Plan – 1 time (4 weeks)

These totally take 25 weeks, and not much time is left to the planning engineer for the works like reserves calculations, mine design, mine planning and reconciliation.

It is anticipated that these intense scheduling works will continue with the same intensity and perhaps even get more through the end of mine life with the need of "what if" scenarios.

The traditional method with the use of AutoCAD sections and Excel spreadsheets is time consuming and mining specific tools. As they do not offer 3D visualization of the schedule, the planner cannot visually check for errors and it is difficult to communicate. Data preparation depends on the skills of the planner.

Furthermore, it requires quite amount of repetitive work when different scheduling options are needed to be assessed, or a part of the scheduling is needed to be revised.
Because of reasons explained above, it has been decided to purchase a scheduling tool.

4.1 Software Selection

Evaluating and selecting a suitable software package for ÇBİ was the most critical risk. The most practical and efficient system that fits to the following was important:

- Underground mining
- ÇBİ's mining method and conditions
- Working compatible with planning tool MineSight
- Scheduling for both short and long term

Normally the best approach would be to purchase the scheduler of MineSight, which was ÇBİ's existing geological modeling and planning tool, not to have compatibility issues, however, Mintec's scheduling packages were all for open pit mines at that time. They were developing and underground scheduler but it would not be available before 2012.

It's been decided to purchase and implement Gemcom's MineSched after an evaluation process.

5 IMPLEMENTATION OF MINESCHED AT ÇBİ

It's been realized during the implementation and training period of MineSched that the software was not completely fulfilling mine's some specific needs, particularly on underground scheduling system with an extreme amount of stope production sequencing required. Thereafter, collective studies started with Gemcom to adapt the software to the mine's specific needs at the highest level possible. The deficiencies determined have been submitted to Gemcom and it was requested to enhance the software upon these requests. Gemcom has eliminated such deficiencies and re-designed the software to ÇBİ's specific needs.

5.1 Enhancements Requested and Implemented in MineSched

A number of new enhancements for MineSched have been created after ÇBİ's requests in 2011 by the MineSched development team.
Some of the critical enhancements were explained below in detail.

Surpac was made able to read all attributes generated in a MineSight polyline file, but also data from MineSched solids. This greatly eased exchange of data between MineSight and MineSched. A custom made script (macro) was created for ÇBİ to automate the importing process of MineSight block models into MineSched. These resulted with the import of MineSight files with simple one click or drag and drop solutions.

For an operation such as ÇBİ, the ability to view current workings (as-builds) alongside planned development and production locations (stopes) was seen as vital. As such the 3D canvas in MineSched has been enhanced to allow the drag and drop of any .dtm file from Surpac to be loaded and displayed in MineSched (Figure 4).

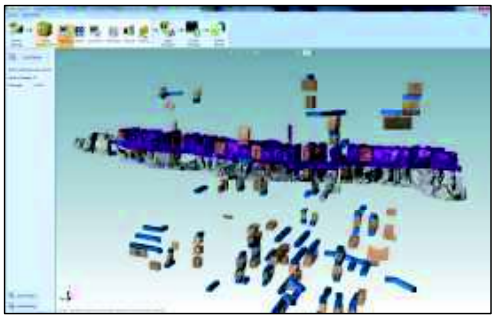

Figure 4. Display of "as build" solids, stopes and headings

Files with the .dtm (digital terrain model) file extension contain three-dimensional images that show the plans for mines. The creation of these .dtm files is a simple two click conversion from .msr (MineSight resource file) files.

The ability to group development and location by a zone or block number was seen as important to the workflow of creating the schedule and reporting. As such new user defined attributes and stope collections made available across MineSched. In ÇBİ this means that a group of stopes or headings can be displayed to report or define a sequence.

A critical enhancement for MineSched was the ability to sequence in a graphical manner. This functionality had already existed for headings but not for locations (stopes). MineSched now has the ability to link different locations and development to each other by a simple two click process. Red arrows in Figure 5 are displayed to show the planner where the sequences are. A delay between the two locations can also be added in order to simply model support work (barricade – paste fill – etc).

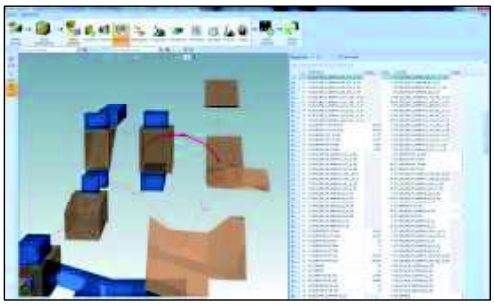

Figure 5. Graphical sequencing with red arrows

5.2 Preparation of 2013 Budget and LOM Plan with MineSched

The budget and LOM plan preparations for 2013 has started after the final MineSched training on site in June 2012 had completed. Firstly, the development polylines and stope solids were designed to be sequenced in MineSight.

As designing tool MineSight and scheduling tool MineSched work with different file types, the files created with MineSight were converted into proper Surpac files, where MineSched is embedded in.

The biggest challenge brought with the implementation of the software was the discrepancy due to difference between the file types in data exchange with the currently used software. Different file types generated by every software cause problems in information exchange between software.

The block model previously generated on MineSight was exported in ASCII format and converted to the proper format by a macro operating on Surpac.

Then the block model was transferred into MineSched (Figure 6). However, another problem encountered at this stage was that the data read by MineSight and MineSched from the block model were different to each other: the Cu and Zn grades extracted from the model were different. As the grade values in MineSight was very well overlapping with the actuals underground, the MineSched outcomes should have been exactly the same as MineSight. The problem was solved when the blocks of 5x5x5 m sizes that constituted the block model were divided into 5 equal parts.

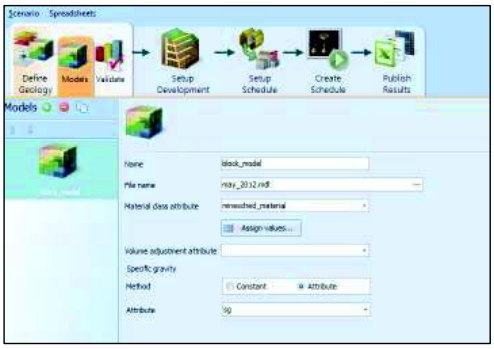

Figure 6. Defining geological model

After the current block model is loaded, recovery and dilution rates were defined. Furthermore, in addition to diluted Cu, Zn, Pb, Au, Ag and NSR values, rock bolt and shotcrete values could have been calculated in this section if required (Figure 7).

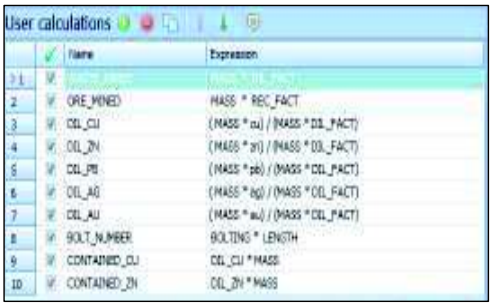

Figure 7. User calculations window

Then, 2013 Budget and LOM sequencing has started. First, ore and waste faces and stope designs were transferred to MineSched. For Budget, 4.400 m face and 171 different stope designs for 2013 Budget, and 16.000 m face and 1.200 different stopes designs for LOM were imported to the software.

After face developments were imported, names, directions and routes of the faces were controlled.

This section also allows specific conditions to be set like starting or stopping a certain face on a certain date (Figure 8).

Then, the designed stopes were imported (Figure 9). The direction of the stope blasting is defined at this stage (as transverse).This section also allows groups to be created, as zones.

In the next step, the activities to be executed during a full production process of a stope at ÇBİ are defined (Figure 10).

Then, it is described to the software to which stockpile the produced ore will be transferred (Figure 11).

After it is made clear where to transport the ore, the ore tonnage and grade from all stopes can be reported with recovery and dilution factors applied.

Then, the most important and critical part of the whole study started. This is the section of the software where development and stopes were sequenced depending on the precedences, planning criteria and planning strategy (Figure 12). This part requires a very accurate and detailed operation.

Then, daily development capacities for waste and ore faces were entered on face basis. At the same time, production rates for stopes were entered separately for secondary, primary and tertiary stopes (Figure 13).

In the next step, the scenario was run and the results were presented in MS Excel spreadsheet and an MS Project Gantt chart format.

6 SPECIFIC BENEFITS OF MINE SCHEDULING AT ÇBİ

6.1 Increased Productivity of the Planners

Such software reduces scheduling times by automation of repetitive tasks, such as development sequencing and stope sequencing. It drives up productivity of the planners by saving labor and time.

More time becomes available to the planning engineers to focus on mine design and planning issues rather than scheduling.

6.2 Easy Evaluation of Scheduling Options

It is easier with the use of MineSched to assess multiple alternatives to determine the optimum development sequence. It enables rapid response to 'what if?' scenarios.

6.3 Improved Communication of Mine Planning

MineSched exports to Excel spreadsheets or Project Gantt charts for a better communication. It also generates real-time 3D animations to provide clarity to the decision makers. This makes budgets and LOM plans more transparent and easy to communicate.

6.4 Integration of Short Term and Life of Mine Plans

MineSched can integrate short-term and Life of Mine plans into a single entity. This ensures quick assessment of any plan modification. For instance, once the link between the 3-months plan and the budget plan is established, any change in the monthly plan will reflect to budget during Q1, Q2 and Q3 forecasts' preparations.

Figure 8. Development strings loaded

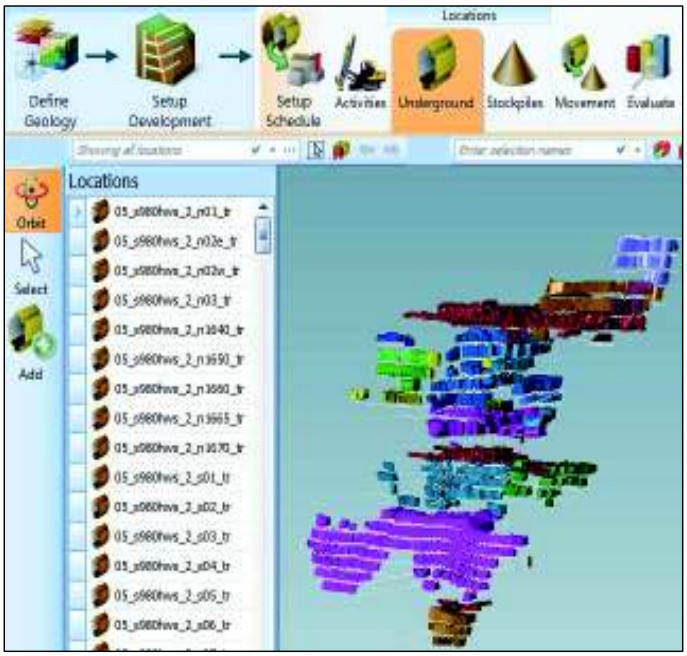

Figure 9. Stopes by different zones

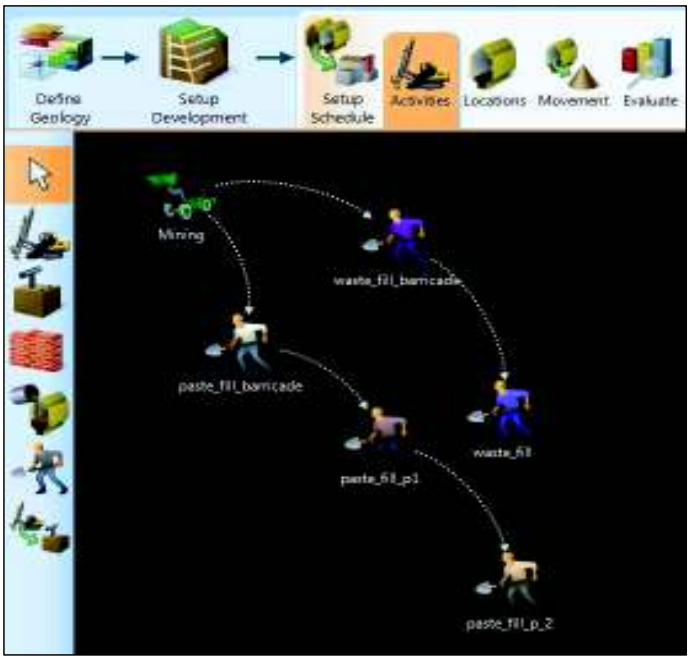

Figure 10. Activities

Figure 11. Stockpiles

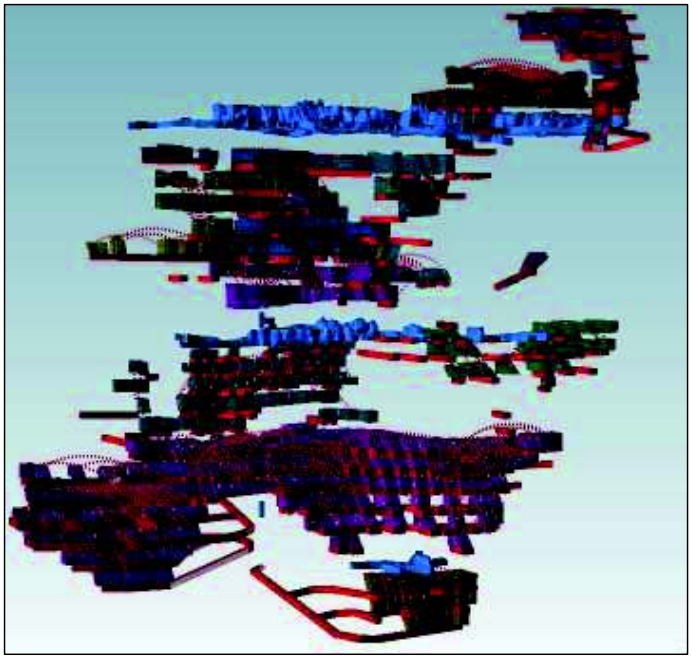

Figure 12. Sequencing

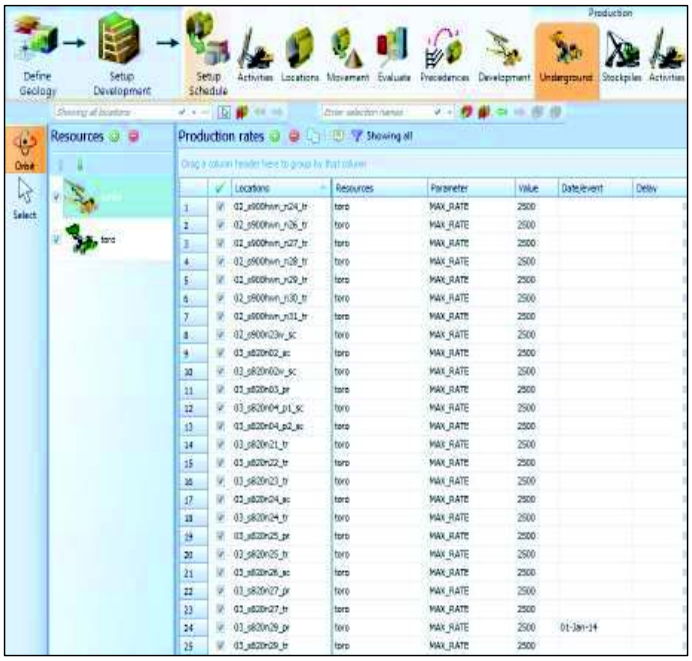

Figure 13. Production rates

7 CONCLUSIONS

The monthly, quarterly, annual and LOM mine plans (schedules) used to be prepared in Excel manually at ÇBİ. Scheduling with those traditional planning systems is labor-intensive and tedious. This also takes considerable time to prepare.

Now, ÇBİ uses specialized mining scheduling software, MineSched, which saves labor and time. It enables multiple scenarios and alternatives to be evaluated to determine the optimum sequence and evaluate constraints and critical path. To change a completed schedule or redo a part of it can be quickly achieved with it, once the data is made proper.

The traditional planning system relies on individuals to apply defined planning standards. This software decreases the dependency to planning personnel as well.

Elimination of negative effects of continuously changing underground conditions on production and safety is only possible by creating new, rapid and safe scenarios. Thanks to this software, a huge amount of time and labor was saved.

An Experimental Study on the Surface Roughness of Rocks Sawn by Diamond Sawblades: Effect of Mineralogical Properties

G. Aydın, I. Karakurt, K. Aydıner

Karadeniz Technical University, Department of Mining Engineering, Trabzon-Turkey

ABSTRACT Surface roughness is a measure of the technological quality of a product and a factor that greatly influences manufacturing costs. In this study, an experimental study on the surface roughness of rocks sawn by sawblades was presented. In the study, major mineralogical properties of the rock affecting surface roughness were investigated. The results showed that among the mineralogical properties; mean grain size of the rock was ranked first in governing surface roughness.

1 INTRODUCTION

The use of granite as a construction and decorative material is continuously increasing worldwide due to their high resistance against to the environmental effects and attractive aesthetic properties. As a result of growing demand, processing of granites by using diamond segmented circular sawblades has found a wide application in the stone industry (Chen and Rowe, 1986). There have been many studies on the investigation of sawing performance of circular diamond sawblades in stone processing. Sawing mechanism (Chen and Rowe, 1986; Konstanty, 1991; Konstanty, 2000; Tönshoff et al., 2002), wearing in diamond sawblades (Luo and Liao, 1993; Ersoy and Atıcı, 1999; Karagöz and Zeren, 2001; Xu, 2001; Denkena et al., 2003; Ersoy et al., 2005; Buyuksagıs, 2007), cut-ability (Wright and Jennings, 1989; Buyuksagıs, 1998; Xu et al., 2003; Wei et al., 2003; Rosa et al., 2004; Delgado et al., 2005; Ucun et al., 2005), modeling and prediction of cutting performance (Buyuksagis, 1998; Di Ilio and Tonga, 2003; Eyuboglu et al., 2003; Kahraman et al., 2004; Buyuksagis and Goktan, 2005; Huang et al., 2006; Fener et al., 2007; Yaşıtlı, 2008; Yılmaz et al., 2011) are among the well-known studies documented so far.

Surface roughness is a measure of the technological quality of a product and a factor that greatly influences manufacturing cost. It describes the geometry and surface textures of the machined parts (Özçelik et al., 2005; Nalbant et al., 2007; Çaydaş and Hasçalık, 2008). Despite the fact that there are many studies on cutting performance of sawblades, until now, no comprehensive study has been specifically conducted for surface roughness of rocks sawn by sawblades. The present contribution attempts to address and fill this gap in the literature. This work aims at investigating the relationship between surface roughness and mineralogical properties of rocks tested.

2 MATERIAL AND METHOD

For the execution of experiments, nine granitic rocks having different percentages of minerals, different grain size distributions and substantial market potential were selected from a stone processing plant and dimensioned according to the requirements of experimental studies. The samples have a length of 30 cm and 10 cm × 3 cm section. Petrographic studies conducted in the study include the determination of composition and grain-size of the minerals. For this purpose, thin sections for each rock were

prepared and examined under the polarizing microscope. Polished hand specimens were also examined for the grain size characterization for the coarse-grained rock samples. Mineralogical compositions and grain size ranges of the studied rocks are given in Table 1.

Table 1. Mineralogical properties of the rocks

Rock Type	*Mineral*	*Grain Size (mm)*			*Prp. (%)*
		Min.	**Max.**	**Mean**	
Verde Butterfly	Alkali feldspar (orthoclase)	0.56	20.00	5.2	41
	Plagioclase	0.40	3.76	1.6	29
	Quartz	0.16	6.00	2.5	11
	Pyroxene	0.24	2.00	0.4	9
	Biotite	0.32	3.60	1.5	6
	Garnet	0.80	6.56	2.4	2
	Opaque	0.08	0.80		2
Giallo Fiorito	Alkali feldspar (orthoclase, microcline)	0.80	18.00	12	41
	Quartz	0.40	9.60	4	32
	Plagioclase	0.40	2.40	1.8	14
	Biotite	0.16	1.60	0.7	12
	Other and sec. components	0.08	0.16		1
Porto Rosa	Alkali feldspar (orthoclase, microcline)	0.80	12.0	8	44
	Quartz	0.40	4.00	0.7	24
	Plagioclase	0.96	6.80	1.7	24
	Biotite	0.16	2.00	0.7	6
	Other and sec. components	0.24	0.48		2
Crema Lal	Alkali feldspar (orthoclase, microcline)	0.48	4.80	0.8	39
	Quartz	0.24	2.24	1.7	27
	Plagioclase	0.56	3.60	2.0	22
	Biotite	0.32	1.60	0.4	10
	Other and sec. components	0.08	0.56		2
Giresun Vizon	Alkali feldspar (orthoclase)	0.80	6.80	1.1	47
	Plagioclase	0.32	4.88	2.2	27
	Quartz	0.24	2.40	1.9	16
	Amphibole	0.16	0.96	0.2	4
	Biotite	0.48	3.44	1.4	4
	Other and sec. components	0.16	0.36		2
Balaban Green	Alkali feldspar (orthoclase. microcline)	0.80	6.80	2.1	38
	Quartz	0.16	5.60	2.7	25
	Plagioclase	0.96	5.20	2.2	14
	Amphibole	0.24	1.20	0.4	10
	Epidot	0.08	0.40	0.1	6
	Biotite	0.48	3.20	0.7	4
	Other and sec. components	0.16	0.96		3

Table 1 continued

Rock Type	*Mineral*	*Grain Size (mm)*			*Prp. (%)*
		Min.	**Max.**	**Mean**	
Nero Zimbabwe	Plagioclase	0.24	3.36	1.7	48
	Pyroxene	0.24	2.40	1.6	40
	Biotite	0.16	0.32	0.2	4
	Opaque	0.04	0.80	0.1	8
Bergama Gri	Plagioclase	0.32	4.6	1.2	43
	Alkali feldspar (orthoclase)	0.32	2.98	1.3	20
	Quartz	0.24	3.60	1.2	19
	Biotite	0.24	1.60	0.4	10
	Amphibole	0.24	1.60	0.4	6
	Other and sec. components	0.24	0.80		2
Star Galaxy	Plagioclase	0.24	5.20	1.5	40
	Pyroxene	0.24	3.60	1.3	39
	Biotite	0.16	3.20	0.4	10
	Amphibole	0.08	0.36	0.1	7
	Other and sec. comp. (quartz, opaque)	0.08	1.36		4

Cutting tests were performed on a high precision experimental cutting machine (Fig. 1).

Figure 1. Experimental set-up

The diamond sawblade used in the tests was of 40 cm diameter, having 28 impregnated diamond segments (circumferential length 40 mm, width 3.5 mm and height 10 mm). The diamonds were sized at 40/50 US mesh with a concentration of 30 which is recommended for the sawing of hard materials. Disc movements forward-backward in the horizontal plane and up-down in the vertical plane were driven with two 0.75 kW ac motors, while the turn of the disc were driven with 4 kW ac motor. Moreover, 0.75 kW ac motor was used to move the wagon in the cutting line. Operating variables such as peripheral speed, traverse speed, cutting depth, flow rate of cooling fluid, vertical, horizontal, axial forces were measured using sensors, load cells, transducers and an encoder in the monitoring system. All movements of the cutting machine were controlled using processing software.

The cutting experiments were conducted in the down-cutting mode. Each experiment was repeated five times to increase the accuracy of the results obtained. In the cutting tests, a constant specific removal rate of 120 cm^2/min was employed so that all granite types could be easily sawn within the available power limits of the cutting machine. The same cutting rate enabled a direct comparison of results obtained for all the rock samples.

There are several ways to describe surface roughness, such as the roughness average (R_a), the root-mean-square (rms) roughness (R_q) and the maximum peak-to-valley roughness (R_{max}), etc. Ra is defined as the arithmetic value of the profile from centerline along the sampling length (Özçelik et al., 2005). Surface roughness measurements of the cut surfaces of the

rocks were made using a stylus-type profilometer, Mitutoyo Surftest SJ-301 whose principals are schematically described in Fig. 2. Surface roughness measurements were made at the middle zone of the cut surface to compare the obtained data for each rock. Due to the variability of data, 20 measurements for each surface and totally 10x20 readings (Ra) were taken for each experiment.

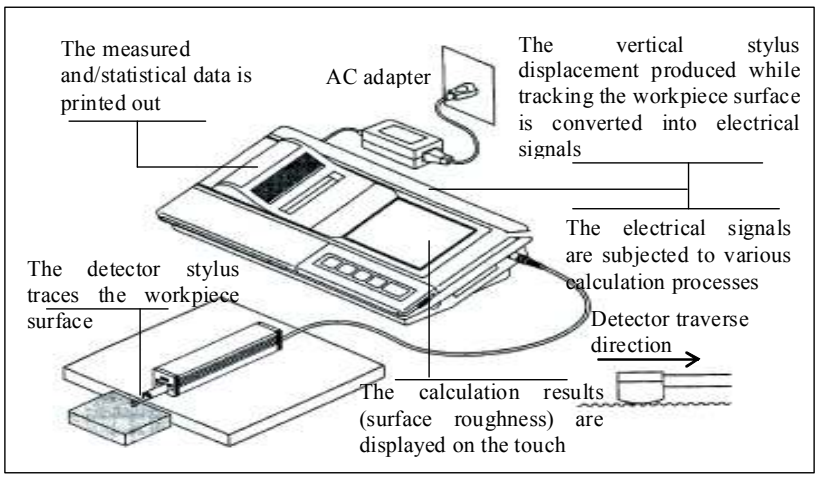

Figure 2. A schematic description of Mitutoyo Surftest SJ-301

3 RESULTS AND DISCUSSIONS

Regression analysis was carried out to determine relations between surface roughness and the mineralogical properties (see Table 2). Relations between material properties and surface roughness were investigated on the basis of some statistical approaches such as linear, logarithmic, exponent and exponential. As can be understood, good correlation was obtained between rock grain size and surface roughness.

Table 2. Regressions analysis concerning the mineralogical properties and surface roughness

Mineralogical Properties	*Regression equation*	R^2
Plagioclase content (%)	SR = 0.0362x + 3.7661	0.3698
	SR = 0.9552 Ln(x) + 1.6822	0.3462
	SR = 2.3293 $x^{0.2179}$	0.3458
	SR = 3.7659 $e^{0.0081x}$	0.3538
Feldspar content (%)	SR = -0.0213 x + 5.4558	0.2940
	SR = 5.4611 $e^{-0.0046x}$	0.2600
Quarts content (%)	SR = -0.028 x + 5.2954	0.1932
	SR = 5.3296 $e^{-0.0066x}$	0.2060
Biotite content (%)	SR = -0.0692 x + 5.3245	0.0896
	SR = -0.4517 Ln(x) + 5.6766	0.0783
	SR = 5.9343 $x^{-0.1157}$	0.0987
	SR = 5.4323 $e^{-0.018x}$	0.1161
Mean grain size of plagioclase (mm)	SR = -0.3233 x + 5.3878	0.0210
	SR = -0.7274 Ln(x) + 5.2189	0.0369
	SR = 5.1605 $x^{-0.1457}$	0.0284
	SR = 5.3148 $e^{-0.0623x}$	0.0150

Table 2 continued

Mineralogical Properties	*Regression equation*	R^2
Mean grain size of feldspar (mm)	SR = -0.1566 x + 5.3472	0.7996
	SR = 5.3812 $e^{-0.0361x}$	0.8175
Mean grain size of quartz (mm)	SR = -0.4451 x + 5.6031	0.5240
	SR = 5.7144 $e^{-0.1033x}$	0.5420
Mean grain size of biotite (mm)	SR = -0.7937 x + 5.3811	0.2427
	SR = -0.6674 Ln(x) + 4.4691	0.3464
	SR = 4.4303 $x^{-0.1383}$	0.2857
	SR = 5.3384 $e^{-0.1609x}$	0.1916
Mean grain size of rock (mm)	SR = -0.3584 x + 5.7084	0.8316
	SR = -1.0344 Ln(x) + 5.5548	0.7949
	SR = 5.6345 $x^{-0.236}$	0.7947
	SR = 5.8549 $e^{-0.0831x}$	0.8590
Max. grain size of plagioclase (mm)	SR = 0.1487 x + 4.159	0.0694
	SR = 0.9155 Ln(x) + 3.4925	0.1472
	SR = 3.3595 $x^{0.2411}$	0.1961
	SR = 3.9665 $e^{0.0413x}$	0.1028
Max. grain size of feldspar (mm)	SR = -0.0847 x + 5.4881	0.7138
	SR = 5.5322 $e^{-0.0189x}$	0.6850
Max. grain size of quartz (mm)	SR = -0.2025 x + 5.5996	0.6374
	SR = 5.7122 $e^{-0.041x}$	0.6624
Max. grain size of biotite (mm)	SR = -0.1464 x + 5.1512	0.0505
	SR = -0.3105 Ln(x) + 5.017	0.1029
	SR = 4.9439 $x^{-0.0584}$	0.0699
	SR = 5.0281 $e^{-0.0239x}$	0.0258
Plagioclase content (%) x its mean grain size (mm)	SR = 2.5796 x + 3.5561	0.3568
	SR = 1.3116 Ln(x) + 5.8278	0.4087
	SR = 6.0236 $x^{0.3051}$	0.4247
	SR = 3.5694e0.5896x	0.3579
Feldspar content (%) x its mean grain size (mm)	SR = -0.3722x + 5.3319	0.8078
	SR = 5.3592 $e^{-0.0855x}$	0.8185
Quartz content (%) x its mean grain size (mm)	SR = -1.2409 x + 5.2839	0.4593
	SR = 5.3282 $e^{-0.2989x}$	0.5117
Biotite content (%) x its mean grain size of (mm)	SR = -23.321 x + 5.9257	0.6798
	SR = -0.7334 Ln(x) + 2.4538	0.5077
	SR = 2.8345 $x^{-0.161}$	0.4697
	SR = 6.1021 $e^{-5.2183x}$	0.6536

Roughness profiles of the measurements were also investigated. A representative profile for both fine-grained and coarse-grained rocks is presented in Fig.3a and Fig.3b, respectively. Main factors affecting surface roughness were determined in the related figures. The findings are in accordance with the results obtained. In grain boundaries, surface roughness presents a peak while it changes relatively stable inside the mineral. In coarse-grained granite, there is relatively lower amount of grain boundaries in a specific area, and thus there is a minor effect on the friction coming from the grain boundaries that have relatively higher roughness. Whereas, fine-grained structures have much more grains that have higher amount of grain boundaries along a specific line. Therefore, during measuring the friction coefficient, the possibilities of intersecting the grain boundaries which have higher roughness compared to the grain interior are higher than the coarse-grained granites.

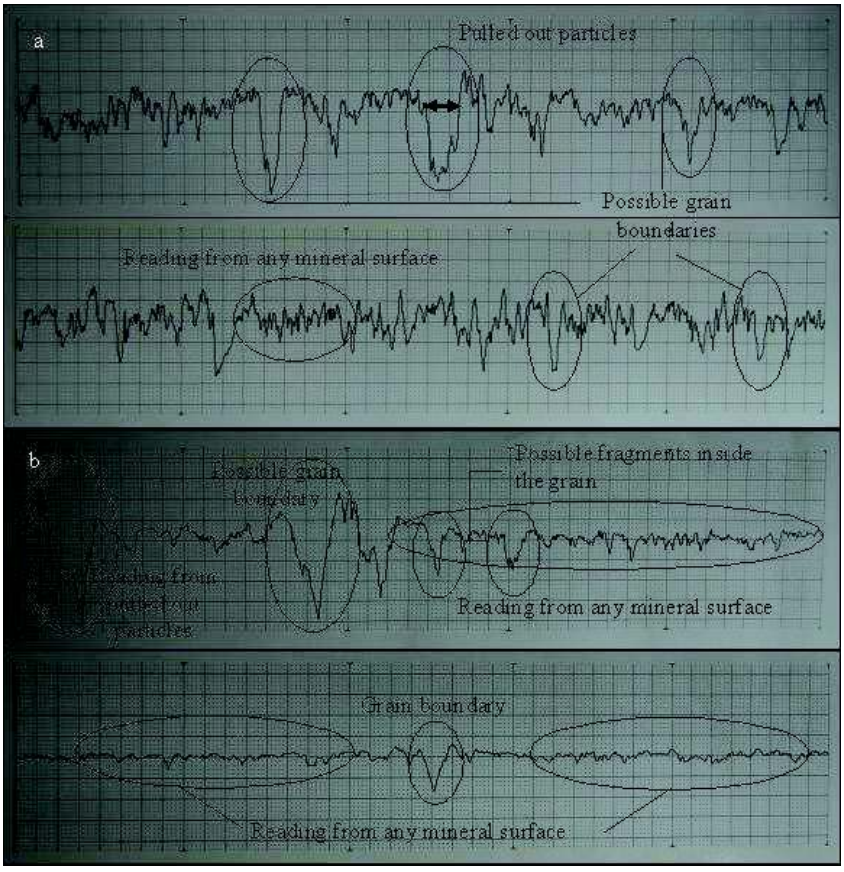

Figure 3. Representative roughness profiles of rocks, a) profile from rocks having finer grains and b) profile from the rocks having larger grains

This results in intersecting higher number of grain boundaries leading to high friction coefficient. Some peaks were also observed due to the fracture occurred inside the minerals due to the cutting forces.

4 CONCLUSIONS

Surface roughness is an important measure of the quality of a rock and a factor that greatly influences manufacturing costs. As a result of the study, it was determined that rock grain size is the main mineralogical property affecting the surface roughness. It was also seen that roughness profiles supports the results obtained.

ACKNOWLEDGEMENTS

The authors would like to thank to the Scientific Research Fund of Karadeniz Technical University for the financial support of this work (No. 2009.112.008.3). Additionally, the authors are most grateful to Granitaş A.Ş. stone processing company for supporting this research by providing dimensioned rock samples for the sawing experiments.

REFERENCES

Buyuksagis, I.S., Goktan, R.M., 2005. Investigation of marble machining performance using an instrumented block-cutter. Journal of

Materials Processing Technology 169, 258-262.

Buyuksagis, I.S., 1998. Dairesel testereli blok kesme makinelerinde mermerlerin kesilebilirlik analizleri. PhD thesis, Osmangazi University Institute for the Natural and Applied Sciences, Turkey, 1998 (in Turkish).

Buyuksagis, S.I., 2007. Effect of cutting mode on the sawability of granites using segmented circular diamond sawblade. Journal of Materials Processing Technology 183, 399–406.

Çaydaş, U., Hasçalık, A., 2008. A study on surface roughness in abrasive waterjet machining process using artificial neural networks and regression analysis method. Journal of Materials Processing Technology 202, 574–582.

Chen, X., Rowe, B.W., 1996. Analysis and simulation of the grinding process: Part II mechanics of grinding. International Journal of Machine Tools and Manufacture 36(8), 883-896.

Delgado, S.N., Rodríguez-Rey, A., Suárez del Río, ML., Díez Sarriá, I., Calleja, L., Ruiz de Argandoña, G.V., 2005. The ifluence of rock microhardness on the sawability of pink porrino granite (Spain). International Journal of Rock Mechanics and Mining Sciences 42, 161–166.

Denkena, B., Tönshoff, H.K., Friemuth, T., Glatzel, T., 2003. Development of advanced tools for economic and ecological grinding of granite. Key Engineering Materials 250, 21-32.

Di Ilio, A., Tonga, A., 2003. A theoretical wear model for diamond tools in Stone cutting. International Journal of Machine Tools and Manufacture 43,1171–1177.

Ersoy, A., Atıcı, Ü., 1999. Wear mechanism of marble cutters. In proceedings of 16th. Mining Congress of Turkey, pp. 107-115, Ankara (in Turkish).

Ersoy, A., Buyuksagis, S.I., Atici, U., 2005. Wear characteristics of circular diamond saws in the cutting of different hard abrasive rocks. Wear 258(9), 1422-1436.

Eyuboglu, S.A., Ozcelik, Y., Kulaksiz, S. Engin, C.I., 2003. Statistical and microscopic investigation of disc segment wear related to sawing Ankara andesites. International Journal of Rock Mechanics and Mining Sciences 40, 405–414.

Fener, M., Kahraman, S., Özder, M.O., 2007. Performance prediction of circular diaomond saws from mechanical rock properties in cutting carbonate rocks. Rock Mechanics and Rock Engineering 40(5), 505–517.

Huang, S., Wang, C., Chen, B., Hu, Y., 2006. Dry-cutting concrete study of diamond saw blade with different segment width. Materials Science Forum 532-533, 321-324.

ISRM., 1981. Rock characterization testing and monitoring suggested methods, in: E.T. Brown (Ed.), Pergamon Press.

Kahraman, S., Fener, M., Günaydın, O., 2004. Predicting the sawability of carbonate rocks using multiple curvilinear regresion analysis. International Journal of Rock Mechanics and Mining Sciences 41, 1123-1131.

Karagöz, Ş., Zeren, M., 2001. The microstructural design of diamond cutting tools. Materials Characterization 47, 89-91.

Konstanty, J., 2000. Diamond bonding and matrix wear mechanisms involved in circular sawing on stone. Industrial Diamond Review 60, 55-65.

Konstanty, J., 1991. The materials science of stone sawing. Industrial Diamond Review 51, 27-31.

Luo, S.Y., Liao, Y.S., 1993. Effects of diamond grain characteristics on sawblade wear. International Journal of Machine Tools and Manufacture 3(2), 257-266.

Nalbant, M., Gökkaya, H., Sur, G., 2007. Application of Taguchi method in the optimization of cutting parameters for surface roughness in turning. Materials and Design 28, 1379–1385.

Özçelik, B., Öktem, H., Kurtaran, H., 2005. Optimum surface roughness in end milling inconel 718 by coupling neural network model and genetic algorithm. International Journal of Advanced Manufacturing Technology 27, 234–241.

Rosa, L.G., Amaral, M.P., Anjinho, C.A., Fernandes, J.C., 2004. Evaluation of diamond tool behaviour for cutting stone materials. Industrial Diamond Review 1, 45-50.

Tönshoff, H.K., Hillmann-Apmann, H., Asche, J., 2002. Diamond tools in stone and civil engineering industry: cutting principles, wear and applications. Diamond Related Materials 11, 736-741.

Ucun, I., Büyüksagis, S.I., Aslantas, K., 2009. Investigation of the effect on disc performance of coolant containing boron oil in marble sawing process. Journal of Faculty of Engineering and Architecture of Gazi University 24(3), 435-441 (in Turkish).

Wei, C., Du, H.W., Wang, C.Y., Frag, Y.L., 2003. Investigation on cutting forces in concrete sawing process. Key Engineering Materials 250, 181-186.

Wright, D.N., Cassapi, V.B., 1985. Factors influencing stone sawability. Industrial Diamond Review 45, 84-87.

Wright, D.N., Jennings, M., 1989. Guidelines for sawing stone. Industrial Diamond Review 70-75.

Xu, X., 2001. Study on the thermal wear of diamond segmented tools in circular sawing of granites. Tribology Letters 10(4), 245-250.

Xu, X.P., Li, Y., Yu. Y., 2003. Force ratio in the circular sawing of granites with a diamond segmented blade. Journal of Materials Processing Technology 139, 281-285.

Yaşıtlı, E.N., 2008. Numerical modeling of circular sawing mechanism. PhD thesis, Hacettepe University Institute for the Natural and Applied Sciences, Turkey (in Turkish).

Yılmaz, G.N., Goktan, M.R., Kibici, Y., 2011. An investigation of the petrographic and physico-mechanical properties of true granites influencing diamond tool wear performance, and development of a new wear index. Wear 271(5-6), 960-969.

Numune Boyutunun Macun Dolgu Dayanımına Etkisi
Effect of Sample Size on the Strength of Paste Backfill

T. Yılmaz, M. İzki, B. Erçıkdı
Karadeniz Teknik Üniversitesi, Maden Mühendisliği Bölümü,Trabzon

ÖZET: Pratikte macun dolgunun dayanımı, genellikle 10x20 cm (boy/çap oranı 2) boyutundaki silindirik örnekler üzerinde yapılan tek eksenli basınç dayanımı deneyi ile belirlenmektedir. Son yıllarda bazı araştırmacılar dolgunun dayanımını belirlemek için 5x10 cm boyutundaki silindirik numuneleri kullanmaya başlamışlardır. Bu çalışmada Kastamonu-Küre bakır işletmeleri atık barajından sağlanan tesis atığı kullanılarak farklı karışım özelliklerinde (farklı bağlayıcı oranı, su/çimento oranı, bağlayıcı tipi ve atık tane boyutu sınıflarında) 10x20 cm ve 5x10 cm boyutunda numuneler hazırlanmıştır. 7-56 günlük kür süreleri sonunda numuneler üzerinde tek eksenli basınç dayanımı testi gerçekleştirilmiş ve numune boyutunun macun dolgu dayanımına etkisi incelenmiştir. 5x10 cm boyutundaki macun dolgu numuneleri bütün kür sürelerinde ve karışım özelliklerinde %6-75 oranında daha yüksek dayanım üretmiştir. Ayrıca kür süresinin artmasıyla birlikte numuneler arasındaki dayanım farkı azalmıştır. Elde edilen sonuçlardan emniyetli ve ekonomik bir dolgu tasarımı için numune boyutunun göz önüne alınması gerektiği anlaşılmıştır.

ABSTRACT: In practice, the strength of cemented paste backfill (CPB) has been generally determined with unconfined compressive strength (UCS) test using plastic cylinders with a diameter x height of 10x20 cm. In recent years, some researchers have used plastic cylinders with a diameter x height of 5x10 cm in order to determine the strength of CPB. In this study, CPB samples produced from dam tailings obtained from Kastamonu-Küre copper mine using 5x10 cm and 10x20 cm plastic cylinders were prepared at different mixture properties (at varying binder dosages, water to cement ratios, binder types and particle size distributions). The CPB samples were subjected to the UCS tests over a curing period of 7-56 days and the effect of sample size on the strength development of CPB was investigated. CPB samples with a diameter x height of 5x10 cm were observed to produce 6-75% higher UCSs than those of 10x20 cm at all curing times and mixture properties. Additionally, the strength gap between small and large samples decreased with increasing curing time. These findings revealed that sample size should be taken into consideration for a reliable and economical paste backfill design.

1 GİRİŞ

Son yıllarda cevher zenginleştirme atıklarının çimentolu macun dolgu (CPB) ile yeraltı üretim boşluklarına depolanması birçok yeraltı madeninde madencilik faaliyetlerinin önemli bir parçasını oluşturmaktadır. Teknik, ekonomik ve çevresel açıdan sağladığı yararlar nedeniyle özellikle Kanada ve Avustralya yeraltı madenciliğinde giderek yaygınlaşmakta olan teknoloji, ülkemizde son on yıldır Çayeli Bakır İşletmelerinde (ÇBİ) kullanılmakta olup, 2013 yılı içerisinde ise Efemçukuru Altın madeni ve Küre bakır işletmelerinde uygulamaya konulacaktır (Yumlu, 2010, Erçıkdı vd., 2012). Yeraltı üretim boşluklarının doldurulması i) topuklardan cevher kazanımı sağlamakta ve tahkimat işlevi görerek yan odaların (stope) üretimi esnasında emniyetli çalışma koşulları

oluşturmaktadır, ii) yerüstü tasman oluşumunu minimize etmektedir ve iii) tesis atıklarının yeraltında depolanmasını sağlamaktadır. Çimentolu macun dolgunun işletme maliyetleri kaya ve hidrolik dolguya kıyasla daha düşük olup, tesis atıklarının %65-70'inin yeraltı üretim boşluklarında depolanmasına imkan sağlamakta ve yerüstü atık depolama ve rehabilitasyon maliyetlerini azaltmaktadır. Uygun bir atık yönetimi yöntemi olan macun dolgu ayrıca, atmosferik koşullar altında depolanması durumunda çevresel problemlere (AMD oluşumu vb.) yol açabilecek sülfürlü atıkların emniyetli bir şekilde depolanmasını sağlamaktadır (Çetiner vd., 2006, Akçil ve Koldaş, 2006).

Çimentolu macun dolgu; ince boyutlu cevher zenginleştirme atıkları (ağırlıkça katı oranı %75-85), bağlayıcı (katı miktarına göre ağırlıkça %3-8) ve istenen akışkanlığı ve katı oranını (%70-80) sağlamak için ilave edilen suyun başarılı bir karışımı olarak ifade edilmektedir. Dolguyu oluşturan bileşenlerin (atık, bağlayıcı ve karışım suyu) fiziksel, kimyasal ve mineralojik karakteristiği dolgunun kısa ve uzun dönem performansı (dayanım, duraylılık vb.), taşınması ve yeraltı üretim boşluklarına yerleştirilmesi açısından önemli bir rol oynamaktadır. Tek eksenli basınç dayanımı (UCS) ve duraylılık (uzun dönemde fiziksel ve kimyasal etkilere karşı bütünlüğünü koruması) çimentolu macun dolgu kalitesini belirleyen en önemli parametrelerdir. İstenen limit dayanım değerleri dolgunun yeraltındaki işlevine bağlıdır. Örneğin, yeraltı üretim boşluğuna yerleştirilen macun dolgunun yan odaların üretimi ve dolgu ile doldurulması işlemleri tamamlanıncaya kadar geçen sürede kendi stabilitesini sağlaması için 28 günlük kür süresinde en az 0,7 MPa dayanıma sahip olması ve 90 gün boyunca duraylılığını koruması gerekmektedir (Brackebusch, 1994). Tavan tahkimatı için ise en az 4 MPa dayanıma sahip olmalıdır. Ayrıca daha erken kür süresinde dayanımın kazanılması madencilik işlemlerini (ocağın döngü süresi) kısaltmakta ve üretim işlemlerini hızlandırmaktadır.

Dolgunun dayanım ve durabilitesi dolguyu oluşturan bileşenlerin fiziksel (tane boyut dağılımı, özgül ağırlığı vb.), kimyasal (bağlayıcı tipi vb.) ve mineralojik (pirit ve kil minerali içeriği vb.) özellikleri ve yeraltı kür koşulları (sıcaklık, yanal basınç etkisi, konsolidasyon, patlatma kaynaklı titreşimler vb.) ile ilişkilidir. Son yıllarda dolguyu oluşturan bileşenlerin özelliklerinin ve yeraltı kür koşullarının dolgu performansına etkisine yönelik çok sayıda çalışma gerçekleştirilmesine karşın numune boyutunun etkisi gözardı edilmiştir. Bu çalışmada aynı boy/çap oranına (2:1) sahip farklı numune boyutlarının dolgu dayanımına etkisi detaylı olarak incelenmiştir.

1.1 Numune Boyutunun Önemi

Numune boyutunun kaya ve çimento içerikli (beton ve dolgu) malzemelerin mekanik performansını etkilediği belirtilmiştir. Brace (1981) ve Hoek (2000), kayalarda numunenin boyutu arttıkça, diğer bir ifade ile hacmi arttıkça, kaya içerisindeki muhtemel mikro çatlak sayısının ve zayıflık düzlemlerinin arttığını ve dayanımın düştüğünü ifade etmiştir. Darlington vd. (2011), numune boyutunun betonun dayanımına etkisini araştırmak için boy/çap oranı 2:1 olan farklı boyutlarda beton numunesi hazırlamıştır. 28 günlük kür süresi sonunda gerçekleştirilen tek eksenli basınç dayanım testi, 6,35x12,7 cm (çap x boy) boyutundaki numunelerin 8,35x16,7 cm boyutundaki numunelere kıyasla yaklaşık %10 daha fazla dayanım ürettiğini göstermiştir. Benzer şekilde Felekoğlu ve Türkel (2005), numune boyutunun beton örneklerinin dayanımına etkisini araştırmak amacıyla farklı boyuttaki (boy/çap oranı:2) numuneler üzerinde dayanım testi gerçekleştirmiştir. Araştırmacılar, 10x20 cm (çapxboy) boyutundaki numunelerin 15x30 cm boyutundaki numunelere kıyasla 28 günlük kür süresi sonunda daha yüksek (%3.6-21.8 oranında) dayanım ürettiğini ve bunun nedeninin küçük boyutlu numunelerde "çeper etkisi" nedeniyle iri agrega tanelerinin askıda kalması (kalıba sürtünmeden dolayı) sonucu oluşan düşük kompaksiyondan kaynaklandığı belirtilmiştir. Ayrıca iri taneli malzemelerin boyutu, şekli (yuvarlak ve

köşeli olması) ve kenetlenme derecelerinin de dayanım kazanımında etkili olduğu bilinmektedir.

Hassani vd. (2007), üç farklı çimentolu dolgu tipinde (atık- kum karışımı dolgu, agrega karışımlı macun dolgu ve kaya dolgu) farklı çaplardaki silindirik numunelerin dayanım testlerini yapmışlardır. Kaya dolgu ile hazırlanan örneklerin dayanımı numune boyutunun artmasıyla birlikte azalmıştır. Atık-kum karışımı dolgu ile hazırlanan numunelerin dayanımı ise 15,2 cm çapa sahip numune boyutuna kadar artmış, fakat daha sonra örnek boyutunun artmasıyla birlikte dayanım azalmıştır. Agrega karışımlı macun dolgu ile hazırlanan numunelerin dayanımlarında ise boyut etkisinin gözardı edilebilecek seviyede olduğu tespit edilmiştir.

Çimentolu macun dolgu numunelerinin tek eksenli basınç dayanımı genellikle 10x20 cm (çap x boy) boyutundaki silindirik numunelerden elde edilmektedir (Benzaazoua vd., 1999, Hassani vd., 2001; Kesimal vd., 2004, Fall vd., 2008; Tariq ve Nehdi, 2007; Yılmaz vd., 2009; Erçıkdı vd., 2010a,b; Cihangir vd., 2012; Yin vd., 2012). Ayrıca tesis uygulamalarında da maden operatörleri macun dolgu karışım dizaynını 10x20 cm boyutundaki numuneden elde ettikleri dayanım sonuçlarına göre yapmaktadırlar (Landriault ve Deneka, 2000; Benzaazoua vd., 2005; Kesimal vd., 2010, 2012). Son yıllarda bazı araştırmacılar (Klein ve Simon, 2006; Fall ve Pokharel, 2010; Fall vd., 2010) kullanılan atık malzeme miktarını ve iş yükünü azaltmak için boy/çap oranı 2:1 olan 5x10 cm (çap x boy) boyutundaki numuneleri dayanım testine tabi tutmaktadırlar. Ancak araştırmacılar numune boyutunun kaya ve betonda olduğu gibi çimentolu macun dolgu dayanımı üzerinde de etkisinin olabileceğini göz önünde bulundurmamışlardır. Benzer şekilde yeraltından alınan macun dolgu karot örneklerinin boy/çap oranı 2:1 olmasına karşın boyutu küçük (NX boyutlu) olabilmektedir. Revell (2004), numune boyutunun çimentolu macun dolgu dayanımına etkisini araştırmak amacıyla boy/çap oranı 2:1 olan 10x20 cm ve 4x8 cm (çap x boy) boyutundaki silindirik numune kaplarını kullanarak %6 bağlayıcı oranında numuneler hazırlamış ve 7-28 günlük kür sürelerinde dayanım testine tabi tutmuştur. 4x8 cm boyutundaki numuneler 10x20 cm boyutundaki numunelere kıyasla %6-10 oranında (7 ve 28 günlük) daha yüksek dayanım üretmiştir.

2 DENEYSEL ÇALIŞMALAR

2.1 Atık Malzeme

Atık malzeme, Eti Bakır Kastamonu – Küre işletmesi atık barajından alınmış, belli bir miktarı hidrosiklon vasıtasıyla sınıflandırma işlemine tabi tutularak ince (şlam) boyutlu malzeme uzaklaştırılmış ve 500 kg kapasiteli varillere doldurularak KTÜ Macun Dolgu Laboratuarına getirilmiştir.

Malvern Mastersizer ile atık malzemeler üzerinde yapılan tane boyut dağılımı analizi sonuçlarına göre 20 µm altı malzeme miktarı referans baraj atığı için %58,42, sınıflandırılmış (şlamı uzaklaştırılmış) baraj atığı için %35,04 olarak belirlenmiştir (Şekil 1). Referans baraj atığının ince boyutlu macun dolgu malzemesi (malzemenin ağırlıkça %60-90' <20 µm) sınıfına yakın seviyede olduğu, sınıflandırılmış atığın ise orta taneli macun dolgu malzemesi (malzemenin ağırlıkça %60-90' <20 µm) sınıfına girdiği görülmektedir. İri taneli atıkların drenaj yoluyla daha fazla su bıraktığı ve ince taneli atıklara kıyasla daha yüksek dayanım ürettiği belirtilmektedir.

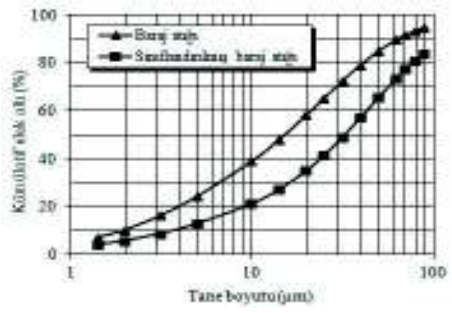

Şekil 1. Atıkların tane boyut dağılımları

Atıkların kimyasal bileşimi XRF ve yaş kimyasal analiz sonucu ICP AES cihazı ile sülfür içeriği ise gravimetrik analizle belirlenmiştir (Tablo 1). Referans ve sınıflandırılmış baraj atıklarının sülfür içeriği oldukça yüksektir. Sınıflandırma işlemi (şlam uzaklaştırma) sonucu ince fraksiyonlardaki silikat minerallerinin uzaklaşmasıyla baraj atığının SiO_2+Al_2O_3 içeriği azalmış ve sülfür içeriği artmıştır (%27.82). Örneğin, atık içerisindeki ince malzeme miktarının azalmasıyla baraj atığının SiO_2+Al_2O_3 içeriği %32,48'den %26,63'e düşmüştür. Ayrıca atık içerisindeki iri tane miktarının artmasıyla birlikte özgül yüzey alanın azaldığı ve özgül ağırlığın arttığı görülmüştür.

Tablo 1. Atıkların kimyasal ve fiziksel bileşimi

Özellikler	Baraj atığı (%)	Sınıflandırılmış baraj atığı (%)
Kimyasal bileşim		
SiO_2	25,80	21,21
Al_2O_3	6,68	5,42
Fe_2O_3	39,83	45,43
MgO	2,14	2,21
CaO	2,79	1,64
Na_2O	0,35	0,24
K_2O	0,42	0,31
TiO_2	0,43	0,38
P_2O_5	0,03	0,03
MnO	0,06	0,05
Cr_2O_3	0,02	0,017
Kızdırma kaybı	20,6	21,9
Toplam	99,15	98,84
Sülfür içeriği (S^{-2}) (%)	23,18	27,82
Pirit içeriği (FeS_2) (%)	43,47	52,16
Fiziksel özellikler		
Özgül ağırlık	3,66	3,81
Özgül yüzey (cm^2/g)	4630	1810
Eğrilik katsayısı ($C_c=(D_{30})^2/(D_{10}\times D_{60})$)	0,99	1,74
Üniformluk katsayısı ($C_u=(D_{60}/D_{10})$)	11	10,84

2.2 Bağlayıcı Malzeme

Deneysel çalışmalarda bağlayıcı malzeme olarak; Akçansa çimento fabrikasından temin edilen Portland (CEM I 42,5) ve sülfata dayanıklı çimento (SDÇ 32,5) ile Karçimsa'dan temin edilen yüksek fırın cüruflu çimento (CEM III/A 42,5 N) kullanılmıştır. Kullanılan bağlayıcıların kimyasal, fiziksel ve mineralojik özellikleri Tablo 2'de verilmiştir. CEM III/A 42.5 N tipi çimento dayanım ve duraylılığı artırmak ve bağlayıcı maliyetlerini azaltmak için %35 oranında öğütülmüş yüksek fırın cürufu içermektedir.

CEM I 42,5 tipi çimentonun kalsiyum silikat içeriği (C_3S ve C_2S) SDÇ 32,5'e yakın olmasına karşın alkali-silika ve asit/sülfat etkisi gibi zararlı kimyasal reaksiyonlarda önem arz eden C_3A içeriği yüksektir. Sülfür içeriği yüksek atıklardan üretilen macun dolguda asit ve sülfat etkisi nedeniyle oluşabilecek duraylılık kaybını engellemek için C_3A içeriği düşük veya mineral katkı maddesi (cüruf vb.) içeren bağlayıcıların kullanılması önerilmektedir. Ancak bu çalışmada uzun dönem dayanım testleri yapılmadığından bağlayıcıların olası asit ve sülfat etkisine karşı performansları değerlendirilmemiştir.

Tablo 2. Bağlayıcıların fiziksel, kimyasal ve mineralojik özellikleri

Özellikler	CEM I 42,5 (%)	CEM III/A 42,5 N (%)	SDÇ 32,5 (%)
Kimyasal bileşim			
SiO_2	20,57	27,58	20,88
Al_2O_3	4,81	7,04	3,84
Fe_2O_3	3,67	2,37	4,52
MgO	1,35	3,91	1,49
SO_3	2,97	2,91	2,84
CaO	65,27	52,75	64,56
Na_2O	0,41	0,25	0,31
K_2O	0,85	1,06	0,67
TiO_2	0,45	0,40	0,33
P_2O_5	0,13	0,03	0,10
MnO	0,11	1,00	0,12
Cr_2O_3	0,075	0,015	0,177
Serbest CaO	1,19	-	0,43
Kızdırma kaybı	2,1	2,8	2,8
Toplam	99,90	99,87	99,87
Fiziksel özellikler			
Özgül ağırlık	3,14	3,08	3,27
Özgül yüzey (cm^2/g)	4335	4260	3170
Mineralojik bileşim			
C_3S	58,44	-	61,96
C_2S	14,95	-	13,18
C_3A	6,54	-	2,54
C_4AF	11,16	-	13,74

2.3 Numune Hazırlama ve Dayanım Testi

Atık, bağlayıcı ve su kullanılarak farklı karışım özelliklerinde (farklı bağlayıcı oranı, su/çimento oranı vb.) hazırlanan 5x10 cm ve 10x20 cm boyutundaki macun dolgu numuneleri önceden belirlenmiş kür süreleri (7, 14, 28 ve 56 gün) sonunda tek eksenli basınç dayanımı testine tabi tutulmuştur. Bağlayıcı malzeme karışıma, deneylerde kullanılan slamp değerlerine karşılık gelen katı oranlarına (%73,58-80,17) göre hesaplanarak ilave edilmiştir. Macun dolgu karışımının istenen akışkanlığa (kıvama) gelmesi için karışım içerisine gerekli miktarda musluk suyu ilave edilmiştir. Karışımın (atık malzeme, bağlayıcı ve su) homojen bir şekilde hazırlanması için 20,8 lt kapasiteli Univex SRMF 20 model mikser kullanılmıştır. Karıştırma işlemi 105 devir/dk'lık dönme hızında 7 dakika süreyle yapılmıştır.

Bağlayıcı oranının etkisi %5, 6 ve 7 çimento oranında ve sabit akışkanlıkta (19,05 cm slamp) değerlendirilmiştir. Su/çimento oranının etkisi sabit bağlayıcı oranında ve farklı su çimento oranlarında (4,62, 4,87 ve 5,13) incelenmiştir. Bağlayıcı tipinin dayanıma etkisi sabit bağlayıcı oranı (%7) ve akışkanlıkta (19,05 cm slamp) farklı bağlayıcılar (CEM I 42,5, CEM III/A 42,5 N ve SDÇ 32,5) kullanılarak araştırılmıştır. Tane boyut dağılımının etkisi ise sabit bağlayıcı oranı (%7), akışkanlık (19,05 cm slamp) ve çimento tipinde (CEM III/A 42,5 N) referans baraj atığı ve şlamı uzaklaştırılmış (sınıflandırılmış) baraj atığı kullanılarak değerlendirilmiştir.

Hazırlanan macun dolgu karışımı 5x10 cm ve 10x20 cm boyutlarındaki drenajlı silindir numune kalıplarına dökülmüş ve 7-56 günlük kür süresi aralığında kür odasında (%80 nem ve 25 C° sıcaklık) bekletilmiştir. Her bir kür süresi için 3 adet 5x10 cm boyutunda ve 3 adet 10x20 cm boyutunda olmak üzere 6 adet numune hazırlanmıştır (Şekil 2). Toplam 192 adet numunenin tek eksenli basınç dayanımı önceden belirlenen kür süreleri sonunda yük kapasitesi 50 kN ve 0,5 mm/dk'lık bir yükleme hızına sahip ELE marka bilgisayar kontrollü basınç ve deformasyon ünitesinde ASTM C 39 (2005) tarafından önerilmiş yönteme göre gerçekleştirilmiştir. Her iki boyuttaki silindirik numunelerin boy/çap oranı 2:1 olup, numunelerin alt ve üst yüzeyleri deney öncesi düzeltilmiştir. Her bir kür süresi için 3'er adet numune test edilmiş ve bulguların yorumlanmasında elde edilen ortalama dayanım değerleri kullanılmıştır.

Şekil 2. Farklı boyuttaki (5x10 cm ve 10x20 cm) numunelerin görünümü

3 BULGULAR VE TARTIŞMA

3.1 Bağlayıcı Oranının Etkisi

Bağlayıcı oranı, macun dolgunun mekanik performansı ve işletme maliyetleri üzerinde önemli bir rol oynar. Kullanılan bağlayıcının dolgu işletme maliyetlerinin %40-75'ini teşkil ettiği göz önüne alındığında, istenen dayanımı verecek optimum bağlayıcı oranının belirlenmesi önemli ekonomik kazanımlar sağlayacaktır. Şekil 3, baraj atığı ve CEM III/A 42,5 N kullanılarak farklı bağlayıcı oranı (%5-7) ve numune boyutunda hazırlanan macun dolgu numunelerinin 7-56 günlük kür süresi sonundaki tek eksenli basınç dayanımı sonuçlarını göstermektedir. Beklenildiği üzere, her iki numune boyutunda da bağlayıcı oranının ve kür süresinin artmasıyla birlikte dayanım kazanımının arttığı görülmektedir. Bağlayıcı miktarı arttıkça ortamda daha fazla bağlayıcı jeli (C-S-H ve portlandit) oluşmakta ve dolgunun dayanımı artmaktadır.

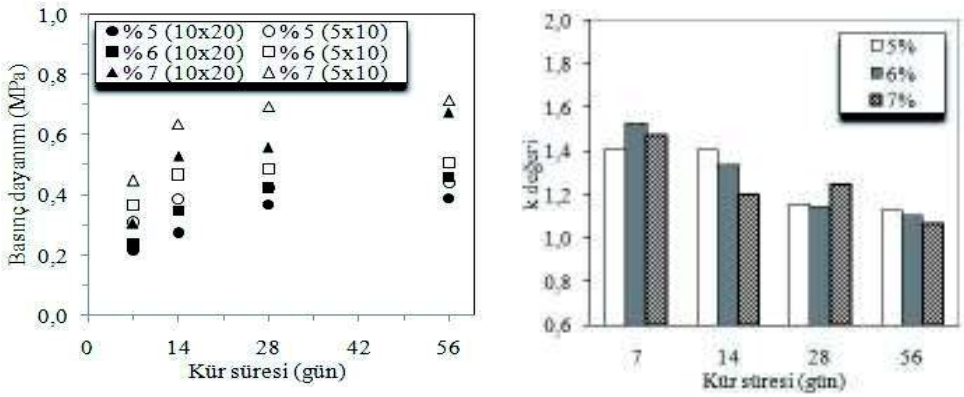

Şekil 3. Bağlayıcı oranının dolgu dayanımına etkisi (a) ve kür süresine bağlı k değerleri (b)

28 günde en yüksek dayanımı (0,695 MPa) 5x10 cm boyutunda hazırlanan numunelerin sağladığı görülmektedir. Pratikte istenen 28 günlük dayanım değerine (≥0,7 MPa) hiçbir bağlayıcı oranı ve numune boyutunda ulaşılamamıştır.

5x10 cm boyutuna sahip macun dolgu numuneleri, 10x20 cm boyutlu numunelere kıyasla bütün bağlayıcı oranları ve kür sürelerinde daha yüksek basınç dayanımı üretmiştir (Şekil 3a). Kaya ve beton malzemesine kıyasla daha homojen bir yapıda olmasına ve görünürde belirgin bir farklılık olmamasına karşın, numune boyutunun artmasıyla birlikte örnek içerisinde kusur olma olasılığı (mikro boşluklar ve zayıflık düzlemleri) artmaktadır. Yüklemeye devam edildikçe örneğin içinde bulunan mikro-kusurlar çevresinde gerilme birikimleri oluşmaktadır. Deformasyonun artmasıyla bu kusurlar büyümekte ve kırılma düzlemi/düzlemleri oluşarak malzeme yenilmektedir. Dolayısıyla numune boyutunun artmasıyla oluşacak daha fazla mikro-kusur boyunca deformasyonlar oluşmaya başlayacak ve sonuçta malzemenin daha kolay yenilmesine yol açacaktır (Ünver, 2012).

5x10 cm boyutlu numunelerin dayanım değerlerinin 10x20 cm boyutlu numunelerin dayanım değerlerine bölünmesiyle elde edilen k ($T.E.B.D_{5x10}/T.E.B.D_{10x20}$) değerleri incelendiğinde (Şekil 3b), 5x10 cm boyutundaki numunelerin 10x20 cm boyutlu numunelere kıyasla 1,06-1,52 kat daha yüksek dayanım ürettiği görülmektedir. Ayrıca iki farklı numune boyutu arasındaki dayanım farkı erken kür sürelerinde (7-14) yüksek, ilerleyen kür sürelerinde (28-56) ise nispeten düşüktür. Küçük boyutlu numunelerin daha hızlı kuruması ve nem içeriklerinin düşük olması nedeniyle erken kür sürelerinde daha yüksek dayanım kazanımının gerçekleştiği düşünülmektedir. Buna karşın büyük boyutlu numunelerin kuruması başlangıçta nispeten daha yavaş olmakta ve bu nedenle erken kür sürelerinde dayanım farkı artmaktadır. Kür süresinin artmasıyla birlikte büyük boyutlu numunelerin nem içeriği azaldığından dolayı ilerleyen kür sürelerinde dayanım farkı erken kür sürelerine kıyasla daha düşük seviyede olmaktadır.

3.2 Su-Çimento Oranının Etkisi

Dolgunun tesisten yeraltı üretim boşluklarına borularla nakledilebilmesi için belli bir akışkanlığa (6-10" slamp) sahip olması gerekmektedir. Ancak akışkanlık arttıkça su/çimento oranı artmakta ve dolgunun dayanımını olumsuz yönde etkilemektedir. Bu nedenle optimum su/çimento oranının belirlenmesi hem dolgunun mekanik performansı hem de yeraltına taşınabilirliği açısından önem arz etmektedir.

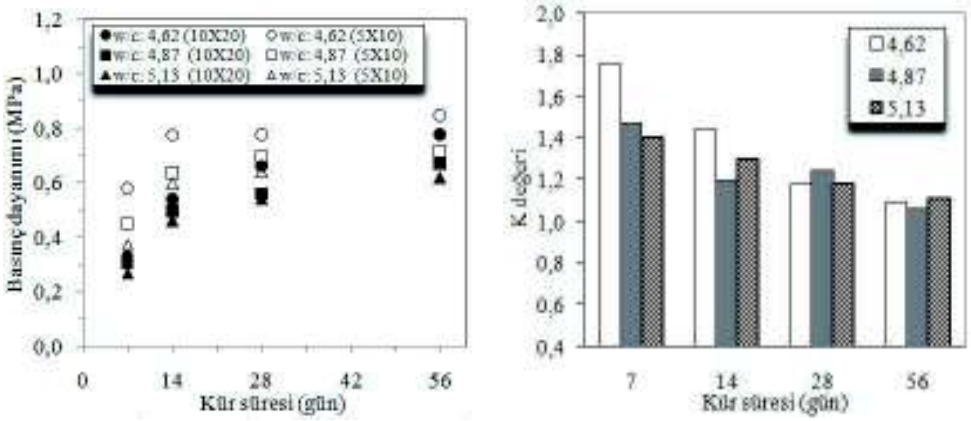

Şekil 4. Su çimento oranının dolgu dayanımına etkisi (a) ve kür süresine bağlı k değerleri (b)

Şekil 4, 6,5-8,5" slamp akışkanlığa karşılık gelen su/çimento oranlarında (4,62, 4,87, 5,13) CEM III/A 42,5 N tipi çimento kullanılarak %7 çimento oranında hazırlanan 10x20 cm ve 5x10 cm boyutlarındaki macun dolgu numunelerinin 7-56 günlük kür süresi sonundaki tek eksenli basınç dayanımı sonuçlarını göstermektedir. Beklenildiği üzere, her iki numune boyutunda da su/çimento oranının azalmasıyla dayanım artış göstermiştir (Şekil 4a). Su/çimento oranının 5,13'den 4,62'ye düşmesiyle basınç dayanımı 1,17-1,54 kat artmıştır. Benzer şekilde, 5x10 cm boyuta sahip numuneler bütün kür sürelerinde 10x20 cm boyutundaki numunelere kıyasla daha yüksek basınç dayanımı üretmiştir. 28 günlük kür süresi sonunda istenen dayanımı (≥0,7 MPa) 10x20 cm boyutundaki hiçbir numune sağlamamış olup, sadece en düşük su çimento oranında hazırlanan 5x10 cm boyutundaki numuneler sağlamıştır (0.777 MPa).

Kür süresine bağlı olarak aynı karışım özelliklerine sahip farklı numune boyutundaki numunelerin dayanım farkları incelendiğinde (Şekil 4b), k değerlerinin ($T.EB.D_{5x10}/T.E.B.D_{10x20}$) 7-14 günlük kür sürelerinde 1,28-1,75 arasında, 28-56 günlük kür sürelerinde ise 1,06-1,25 arasında değiştiği görülmektedir.

3.3 Bağlayıcı Tipinin Etkisi

Sabit bağlayıcı oranında (%7) CEM I 42,5, SDÇ 32,5 ve CEM III/A 42,5 tipi çimento kullanılarak hazırlanan 10x20 cm ve 5x10 cm boyutlarındaki macun dolgu numunelerinin dayanım sonuçları Şekil 5'de verilmiştir. Her iki numune boyutunda da en yüksek dayanımı Portland çimentosu (CEM I 42,5) ile hazırlanan numuneler, en düşük dayanımı ise sülfata dayanıklı çimento (SDÇ 32,5) ile hazırlanan numuneler üretmiştir. Bunun başlıca nedeni Portland çimentosunun 28 günlük basınç dayanımının (42,5 MPa) daha yüksek olmasından kaynaklanmaktadır. Ancak sülfür içeriği yüksek atıklardan hazırlanan numunelerde Portland çimentosu gibi C_3A içeriği yüksek bağlayıcıların kullanılması durumunda asit ve sülfat etkisi nedeniyle uzun dönemde (≥90 gün) dayanım kaybı oluşabilmektedir. Bu gibi durumlarda sülfata dayanıklı çimento veya portland kompoze çimento kullanımı önerilmektedir. CEM III/A 42,5 N tipi çimento ile hazırlanan numunelerin dayanımı erken kür sürelerinde (7-14 gün) CEM I 42,5 ile hazırlanan numunelere kıyasla düşük olmasına karşın, ilerleyen kür sürelerinde (28 ve 56 gün) CEM I 42,5'e yakın dayanım kazanımı elde ettikleri görülmektedir. Demirboğa vd. (2004) puzolanların hidratasyon ısısını düşürdüğünü ve dayanım kazanımı için daha uzun kür süresine ihtiyaç duyulduğunu belirtmiştir.

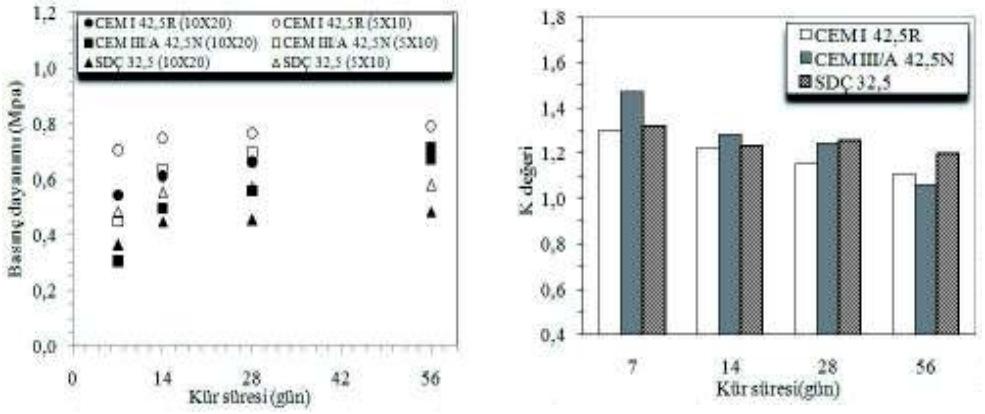

Şekil 5. Bağlayıcı tipinin dolgu dayanımına etkisi (a) ve kür süresine bağlı k değerleri (b)

Ayrıca belirli bir hidrolik bağlayıcı özelliği (CaO içeriğinin yüksek olmasından dolayı) bulunan öğütülmüş yüksek fırın cürufu, klinkerin hidratasyonu sonucu açığa çıkan $Ca(OH)_2$ ile reaksiyona girerek bağlayıcı jeli (C-S-H) oluşturmakta ve bu nedenle CEM III/A 42,5 N tipi çimentonun yeterli dayanım kazanımı için daha uzun kür süresine ihtiyaç duyulmaktadır. Karışımın hazırlanmasında bağlayıcı olarak Portland çimentosu (CEM I 42,5 R) kullanılması ve boyutu 5x10 cm olan numunelerin seçilmesi durumunda istenen mekanik performans (28 günde ≥0,7 MPa) için %7 bağlayıcı oranının yeterli olduğu görülmektedir (Şekil 5a). Ancak, 10x20 cm boyutundaki numunelerin 28 günde istenen dayanımı sağlaması için daha fazla çimentoya gereksinim duydukları anlaşılmaktadır. Bu durum emniyetli, ekonomik bir dolgu tasarımı açısından numune boyutunun önemini ortaya koymaktadır.

5x10 cm boyutlu numunelerin dayanım değerlerinin 10x20 cm boyutlu numunelerin dayanım değerlerine bölünmesiyle elde edilen k ($T.EB.D_{5x10}/T.E.B.D_{10x20}$) değerleri kür süresinin artmasıyla birlikte azalmıştır (Şekil 5b). k değerleri erken kür sürelerinde 1,22-1,47 arasında, ilerleyen kür sürelerinde ise 1,06-1,26 arasında değişmektedir.

3.4 Tane Boyut Dağılımının Etkisi

Atık tane boyutu, dolgunun mekanik ve reolojik (akışkanlık) özelliklerini etkilemektedir. Fall vd. (2005) iri taneli atıklardan hazırlanan macun dolgu karışımlarının iri ve orta taneli atıklardan hazırlanan karışımlara kıyasla drenaj yoluyla daha fazla su bıraktığını belirtmiştir. Daha fazla suyun drene olması, mikro yapının iyileşmesine (düşük porozite ve boşluk oranının oluşması) ve dolgu dayanımının artmasına neden olmaktadır. Ancak bu durumda macun dolgunun borularla yeraltına taşınması ve mikserde karıştırılması esnasında oturma ve ayrışma oluşabilir (Erçıkdı vd., 2013). Bu nedenle optimum atık tane boyut dağılımının belirlenmesi kritik öneme sahiptir. Daha önce yapılan çalışmalarda dolgu dayanımı ve reolojik özellikleri açısından optimum 20 µm altı ince malzeme miktarının ağırlıkça %25-30 oranında olması gerektiği belirtilmiştir (Kesimal vd., 2003; Fall vd., 2005).

Şekil 6, referans ve sınıflandırılmış (şlamı uzaklaştırılmış) baraj atığı kullanılarak farklı numune boyutunda ve sabit bağlayıcı oranı (%7) ile slampta (19.05 cm) hazırlanan dolgu numunelerinin 7-56 günlük kür süresi sonundaki dayanımını göstermektedir.

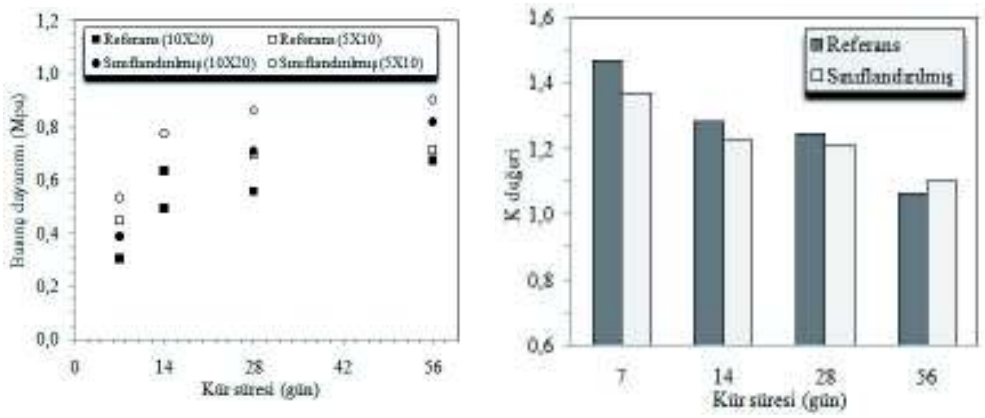

Şekil 6. Atık tane boyutunun dolgu dayanımına etkisi (a) ve kür süresine bağlı k değerleri (b)

Sınıflandırılmış (şlamı uzaklaştırılmış) baraj atığı ve CEM III/A 42,5 N kullanılarak farklı boyutlarda hazırlanan numuneler aynı bağlayıcı oranı (%7) ve akışkanlıkta (19,05 cm) referans atıkla hazırlanan numunelere kıyasla daha yüksek dayanım üretmiştir. Sadece sınıflandırılmış baraj atığı kullanılarak hazırlanan 10x20 cm boyutundaki numuneler 28 günde istenen dayanım değerini vermiştir (0,711 MPa) (Şekil 6a). Ayrıca numune boyutu arttıkça dayanım azalma göstermiş ve kür süresinin artmasıyla birlikte numune boyutları arasındaki dayanım farkı azalmıştır (Şekil 6b). Sınıflandırmanın (şlam uzaklaştırma) dayanım kazanımına olumlu etkisi su bırakma kapasitesindeki artış (çimento/su oranında artış vb.) ve tane boyut dağılımındaki iyileşme ile ilişkilendirilebilir. Karışım içerisinde ince tane miktarı azaldıkça çimento ve su ile etkileşimi gerekli yüzey alanı azalmaktadır. Bu nedenle sınıflandırılmış atıklardan hazırlanan macun dolgu karışımı aynı akışkanlığa daha yüksek katı oranında ulaşmaktadır. İstenen akışkanlığı (19,05 cm slamp) sağlayan katı oranının artması yeraltı üretim boşluklarına daha fazla atık malzemenin depolanmasına imkân sağlamaktadır. Erçıkdı vd. (2013) sınıflandırılmış atıklardan hazırlanan macun dolgu uygulamasının bağlayıcı tüketimini %13-25 oranında azalttığını ve özellikle sülfürlü atıklardan üretilen dolgunun uzun dönem duraylılığını iyileştirdiğini belirtmiştir.

4 SONUÇLAR

Bu çalışmada farklı boyutlarda (boy/çap oranı 2:1) ve karışım özelliklerinde (farklı bağlayıcı tipi ve oranı, su/çimento oranı vb.) hazırlanan silindirik numunelerin macun dolgu dayanımına etkisi incelenmiştir. Kullanılan atık ve bağlayıcıların ayrıntılı fiziksel, kimyasal ve mineralojik karakterizasyonu yapılarak dayanım kazanımına etkileri değerlendirilmiştir. Genel olarak bağlayıcı oranının artması ve su/çimento oranının azalmasıyla bütün kür sürelerinde dayanım artış göstermiştir. Atığa uygun bağlayıcı tipinin belirlenmesinin dolgu dayanım ve duraylılığı açısından önemli olduğu ortaya konulmuştur. Sınıflandırma (şlam uzaklaştırma) işleminin dolgu dayanımı üzerinde olumlu bir etki yaptığı belirlenmiştir. Genel olarak bütün kür sürelerinde ve karışım özelliklerinde küçük boyutlu (5x10 cm) numunelerin daha yüksek dayanım ürettiği ve istenen mekanik dayanım için daha az çimento kullanımının yeterli olacağı görülmüştür. Ancak başlangıçta 10x20 cm boyutundaki numunelerden elde edilen sonuçlara göre tasarımı yapılan dolgunun performansının takibi farklı boyutlardaki numunelerle gerçekleştirilmesi durumunda yanıltıcı

sonuçlar elde edilecektir. Bu durumda yeraltında bazı sorunlarla (küçük çaplı göçük vb.) karşılaşılacak ve sonuçta iş gücü kaybına ve üretim veriminin azalmasına neden olacaktır. Bu nedenle emniyetli ve ekonomik bir dolgu uygulaması açısından numune boyutunun dayanım üzerine etkisi göz önüne alınmalıdır.

TEŞEKKÜR

Desteklerinden dolayı Karadeniz Teknik Üniversitesi Bilimsel Araştırma Projeleri Koordinasyon Birimine (2010.112.008.2 no'lu proje) ve Eti Bakır AŞ'ye teşekkür ederiz.

KAYNAKLAR

Akcil, A. ve Koldaş, S., 2006. Acid mine drainage (AMD): Causes, treatment and case studies, *Journal of Cleaner Production*, 14, 12-13, s. 1139-1145.

Benzaazoua, M., Ouellet, J., Servant, S., Newman, P. ve Verburg, R., 1999. Cementitious backfill with high sulfur content physical, chemical, and mineralogical characterization, *Cement and Concrete Research*, 29, 5, s.719-725.

Benzaazoua M., Yilmaz E., Belem T., Bussière B. ve Bordeleau H. 2005. Laboratory investigation of cemented paste backfill samples made of mill tailings from Garpenberg Sulfide Mine, Sweden. Final Technical Report, Outokumpu Technology Ab, Boliden Mineral Ab, s.16.

Brace, W.F., 1981. The effect of size on mechanical properties of rock, *Geophysical Research Letters*, 8, 7, s.651–652.

Brackebusch, F.W., 1994. Basics of cemented paste backfill systems, *Mining Engineering*, 46, 10, s.1175-1178.

Cihangir, F., Ercikdi, B., Kesimal, A., Turan, A. ve Deveci, H., 2012. Utilization of alkali–activated blast furnace slag in paste backfill of high–sulphide mill tailings: Effect of binder type and dosage, *Minerals Engineering*, 30, s.33-43.

Çetiner, E.G., Ünver, B. ve Hindistan, M.A., 2006. Regulations related with mining wastes: European Community and Turkey, *Madencilik*, 45, 1, s. 23-34.

Darlington, W.J., Ranjith, P.G. ve Choi, S.K., 2011. The effect of specimen size on strength and other properties in laboratory testing of rock and rock–like cementitious brittle materials, *Rock Mechanics* and *Rock Engineering*, 44, s.513–529.

Demirboğa, R., Türkmen, İ. ve Karakoç, M.B., 2004. Relationship between ultrasonic velocity and compressive strength for high-volume mineral admixture concrete, *Cement and Concrete Research*, 34, s.2329-2336.

Erçıkdı, B., Cihangir, F., Kesimal, A., Deveci, H. ve Alp, İ., 2010a. Effect of natural pozzolans as mineral admixture on the performance of cemented paste backfill of sulphide–rich tailings, *Waste Management Research*, 28,5, s.430-435.

Erçıkdı, B., Cihangir, F., Kesimal, A., Deveci, H. ve Alp, İ., 2010b. Utilization of water–reducing admixtures in cemented paste backfill of sulphide–rich mill tailings, *Journal of Hazardous Materials*, 179, s.940–946.

Erçıkdı, B., Cihangir, F., Kesimal, A. ve Deveci, H., 2012. Tesis atıklarının yönetiminde macun dolgu teknolojisi, *Madencilik Türkiye*, 24, s.54-59.

Erçıkdı, B., Baki, H. ve İzki, M., 2013. Effect of desliming of sulphide-rich mill tailings on the long-term strength of cemented paste backfill, *Journal of Environmental Management*, 115, s.5-13.

Fall, M. ve Pokharel, M., 2010. Coupled effects of sulphate and temperature on the strength development of cemented tailings backfill: Portland cement-paste backfill, *Cement and Concrete Composites*, 32, 10, s.819–828.

Fall, M., Benzaazoua, M. ve Ouellet, S., 2005. Experimental characterization of the influence of tailings fineness and density on the quality of cemented paste backfill, *Minerals Engineering*, 18, s.41-44.

Fall, M., Benzaazoua, M. ve Saa, E.G., 2008. Mix proportioning of underground cemented tailings backfill, *Tunnelling and Underground Space Technology*, 23, s.80–90.

Fall, M., Celestin, J.C., Pokharel, M. ve Toure, M., 2010. A contribution to understanding the effects of curing temperature on the mechanical properties of mine cemented tailings backfill, *Engineering Geology*, 114, 3-4, s.397–413.

Felekoğlu, B. ve Türkel, S., 2005. Effects of specimen type and dimensions on compressive strength of concrete, *Gazi Üniversitesi Fen Bilimleri Dergisi*, 18,4, s.639–645.

Hassani, F.P., Ouellet, J. ve Hossein, M., 2001. Strength development in underground high

sulphate paste backfill operation, *CIM Bulletin*, 94, 1050, s.57-62.

Hassani, F.P., Nokken, M.R. ve Annor, A., 2007. Physical and mechanical behaviour of various combinations of minefill materials, *CIM Bulletin*, 100, 1101, s.1–6.

Hoek, E., 2000, Rock engineering course notes by Evert Hoek, http://www.rockscience.com/education/hoeks_corner, (09.08.2012).

Kesimal, A., Ercikdi, B. ve Yilmaz, E., 2003. The effect of desliming by sedimentation on paste backfill performance, *Minerals Engineering,* 16, s.1009-1011.

Kesimal, A., Yılmaz, E. ve Ercikdi, B., 2004. Evaluation of paste backfill test results obtained from different size slumps with varying cement contents for sulphure rich mill tailings, *Cement and Concrete Research*, 34, 10, s.1817-1822.

Kesimal, A., Deveci, H., Alp, İ., Erçıkdı, B., ve Cihangir, F., 2010. Optimization of paste backfill performance for different ore types in Cayeli copper mine, *Project report*, s.42, Karadeniz Teknik Üniversitesi, Trabzon.

Kesimal, A., Deveci, H., Erçıkdı, B., Cihangir, F., İzki, M., ve Baki, H., 2012. Evaluation of paste backfill performance of different mill tailings in Küre copper mine, *Project report*, s.42, Karadeniz Teknik Üniversitesi, Trabzon.

Klein, K. ve Simon, D., 2006. Effect of specimen composition on the strength development in cemented paste backfill, *Canadian Geotechnical Journal*, 43, s.310–324

Landriault, D. ve Deneka, E., 2000. Comparision laboratory study of Cayeli Mine's Clastic ore and Spec ore tailings in paste form, *Golder PasteTec Project Report*, Ontario, Canada, 23p.

Revell, B., 2004. Paste–how strong is it?, *Proceedings of The 8th International Symposium with Backfill*, Beijing, China, s.286–294.

Tariq, A. ve Nehdi, M., 2007. Developing durable paste backfill from sulphidic tailings, *Waste Management Research*, 160, 4, s.155–166.

Ünver, B., 2012. Kişisel görüşme. Hacettepe Üniversitesi Maden Mühendisliği Bölümü, Ankara.

Yılmaz, E., Benzaazoua, M., Belem, T. ve Bussiere, B., 2009. Effect of curing under pressure on compressive strength development of cemented paste backfill, *Minerals Engineering*, 22, 9-10, s.772-785.

Yin, S., Wu, A., Hu, K., Wang, Y. ve Zhang, Y., 2012. The effect of solid components on the rheological and mechanical properties of cemented paste backfill, *Minerals Engineering*, 35, s.61–66.

Yumlu, M., 2010. Pastefill - becoming a feasible and popular option for ensuring recovery of high grade deposits, *Cobar Mining Seminar 2010*, The Australasian Institute of Mining & Metallurgy, New South Wales, Australia, s.26.

Zayıf Kayaçlarda Kohezyonun Dolaylı Olarak Tahmini
Indirect Estimation of Cohesion in Weak Rocks

E. Köken
Bülent Ecevit Üniversitesi, Maden Mühendisliği Bölümü, Zonguldak

ÖZET Zayıf kayaçların jeomekanik özelliklerinin belirlenmesi, uygun boyutlarda karot alınmasının zorluğu ve deneyler sırasında sıklıkla karşılaşılan sorunlar (oluşan yenilme yüzeyinin düzensizliği, üç eksenli basınç deneyindeki yanal basınç seçimi, deney esnasında kayaçtaki ezilmeler vb.) sebebiyle çoğu kez güvenilir bir şekilde gerçekleştirilememektedir. Özellikle bu durum tek eksenli basınç, üç eksenli basınç ve deformobilite deneylerinde kendini açıkça göstermektedir. Bu çalışmada zayıf kayaçların (σ_c<50MPa) kohezyonunun dolaylı olarak belirlenmesi için 13 farklı kayaç üzerinde (kiltaşı, silttaşı, traverten, kumtaşı, andezit, konglomera, tüf vb.) bir dizi kaya mekaniği deneyleri yapılmıştır. Deney yöntemlerinin seçiminde numunelerin kolay hazırlanması ve pratik deneyler (dolaylı çekme dayanımı, P-dalgası hızı vb.) olmasına dikkat edilmiştir. Ayrıca, kayaçların ayrışma-bozunma durumları da gözönünde bulundurularak basit ve çoklu regresyon analizleri gerçekleştirilmiştir. Geliştirilen modellerin uygunluğu ki-kare uygunluk testi ile kontrol edilmiş ve önerilen görgül bağıntıların geçerli olduğu görülmüştür. Sonuç olarak, zayıf kayaçların kohezyonunun önerilen görgül bağıntılar ile yeterli güvenilirlikte dolaylı olarak tahmin edilebileceği belirlenmiştir.

ABSTRACT Estimation of the geomechanical properties of weak rocks cannot usually be realized reliably due to the difficulties encountered in obtaining the core samples with proper dimensions and those encountered during the tests (i.e. disorder in the failure surfaces occurred, selection of the confining pressure in triaxial tests and crushing in core samples during the test). This situation is seen in uniaxial compression, triaxial compression and deformability tests in particular. In this study, several rock mechanics tests have been performed on thirteen different rock types (i.e. claystone, siltstone, travertine, sandstone, andesite, conglomerate, tuff etc.) in order to indirect estimate the cohesion of weak rocks (σ_c<50MPa). In selection of the tests, special attention has been paid to ease of preparation of rock samples and selecting tests that are practically performable (i.e. indirect tensile strength test, P-wave velocity etc.). Besides, simple and multiple regression analysis have been conducted considering the weathering degree of the rocks used. The convenience of developed models has been verified by x^2 suitability test and it has been seen that the models are eligible. It was concluded that the cohesion of weak rocks could be estimated with sufficient reliability by the proposed empirical formulas.

1 GİRİŞ

Zayıf kayaçların jeomekanik özelliklerinin net olarak ortaya konması, çoğu kez sağlıklı bir şekilde gerçekleştirilememektedir. Uygun boyutlarda karot alınamayışı, kayaçların suya olan hassasiyetleri, ayrışma-bozunma durumları ve deney esnasında karşılaşılan sorunlar sağlıklı deney sonuçlarının elde edilmesini güçleştirmektedir. Bu durum saha ve proje mühendislerinin çoğu kez en uygun mühendislik tasarımını yapabilmelerine engel olmaktadır. Bazı durumlarda ise tasarım için gerekli girdi parametrelerinin sayısal olarak temin edilemeyişi, bunun yerine eski tecrübelerin kullanılışı (özellikle tünel, şev, temel ve tahkimat

tasarımında), proje maliyeti, güvenilirliği ve iş güvenliğini doğrudan etkilemektedir. Çağın gereklerine uygun mühendislik tasarımı; yeterli sayıda güvenilir verinin tecrübeli ekipler tarafından değerlendirilmesi ve bu doğrultuda yapılan çalışmaların bir bütünü olarak tanımlanmaktadır.

Olaya bu açıdan bakıldığında, kaya malzemesi daha geniş anlamıyla da malzeme bilimi ile ilgilenen bütün disiplinlerde, kullanılacak malzemeye ait istenen fiziksel ve mekanik büyüklüklerin belirlenmesinde ilgili standartlara uygun boyutlarda numune hazırlamak oldukça önemlidir. Çelik, beton, demir ve teknolojik imkânlar dâhilinde hazırlanan diğer malzemeler genellikle homojen ve izotrop olarak kabul edilmektedir. Bu malzemelerden elde edilen deney sonuçlarındaki sapmalar ve olası sorunlar, genellikle imalat hataları, operatör etkisi ile kullanılan deney setindeki problemlerden kaynaklanmaktadır. Buna karşın, kaya malzemesi ve kütlesi ile ilgilenen disiplinlerde (kaya mekaniği, mühendislik jeolojisi vb.) ise, sağlıklı deney sonuçlarının alınamayışının birden çok sebebi olabilir. Bu sebeplerin başında kullanılan malzemenin doğası gereği var olan düzensizlikler akla gelmektedir. Bu düzensizlikler; kayaçtaki makro ve mikro süreksizlikler, tabakalanma, kayacın dolgu durumu, mineralojik bileşim, ayrışma-bozunma durumu ve anizotropi özelliği olarak sıralanabilir.

Araziden alınan, ayrışmamış, az sayıda süreksizlik içeren ve en az derecede örselenerek temin edilmiş kaya bloklarından hazırlanan, süreksizlik ve herhangi bir arıza içermeyen numuneleri homojen ve izotrop kabul ederek kayaçlara ait istenen fiziksel ve mekanik büyüklükler elde edilmektedir. Ancak belirgin olarak ayrışmış, suya karşı hassasiyeti olan, çok sayıda süreksizlik içeren ve dayanımı düşük kayaçlardan hazırlanan numuneleri homojen ve izotrop olarak kabul etmek tartışmaya açık bir konu olmakla birlikte, bu tür kayaçlarla çalışmak çoğu kez sorunları beraberinde getirir. Zayıf kayaçlar üzerinde doğrudan yapılamayan deneyler için yaklaşık çözüm; daha kolay yapılabilen deney sonuçlarından türetilen görgül bağıntıları kullanarak istenilen büyüklüğü belirli bir güven aralığında dolaylı olarak tahmin etmektir.

Kohezyon kısaca, normal gerilmenin etkimediği bir düzlem boyunca, kaya malzemesinin yenilmesi için gerekli olan kayma gerilmesi olarak tanımlanmakta ve özellikle kaya mekaniği ile mühendislik jeolojisinde önemli bir girdi parametresi olarak kabul edilmektedir. Kaya malzemesinin kohezyonu yaygın olarak, farklı yanal basınçlar altında gerçekleştirilen üç eksenli basınç deneyleri ile belirlenmektedir. Üç eksenli basınç deneyleri dışında kaya malzemesinin kohezyonun doğrudan belirlenmesi için, Prodotyakonov (1969) ve Vutukuri (1974) ise tek kesme yüzeyli ve çift kesme yüzeyli deney düzeneklerini kullanmıştır. Lundborg (1968) ve Andreev (1995) ise, basınç uygulayan çift kesme yüzeyli deney düzeneğini kullanarak elde ettiği kohezyon değerlerinin üç eksenli basınç deneylerinden elde edilen kohezyon değerinden yüksek olduğunu belirtmiştir. Yaralı (1999) geliştirdiği tek kesme yüzeyli çift yükleme bloklu deney düzeneğini beton, alçı, kumtaşı, kireçtaşı ve marn örneklerini kullanarak elde ettiği kohezyon değerlerinin üç eksenli basınç deneylerinden elde edilen kohezyon değerlerine yakın olduğunu belirlemiştir.

Kaya malzemesine ait kohezyonun doğrudan kestirimi için diğer bir yöntem ise Wuerker (1959) yöntemidir. Bu yöntem üç eksenli basınç deneylerinin yapılamadığı durumlarda kaya malzemesi kohezyonunun kabaca tahmin edilmesi için kullanılmaktadır (Şekil 1).

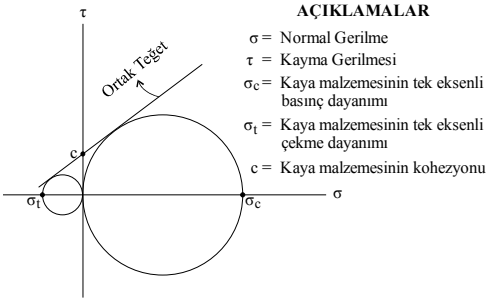

Şekil 1. Wuerker (1959) yöntemine göre kaya malzemesinin kohezyonun kestirimi

Cuisiat (2011) ise şeyller üzerinde yaptığı deneylerde, kaya malzemesi kohezyonu (c, MPa) ile görünür porozite arasında anlamlı bir ilişki tespit etmiştir. Buna göre, şeyllerin görünür porozitesinin (n, %) 7–38 aralığındaki kohezyonu Eşitlik 1 ile tahmin edilebilmektedir.

$$c = 57,868 \times n^{-0,859}, R^2 = 0,85 \quad (1)$$

Kaya malzemesi kohezyonu ve içsel sürtünme açısının tahmininde günümüzde oldukça sık kullanılan diğer görgül bağıntılar ise Hoek vd. 2002 tarafından önerilmiştir. Eşitlik 2, Hoek – Brown yenilme ölçütüne göre kaya malzemesinin kohezyonu, Eşitlik 3 ise kaya malzemesinin içsel sürtünme açısının belirlenmesi için kullanılmaktadır. Eşitlik 2 ve Eşitlik 3'te yer alan σ'_{3n} ifadesi ise Eşitlik 4 kullanılarak bulunur.

Hoek – Brown yenilme ölçütüne göre, kaya malzemesinin a üstel katsayısı 0,5, kaya malzemesinin çatlaklılık durumunu ifade eden s parametresi ise 1 olarak kabul edilmektedir. Eşitlik 2 ve Eşitlik 3'te yer alan m_i parametresi ise kaya malzemesinin kendine özgü bir dayanım parametresi olarak düşünülebilir. m_i parametresi üç eksenli deney sonuçlarına göre belirlenebildiğini gibi, Aydan vd. (2012) m_i parametresinin belirlenmesi için kaya malzemesinin tek eksenli basınç ve çekme dayanımına bağlı olduğunu belirtmektedir. Pratik olarak kaya malzemesine ait m_i değeri Eşitlik 5 ile belirlenebilir. Konu ile ilgili diğer ayrıntılar Hoek vd. 2002'de yer almaktadır.

$$c = \frac{\sigma_c[2+(0,5m_i\sigma_{3n})][1+m_i\sigma_{3n}]^{-0,5}}{3,75\sqrt{0,27+\left(0,8m_i(1+m_i\sigma_{3n})^{-0,5}\right)}} \quad (2)$$

$$\phi = \sin^{-1}\left[\frac{3m_i(1+m_i\sigma_{3n})^{-0,5}}{7+3m_i(1+m_i\sigma_{3n})^{-0,5}}\right] \quad (3)$$

$$\sigma_{3n} = \frac{1,875}{(m_i+16)(m_i+4)^{-0,5}} \quad (4)$$

$$m_i = \left|\frac{16\sigma_{tB}}{\sigma_c} - \frac{\sigma_c}{\sigma_{tB}}\right| \quad (5)$$

Bunun yanı sıra, kaya malzemesinin tek eksenli basınç dayanımı ile kohezyonu arasında sıkı bir ilişki olduğu bilinmektedir. Dayanımın bir ölçüsü olarak da düşünülebilen kohezyon ile kayaçların diğer mekanik özellikleri ile bireysel ilişkiler kurmak mümkündür. Buna çift makaslama dayanımı (BPI, MPa) örnek gösterilebilir. Ulusay ve Gökçeoğlu 1997 ile Ulusay vd. 2001 çift makaslama dayanımı ile kaya malzemesinin tek eksenli basınç ve dolaylı çekme dayanımı arasında anlamlı ilişkiler olduğunu tespit etmiştir. Sülükçü ve Ulusay (2001) çift makaslama deneyi üzerine çalışmalarına devam ederek, kaya malzemesinin kohezyonu ile çift makaslama dayanımı arasında anlamlı bir ilişki belirlemiştir (Bkz. Eşitlik 6).

$$c = 1,207BPI \quad (6)$$

Özetle, üç eksenli basınç dayanımı deneyi, tecrübe gerektiren zahmetli ve önemli bir kaya mekaniği deneyidir. Zayıf kayaçlarda yanal basınç seçimi, numune hazırlama, kullanılan malzemenin doğası gereği düzensiz oluşu ve olası operatör hataları kaya malzemesinde kohezyonun sağlıklı bir şekilde belirlenmesini güçleştirmektedir. Uygulamalarda saha mühendislerine kolaylık sağlamayı amaçlayan bu çalışma, yapılması kolay, maliyeti ucuz ve tekrarlanabilirliği yüksek olan deneylerle kaya malzemesinde kohezyonun dolaylı olarak tahmini üzerine bir incelemesini içermektedir.

2 NUMUNE HAZIRLAMA

13 farklı kayaç üzerinde yapılan kaya mekaniği deneylerinde, boy (*l*) / çap (d) oranları 0,5–2 arasında değişen silindirik numuneler alınmıştır. Silindirik numuneler NX (54± 0,4 mm çapında) ve BX (42± 0,6 mm çapında) tip karotiyerler kullanılarak temin edilmiştir.

Dolaylı çekme dayanımı deneyleri için l/d oranı 0,5, P dalga hızının ölçülmesi ve tek eksenli basınç dayanımı deneylerinde l/d oranı 1–2 arasında, üç eksenli basınç deneylerinde ise l/d oranı 2 olan silindirik numuneler hazırlanmıştır. Numune litolojileri, alındığı bölgeler ve yapılan deneylerde kullanılan numune sayıları Çizelge 1'de verilmiştir.

Çizelge 1. Çalışmada kullanılan kaya türleri, alındığı bölgeler ve numune sayıları

Kaya Türü	Örnek No	Alındığı Yer	Numune Sayısı			
			TEBD	DÇD	ÜEBD	PDH
Tüf[1]	1	Havran - Balıkesir	8	10	4	8
Traverten	2	Honaz - Denizli	9	12	4	9
Andezit	3	Havran - Balıkesir	9	10	3	9
Konglomera	4	Havran - Balıkesir	5	5	3	5
Çamurtaşı	5	Havran - Balıkesir	4	5	3	4
Şeyl	6	Havran - Balıkesir	5	5	3	5
Tüf[2]	7	Develi - Kayseri	7	10	3	7
Kumlu Kireçtaşı	8	Havran - Balıkesir	5	6	2	5
Siltli Çamurtaşı	9	Edremit - Balıkesir	6	5	3	6
İnce Taneli Kumtaşı	10	Havran - Balıkesir	5	5	3	5
Silttaşı	11	Üzülmez - Zonguldak	9	8	3	9
Kiltaşı	12	Üzülmez - Zonguldak	5	5	3	5
Orta Taneli Kumtaşı	13	Bor - Niğde	5	5	4	5

AÇIKLAMALAR

TEBD: Tek eksenli basınç dayanımı — PDH: P dalga hızı

ÜÇBD: Üç eksenli basınç dayanımı — DÇD: Dolaylı çekme dayanımı

3 DENEYSEL ÇALIŞMALAR

Bu çalışma kapsamında; en çok kullanılan, numune hazırlaması ve yapılması kolay deneylerin seçilmesine özen gösterilmiştir. Bu sebepten zayıf kayaçların kohezyonun dolaylı olarak belirlenmesi için, dolaylı çekme dayanımı (DÇD), tek eksenli basınç dayanımı (TEBD), üç eksenli basınç dayanımı (ÜEBD) ile P dalgası hızı (PDH) deneyleri yapılmıştır. Yapılan deneylerde ISRM (1981) tarafından önerilen yöntemler esas alınmıştır. Gerçekleştirilen bütün deneyler kuru şartlar altında gerçekleştirilmiş olup, deney sonuçları Çizelge 3'te toplu olarak verilmiştir.

Ayrıca numunelerin hazırlanma süreçlerinde kayaçların ayrışma-bozunma durumları, ayrışmış ve ayrışmamış durumlardaki renk ve dokusal değişimi göz önünde bulundurularak ISRM (1981)'e göre sınıflandırılmıştır. Buna göre çalışmada kullanılan kayaçlar ayrışmamıştan (W_1) ileri derecede ayrışmış kayaca (W_4) değişen bir aralıktadır.

3.1 Tek Eksenli Basınç Dayanımı Deneyi

Tek eksenli basınç dayanımı deneyleri ISRM 1981 tarafından önerilen yöntem ile ASTM D2938' e uygun olarak gerçekleştirilmiştir. Deneylerdeki yükleme hızı zayıf kayaçlar için yaklaşık 0,5MPa/s olarak tercih edilmiştir. Araziden temin edilen kaya bloklarının içerdiği süreksizlikler ve ayrışma-bozunma durumları ve numune alma esnasında karotların parçalanmaları dikkate alındığında, deney için gerekli geometrik şartlar (Bkz. ASTM D2938–95, ISRM 1981) çoğu kez sağlanamamıştır.

Bu sebepten uygun boyutlarda alınamayan karotlarda yapılan deney sonuçları *l*/d=2 oranı dikkate alınarak ASTM D2938-95'e göre Eşitlik 7 kullanılarak düzeltilmiştir. Eşitlik 7, *l*/d oranının 1–2 aralığında olması durumunda geçerlidir.

$$\sigma_{(2/1)} = \frac{\sigma_{(l/d)}}{0,24 \times \frac{d}{l} + 0,88} \quad (7)$$

Yapılan tek eksenli basınç dayanımı deney sonuçlarına göre, 13 farklı kayacın tek eksenli basınç dayanımları *l*/d=2 düzeltmesi ile ortalama 16,15MPa ile 47,97 MPa arasında değişmektedir. ISRM (1981)' göre çalışmada kullanılan kayaçlar düşük ve orta dayanımlı, Deere ve Miller (1966)'a göre ise düşük dayanımlı kayaç sınıfında yer almaktadır.

3.2 P Dalgası Hızı Deneyi

P dalga hızı deneyi, kayacı örselememesi, tekrarlanabilirliği yüksek bir deney olması ve kaya malzemesinin bazı fiziksel ve mekanik özellikleri ile anlamlı ilişkilere sahip olması sebepleriyle son zamanlarda kaya mekaniğinde sıklıkla kullanılmaktadır. P dalga hızı deneyleri, P dalga hızı (V_p), karotun bir ucundan diğer ucuna gönderilen ultrasonik dalganın hızıdır (Bkz. Eşitlik 8).

$$V_p = \frac{L}{\eta} \quad (8)$$

Eşitlik 8'de ifade edilen L karot boyunu (mm), η ise karotun bir ucundan diğer ucuna geçen ultrasonik dalganın geçtiği süreyi (μs) ifade etmektedir. Pundit Plus deney aleti kullanılarak ASTM D2845-69'a uygun olarak yapılan deney sonuçlarına göre ortalama V_p hızları 1,47 km/s – 4,03 km/s arasında değişmektedir.

Kayaçların ayrışma-bozunma derecelerinin (W_d) sayısal olarak belirlenmesi ve analizlere dahil edilebilmesi için, P dalga hızları istatistiksel kurallar dahilinde kullanılmıştır. İstatistikte herhangi bir büyüklüğün (örneğin β) alabileceği en yüksek ve en düşük değeri Eşitlik 9 ile belirlenmektedir.

$$\beta_{\max} = \beta_{ort} \pm 3ss \quad (9)$$

Burada β_{max} ve β_{ort} sırasıyla herhangi bir büyüklüğün en yüksek ve ortalama değerleri, ss ise bu büyüklüğe ait standart sapma olarak tanımlanmaktadır. Bu istatistiksel kural doğrultusunda W_d değeri P dalga hızına göre Eşitlik 10 ile belirlenmiştir.

$$W_d = \frac{V_{p(ort)} + 3ss}{V_{p(ort)} - 3ss} \quad (10)$$

Burada $V_{p(ort)}$ kayaçların ortalama P dalga hızı (km/s), ss ise p dalga hızlarına ait standart sapma değerlerini ifade etmektedir. Buna göre ISRM (1981) tarafından önerilen ayrışma-bozunma sınıflamasına göre, kayaçların ayrışma bozunma indeksi değer aralığı Çizelge 2'de verilmiştir.

Çizelge 2. Kayaçların ayrışma-bozunma indeksi değerleri

Ayrışma-Bozunma Derecesi	Tanımlama	W_d
W_1	Ayrışmamış	1-1,6
W_2	Az Ayrışmış	1,6-2,5
W_3	Orta Derecede Ayrışmış	2,5-3,4
W_4	İleri Derecede Ayrışmış	>3,4

3.3 Dolaylı Çekme Dayanımı Deneyi

Dolaylı çekme dayanımı deneyi (Brazilian Deneyi) gerek numune hazırlaması kolay, gerekse pratik bir deney olması sebebiyle yaygın olarak kullanılmaktadır. Kayaçların dolaylı çekme dayanımı Eşitlik 11 ile belirlenmektedir.

$$\sigma_{tB(MPa)} = \frac{2F}{\pi Dt} \quad (11)$$

Burada F kırılma yükü (N), D numune çapını (mm), t ise numune kalınlığını (mm) göstermektedir. Buna göre 13 farklı kayaçtan hazırlanan disk numuneler üzerinde yapılan deney sonuçlarına göre, kayaçların ortalama dolaylı çekme dayanımı 0,7MPa ile 6,3MPa arasında değişmektedir.

3.4 Üç Eksenli Basınç Dayanımı Deneyi

Üç eksenli basınç deneyi, farklı yanal basınçlar altında (σ_3) kaya malzemesinin dayanımının belirlenmesi olarak tanımlanabilir. σ_3= 0 durumunda kaya malzemesini yenmek için gerekli olan gerilme kayacın tek eksenli basınç dayanımı olarak tanımlanmakta olup, farklı σ_3 değerleri altında kayacın dayanımını yanal sıkışmaya bağlı olarak artacaktır. Deneyin amacı, en temel olarak kaya malzemesinin kayma parametrelerinin belirlenmesi (kohezyon ve içsel sürtünme açısı) olarak düşünülebilir. Mohr – Coulomb yenilme ölçütüne göre kaya malzemesinin kayma parametreleri içsel sürtünme açısı (ϕ, °) ve kohezyon (c, MPa) olarak tanımlanmaktadır.

Bunun için farklı yanal basınçlarda yapılan 3–4 deney ile kaya malzemesine ait yenilme zarfi oluşturularak kayacın c ve ϕ değerleri ayrıca Hoek-Brown sabitlerinden m_i bulunur. Kaya malzemesinin c ve ϕ değerleri ISRM (1981)'e göre üç farklı şekilde belirlenebilir. Bu çalışmada farklı karotların değişik yanal basınçlar altındaki eksenel dayanım değerleri tespit edilerek kayma parametreleri belirlenmiştir.

Kayaçların kohezyonu için Eşitlik 12, içsel sürtünme açılarının belirlenmesi için ise Eşitlik 13 kullanılmıştır.

$$c = q \times \frac{1-\sin\phi}{2\times\cos\phi} \qquad (12)$$

$$\phi = \arcsin\left(\frac{m-1}{m+1}\right) \qquad (13)$$

Burada q, $\sigma_1 - \sigma_3$ uzayındaki dayanım zarfının σ_1 eksenini kestiği noktanın değeridir. Başka bir deyişle q değeri, $\sigma_3 = 0$ olduğu durumdaki eksenel gerilmenin büyüklüğü olarak tanımlanan dayanım zarfindaki tek eksenli basınç dayanımı değeridir. m değeri ise dayanım zarfının eğimi olarak tanımlanmaktadır.

Yapılan üç eksenli deney sonuçlarında zayıf ve orta dayanımlı kayaçlar için yanal basınçlar (σ_3) 2MPa ile 15MPa arasında seçilmiştir. Buna göre 13 farklı kaya malzemesinin c değerleri 3MPa ile 10MPa arasında, ϕ değerleri ise 32° ile 51° arasında değiştiği belirlenmiştir (Çizelge 3).

4 İSTATİSTİKSEL ANALİZ

Kayaçların farklı fiziksel ve mekanik özellikleri arasındaki anlamlı ilişkileri göz önünde bulundurulduğunda, kaya malzemesinin kohezyonu ile bazı mekanik özellikleri arasında bireysel ilişkiler kurulabileceği daha önce belirtilmişti. Örneğin, kayaçların dayanımı ile kohezyonu arasında genellikle doğrusal bir ilişki vardır. Ancak doğadaki kayaçların litolojik çeşitliliği ve ayrışma-bozunma durumları kayaçların herhangi bir fiziksel veya mekanik özelliğinin kestirimi için genel bir yaklaşım ortaya koymayı güçleştirmektedir.

Bu kapsamda, düşük dayanımlı kayaçların σ_c, V_p, σ_{tB} ve W_d değerleri kullanılarak, bu analizlerine ilave edilmiştir. Gerçekleştirilen basit ve çoklu regresyon analizlerinde kullanılacak olan değişkenlerin birimleri; c = MPa, σ_c = MPa, σ_{tB} = MPa ve V_p = km/s olup, geliştirilen eşitlikler boyut analizi içermemektedir.

Kayaçların dayanımı arttıkça genellikle, c, σ_c, V_p ve σ_{tB} değerlerinin de artması beklenir. Kayaçların litolojik farklılıkları, ayrışma-bozunma durumları, dayanım anizotropisi gibi özellikleri bu büyüklükler arasından dolaylı çekme dayanımının P dalgası hızına oranının ($\psi = \sigma_{tB} / V_p$) kayaçtan kayaca farklı olmasına sebep olmaktadır. Burada tanımlanan ψ değerindeki bu değişimin zayıf kayaçların kohezyonunun bir ölçüsü olup olmadığı bu çalışmada bir hipotez olarak ileri sürülmüş ve basit regresyon analizi ile irdelenmiştir.

İstatistiksel analizlere geçmeden önce yukarıda tanımlanan ψ değer aralığının belirlenmesi gerekmektedir. Bu kapsamda ψ değerinin tanımlanabilen en geniş tanım kümesi, literatürde bilinen en yüksek ve en düşük σ_{tB} ve V_p değerlerinin kendi aralarında çaprazlama yapılması ile elde edilebilir.

Çizelge 3. Deney sonuçlarının toplu gösterimi

Kaya Türü	Örnek No	σ_c (MPa)*	σ_{tB} (MPa)	V_p (km/s)	c (MPa)	ϕ (°)	m_i	Ayrışma Derecesi**	
								Tanım	W_d
Tüf[1]	1	16,1± 6,6	0,7±0,1	1,4±0,3	3,2	50,4	15,8	W_4	4,3
Traverten	2	25,7± 12,2	2,1±0,7	2,2±0,4	5,6	40,1	12,3	W_4	3,4
Andezit	3	41,4 ± 7,1	5,3±0,5	3,3±0,5	8,1	37,9	10,4	W_3	2,8
Konglomera	4	26,2±5,9	1,7±1,2	2,7±0,4	4,3	43,5	14,7	W_3	2,7
Çamurtaşı	5	33,4±6,7	2,4±0,5	2,3±0,3	6,5	36,8	11,2	W_2	2,2
Şeyl	6	23,8±9,5	1,5±0,5	2,2±0,3	4,8	39,1	9,0	W_2	2,5
Tüf[2]	7	40,2±12,2	2,9±0,8	3,1± 0,4	7,3	45,9	12,7	W_3	2,6
Kumlu Kireçtaşı	8	32,7±10,1	3,3±1,6	2,7± 0,3	6,9	42,7	10,1	W_2	2,0
Siltli Çamurtaşı	9	41,8±8,2	2,8±0,3	2,4±0,3	8,4	32,0	14,1	W_2	2,3
İnce Taneli Kumtaşı	10	24,0±14,9	1,85±0,44	1,8±0,3	5,7	39,7	7,9	W_3	3,1
Silttaşı	11	40,9±13,6	3,1±1,2	2,1±0,21	8,6	34,6	9,4	W_2	1,9
Kiltaşı	12	36,5±7,3	6,3±0,9	4,1±0,2	9,5	38,1	5,8	W_1	1,4
Orta Taneli Kumtaşı	13	47,9±9,1	5,7±1,1	3,9±0,4	9,1	40,7	9,2	W_2	1,9

AÇIKLAMALAR

*: Ortalama (ort) ± standart sapma (ss)

**: ISRM (1981)'e göre kayaçların ayrışma dereceleri

Kayaçların V_p hızları genellikle 1km/s ile 7,7km/s arasında değişmektedir (Castagna vd. 1985, Franklin ve Dusseault, 1989, Goodman 1989, Tercan vd. 2005, Zamora vd. 1994, Schön 1996, Tuğrul ve Zarif 1999, Kahraman 2001, Zarif ve Tuğrul 2003, Teymen 2005, Sharma ve Singh 2008, Yağız 2011, Altındağ 2012). Kayaçların σ_{tB} değerleri ise genel olarak 0,1MPa ile 42 MPa arasındadır (Çolak 1998, Zhang 2005, Tercan vd. 2005, Mosch ve Siegesmund 2007, Dai ve Xia 2009, Mendoza-Chavez vd. 2012).

Bu kapsamda kayaçlara ait ψ değerinin en geniş tanım kümesinin 0,013 (σ_{tB} = 0,1MPa ve V_p = 7,7km/s değerleri için) ile 42 (σ_{tB} = 42MPa ve V_p = 1km/s değerleri için) arasında değiştiği matematiksel olarak mümkündür. Ancak uygulamalarda bu kadar geniş bir aralığın varlığından söz etmek doğru olmayabilir. Dayanımı artan kayaçta genel olarak artması beklenen σ_{tB} ve V_p gibi büyüklüklerin zayıf ve yüksek dayanımlı kayaçlara ait olan değerleri kendi aralarında değerlendirilirse gerçeğe daha yakın bir tanım kümesi oluşturulabilir. Buna göre Deere ve Miller (1966)'a göre düşük dayanımlı olarak tanımlanan kayaçlar için (σ_c < 50MPa olan kayaçlar) ψ değerinin üst sınırı (V_p = 4km/s ve σ_{tB} = 10MPa değerleri için), ψ = 2,5olurken, alt sınır ise (V_p = 1km/s ve σ_{tB} = 0,1MPa değerleri için) ψ = 0,1 olarak ifade edilebilir. Buradan zayıf kayaçların dayanımının değişmesi ile ψ değerinin 0,1 ile 2,5 arasında değişebileceği söylenebilir. (Şekil 2).

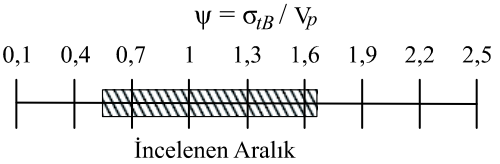

Şekil 2. Zayıf kayaçlar için ψ değerinin değişimi ve incelenen aralık

4.1 Basit Regresyon Analizi

Basit regresyon analizi için Menten – Michaelis (1913) tarafından önerilen analitik model kabul edilmiş ve en küçük kareler yöntemi ile çözülmüştür. Analitik model Eşitlik 14'te ifade edilmektedir. Herhangi bir denklem sisteminin en küçük kareler yöntemi ile çözülmesi için denklem

sisteminde yer alan bilinmeyenlerin (m_1 ve m_2 gibi) doğrusal bir denklem sisteminde yer alması gerekmektedir. Eşitlik 8'deki bağımlı ve bağımsızlık değişkenler sırasıyla; y = c ve $x = \psi = \frac{\sigma_{tB}}{V_p}$ olarak tanımlanmaktadır. Eşitlik 14'te verilen denklem sisteminin doğrusal hale getirilmesi ve en küçük kareler yöntemin uygulanması ile Eşitlik 15 elde edilmiştir.

$$y = \frac{m_1 \times x}{m_2 + x} \tag{14}$$

$$c = \frac{54,94\sigma_{tB}}{7,82V_p + \sigma_{tB}}, R^2 = 0,85 \tag{15}$$

4.2 Çoklu Regresyon Analizi

Çoklu regresyon analizleri, $\sigma_c - W_d$, $\sigma_c - \sigma_{tB}$ ve $\sigma_{tB} - V_p$ veri çiftleri kullanılarak gerçekleştirilmiştir. $\sigma_c - \sigma_{tB}$ çifti ile çoklu doğrusal regresyon analizi, $\sigma_{tB} - V_p$ ve $\sigma_c - W_d$ veri çiftleri kullanılarak ise doğrusal olmayan çoklu regresyon analizi yapılmıştır. Çoklu doğrusal regresyon analizlerinde kullanılan analitik model Eşitlik 16'da verilmiştir.

$$y = ax_1 + bx_2 \tag{16}$$

$\sigma_c - \sigma_{tB}$ veri çifti kullanılarak gerçekleştirilen çoklu regresyon analizi sonucunda Eşitlik 17 elde edilmiştir.

$$c = 0,16\sigma_c + 0,37\sigma_{tB}, R^2 = 0,82 \tag{17}$$

Doğrusal olmayan çoklu regresyon analizlerinin ilki için $\sigma_{tB} - V_p$ veri ikilisi kullanılmış olup, regresyon analizinde Eşitlik 18'deki analitik model benimsenmiştir. Eşitlik 18'de, y = c, $x_1 = \sigma_{tB}$ ve $x_2 = V_p$ için Eşitlik 19 elde edilmiştir.

$$y = t_1 \times x_1^{t_2} \times x_2^{t_3} \tag{18}$$

$$c = 5,12\sigma_{tB}^{0,75}V_p^{-0,53}, R^2 = 0,88 \tag{19}$$

Benzer şekilde Eşitlik 18'deki analitik model kullanılarak $\sigma_c - W_d$ veri çifti ile ikinci doğrusal olmayan çoklu regresyon analizi gerçekleştirilmiştir. y = c, $x_1 = \sigma_c$ ve $x_2 = W_d$ olmak üzere Eşitlik 20 elde edilmiştir.

$$c = 0,48\sigma_c^{0,81}W_d^{-0,26}, R^2 = 0,86 \tag{20}$$

5 TARTIŞMA VE SONUÇLAR

Yapılan basit ve çoklu regresyon analizlerinden elde edilen görgül bağıntıların uygunluğu ki kare (x^2) testi ile kontrol edilmiştir. Ki kare testine göre bir modelin uygun olup olmadığı modelden elde edilen değerlerin (gözlenen değer, o_i) deneysel değerlere (beklenen değer, e_i) olan yakınlığı ile ilgilidir. Bu bağlamda x^2 değeri Eşitlik 21 yardımı ile belirlenecektir. Bir modelin geçerli olup olmadığı, elde edilen x^2 değerinin belirli bir güven aralığında (G) ve buna bağlı serbestlik derecesinde (λ) tabloda verilen x^2 değerinden küçük olmasına bağlıdır. Aksi halde önerilen model reddedilecektir. Geliştirilen bağıntıların geçerliliği bu şekilde irdelenmiştir. Modellerin serbestlik dereceleri $\lambda = n - v - 1$ şeklinde belirlenmiştir. Burada n örnek sayısını, v analizlerde kullanılan değişken sayısını ifade etmektedir.

$$x^2 = \sum_{i=1}^{n=13} \frac{(o_i - e_i)^2}{o_i} \tag{21}$$

Buna göre, geliştirilen eşitliklere ait x^2 değerlerinin G = 0,9 güven aralığı ve $\lambda = 9$ koşullarında geçerli olduğu Çizelge 4'ten anlaşılmaktadır.

Çizelge 4. x^2 uygunluk testi sonuçları

Eşitlik No	15	17	19	20
x^2	0,864	1,047	0,716	0,88
x^2 Tablo (G=0,9)	4,168	4,168	4,168	4,168
Serbestlik Derecesi (λ=n-v-1)	9	9	9	9

Eşitliklerden tahmin edilen kohezyon değerleri ise; birbirleri, deney sonuçları ve Hoek vd. 2002'den tahmin edilen kohezyon değerleri ile karşılaştırılmıştır. Buna göre 13 farklı kayacın kohezyonu, en fazla yüzde 14'lük hata payı ile tahmin edilebildiği Şekil 3'ten anlaşılmaktadır.

Kayaçların ilerleyen ayrışma-bozunma evrelerinde (fiziksel, kimyasal veya biyolojik bozunma evrelerinde) kaya malzemesinin içyapısında tane sınırları genişlemekte, başka bir deyişle kayaç içindeki atomik bağlar

zayıflamaktadır. Bu bağların zayıflaması ve buna bağlı kayaçta oluşan makro ve mikro ölçekteki kırıklı yapıların varlığı kaya malzemesinin kohezyonunu önemli ölçüde düşürmektedir (Baynes ve Dearman 1978).

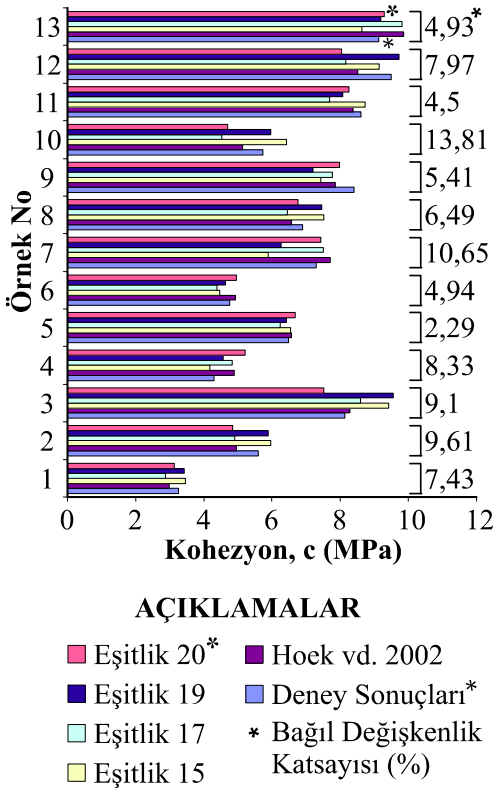

Şekil 3. Görgül bağıntıların karşılaştırılması

Bu bulgu, Arel ve Önalp (1998)'in granodiyoritler üzerinde yaptığı çalışmalarla da desteklenmiştir. Bu çalışmada da zayıf kayaçların ayrışma – bozunma durumları dikkate alınmış ve ayrışmanın kaya malzemesinin kohezyonunu azalttığı niceliksel olarak belirlenmiştir. Eşitlik 20 bu açıdan incelendiğinde, 10MPa < σ_c < 50MPa aralığında kalan kayaçlar için, ilerleyen ayrışma derecesinin kaya malzemesindeki kohezyonu %30 oranında düşürdüğü Şekil 4'ten anlaşılmaktadır.

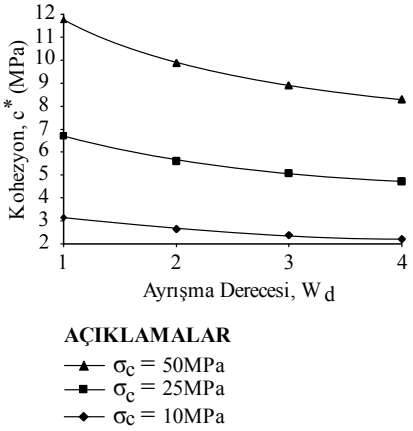

* Eşitlik 20 ile belirlenen kohezyon değerleridir.

Şekil 4. İlerleyen ayrışma derecesinin kohezyon üzerine etkisi

Yürütülen deneysel çalışmalar ve istatistiksel analizler sonucunda bu çalışmadan elde edilmiş bazı sonuçlar aşağıdaki gibi özetlenmiştir.

1- Bu çalışmada önerilen bağıntılar aşağıdaki sınırlamalar dikkate alındığında güvenle kullanılabilir.

- 10 MPa < σ_c < 50 MPa
- 0,7 MPa < σ_{tB} < 6,3 MPa
- 1,4 km/s < V_p < 4 km/s
- 5 < m_i < 16

2- Bu çalışmada kullanılan kayaçlarda yapılan üç eksenli basınç deneylerinde, yanal basınç seçimi kayacın tek eksenli basınç dayanımının en fazla beşte biri ile sınırlı kalmalıdır. Aksi durumlarda anlamsız sonuçlar elde edilmektedir.

3- Kayaçlarda ilerleyen ayrışma derecesinin kaya malzemesinin kohezyonunu üzerine olan etkisi niceliksel olarak belirlenmiştir.

4- Zayıf kayaçlarda kohezyonun dolaylı tahmini üzerine yapılmış olan bu çalışma, örnek sayısı arttırılarak daha sağlıklı ve genel görgül bağıntıların geliştirilmesi için bir başlangıç çalışması olarak kabul edilebilir.

KAYNAKLAR

Altındağ, R. 2012. Correlation between P-wave velocity and some mechanical properties for sedimentary rocks, The Journal of The Southern African Institute of Mining and Metallurgy, Vol: 112, pp. 229-237.

Andreev, G. 1995. Brittle Failure of Rock Materials, Tests, Results and Constitutive Models, A.A. Balkema pp. 411.

Arel, E. ve Önalp, A. 1998. Granitik bir kayada marka ve mikro porozite ile basma dayanımı bağıntısı, 4. Ulusal Kaya Mek. Semp. Bild. Kit. ss. 75-83, Zonguldak.

ASTM D2664-95a. Standard Test Method for Triaxial Compressive Strength of Undrained Rock Core Specimens Without Pore Pressure Measurements.

ASTM D2938-95. Standard Test Method for Unconfined Compressive Strength of Intact Rock Core Specimens.

ASTM D2845-69 Laboratory determination of pulse velocties and ultrasonic elastic constants of rocks.

Aydan, Ö., Tokashiki, N., Geniş, M. 2012. Some Considerations on Yield (failure) Criteria in Rock Mechanics, 46th US Rock Mechanics /Geomechanics Symposium, ARMA: American Rock Mechanics Association 12-640, pp. 8, Chicago.

Baynes, J. ve Dearman, W.R. 1978. The relationship between microfabric and the engineering properties of weathered granite, International Association of Engineering Geology, Vol: 18, pp. 191-198.

Castagna, J.P., Batzle, M.L. ve Eastwood, R.L. 1985. Relationships between compressional-wave and shear wave velocities in clastic silicate rocks, Geophysics. 50, pp. 571–581.

Cuisiat, F. 2011. Cap rock fracturing criteria, Tech. Rep., NGI pp. 23.

Çolak, K. 1998. Zonguldak Kömür Çevre Kayaçlarının Dayanım ve Deformasyon Anizotropisinin İncelenmesi, Doktora Tezi, ZKÜ Fen Bil. Ens., s. 214, Zonguldak.

Dai, F. ve Xia K. 2009. Tensile strength anisotropy of Barre Granite, ROCKENG09: Proceedings of the 3rd CANUS Rock Mechanics Symposium, Toronto.

Deere, D.U. ve Miller, R.P. 1966. Engineering classification and index properties for intact rock. Tech. Rep. No: AFWL-TR-65-116, Air Force Weapons Lab., Kirtland Air Force Base.

Franklin, J.A ve Dusseault M.B 1989. Rock Engineering, McGraw-Hill Pub., pp. 600, USA.

Goodman, R.E, 1989. Introduction to rock mechanics, Second Edition, John and Wiley Pub., pp. 562.

Haik, Y., ve Shahin T. M., 2003. Engineering Design Process. Cengage Learning, 304s. Stamford.

Hoek E., Carranza-Torres C.T. ve Corkum, B., 2002. Proceedings of the fifth North American rock mechanics symposium Vol: 1, pp. 267–273.

Hoffman, J.D. 1992. Numerical Methods for Engineers and Scientists, Second Edition, McGraw-Hill, pp. 825, Newyork.

ISRM .1981. Rock Characterization, Testing and Monitoring –ISRM Suggested Methods, E.T. Brown ed. Pergamon Press, Oxford.

Kahraman, S., 2001. Evaluation of simple methods for assessing the uniaxial compressive strength of rock, Int. J. Rock Mech.Min. Sci., 38, pp. 981–994.

Kılıç, A., Teymen, A., 2008. Determination of mechanical properties of rocks using simple methods. Bulletin of Engineering Geology and the Environment 67 (2), 237–244.

Lundborg, N. 1968. Strength of rock-like materials. Int. J. Rock Mech. Min. Sci., 5, pp. 427-454.

Mendelson, E. 1988, 3000 Solved Problems in Calculus, McGraw-Hill, 455pp.

Mendoza-Chavez, G., Martínez-Mártinez, L. H., Delgado-Hernandez, D.J., De León Escobedo, D., Alonso-Guzmán, E.M., Martínez-Molina, W., Arreygue-Rocha, E., havez-Garcia, H. L. ve Arteaga-Arcos J. C. 2012. Mechanical properties of rocks used for the construction of vehicular bridges supported by pier masonry, Advanced Materials Research, Vols. 535-537, pp. 1881-1888.

Menten, L. ve Michaelis, M.I. (1913), Die Kinetik der Invertinwirkung, Biochem Z 49: pp. 333–369.

Mosch S. ve Siegesmund, S. 2007. Statistische Bewertung gesteintechnischer Kenndaten von Natursteinen. Z dtsch Ges Geowiss 158/4, pp. 821–868.

Obert, L. ve Duvall, W.I. 1967. Rock mechanics and the design of structures in rock. John Wiley, New York, 1967. p. 650.

Prodotyakonov, M.M. 1969. Methods of determining the shearing strength of rocks; Mechanical Properties of Rocks, Wiener-Bindery Ltd. pp. 175, Jerusalem.

Schön, J.H. 1996. Physical properties of rocks – Fundamentals and principles of petrophysics, Pergamon Press, Oxford.

Sharma, P. K. ve Singh T.N. 2008. A correlation between P-wave velocity, impact strength index, slake durability index and uniaxial compressive strength, Bull. Eng. Geol. Environ., 67, 17–22.

Siegesmund, S. ve Sbethlage, R. 2011. Stone in Architecture, pp. 97-227, Berlin.

Sülükçü, S., ve Ulusay, R., 2001. Evaluation of the block punch index test with particular reference to the size effect, failure mechanism and its effectiveness in predicting rock strength. International Journal of Rock Mechanics and Mining Sciences, 38, pp. 1091-1111.

Tercan, A.E., Ünver, B., Tiryaki B. ve Özbilgin, D. 2005. A study of relationships among mechanical, index and petrographic properties of some sandstones using canonical correlation analysis, (in Turkish). Madencilik Dergisi, s. 3–14.

Teymen, A. 2005. Bazı kayaçların petrografik, fiziksel ve mekanik özellikleri arasındaki ilişkilerin incelenmesi, Y. Lisans Tezi, Çukurova Fen. Bil. Ens., s. 136, Adana.

Tuğrul, A. ve Zarif, I.H. 1999. Correlation of mineralogical and textural characteristics with engineering properties of selected granitic rocks from Turkey, Engineering Geology, 51, 1999. pp. 303–317.

Ulusay, R. ve Gökçeoğlu, C. 1997. The modified block punch index test. Can. Geotech. J., Vol : 34, pp. 991–1001.

Ulusay, R., Gökçeoğlu C. ve Sülükçü, S. 2001. Draft ISRM suggested method for determining block punch strength index (BPI), International Journal of Rock Mechanics and Mining Sciences, 38, pp. 1113–1119.

Vutukuri, V.S., Lama, R.D. ve Saluja, S.S. 1974. Handbook of mechanical properties of rocks, Testing, Techniques, and Results, vol: 1, Trans Tech Publications, pp. 141–173 ABD.

Yağız, S. 2011. P-wave velocity test for assessment of geotechnical properties of some rock materials, Bull. Mater. Sci., 34, 4, pp. 947–953.

Yaralı, O. 1999. Kaya malzemesinin kohezyonunun doğrudan tayininde bir deney yönteminin geliştirilmesi, Doktora Tezi, ZKÜ Fen. Bil. Ens. S. 198., Zonguldak.

Zhang, L. 2005. Engineering Properties of Rocks, Elsevier Geo-Engineering Book Series Vol:4, pp. 290., USA.

Zamora, M., Sartoris, G. ve Chelini W. 1994. Laboratory measurements of ultrasonic wave velocities in rock from the Campi Flegrei volcanic system and their relation to other field data, journal of geophysical research, vol: 99, pp. 553–561.

Zarif, I.H. ve Tuğrul, A. 2003. Aggregate properties of Devonian limestones for use in concrete in Istanbul, Turkey. Bulletin of Engineering Geology and the Environment, 62, pp. 379–388.

Wuerker, R.G. 1959. The shear strength of rocks, Min. Eng., Vol:11, No:10, pp. 1022–1026.

Patlatma Sonrası Oluşacak Yığının Ortalama Boyutu ile Jeolojik Dayanım İndeksi (GSI) İlişkisinin Araştırılması

Investigation of Relationship between Mean Fragment Size of The Blast Pile and Geological Strength Index (GSI)

T. Öngen, D. Karakuş, G. Konak, A. Tosun, A.H. Onur
Dokuz Eylül Üniversitesi, Maden Mühendisliği Bölümü, İzmir

ÖZET: Açık ocak madenciliğinde üretim aşamasında yaygın olarak patlatma işlemleri gerçekleştirilmektedir**.** Patlatma işlemi sonucunda oluşan yığının parça boyut dağılımına etki eden birçok faktör mevcuttur. Bu faktörlerin en önemlileri, patlayıcı madde cinsi ve patlatma tasarımı ile birlikte çalışılacak arazinin jeolojik yapısıdır. Özellikle ayna yüzeyinde gözlenen süreksizlik aralığı, dolgu durumu gibi parametreler patlatma sonrası yığın boyut dağılımında etkendir. Kaya kütlesi özelliklerini inceleyen yaklaşımlardaki ortak sonuç, kayacın süreksizlik özelliklerinin patlatma sonuçlarını etkileyeceği şeklindedir. Süreksizlik tanımlaması yapmak için çeşitli sınıflama yöntemleri mevcuttur. Hazırlanan bu çalışmada, Işıkkent mevkiinde bulunan bir agrega ocağında toplam 11 adet patlatma deneyi yapılarak, süreksizlik özelliklerinin sınıflamasını ve değerlendirmesini yapan Jeolojik Dayanım İndeksi (GSI) ile patlatma sonucu oluşan yığının ortalama tane boyutu arasındaki ilişki irdelenmiştir.

ABSTRACT Blasting operations are commonly realised in open-pit mining at the production phase. There are many factors that affect the distribution of particle size of the pile which is formed as a result of blasting operation. The most important of these factors are type of explosives, blasting design and the geological structure. Particularly, parameters such as filling material between discontiunities, joint space observed in the blast face are effective in the pile size distrubution which occured after blasting. Common result of approaches that analyzed rock mass properties; characteristics of rock discontinuities influence the blast result. Various classification methods to make identification of discontinuities are available. In this study, an 11 blast experiments were performed in an aggregate quarry which is located Işıkkent. The relationship between mean fragment size of the blast pile and geological strength Index (GSI) which make the classification and assesment of geological properties of discontiunity have been investigated.

1 GİRİŞ

Madencilikte, özellikle açık ocak madenciliğinde kayaçların parçalanması için genellikle patlayıcı maddelerden yararlanılmaktadır. Patlayıcı madde kullanılarak yapılan üretimlerde oluşan yığının parça boyut dağılımı yükleme, nakliye ve kırma proseslerinin ekonomikliğini doğrudan etkilemektedir. Bu etki göz önüne alındığında, patlatma sonrası oluşacak yığın boyut dağılımının denetlenebilmesi önem kazanmaktadır. Boyut dağılımına etki eden faktörler iki ana başlık altında toplanabilir. Bunlar; kontrol edilebilir parametreler (delik çapı, patlatma yönü, delik eğimi, dilim kalınlığı vb.) ve

kontrol edilemeyen (tabakalanma, çatlak setleri, süreksizlikler vb. gibi kaya kütlesi yapısal özellikleri) parametrelerdir. Kontrol edilemeyen yapısal özelliklerin patlatma sonucu oluşacak yığın boyut dağılımı üzerinde azımsanmayacak bir etkisi vardır. Bir bölgedeki patlatma tasarımının etkilerini analiz edebilmek için farklı kaya birimlerinin doğru bir şekilde tanımlanması oldukça önemlidir. Kayaçların tanımlanabilmesinde kullanılan en etkili yöntem, jeolojik olarak sınıflandırılmalarıdır (Hopler, 1998).

İki süreksizliğin arasının kapalı, boşluklu ya da dolgulu olmasına bağlı olarak bu süreksizlikler patlatma ile oluşan basınç dalgalarını farklı iletmektedirler (Obert ve Duvall, 1950). Sistematik eklemler kayacın patlatılmasını daha zor bir duruma sokabilir, zayıf zon ve damarlar veya boşluklu süreksizlik yapısı patlayıcının infilak koşullarını değiştirip, açığa çıkan enerjiyi azaltır ve bu enerjinin istenmeyen yönlerde yayılımına sebep olur. Süreksizliklerin arasının kapalı olması dalgaların iletimini etkilemezken, kayaç yapısında boşluklu ya da dolgulu süreksizlik mevcutsa basınç dalgasını farklı yönlere yansıtmakta ve kuvvetini azaltmaktadır. (Zagreba, 2003). Böyle durumlarda kaya kütlesi daha az kırılır ve patarlanacak kadar büyük boyutlu malzemeler açığa çıkar.

Fourney ve Diğerleri (1983), laboratuar boyutunda yapmış olduğu çalışmalarında parçalanma mekanizması ile çatlak takımları arasında ilinti kurmuştur. Homojen kayaya nazaran süreksizlik içeren kayalarda elde edilen ortalama tane boyutunun daha küçük olduğunu, yaklaşık 1,5 kat daha aza indirgendiğini öne sürmüşlerdir. Harries (1983), arazi çalışmalarında gerçekleştirmiş olduğu tam ölçekli basamak patlatmalarında; çatlak setleri ve/veya tabakalanma arasındaki ortalama mesafenin artmasının patlatma sonucu oluşacak kırılma derecesini de arttıracağını ileri sürmüştür.

Literatürde bulunan çalışmalardan elde edilen ortak sonuç, açık ocak işletmeciliğinde ekonomikliğe de bağlı olarak en iyi verime ulaşabilmek için süreksizliklerin patlatma tasarımı yapılırken göz önüne alınması gerektiğidir.

Hazırlanan bu bildiri kapsamında, süreksizliklerin yığın boyut dağılımına etkisinin belirlenmesi için Jeolojik Dayanım indeksi (GSI) ile patlatma sonrası yığından alınan görüntülerin görüntü analizi yöntemiyle elde edilen ortalama tane boyutları arasındaki ilişki araştırılmıştır.

2 ORTALAMA TANE BOYUTUNUN BELİRLENMESİ VE GSI

Verimli bir patlatma sonucunda homojen dağılım gösteren bir yığın elde edildiğinde, ardışık işlemler örneğin yükleme, nakliye ve kırma işlemleri de verimlilik kazanmaktadır. İdeal şartlar altında süreksizlik içermeyen homojen kayaçlarda gerçekleştirilecek patlatma sonrası yığın boyut dağılımını modellemek basit iken, gerçekte kayacın yapısını oluşturan süreksizlikler dolayısı ile parçalanmaya etki eden değişkenlerin artmasıyla ampirik yaklaşımların haricinde yığın boyut dağılımının tahmin edilebildiği bir model bulunmamaktadır. Ortalama tane boyutunun ve dağılımının tahmini için literatürde kabul görmüş birçok model olmasına rağmen yaygın olarak kullanılan model Cunnigham'ın (1983, 1987) geliştirdiği "Kuz-Ram" modelidir. Bu modelden hariç Langefors ve Kihlström (1963)'ün ilk çalışmalarına dayanarak, Holmberg ve Larsson (1974) "SveDeFo Eşitliği" olarak adlandırdıkları tahmin eşitliğini ortaya koymuşlardır (Eşitlik 1).

$$X_{50}=0{,}143 \times f\left(\frac{L_{tot}}{H}\right) \times \left\{B^2 \sqrt{\frac{1{,}25}{\frac{S}{B}}}\right\}^{0{,}29} \times \left(\frac{C_{rock}}{S_{Dx} q}\right)^{1{,}35} \quad \textbf{(1)}$$

Burada;

L_{tot} :Toplam şarj uzunluğu (m)
H : Delik boyu (m)
f : Geometrik faktör; $1+4{,}67(1-L_{tot} / H)^{2.5}$
B : Dilim kalınlığı (m)
S : Delikler arası mesafe (m)
C_{rock} : Kaya sabiti
S_{Dx} : Patlayıcı gücü oranı
Q : Özgül şarj (kg/cm^3)

Holmberg ve Larsson (1974) kaya kütlesinin ne kadar kırılmış olduğunu dikkate alan bir sayısal çarpanı Eşitlik 1'de

kullanmaktadır. Bu çarpan; homojen masif kayaya nazaran çok kırıklı bir kayaç için % 50 daha fazladır. Bu parçalanma eşitliğinin bir versiyonu da Dyno Nobel patlatma programı olan Blastec'te kullanılmıştır.

Kou ve Rustan (1993) ortalama boyut tahmini için, model ölçekli patlatma testlerinden elde edilen kapsamlı bir model ve literatür çalışmalarına dayanarak farklı bir parçalanma teorisi sunmuştur. Bu teori, %50'den geçen tane boyutunu vermekte fakat parçalanma dağılım eğrisinin şeklini vermemektedir (Eşitlik 2).

$$x_{50} = 0{,}01 \times \rho c^{0,6} \times B^{0,2} \times \frac{\left(\frac{S}{B}\right)^{0,5} \times \left(\frac{H}{L_{tot}}\right)^{0,7}}{\left(\frac{D^{0,4}}{q}\right)} \quad \textbf{(2)}$$

Eşitlik 2'de görüldüğü gibi ortalama tane boyutunun tahmininde kaya kütlesinin dayanım özellikleri (ρc) faktörüne bağlıdır. Patlayıcının kuvveti D faktörü ile verilmiştir. Bu eşitlik 1987 yılında dirence bağlı olan üniformluk indeksinin kullanıldığı Rustan ve Nie'ye ait olan eşitliğin geliştirilmesi ile elde edilmiştir. Bu eşitlik X_{50} değeri için S/B oranı hariç diğer parametreler değiştiğinden SveDeFo parçalanma eşitliği ile çelişmektedir.

Kuznetsov (1973) özgül şarj ile patlatma sonrası yığının ortalama boyutu arasındaki ilişkiyi kaya kütlesini bir girdi parametresi olarak kullanarak aşağıda verilen eşitliği (3) önermiştir.

$$X_{50} = A\left(\frac{V_o}{Q_e}\right)^{0.8} Q_e^{1/6} \quad \textbf{(3)}$$

Burada;

X_{50} :Ortalama boyut (cm),

A :Kaya faktörü,

V_o :Delik başına patlatılacak hacim (dilim kalınlığı x delikler arası mesafe x basamak yüksekliği, m^3),

Q_e :Delik başına kullanılan nitrogliserin esaslı patlayıcı (kg).

Ortalama boyut tahmini için verilen bu formül nitrogliserin esaslı detonasyon hızı fazla patlayıcı maddeler için önerilmiştir.

Bu patlatıcıların gücü Anfoyla karşılaştırıldığında daha fazladır. Patlayıcı madde olarak Anfo kullanıldığında düzeltme katsayısı kullanılarak formül, eşitlik 4'teki şekli almıştır.

$$X_{50}=A\left(\frac{V_o}{Q_e}\right)^{0.8} Q_e^{\frac{1}{6}} \left(\frac{S_{Anfo}}{115}\right)^{\frac{19}{30}} \quad \textbf{(4)}$$

Patlayıcı olarak Anfo kullanıldığında S_{Anfo} =100 olarak alınır. (Kuznetsov, 1973)

Bu formüle girdi olarak etki eden özgül şarj birim hacim başına kullanılan patlayıcı miktarı olarak tanımlanmaktadır. Özgül şarj miktarının tespiti için kullanılan bağıntı eşitlik 5'te verilmiştir.

$$\frac{1}{q}=\frac{V_0}{Q_e} \quad \textbf{(5)}$$

Kullanılan patlayıcı miktarı ve özgül şarj miktarını ölçülen değerlerden hesaplamak mümkün iken kaya kütlesinin etkisi katsayı düzeltmesi olarak formüle yansımaktadır. Kaya kütle katsayısı A; 7 ile 13 arasında değerler almaktadır.

Kaya kütle katsayısının kayacın karakteristik özelliklerini yansıtmadığını düşünen Cunnigham (1983) Kaya kütlesi patlatılabilirliği ile ilgili Lilly (1986) tarafından önerilen kaya kütlesi patlatma indeksini ortalama boyut tahmini için önerilen eşitlikteki kaya katsayısının belirlenmesinde kullanmıştır (Eşitlik 6).

$$A = 0{,}06(RMD + JF + RDI + HF) \quad \textbf{(6)}$$

A katsayısının bulunmasında kullanılan parametreler Tablo 1'de verilen değerlendirmeler neticesinde tespit edilmektedir.

Tablo 1. A Katsayısının Tespitinde Kullanılan Parametreler ve Bu Parametrelerin Belirlenmesi (Cunnigham,1983).

RMD Kaya kütle sayısı	
Eğer kaya kütlesi kırılgan gevrek yapıdaysa	RMD = 10
Eğer düşey yönde süreksizlikler varsa	RMD = JF
Eğer masif yapıdaysa	RMD = 50
JF Kaya Kütlesi Süreksizlik Katsayısı	
	JF = JPS+JA
JPS Düşey Süreksizlik aralığı	
Eğer ortalama süreksizlik aralığı < 0,1m	JPS = 10
Eğer ortalama süreksizlik aralığı 0,1m < X < İri Blok boyutlu (~ 0.5m)	JPS = 20
Eğer ortalama süreksizlik aralığı iri blok < X < Dilim Kalınlığı (m)	JPS = 50
JPA Süreksizlik düzlemi açısı	
Eğer düzlem açısı yüzeyin dışına doğru ise	JPA = 20
Eğer düzlem açısı yüzeye dik ise	JPA = 30
Eğer düzlem açısı yüzeyin içinde kalıyorsa	JPA = 40
RDI Kayaç yoğunluğu Faktörü	
Kayaç Yoğunluğu RD (t/m^3)	RDI = 25 RD-50
HF Sertlik faktörü	
Eğer Young Modülü Y<50	HF = Y/3
Eğer Young Modülü Y>50	HF = σb/5

"A" katsayısının belirlenmesinde süreksizliklerin bir takım özellikleri (dolgu durumu, birden fazla çatlak seti varlığı vs.) hesaba katılmamaktadır. Ayrıca A katsayının tespitinde kullanılan RMD değerinin de pratikte belirlenmesi zordur. Bu sebeple genel bir değerlendirme yapılmış ve kayacın sertliğine göre;

Orta sert kaya kütleleri için; A= 7
Sert çok fisürlü kaya kütleleri için; A=10
Sert az fisürlü kaya kütleleri için; A=13

olarak pratikleştirilmiştir.

Cunningham (1983, 1987), Kuz-Ram boyut dağılım tahmin modeli uygulamasında ateşleme sırası ve gecikme aralığının modelde yer almadığı belirtmiş, ayrıca çok süreksizlik içeren kaya yapılarında patlatma sonrası boyut dağılımını belirleyen en etkin parametrenin kaya kütle özellikleri olduğunu vurgulamıştır (Hustrulid,1999).

Ortalama tane boyutunun tahmininde kullanılan yaklaşımlarda küçük çelişkiler olsa da genel olarak bütün eşitliklerde kaya kütlesi sayısallaştırılarak kullanılmakta, patlayıcı miktarı ve patlatmanın geometrisini temsilen özgül şarj ise ya bölümlenerek ya da doğrudan kullanılmaktadır. Konuyla ilgili bir diğer değerlendirme de patlatılacak aynanın sayısallaştırılmasında kullanılacak yöntemlerin çeşitliliğidir. Bu konuda kimi yaklaşımlarda doğrudan kayaç malzemesinin mekanik özelliklerine dayanan parametreler, kimi yaklaşımlarda ise doğrudan süreksizlik özelliklerine dayanan parametreler kullanılmaktadır.

Kaya kütlesinin homojen olduğu varsayıldığında tahmin modellerinden elde edilen değerler gerçeğe yakın değerler vermektedir. Fakat kaya kütlesindeki süreksizliklerden dolayı arazideki gerçek değerler ile tahmin modellerinde elde edilen değerler farklılık göstermektedir. Bu farkları en aza indirmek amacıyla süreksizlik özellikleri katsayı olarak tahmin modellerine eklenmekte, kaya kütle özellikleri sayısallaştırılmaya çalışılmaktadır.

Doucent (1995) kaya kütlesi sınıflama sistemlerinden RMR sınıflama sitemi, Q sınıflama sitemi ve RQD kaya kalite göstergesi ile boyut dağılımı arasındaki ilişkiyi araştırmıştır. Buna göre sınıflama sistemlerinde düşük kaya kütlesi özelliklerinin üniform olmayan boyut dağılımına neden olduğu sonucunu rapor etmiş ve boyut dağılımının tahmin modellerinde gerçekçi yaklaşımların yapılabilmesi için kaya kütle sınıflama sistemlerinin kullanılması gerektiğini önermiştir (Karakuş, 2010).

Bu bildiri kapsamında hazırlanan çalışmada kaya kütle sınıflama sistemlerinden olan "Jeolojik Dayanım İndeksi (GSI)" kullanılarak patlatma aynasına ait karakteristikler sayısallaştırılıp patlatma sonrası oluşan boyut dağılımı ile ilişkilendirilecektir.

3 JEOLOJİK DAYANIM İNDEKSİ (GSI)

Hoek (1995) tarafından önerilen Jeolojik Dayanım İndeksi (GSI), daha sonra Sönmez ve Ulusay (2007), tarafından çok daha kullanışlı hale getirilmiştir. GSI abağı kullanılarak kaya kütle özellikleri sayısal formda tespit edilebilir. GSI, 10'dan 85' e kadar çok farklı değerler alabilmektedir. Bu yöntemde süreksizliklerin yüzey koşulunu ve kaya kütle yapısını temel alan iki parametre bulunmaktadır.

Kaya kütlesinin "çatlaklılık" durumunu belirten yapısal özellik puanı kaya kütlesinin hacimsel çatlak sayısından "J_v" hesaplanabilir (Eşitlik 7).

$$SR = -17{,}5 \ln J_v + 79{,}8 \qquad \textbf{(7)}$$

Çatlak aralık ölçümlerinden J_v'nin belirlenmesi için Palmström (1996) aşağıdaki eşitliği önermiştir (Eşitlik 8).

$$J_v = \frac{N_1}{L_2} + \frac{N_2}{L_2} + \cdots + \frac{N_n}{L_n} \qquad \textbf{(8)}$$

J_v :Hacimsel çatlak sayısı (çatlak adeti/m^3),

L_n : Her çatlak takımına (1'den n' e kadar) dik yöndeki ölçüm hattının uzunluğu,

N_n : Her çatlak takımındaki (1'den n' e kadar) çatlak sayısı,

n :Çatlak takımı sayısı.

Genellikle hat etütlerinin her çatlak takımına dik yönde yapılması güçtür. Çünkü çatlak takımları farklı yönelimlere sahiptir. Bu zorluğu ortadan kaldırabilmek amacıyla Sönmez ve Ulusay (1999) eşitlik 9'da verilen ifadeyi önermişlerdir (Arıoğlu, 2009).

$$J_v = \frac{1}{S_1} + \frac{1}{S_2} + \cdots + \frac{1}{S_n} = \sum_{i=1}^{n} \left(\frac{1}{S_i}\right) \qquad \textbf{(9)}$$

S : Her çatlak takımının gerçek aralığı;

n : Çatlak takımı sayısı.

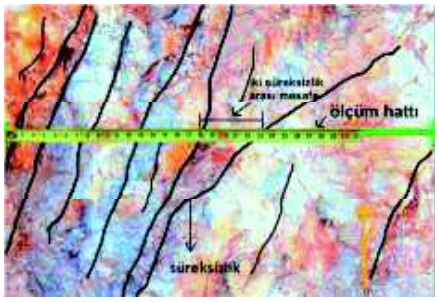

Şekil 1. Bir fotoğraf üzerinde şematik hat etüdü gösterimi.

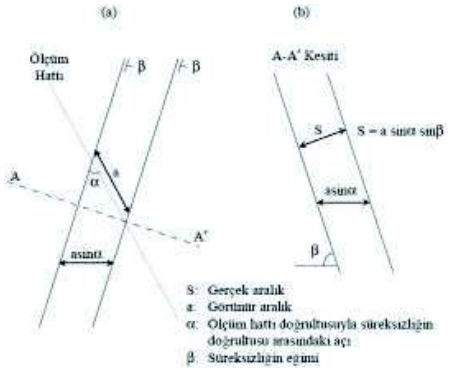

Şekil 2. Görünür (a) ve gerçek aralık (s) parametreleri arasındaki ilişki (Sönmez ve Ulusay, 2007)

İleri derecede eklemli aşırı derecede parçalanmış kaya kütlelerinde eklem takımlarının ayırtlanması oldukça güçtür. Bu nedenle, bu tür kaya kütlelerinde J_v'nin tahmini için birbirine dik üç yönde yapılan hat etütleriyle belirlenen eklem sayıları esas alınarak eşitlik 10 önerilmiştir (Sönmez ve Ulusay, 1999).

$$J_v = \frac{1}{S_x} \times \frac{1}{S_y} \times \frac{1}{S_z} \quad \text{adet/m}^3 \qquad \textbf{(10)}$$

$S_{x,y,z}$: Birbirine dik x, y ve z yönlerindeki ortalama süreksizlik aralıkları.

İleri derecede eklemli homojen kaya kütlelerinde $S_x \approx S_y \approx S_z$ kabul edilerek eşitlik aşağıdaki halini almıştır.

$$J_v = \left(\frac{1}{S}\right)^3 \quad \text{adet/m}^3 \qquad \textbf{(11)}$$

Buradaki S; ortalama süreksizlik aralığıdır. Sönmez ve Ulusay (1999) J_v için aralık değerlerini ISRM (1981)' den almış ve GSI sistemine uyarlamıştır. Daha sonra 2002 yılında modifiye edilerek sağlam veya masif kaya grubu da sınıflamaya eklenmiştir. Yukarıdaki eşitliklerden hesaplanan J_v değeri çatlak takım sayıları dikkate alınmadığından doğru olmayabilir ve gerçekte olacak değerden daha yüksek değerler elde edilebilir. Bu sorunu ortadan kaldırmak için Sönmez ve Ulusay (2002) aşağıdaki eşitliği önermişlerdir (Eşitlik 12):

$$J_v = D_n \left(\frac{1}{S}\right) \qquad \text{adet/m}^3 \qquad \textbf{(12)}$$

D_n : Birbirine paralel veya paralele yakın olan süreksizlikler aynı çatlak takımında kabul edilerek belirlenen çatlak takımı sayısı

S : Ortalama süreksizlik aralığı

SR hesaplanırken Eşitlik 7 kullanılabileceği gibi, GSI abağının sol üst köşesinde yer alan grafikten de yararlanılabilmektedir.

Süreksizlik çatlak koşulu puanlaması için süreksizlik yüzeylerinin pürüzlülüğü, bozunma derecesi ve süreksizlik arası dolgu durumu dikkate alınmaktadır. Buna göre;

$$SCR = R_r + R_w + R_f \qquad \textbf{(13)}$$

R_r :Çatlak yüzeylerinin pürüzlülüğüne ilişkin puan; (0 – 6)

R_w : Bozunma – ayrışma – derecesi ile ilgili puan; (0 – 6)

R_f :Çatlak içi malzemesine ilişkin puan; (0 – 6)

Kaya kütlesi incelenerek söz konusu faktörlere puanlar verilir. SR ve SCR büyüklükleri belli olunca kaya kütle özelliklerini sayısallaştıran GSI abağından GSI değeri bulunabilir. GSI abağı Şekil 3' te verilmiştir.

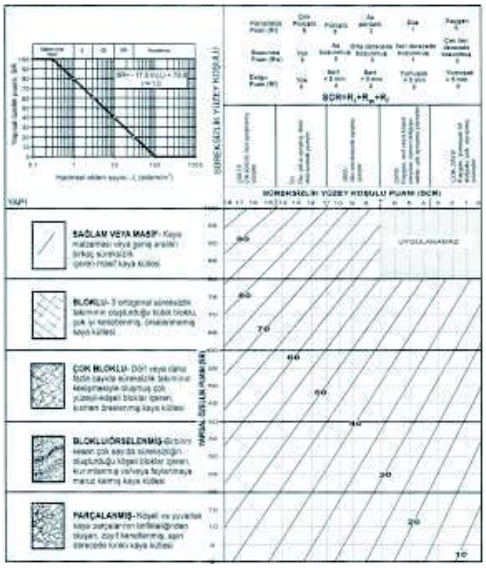

Şekil 3. GSI sınıflama sistemi abağı (Sönmez ve Ulusay 2002)

4 ARAZİ ÇALIŞMASI

İzmir Işıkkent mevkiinde bulunan bir agrega ocağında 11 adet patlatma takip edilmiştir. Öncelikli olarak takibi yapılacak patlatmaların teknik parametreleri (basamak boyu, dilim kalınlığı, kullanılan patlayıcı madde miktarı vb.) kayıt altına alınmış ve özgül şarj değerleri belirlenmiştir. Ocakta uygulanan delik geometrisi ve patlatma deliği düşey kesiti Şekil 4'te gösterilmiştir. Her patlatma çalışması için belirlenen özgül şarj değerleri de Tablo 2'te verilmektedir. 11 adet patlatmaya ait özgül şarj değerlerine bakıldığında 0,5 kg/m^3 ile 0,6 kg/m^3 arasında değişmektedir. Bu durum, patlatma sonrası oluşacak tane boyut dağılımında etken parametrenin kaya kütle özellikleri olduğunu göstermektedir.

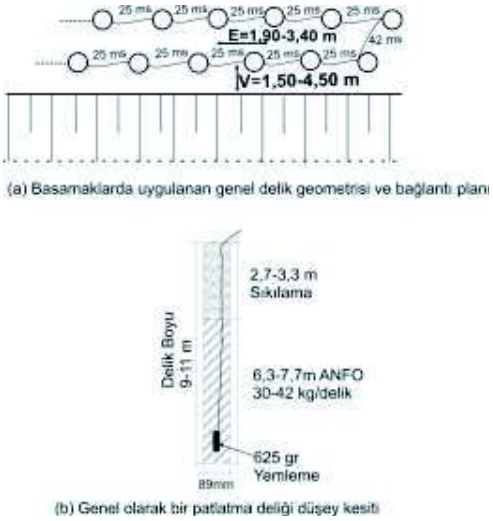

Şekil 4. Ocakta uygulanan patlatma plan görüntüsü, (a) Temsili delik geometrisi ve bağlantı planı, (b) Delik düşey kesiti

Tablo 2. 11 Adet Patlatma Çalışmasına ait Özgül Şarj Değerleri

Patlatma No	Özgül Şarj (kg/m^3)
1	0,60
2	0,57
3	0,54
4	0,56
5	0,54
6	0,54
7	0,55
8	0,51
9	0,50
10	0,53
11	0,49

Patlatma aynalarına ait teknik verilerinin elde edilmesinin ardından, hat etüdü yöntemi kullanılarak arazi çalışmasının gerçekleştirildiği açık ocak sahasında süreksizlik aralıkları ve dolgu durumları belirlenmiş ve kaydedilmiştir (Tablo 4). Tablo 3'te Patlatma-1 araştırması için yapılan hat etüdü değerleri verilmektedir. Arazi çalışmasının gerçekleştirildiği ocakta jeolog pusulası kullanılarak süreksizlik eğim yönü/eğim değerleri elde edilen her aynaya ait kontur diyagramları (stereonet) çizilerek süreksizlik takımlarının sayısı belirlenmiştir (Tablo 4). Örnek olması amacıyla Şekil 5'te Patlatma-1 araştırmasına ait stereonet verilmektedir.

Tablo 3. Patlatma-1 Araştırması için Aynadan Alınan Hat Etüdü Sonuçları ve Elde Edilen Süreksizlik Aralığı Değeri

0.cm, 2.cm, 7.cm, 31-50.cm ***(parçalanmış zon)***, 55.cm, 58.cm, 66.cm, 77-81.cm ***(kil, kalsit),*** 89.cm, 110-112.cm ***(kil, kireçtaşı),*** 142.cm, 195.cm, 239.cm, 271.cm, 286.cm, 308-309.cm ***(kireçtaşı),*** 330.cm, 378.cm, 392.cm, 422.cm, 478-480.cm ***(kireçtaşı),*** 535.cm, 560.cm, 580.cm, 603.cm, 667.cm, 793.cm, 825.cm, 990.cm, 1041.cm, 1052.cm, 1084.cm, 1114.cm, 1150.cm, 1183.cm, 1198.cm, 1221.cm, 1272.cm, 1305.cm.

Süreksizlik aralığı =1305/43= 30,35cm =***0,3035m***

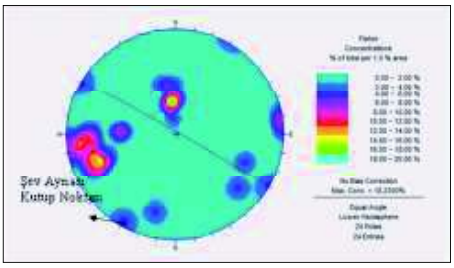

Şekil 5. Patlatma-1 araştırması için aynadan elde edilen süreksizlik eğim yönü/eğim değerlerine ait stereonet

Patlatma sonrası oluşan yığını bölümlere ayrılarak, yığını temsil edecek sayıda ölçekli görüntüler alınmış, görüntü işleme teknikleriyle zenginleştirilen görüntülerin boyut dağılım analizleri WIPFRAG programı kullanılarak yapılmış, her görüntüye ait dağılım grafikleri bulunmuştur. Bu grafiklerden elde edilen veriler derlenerek bütün yığına ait ortalama tane boyut dağılım grafiği elde edilmiştir. Patlatma-1 araştırması için yığından alınan görüntülerden birine ait analiz aşamaları Şekil 6'te verilmektedir. Bu yöntem her patlatma için tekrarlanarak her bir patlatmaya ait boyut dağılımı ve ortalama tane boyutu (D_{50}) tespit edilmiştir (Tablo 4).

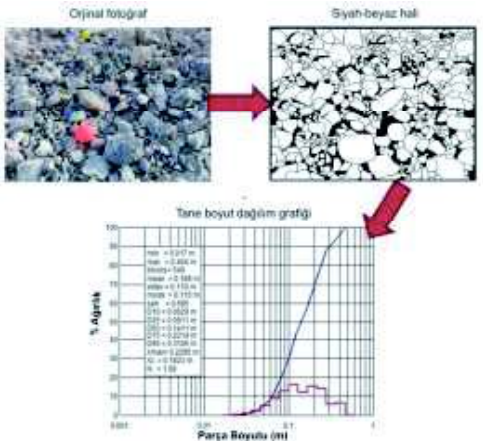

Şekil 6. Patlatma-1 araştırmasına ait yığından elde edilen görüntünün analiz aşamaları

11 adet aynadan elde edilen süreksizlik verileri neticesinde SCR ve SR puanları hesaplanarak Jeolojik Dayanım İndeksi (GSI) abağından her patlatma aynasına ait GSI değerleri tespit edilmiştir (Şekil.7).

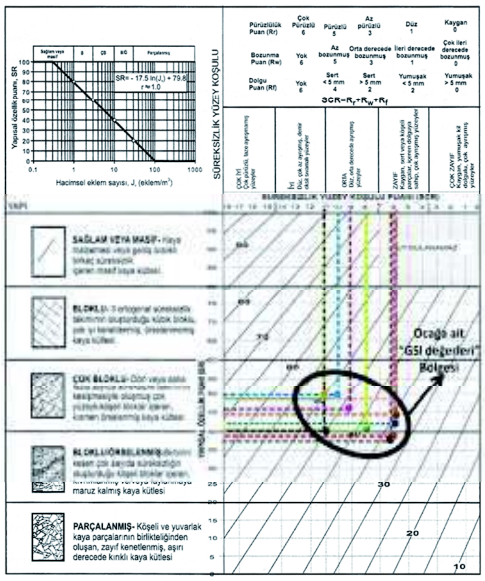

Şekil 7. Çalışılan agrega ocağında ölçüm alınan aynalara ait GSI değerlerinin gösterimi ve ocağa ait GSI değerleri

Yukarıdaki şekil incelendiğinde çalışılan ocağa ait GSI değerlerinin yaklaşık 35 ile 50 değerleri arasında olduğu görülmektedir. Bu sınıflamaya göre incelenen agrega ocağı "ÇOK BLOKLU - *dört veya daha fazla sayıda süreksizlik takımının kesişmesiyle oluşmuş çok yüzeyli-köşeli bloklar içeren, kısmen örselenmiş kaya kütlesi*" yapısal özelliği göstermektedir. Elde edilen GSI değerleri Tablo 4'te verilmektedir.

5 ÖLÇÜM SONUÇLARININ DEĞERLENDİRİLMESİ

Süreksizlikler ile patlatma verimi arasındaki ilişkiyi belirlemek için arazide yapılan patlatmalardan elde edilen veriler kullanılmıştır. Toplam 11 patlatma aynasına ait süreksizlik ölçümlerinden elde edilen veriler kullanılarak GSI değerleri hesaplanmıştır. Her bir patlatma araştırması için WIPFRAG programı ile elde edilen D_{50} ile Patlatma aynalarına ait GSI değerleri arasındaki ilişkinin varlığı, $R^2 = 0,86$ 'lük bir korelasyon katsayısı ile ortaya konulmuştur. (Şekil 8).

GSI ile D_{50} arasındaki grafiksel ilişki incelendiğinde çalışılan ocak için özgül şarj değerleri 0,5-0,6 kg/m^3 aralığındayken GSI değeri arttıkça ortalama tane boyutu irileşmektedir. Farklı bir ifadeyle özgül şarj 0,5-0,6 kg/m^3 aralığındayken patlatılan kayacın homojenliği arttıkça parçalanma derecesi kötüleşmekte ve iri parçalar meydana gelmektedir.

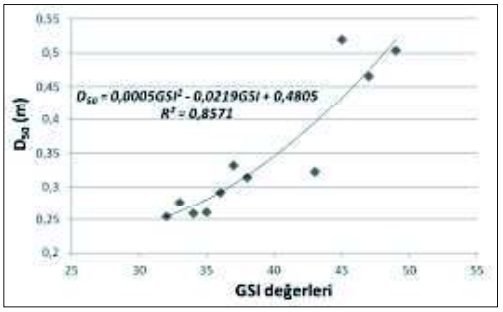

Şekil 8. D_{50} ile GSI değerleri arasındaki grafiksel ilişki

Tablo 4. 11 Adet Patlatma Araştırmasına ait D_{50}, Süreksizlik Aralığı, Çatlak Seti Sayısı, Dolgu Durumu ve GSI Değerleri

		Ortalama Tane Boyutu (D_{50}) (m)	Süreksizlik Aralığı (m)	Çatlak Seti Sayısı	Dolgu Durumu	Hesaplanan GSI Değerleri	Özgül şarj
PATLATMA NO	1	0,2553	30,35	3	kireçtaşı, kil; > 5 mm	32	0,60
	2	0,4662	50,85	3	kil; > 5 mm	47	0,57
	3	0,2774	25,45	3	kil; > 5 mm	33	0,54
	4	0,3323	20,7	2	kalsit; > 5 mm	37	0,56
	5	0,2922	49,65	3	kireçtaşı, kil; > 5 mm	36	0,54
	6	0,3143	35,9	3	kalsit; > 5 mm	38	0,54
	7	0,2598	25,06	2	kil; > 5 mm	34	0,55
	8	0,3233	44,48	3	kalsit; > 5 mm	43	0,51
	9	0,2617	41,62	3	kil; > 5 mm	35	0,50
	10	0,5199	29,33	3	kalsit; > 5 mm	45	0,53
	11	0,5046	31,8	2	kalsit; > 5 mm	49	0,49

6 SONUÇLAR

Patlatma sonucu oluşacak yığının boyut dağılımı ve ortalama tane boyutu patlatmanın verimliliği açısından önemli iki parametredir. Gerçekte bir patlatmada ortalama boyut ve yığın boyut dağılımının oluşumu kaya kütlesi özellikleri ile birlikte delik çapı, delik boyu, delikler arası mesafe delik yükü ve ateşleme sırası ile serbest yüzey oluşum mekanizması tarafından denetlenmektedir. Madencilik sektöründe boyut küçültmenin ilk aşaması olan patlatma işlerinde patlatma sonucu oluşacak yığına ait boyut dağılımının patlatma yapmadan önce tahmin edilebilmesi yukarıda sayılan değişkenleri içeren karmaşık modellemelerle mümkündür. Tahmin modellerinde patlayıcı miktarı, patlatma geometrisi ve patlatılacak şev aynasının kaya kütle özelliklerini içeren ampirik yaklaşımlar yaygın olarak kullanılmaktadır. Bu ampirik yaklaşımlarda özellikle patlatılacak aynanın sayısallaştırılması kısmında bir takım farklı kabuller ve ortalama tane boyutunun belirlenmesinde kullanılan dijital görüntü analiz yöntemleri gibi kısıtlı değerlendirme aşamaları konunun tartışılabilir ve gündemde olmasına neden olmaktadır. Bu çalışmada da kaya kütle sınıflama sistemlerinden birisi olan GSI sınıflama sistemi ile patlatılacak aynanın sınıflaması yapılmış ve ortalama tane boyutu ile ilişkisi değerlendirilmiştir. Buna göre;

1. Literatürde kabul görmüş ortalama tane boyut tahmini için çeşitli ampirik modeller mevcuttur. Bu modellerde farklılıklar olmasına rağmen ortak nokta, ortalama tane boyut tahmini yapan ampirik modellerin hepsinde özgül şarj ile birlikte kaya kütlesi özellikleri kullanılmaktadır.

2. Kaya kütlesi özelliklerinin belirlenip sınıflanması için sürekli gelişen ve güncellenen sınıflama sitemleri bulunmaktadır. Bu sınıflama sistemlerinden GSI'nin bu çalışmada kullanılmasının nedeni; kaya kütlesinin görünen bozunma derecesini en iyi yansıtan sistem olmasıdır.

3. GSI ile ortalama boyut arasındaki ilişkinin araştırılması için 11 adet patlatma takip edilmiş, patlama şev aynasının GSI değerleri belirlenmiştir. Buna göre sahanın yapısal özelliği "ÇOK BLOKLU - dört veya daha fazla sayıda süreksizlik takımının kesişmesiyle oluşmuş çok yüzeyli-köşeli bloklar içeren, kısmen örselenmiş kaya kütlesi" olarak belirlenmiştir. GSI özellikleri belirlenen bu aynaların; 0,5-0,6 kg/m^3 özgül şarj değerleri ile patlatılması sonucu oluşan ortalama tane boyutunun belirlenmesinde dijital görüntü analizi yöntemleri kullanılmıştır.

4. GSI ile ortalama tane boyutu arasında yüksek korelasyonlu doğrusal bir ilişki (R^2 = 0,86) tespit edilmiştir. Bunun anlamı; bloklu, parçalanmış, süreksizlikleri az açıklıklı ve/veya kapalı, süreksizlik araları az dolgulu ve/veya dolgusuz olan kaya kütle özelliklerine sahip aynalarda özgül şarj 0,5-0,6 kg/m^3 aralığında kalmak koşulu ile parçalanma derecesi artmakta, parça boyutu düşmektedir.

Her ne kadar patlatma sonucu oluşan yığın boyut dağılımı ile ortalama tane boyutu arasında ilişki tespit edilmiş olsa da bu değerlendirme, çalışma yapılan agrega sahası ve kireçtaşına özeldir. Diğer taraftan parçalanmanın derecesi ile oluşan yığının boyut dağılımı arasında fark bulunmaktadır. Örneğin ortalama tane boyutu küçük olmasına rağmen; üniform dağılmamış, tane sınıfları arasında fark olan bir yığın ile ortalama tane boyutu kısmen yüksek ama yığını oluşturan tanelerin çoğunun eş boyutlu olması patlatma sonucunun daha verimli olarak değerlendirilmesine neden olabilir. Süreksizlik özelliklerinin az olduğu GSI değeri yüksek kaya kütlesi yapılarında, patlayıcı enerjisi kaya kütlesi içerisinde homojen bir şekilde yayılarak parçalanmanın kontrol edilebilmesini sağlayabilir. Diğer bir değişle kaya kütle özellikleri yüksek, masif ortamlarda parçalanmanın derecesi tahmin edilebilir. Ancak kaya kütle özellikleri zayıf süreksizlik ortamlarda yapılan patlatmalarda ortalama boyut düşük çıksa da kontrol edilemeyen iri boyutlu taneler oluşabilir.

TEŞEKKÜR

2010.KB.FEN.002 No'lu Dokuz Eylül Bilimsel Araştırma Projesi Kapsamında maddi olarak destek veren Dokuz Eylül Üniversitesi Rektörlüğü'ne teşekkür ederiz.

Arazi çalışmaları için gerekli imkânları sağlayan Çimentaş İzmir Çimento Fabrikası Türk A.Ş. 'ye teşekkür ederiz.

KAYNAKLAR

Arıoğlu, E., 2009. İnşaat Müh. Bölümü, Genişletilmiş 4. Bölüm, Tünel ders notları, Yıldız Teknik Üniv.

Cunningham, C. V. B, 1983. The Kuz-Ram Model For Prediction of Fragmentation by Blasting, *In Proc 1st Int Symp on Rock Fragmentation by Blasting,* s.439-453.

Cunningham, C. V. B, 1987. Fragmentation Estimations and The Kuz-Ram Model-Four Years on, *In Proc 2nd Int Symp on Rock Fragmentation by Blasting*, s.475-487.

Doucent, C., 1995, The Effect of Geology on Fragmentation in Small Devolopment Headings, *Master Thesis,McGill University*, Montreal.

Fourney, L.W., Barker, B.D., ve Holloway, C.D., 1983. Fragmentation in Jointed Rock Material. *Proceeding, First Int Symp ın Rock Fragmentation by Blasting,* Lulea, Sweden.

Harries, G., 1983. A Mathematical Model of Cratering and Blasting, *Proceeding National Symposium on Rock Fragmentation, Adelaide.* s.41-54.

Hoek, E., Kaiser, P.K., ve Bawden W.F., 1995. Support of Underground Excavations in Hard Rock. Balkema, Rotterdam, s.214

Holmberg, R., 1974, Charge calculations for bench blasting. SveDeFo report DS 1974:4. *Swedish Detonic Research Foundation,* Stockholm. In Swedish.

Hopler, R.B., 1998. *Blaster's Handbook*, International Society of Explosives Engineers,

Hulstrulid, W.A, 1999. Blasting Princibles for Open-pit Mining, Vol 1: General Design Concepts & Vol 2: Theoretical Foundations, Balkema, Rotterdam

I.S.R.M., 1981. Suggested Methods: Rock Characterization, Testing and Monitoring. *London: E.T. Brown (ed), Pergamon Pres.*

Karakuş, D., Konak, G. ve Onur A. H., 2012. Basamak Patlatması Sonucu Oluşan Yığın Boyut Dağılımının Ampirik Modeller ile Tahmini ve Görüntü Analiz Yöntemleri ile Karşılaştırılması, *Madencilik Dergisi*, Cilt 49, Sayı 1, s.3-16.

Kou, S. ve Rustan, A., 1993. Computerized design and Result Prediction of Bench Blasting. *In Proc 4th Int Symp on Rock Fragmentation by Blasting,* s.263-271

Kuznetsov , V. M., 1973. The Mean Diameter of The Fragments Formed byBlasting Rock. *Soviet Minin Sciense*, Vol 9(2), **s.**144-148

Kuznetsov , V. M. 1973. The Mean Diameter of The Fragments Formed byBlasting Rock, *Soviet Minin Sciense,* 9(2), s.144-148

Langefors, U ve B Kihlström (1963*).* The Modern Technique of Rock Blasting. Almqvist & Wicksell, Uppsala, Sweden.

Larsson, B., 1974. Report on blasting of high and low benches – fragmentation from production blasts. In *Proc Discussion Meeting,* Swedish Rock Construction Committee, Stockholm. In Swedish. S.247-273.

Lilly, P (1986). An empirical method of assessing rock mass blastability. *In Proc Large Open Pit Mining Conference*, AusIMM & Inst Engrs, Newman Cob Group, Melbourne, s.89-92.

Obert, L., ve Duvall, W. I., 1950. Generation and Agitation of Strain Waves in Rock Part I. *USBM,RI 4583,*

Öngen (Toprak), T., 2012. Süreksizliklerin Patlatma Verimi Üzerine Etkisinin Araştırılması,*Yüksek Lisans Tezi, Dokuz Eylül Üniversitesi Fen Bilimleri Enstitüsü*, İzmir.

Palmstrom, A., 1996. RMI- a system of Characterizing Rock Mass Strength for use in Rock Engineering. *Journal of Rock Mechanics and Tunneling Technology, India*, 1(2), s.69-108.

Rosin, P. ve Rammler, E., 1933. The Laws Governing The Fineness Of Powdered Coal, *J Inst Fuel*, (7), s.29-36.

Rustan, A ve Nie, S., 1987. Fragmentation model at rock blasting. Research Rpt TULEA 1987:07. Luleå University of Techn, Luleå, Sweden.

Sönmez, H., ve Ulusay, R., 1999. Modifications to the Geological Strength Index (GSI) and Their Applicability to Stability of Slopes. *International Joutnal of Rock Mechanics and Mining Science,* 36(6), s.743-760

Ulusay, R., Sönmez, H., 2002. *Kaya Kütlelerinin Mühendislik Özellikleri*. Ankara: TMMOB Jeoloji Mühendisleri Odası Yayınları 60

Ulusay, R., Sönmez, H., 2007. *Kaya Kütlelerinin Mühendislik Özellikleri*. Ankara: TMMOB Jeoloji Mühendisleri Odası Yayınları 60 ikinci baskı.

Zagreba, V., 2003. *Fragm: A Blasting Fragmentation Model of Rocks.* Master of Science in Mining Engineering. West Virginia University. Cleveland, Ohio, ISBN: 1-892396-00-9, 17th Edition, USA, pp. 271-286

Evaluation of Squeezing Potential in the Sabzkouh Tunnel

K. Shahriar, M. Ataee Pour, A. Asrari

Department of Mining and Metallurgical Engineering, Amirkabir University of Technology, Tehran, Iran

ABSTRACT In this study, squeezing potential of the Sabzkuh Tunnel was evaluated. The squeezing is common phenomenon in the weak rock masses under high in-situ stress. This phenomenon may slow down TBM operation and increased the pressure on the lining or even damage it. Several parameters such as geological condition, in-situ stress, pore pressure and rock properties affect the behavior of rock mass. Several methods have been proposed for prediction of squeezing potential. In this study, the empirical and semi-empirical approaches were used to determine squeezing potential of the Sabzkuh Tunnel. According to the geological condition, the tunnel is divided to 10 different zones. Squeezing potential was evaluated for each zone and the results show that, the squeezing could happen in the most of the zones. To determine the time dependent behavior of rock, the triaxial creep test performed on the specimens from each zone in the tunnel rout which their results used as input parameters for the numerical modeling of the long-term behavior of rocks.

Keyword: squeezing, Sabzkuh Tunnel, triaxial creep test, numerical method,

1 INTRODUCTION

The squeezing of tunnels are a common phenomenon in poor rock masses under high in situ stress conditions(Singh et al. 2007).It is observed in weak rocks such as Schist, phylitte, mudstone, siltstone, flyschs, Tuff, Shale and etc(Shrestha & Broch, 2008)(Aydan et al. 1996)(Hoek , 2001). The occurrence of this phenomenon is depended on the geological and geotechnical conditions, the in-situ state of stress relative to rock mass strength, the ground water flow and pore pressure, and the rock mass properties. Squeezing is closely related to the excavation and support techniques which are adopted. If the support installation is delayed, the rock mass move into the tunnel and stress redistribution takes place around it. On the contrary, if deformation is restrained, squeezing will lead to long-term load build-up over rock support (Barla, 2001).

The term squeezing has been often vaguely-defined in the literature. In general, definitions of squeezing include the ideas of (i) time-dependent behavior; (ii) failure of the rock mass due to overstressing around the excavation; and (iii) large convergences and/or large loads on the support (Jimenez & Recio, 2011). Conceptually, the term squeezing is different from swelling. The swelling is volume increase of the ground due to water absorption or to other physical–chemical processes (Terzaghi, 1946), while definitions of squeezing published by the International Society for Rock Mechanics (ISRM) is the time dependent large deformation of a rock mass, which occurs around a tunnel, and is essentially associated with creep caused by exceeding a limiting shear stress. Deformations may terminate during construction or continue over a long time period (Barla, 1995).

Such large deformation causes some problems during and/or after construction such as: reductions in the cross-sectional area of an opening, slow down or obstruct TBM operation, increased the pressure on the lining or even damage it and finally resulting in great difficulties for completing underground works, with major delays in

construction schedules and cost overruns. Hence, prediction of squeezing conditions is of great importance to a designer for designing a stable support system of the tunnel (Singh et al., 2007).

2 SQUEEZING ASSESSMENT

Many authors have proposed a number of approaches for the assessment and support design for the squeezing ground in subsurface constructions. These approaches can be grouped in the following categories:
1. Empirical &Semi-Empirical
2. Analytical
3. Numerical modelling

2.1 Empirical & Semi-Empirical Approaches

The Empirical approaches are essentially based on classification schemes. A well-known empirical correlation to anticipate squeezing conditions based on the *Q*-value of the rock mass and overburden (H) was presented by Singh et al.(1992)(Table 1). In addition, similar empirical correlation was submitted by Goel et al.(1995) by considering the tunnel depth (H), the tunnel span or diameter (B), and the rock mass number (N) (Table 1).Recently, a novel empirical method for prediction of squeezing conditions in rock tunnels was proposed by Jimenez et al.(2011) which is based on the application of the theory of linear classifiers to an extensive database of well-documented squeezing case histories from tunnels in the Himalayas. This method allows proposing new class-separation lines to estimate the occurrence of squeezing conditions (squeezing vs. no-squeezing).The equations of 50% squeezing probability line is presented in table 1which could say that is the modified of Singh's et al (1992) correlation.

Semi-empirical approaches offer indicators for predicting squeezing, and also providing some tools for the estimation of the expected deformation around the tunnel and/or the support pressure by using closed form analytical solutions for a circular tunnel in a hydrostatic stress field. The common starting point of all these methods for quantifying the squeezing potential of rock is the use of the "competency factor", which is defined as the ratio of uniaxial compressive strength of rock/rock mass to overburden stress (Barla, 2001). For instance, Jethwa et al. (1984) predicted tunnel squeezing based on the ratio between rock mass uniaxial strength (σ_{cm}) and in situ stress ($p_0 = \gamma H$) which includes four degrees for classes of squeezing intensity (table1).

Other researchers have also proposed estimates of degrees of squeezing intensity based on estimation of tunnel deformations. Aydan et al. (1993) based on the experience with tunnels in Japan, proposed to relate the strength of the intact rock (σ_{ci}) to the overburden pressure (γH). Squeezing conditions will occur if the ratio ($\sigma_{ci}/\gamma H$) is less than 2.0.also, based on the analogy between the stress-strain response of rock in laboratory testing and tangential stress-strain response around tunnels, they proposed five different degree of squeezing based on the ratio between the peak tangential strain at the tunnel boundary and the elastic strain limit for the rock mass (table 1).

Hoek (1999) showed that the ratio of the uniaxial compressive strength of the rock mass (σ_{cm}) to the in situ stress (p_0) can be used as an indicator of potential tunnel squeezing problems. Also, Hoek et al. (2000) presented a curve to be used as a primary indicator of tunnel squeezing problems. In this curve, proposed five levels of squeezing based on tunnel strain which was plotted against the ratio σ_{cm}/p_0. Table 1.

Singh et al. (2007) used the critical strain to quantify the degree of squeezing potential. In the literature, the value of critical strain is generally taken as 1% but they showed that the critical strain is an anisotropic property that depends on the properties of the intact rock and the joints in the rock mass, and suggested a correlation for estimation of critical strain. Finally, they proposed the Squeezing Index (SI) (defined as expected strain divided by critical strain) to predict levels of squeezing potential in tunnels.

Table1. Empirical and Semi-Empirical methods for squeezing assessment in the tunnels

Considerations	relation	Parameters	methods	
Squeezing: $H \gg 350Q^{\frac{1}{3}}$ Non squeezing: $H \ll 350Q^{\frac{1}{3}}$	$H = 350Q^{\frac{1}{3}}$	Q: rock mass quality H: overburden	Singh et al. (1992)	Empirical
Squeezing: $H \ll (275N^{0.33})B^{-1}$ Non squeezing: $H \gg (275N^{0.33})B^{-1}$	$H = (275N^{0.33})B^{-1}$	N: rock mass number B: tunnel span H: overburden	Goel et al. (1995)	
Squeezing: $H \gg 424.4Q^{0.32}$ No squeezing: $H \ll 424.4Q^{0.32}$	$H = 424.4Q^{0.32}$	Q: rock mass quality H: overburden	Jimenez et al. (2011)	
highly squeezing: $\frac{\sigma_{cm}}{p_0} < 0.4$ moderately squeezing: $0.4 < \frac{\sigma_{cm}}{p_0} < 0.8$ mildly squeezing: $2 < \frac{\sigma_{cm}}{p_0} < 2$ non squeezing: $\frac{\sigma_{cm}}{p_0} > 2$	$N_c = \frac{\sigma_{cm}}{p_0} = \frac{\sigma_{cm}}{\gamma H}$	σ_{cm}: rock mass uniaxial compressive strength p_0: in situ stress γ: rock mass unit weight H: tunnel depth below surface.	Jethwa et al. (1984)	Semi-empirical methods
Non-squeezing: $\varepsilon_\theta^a/\varepsilon_\theta^e \le 1$ Light-squeezing: $1 \le \varepsilon_\theta^a/\varepsilon_\theta^e \le \eta_p$ Fair-squeezing: $\eta_p \le \varepsilon_\theta^a/\varepsilon_\theta^e \le \eta_s$ Heavy-squeezing: $\eta_s \le \varepsilon_\theta^a/\varepsilon_\theta^e \le \eta_f$ Very heavy squeezing: $\eta_f \le \varepsilon_\theta^a/\varepsilon_\theta^e$	$\eta_p = \frac{\varepsilon_p}{\varepsilon_e} = 2\sigma_c^{-0.17}$ $\eta_s = \frac{\varepsilon_s}{\varepsilon_e} = 3\sigma_c^{-0.25}$ $\eta_f = \frac{\varepsilon_f}{\varepsilon_e} = 5\sigma_c^{-0.32}$	σ_c: uniaxial compressive strength of intact rock ε_θ^a: tangential strain of circular tunnel ε_θ^e: elastic strain limit of rock mass ε_e: elastic strain limit of intact rock $\varepsilon_p, \varepsilon_s, \varepsilon_f$:strain values	Aydan et al. (1993)	
few support problems: $\varepsilon < 1$ minor squeezing: $1 < \varepsilon < 2.5$ severe squeezing: $2.5 < \varepsilon < 5$ very severe squeezing: $5 < \varepsilon < 10$ extreme squeezing: $10 < \varepsilon$	$\varepsilon_t = 0.15\left(1 - \frac{p_i}{p_0}\right)$ $\times \frac{\sigma_{cm}}{p_0}^{-\left(\left(3\frac{p_i}{p_0}\right)+1\right)/\left(\left(3.8\frac{p_i}{p_0}\right)+0.54\right)}$ $\sigma_{cm} = (0.0034m_i^{0.8})\sigma_{ci}$ $\times \left[1.029 + 0.025e^{(-0.1m_i)}\right]^{GSI}$	ε_t: tunnel strain p_i:Internal support pressure p_0: In situ stress σ_{cm}: Rock mass strength m_i:Hoek-Brown constant GSI: Geological Strength Index	Hoek and Marinos (2000)	
No squeezing: SI<1.0 Light squeezing: 1.0<SI≤2.0 Fair squeezing: 2.0<SI≤3.0 Heavy squeezing: 3.0<SI≤5.0 Very heavy squeezing: 5.0<SI≤10	$\varepsilon_{cr} = 31.1\frac{(\sigma_{ci})^{1.6}}{E_i\gamma^{0.6}Q^{0.2}}$ $\varepsilon_{cr} = 5.84\frac{(\sigma_{ci})^{0.88}}{E_i^{0.63}Q^{0.12}}$ $SI = \frac{\text{Observed or expected strain}}{\text{Critical strain}}$	Q: rock mass quality γ: density of rock mass σ_{ci}: UCS of intact rock E_i: elastic modulus of the intact rock, ε_{cr}: Critical strain SI: Squeezing Index	Singh et al. (2007)	

However, due to simplicity and ease of use, the Empirical and Semi-Empirical approaches still play a crucial role for squeezing prediction (Jimenez & Recio, 2011) and very useful method in preliminary studies, but in these methods, the results are qualitative and no time variable is taken into account therefore in complex condition, it's preferred to use other method such as analytical and/or numerical modelling approaches.

2.2 Analytical Approaches

Methods for analysis of tunnels in squeezing rock conditions need to consider (Barla, 2001):

- the onset of yielding within the rock mass, as determined by the shear strength parameters relative to the induced stress
- the time dependent behaviour.

In the most of analytical solutions the tunnel is assumed to be circular and the rock mass elasto-plastic and isotropic, subjected to a hydrostatic in situ state of stress. But these models do not consider the time-dependency of the squeezing phenomena.

Nevertheless, some analytical solutions were proposed to consider the time-dependency of deformations in squeezing ground. For instance, Fritz (1984) presented a solution for axisymmetric tunnels in elasto-viscoplastic media. Recently, Fahimifar et al. (2010)proposed an analytical solution for predicting time-dependent deformation of tunnel wall by using the Burger's body which is able to model the primary and secondary creep regions of the rock mass. Also, Nomikos et al.(2011) presented an exact closed form solution for the mechanical behaviour of a linear viscoelastic Burgers rock around an axisymmetric tunnel, supported by a linear elastic ring.

2.3 Numerical Modelling Approaches

Numerical methods which used for modelling of squeezing condition must represent the time-dependent behavior of the rock. Several time-dependant constitutive models have been proposed to model the complex time-dependant behavior of rock mass. Such as these time-dependant constitutive models are rheological models which include:

- Visco – elastic model(Kelvin, Maxwell, Burgers model),
- Visco-elasto-plastic model (CVISC model)
- Elasto-visco-plastic model (Sterpi & Gioda, 2009).

Also, empirical creep models have been used as the time-dependant constitutive models which are usually expressed in simple mathematical forms (power law, hyperbolic law and exponential law (Phienwej et al, 2007) (Shalabi, 2005)) with a small number of parameters. These parameters usually have been defined by using the tunnel monitoring data, which represent the real behaviour of the rock mass at the scale of the tunnel.

Some of these time-dependant constitutive models have been implemented in numerical code to simulate the time-dependent rock mass behavior. For instance, Shalabi (2005) used power and hyperbolic creep models to model ground squeezing by ABAQUS finite element analysis software. Nadimi et al. (2011) implemented power constitutive creep model for back analysis of time-dependent behavior of Siah Bisheh cavern by 3-Dimensional Distinct Element Method (3DEC software).

3 CASE STUDY: SABZKUH WATERTUNNEL

The Sabzkuh water tunnel project is located about 68 km south of Shahr-e-Kord city, in the Chaharmahal-Bakhtyari province in the west of Iran. The project is designed to control flood in the Sabzkuh drainage basin and transfer 75 million m^3 of water annually from the Sabzkuh drainage basin to the Choghakhor dam reservoir in order to provide water for drinking, industry and agricultural development of the region. Outline of the area is shown in Figure 1.

The tunnel has a circular cross section with 4.5 m diameter and has been excavated

with a double shield TBM in the length of about 10 km with gradient approximately 0.001.The maximum over burden in the tunnel route is about1160m.

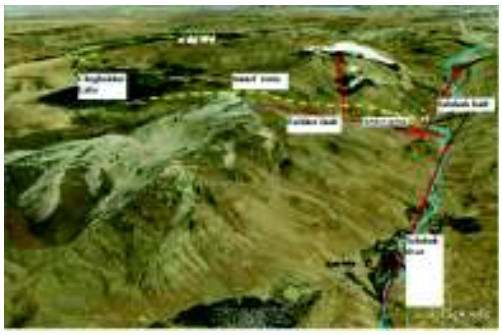

Figure 1-the outline of tunnel area

3.1 Engineering Geology

The study area is situated on the north side of Zagros Mountain which including Paleozoic and Mesozoic units.

The lithology of the tunnel route mainly consists of limestone, marly and dolomitic limestones, dolostone, shale and variable sizes of alluvium. At the project area, there are karstic features and traces, including sinkholes, solution dolines, lapies, poljes and shallow caves, which are locally observed in limestone. Furthermore, 18 faults are detected in these areas which have created crushed zones around them with different thickness. The main geologic structure at the project area is the Sabzkuh syncline.

For geotechnical evaluation and rock mass classification, the field observation, geophysical exploration, the field tests and laboratory experiments have been used and finally, according to geology and geological engineering studies, the tunnel is divided to 10 different zones. The basis of this division is the lithological properties of the layers, as well as structural differences, and therefore geomechanical properties. These zones include: Shale with Marly Limestone (Sh-Ml)،Marlstone and Marly Limestone (Ma-Ml) ،Limestone with Marlstone (Li-Ma), Limestone and Shaly interlayer (Li-Sh) ، Massive Dolomite (M-Do), Dolomitic

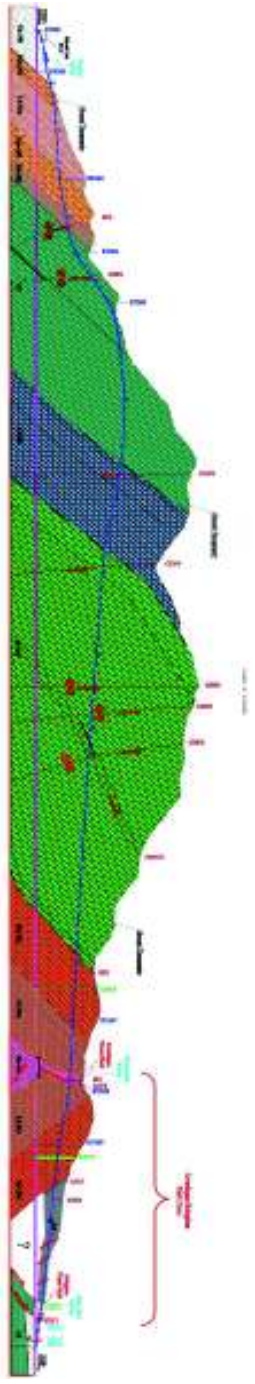

Figure 2. Engineering geological section of Sabzkuh tunnel

Limestone (Do-Li), Brecciated Dolomite (Br-Do), Shale with Sandstone(Sh-Sa) and Crushed Zone (CZ).An engineering geological section of Sabzkuh tunnel is shown in Figure 2.

RQD, RMR, Q, N and GSI systems have been used for classification of rock masses for different zones in the tunnel route. Figure 3 shows the GSI table for different zones in the tunnel rout.

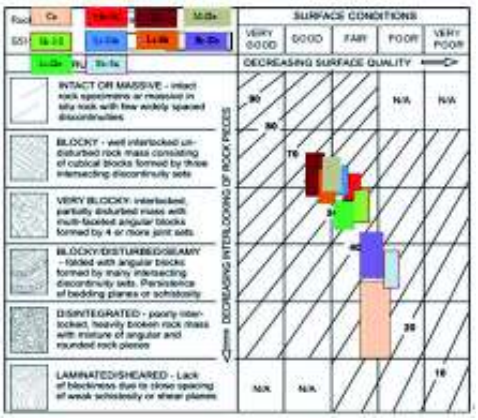

Figure 3. Table of GSI for different zone in the tunnel route

4 PREDICTION OF SQUEEZING IN THE SABZKUH TUNNEL

As previously mentioned rock mass strength and over burden (in-situ stress) are the main factors for the occurrence of squeezing. Many authors use the ratio of uniaxial compressive strength of rock mass to overburden stress for quantifying the squeezing potential of rock. In the Sabzkuh tunnel, due to very high overburden (up to 1160 m) and presence of weak zone, shear or crushed zone, layered formation and fault in the tunnel route, the occurrence of squeezing would be probable.

Hence, for prediction and quantifying of squeezing potential in the Sabzkuh tunnel's zones, the empirical and semi-empirical approaches are implemented. These methods are include: Singhet al.(1992), Goel et al.(1995), Jimenez et al.(2011), Jethwa et al.(1984) and Hoek et al. (2000).The squeezing potential for each zone are evaluated by these methods and the result are shown in the figure 4,5,6,7 & 8 and summered in table 2. In these methods, the average value of geomechanical properties and maximum over burden in the tunnel's zones have been considered.

As can be seen in Table 2, squeezing could happen in the most of tunnel zones.In the initial zone, i.e. Sh-Ml,Ma-Ml&Li-Ma, squeezing is not probable because in these zones, the overburden is low.In the Sh-Ml(ll) zone, according to three methods Singh et al.(1992), Jethwa et al.(1984) and Hoek et al. (2000), squeezing could happen and according to Hoek et al. (2000) method is estimated very severe squeezing.

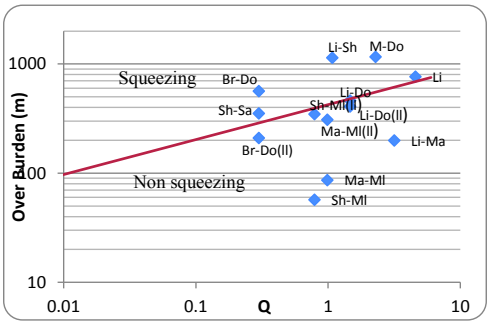

Figure 4. Prediction of squeezing potential for Sabzkuh tunnel's zone by Singhet al.(1992)

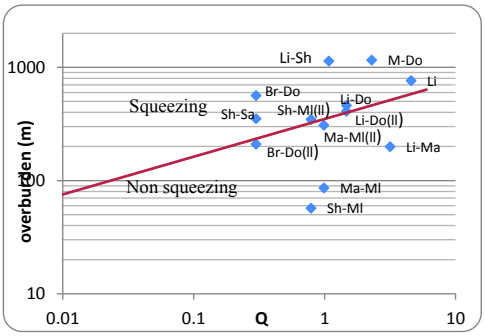

Figure 5. Prediction of squeezing potential for Sabzkuh tunnel's zone by Jimenez et al.(2011)

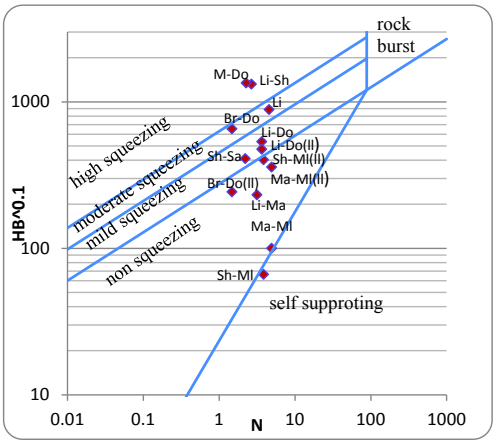

Figure 6. Prediction of squeezing potential for Sabzkuh tunnel's zone by Goel et al.(1995)

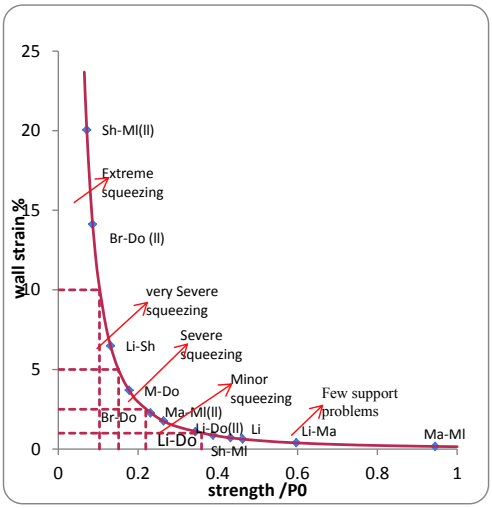

Figure 7- prediction of squeezing potential for Sabzkuh tunnel's zone by Hoek et al.(2000)

The Li, Li-Sh &M-Do zones have a stronger rock mass in the tunnel route but the overburden is very high and faults and discontinuities are presented in these zones. According to table 2, there is a squeezing potential in these zones and degree of intensity is between Fair to heavy squeezing. Also, the risk of rock burst phenomena should be studied in these zones.

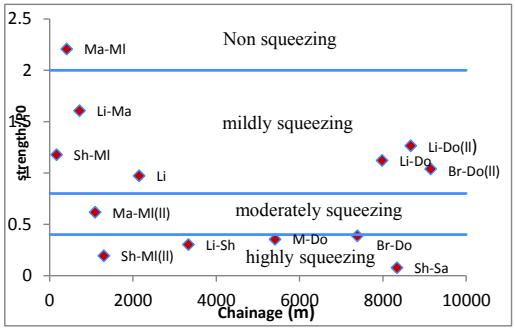

Figure 8. Prediction of squeezing potential for Sabzkuh tunnel's zone by Jethwa et al.(1995)

Br-Do zone is Brecciated Dolomite zone with a weak and jointed rock mass. In this zone, the core recovery is less than 40% and RQD is about 15%. Based on table 2,it is expected that heavy squeezing would be occurred in this part of the tunnel.

Sh-Sa is the critical zone in the route of tunnel. The rock mass is shale and have a very low strength. The maximum overburden in this zone is about 360 m. This zone is the most likely one for the occurrence of squeezing in the tunnel route.

According to table 2, the problems of squeezing are very serious in the Sh-Sa, Br-Do, Sh-Ml(ll),Li-Sh and M-Do zones .the degree of squeezing intensity in these zones are estimated between heavy to very heavy or extreme squeezing condition. So, for better understanding of rock mass behavior, more studies should be done in this zone. These studies are including the time dependent behavior of rock mass. Therefore, to determine the time dependent behavior of rock, the triaxial creep test was performed on the specimens from these tunnel zones. Here, the studies on Br-Do zone are presented.

5 TRIAXIAL CREEP TEST

To study the time dependent behavior of rock, triaxial creep tests have been conducted. In the tests, multiple stress levels were applied to small cylindrical specimens with a diameter of 54 mm and height of 100-110 mm. The stress level increment ranges from 2 to 5 MPa. Each stress level is

maintained for at least one day. The longest test lasted 41 days. Figure 9 show a stress-time and strain-time curves for the test on the specimen CH-T3(1).

The Specimens are prepared from rock cores of CH-T3 borehole that are drilled in the Br-Do zone. Most of these Specimens contain various flaws such as fractures, thin bedding, and pores with or without filling. Presence of these flaws and particularly the filling are the main reason for creep behavior of this rock. Figure 10, show flaws in the rock specimens .

Table 2. squeezing prediction by empirical method

Tunnel zone	from	to	Over burden	Singh (1992)	Jimenez (2011)	Goel (1995)	Jethwa (1984)	Hoek (2000)
Sh-Ml	0+000	0+344	57	NS[1]	NS	Self-supporting	Mildly-squeezing	Few problem support
Ma-Ml	0+344	0+482	86	NS	NS	No-Squeezing	No-Squeezing	Few problem support
Li-Ma	0+482	0+960	199	NS	NS	No-Squeezing	Mildly-squeezing	Few problem support
Ma-Ml(ll)	0+960	1+229	308	NS	NS	No-Squeezing	Moderate-squeezing	Minor squeezing
Sh-Ml(ll)	1+229	1+383	346	S[2]	NS	No-Squeezing	Highly squeezing	Extremely squeezing
Li	1+383	2+914	761	S	S	Moderate-squeezing	Mildly-squeezing	Few problem support
Li-Sh	2+914	3+758	1136	S	S	High-squeezing	Highly squeezing	Very severe squeezing
M-Do	3+758	7+071	1157	S	S	High-squeezing	Highly squeezing	severe squeezing
Br-Do	7+071	7+706	562	S	S	Moderate-squeezing	Highly squeezing	Extremely squeezing
Li-Do	7+706	8+255	460	S	NS	Mild-squeezing	Mildly-squeezing	Minor squeezing
Sh-Sa	8+255	8+430	352	S	S	Mild-squeezing	Highly squeezing	Extremely squeezing
Li-Do(ll)	8+430	8+911	408	S	NS	Mild-squeezing	Mildly-squeezing	Few problem support
Br-Do(ll)	8+911	9+390	209	NS	NS	No-Squeezing	Mildly-squeezing	Minor squeezing

[1] Non-squeezing
[2] squeezing

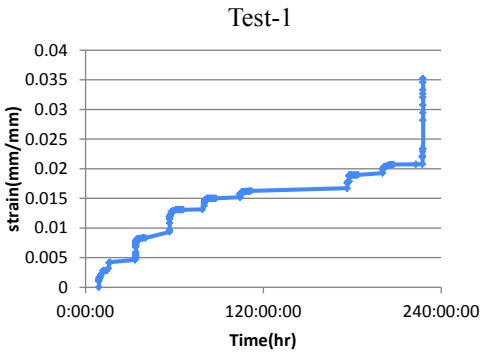

Figure 9. Creep test on Ch-T3(1) specimen

Figure 10. Core rock specimen from 254 to 255m in borehole CH-T3

As discussed in the section 2, many creep models have already been proposed. These reflect the fact that the creep behaviour of rock is very complicated depending on the rock types, stress conditions, temperature and etc. In this study, The Burger creep model was used for the modeling of creep behavior of rock. This model can describe the elastic strain (ε_e), primary creep (ε_1) and secondary creep (ε_2) as follows:

$$\varepsilon = \sigma\left(\frac{2}{9K} + \frac{1}{3G_m}\right) + \frac{\sigma}{3G_k}\left[1 - \exp\left(-\frac{G_k t}{\eta_k}\right)\right] + \frac{\sigma . t}{3\eta_m}$$

Parameters, K, and G_m are the bulk modulus and shear modulus of the spring, η_m is the viscosity coefficient of the dash pot in the Maxwell section and Parameters G_k, and η_k are the shear modulus of the spring, and the viscosity coefficient of the dash pot in the Kelvin body.

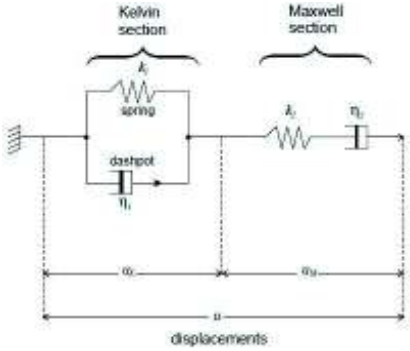

Figure 11. Schematic of Burger model (Itasca, 2002)

For all of the stage tests, the creep parameters of Burger model can be obtained by curve fitting of the axial strain vs. time curves based on Burger creep law. Elastic strain, primary creep and secondary creep were analyzed separately (figure-12). The average creep parameters obtained are shown in Table 3.

Table 3. Creep parameters of Burger model

K	G_m	G_k	η_k	η_m
9.57e9	1.29e9	2.23e9	8.15e10	1.74e13

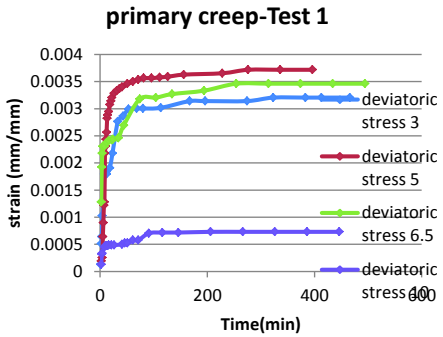

Figure 12. Primary creep in for the stage of tests 1

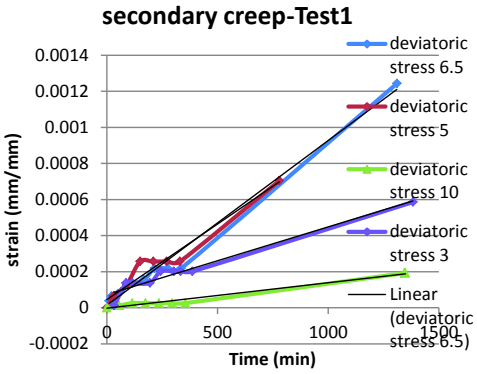

Figure13. Secondary creep for the stage of test-1

6 NUMERICAL SOLUTIONS

In this study, FLAC^{3D} (Version 3) was selected for numerical modelling of Sabzkuh tunnel. The Burgers model has been used for the time dependent behavior of rock. The input data for modeling are shown in the table 3 and a 3D model of excavated tunnel is given in figure 14.

Table 3-model parameters

Parameters	value
K	1.62e9
G_m	0.55e9
G_k	2.23e9
η_k	8.15e10 (min.pa)
η_m	1.74e13 (min.pa)
Over burden	562 m
Density	2.65 (gr/cm3)
K_0	1.35

In modeling, tunnel is assumed to be without support. The purpose of modeling is to study the time dependent convergence of tunnel in delay time which occurred in excavation stages. Numerical modeling was performed for tow time period (one week and one month). Figure 15&16 show the displacement against creep time for sidewall of tunnel.

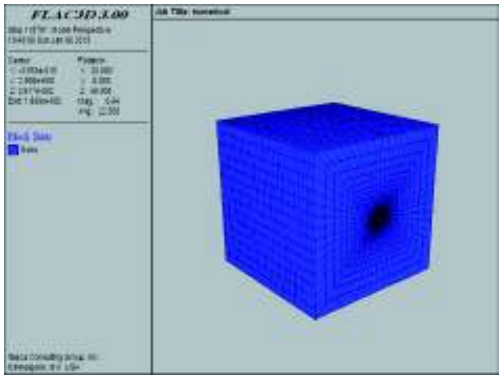

Figure 14. 3D model of excavated model

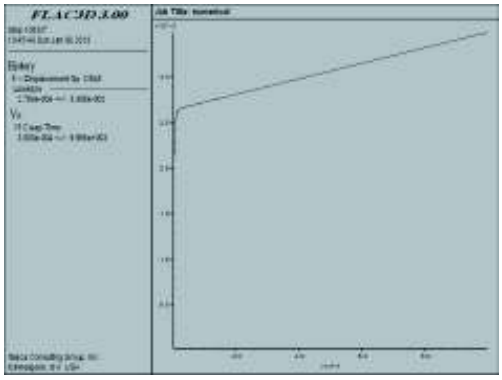

Figure 15. The displacement in the side wall against creep time for a week

Figure 17 shows the displacement around the tunnel after one month. As can be seen the floor convergence is larger than the crown convergence

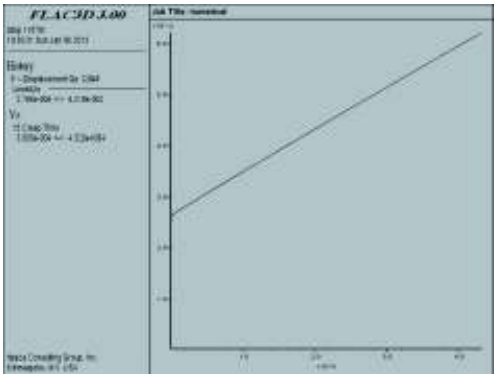

Figure 16. The displacement in the side wall of tunnel against creep time for a month

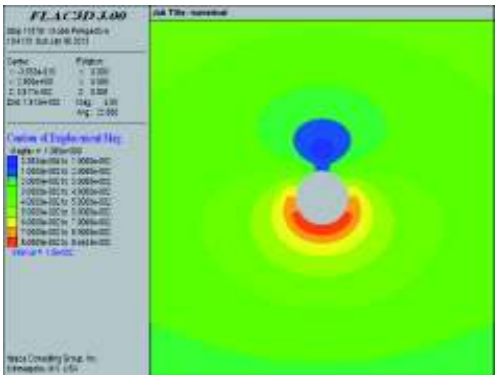

Figure 17. The displacement around the tunnel after one month

7 CONCLUSION

In this study, the squeezing potential of Sabzkuh tunnel was evaluated by empirical and numerical method. In Sabzkuh tunnel, Due to high over burden and weak rock mass, the squeezing could happen in the most part of the tunnel. Empirical methods also predict fair to heavy squeezing for most zones in the tunnel rout.

To study of time dependent behavior of rock masses in the Br-Do zone, triaxial creep was perform on specimens from the CH-T3 drill hole. In the tests, multiple stress levels were applied to the specimens which were constant for 1 to 5 days. The longest test lasted 41 days.

In the numerical modeling of time dependent behavior of rock, the Burger model have been used and creep parameters was obtained by curve fitting of the axial strain vs. time curves based on Burgers creep law. Numerical model showed a high convergence in tunnel. This high convergence causes some problems at the delay time in the excavation stage.

8 REFERENCES

Aydan, O., Akagi, T., & Kawamoto, T. (1993). The squeezing potential of rock around tunnels: theory and prediction. *Rock Mechanics and Rock Engineering , 26*, 137–163.

Aydan, Ö., Akagi, T., & Kawamoto, T. (1996). The squeezing potential of rock around tunnels: Theory and prediction with examples taken from Japan. *Rock Mechanics and Rock Engineering , 29* (3), 125-143.

Barla, G. (1995). Squeezing rocks in tunnels. *3/4*, 44-49.

Barla, G. (2001). *Tunnelling under squeezing rock conditions.* Eurosummer-School in Tunnel Mechanics, Innsbruck.

Fahimifar, A., Monshizadeh Tehrani, F., Hedayat, A., & Vakilzadeh, A. (2010). Analytical solution for the excavation of circular tunnels in a visco-elastic Burger's material under hydrostatic stress field. *Tunnelling and Underground Space Technology , 25* , 297–304.

Fritz, P. (1984). An analytical solution for axisymmetric tunnel problems in elasto-viscoplastic media. *International Journal for Numerical and Analytical Methods in Engineering , 8*, 325–342.

Goel, R., Jethwa, J., & Paithankar, A. (1995). Indian experiences with Q and RMR systems. *Tunnelling and Underground Space Technology , 10* , 97–109.

Hoek, E. (2001). Big tunnels in bad rock. *ASCE Journal of Geotechnical* , 726–740.

Hoek, E. (1999). Support for very weak rock associated with faults and shear zones. In E. Villaescusa, C. Windsor, & A. Thompson (Ed.), *In Rock support and reinforcement practice in mining*, (pp. 19-32). Rotterdam.

Hoek, E., & Marinos, P. (2000,). Predicting tunnel squeezing problems in weak heterogeneous rock masses. *Tunnels and Tunnelling International.*

Jethwa, J., Singh, B., & Singh, B. (1984). Estimation of ultimate rock pressure for tunnel linings under squeezing rock coditions—a new approach. In J. H. E.T. Brown (Ed.), *Design and*

Performance of Underground Excavations, (pp. 231–238). Cambridge .

Jimenez, R., & Recio, D. (2011). A linear classifier for probabilistic prediction of squeezing conditions in Himalayan tunnels. *Engineering Geology , 121* (3-4), 101–109.

Itasca Consulting Group, Inc. FLAC (Fast Lagrangian Analysis of Continua), Version 3.0 Minneapolis:ICG, 2002.

Nadimi, s., Shahriar, K., Sharifzadeh, M., & Moarefvand, P. (2011). Triaxial creep tests and back analysis of time-dependent behavior of Siah Bisheh cavern by 3-Dimensional Distinct Element Method. *Tunnelling and Underground Space Technology , 26* (1), 155–162.

Nomikos, P., Rahmannejad, R., & Sofianos, A. (2011). Supported Axisymmetric Tunnels Within Linear Viscoelastic Burgers Rocks. *Rock Mech Rock Eng , 44*, 553–564.

Phienwej, N., Thakur, P. K., & Cording, E. J. (2007). Time-Dependent Response of Tunnels Considering Creep Effect. *International Journal of Geomechanics , 7*, 296-306.

Shalabi, F. (2005). FE analysis of time-dependent behavior of tunneling in squeezing ground using two different creep models. *Tunnelling and Underground Space Technology , 20*, 271–279.

Shrestha, G., & Broch, E. (2008). Influences of the valley morphology and rock mass strength on tunnel convergence: With a case study of Khimti 1headrace tunnel in Nepal. *Tunnelling and Underground Space Technology , 23*, 638–650.

Singh, B., Jethwa, J., Dube, A., & Singh, B. (1992). Correlation between observed support pressure and rock mass quality. *Tunnelling and Underground Space Technology , 7* (1), 59–74.

Singh, M., Singh, B., & Choudhari, J. (2007). Critical strain and squeezing of rock mass in tunnels. *Tunnelling and Underground Space Technology , 22*, 343–350.

Sterpi, D., & Gioda, G. (2009). Visco-Plastic Behaviour around Advancing Tunnels in Squeezing Rock. *Rock Mech Rock Engng , 42*, 319–339.

Terzaghi, K. (1946). *Rock defects and loads in tunnel supports. Rock tunneling with steel.* Youngstown, Ohio: The Commercial Shearing and Stamping Co.

Behavior Assessment of Seismic Activity in Tabas Coal Mine

H. Kamranpoor Jahromi, K. Shahriar

Department of Mining and Metallurgical Engineering, Amirkabir University of Technology, Tehran, Iran.

ABSTRACT Tabas Coal Mine (TCM) is the first fully mechanized coal mine in Iran. TCM is in an active seismic area with eleven earthquakes of surface wave magnitude of 7 or greater recorded to have occurred in the last 80 years within an approximate radius of 500 kilometers around the mine locality.

With using of different relations of peak horizontal ground acceleration, it was shown that if an earthquake of the same magnitude and focal depth of the Tabas earthquake of 16 September 1978 occur within approximately 9 kilometers of the mine site, then collapse of the mine or severe damage would be expected whilst with distances greater than 50 kilometers no damage would be expected. In addition, the behaviors of induced earthquake on stability of TCM were assessed and were concluded that these earthquakes in distances farther than 20 km cause no damage.

1 INTRODUCTION

One of the stages of underground space design is the assessment of seismic activity and earthquake risk. The importance of this subject is when the area is seismic and major earthquakes were occurred there. The goal of this study is to evaluate the response and the kind of destruction of excavations under seismic loading, and determine the safe scope of mine for prevention and reduction of damage. The behavior of an excavation to an event of seismic loading depends on effects of static and transient related to seismic loading on an excavation (Brady and Brown, 2004).

The effects of the seismic events can be assessed in several ways; the first uses the magnitude of the earthquake, whereas the second considers the intensity, characterized by the relative degrees of shaking observed at the area of specific interest.

1.1 Classification of Earthquakes

Type of earthquakes is divided into four categories by seismologists, which are tectonic, volcanic, collapse and explosion (St. John and Zahrah, 1987). On the other hand, earthquakes can be classified into two types of natural and induced. Triggered or natural earthquakes have been occurred as results of tectonic deformation of drifting plates, volcanic activities (such as volcanic eruptions) and from surface processes like erosion and sedimentation, induced earthquakes have been created from Human activities and specifically induced stress perturbations of large-scale geoengineering constructions, which achieve or exceed triggered levels, though (Klose, 2010). Determination of type of earthquakes (induced or natural) is very difficult, although previous analyses have expressed with appropriate accuracy that large-sized earthquakes (> M6) with deep epicenter (>10 km) can be considered triggered or natural earthquakes, although, exceptions may be existed (Klose, 2013).

1.1.1 Induced earthquakes

Geoengineering activities which are the main cause of creation of induced earthquake include: surface and underground mining, artificial water reservoirs, hydrocarbon production, waste water injections deep underground, injections of carbon dioxide deep underground, deep geothermal energy production, and formation of artificial land (Klose, 2010, 2013). Figures 1-2 illustrate number of human-triggered earthquakes, versus time and the type of geoengineering activity, respectively.

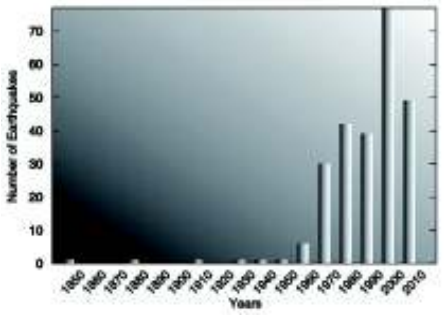

Figure 1. Number of induced earthquakes versus time, which are based on events with moment magnitudes Mw>4.5 (Klose, 2010, 2013)

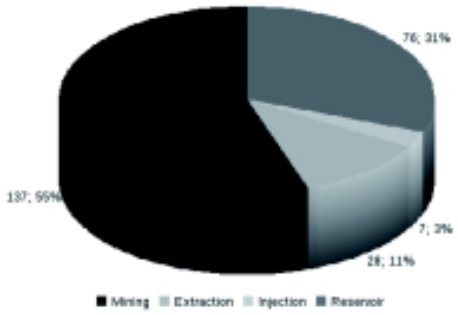

Figure 2. Number of induced earthquakes according to the type of geoengineering activity, which are based on events with moment magnitudes Mw>4.5 (Klose, 2010)

Induced earthquakes are mostly occurred in stable continental regions (>75 %) (Klose, 2007a). In contrast, they are slightly occurred in active continental regions (e.g., California, Japan or Turkey) (<25 %) that might be due to the fact that less attention is paid or assuming of natural origin (Klose, 2013). In general, induced earthquakes tent to occur in regions next to the geoengineering activities, stable continental regions and create lasting seismic activities in there (Klose and Seeber, 2007, Klose 2007, 2013). In addition, human caused earthquakes to nucleate in very shallow depths (<10 km); this assumption is based on that the geomechanical pollution on shallow crustal faults may cause failures (Klose, 2013).

1.2 Earthquake Magnitudes

For engineering purposes, the size of the earthquake is represented by its magnitude. Several magnitude scales currently used are: the local magnitude, the surface wave magnitude, the body wave magnitude and the moment magnitude which are symbolized by M_L, M_s, M_b and M_w, respectively. Definitions and their application of each of these scales are provided by Housner and Jennings (Housner and Jennings, 1982; St. John and Zahrah, 1987). In addition, by the following equations 1-4 for earthquakes with magnitude >M3.0 can be corrected in moment magnitudes M_w. Frequently, M_w is utilized for comparison of seismic events.

$$M_s = 1.27(M_L - 1) - 0.016M_L^2 \quad (1)$$

$$M_w = 0.67(\pm 0.005)M_s + 2.07(\pm 0.03) \quad 3.0 \le M_s \le 6.1 \quad (2)$$

$$M_w = 0.99(\pm 0.02)M_s + 0.08(\pm 0.13) \quad 6.2 \le M_s \le 8.2 \quad (3)$$

$$M_w = 0.85(\pm 0.04)M_b + 1.03(\pm 0.23) \quad 3.5 \le M_s \le 6.2 \quad (4)$$

Where M_L, M_s, M_b and M_w are the local magnitude, the surface wave magnitude, the body wave magnitude and the moment

magnitude, respectively (Kanamori1983; Scordilis, 2006; Klose, 2013).

1.3 Influence of Earthquake on Mines

Intensity of shaking has been proven to be less severe underground than at the surface except for very soft deposits, (Duke and Leeds, 1959; Kuesel, 1969; Dowding and Rozen, 1978; Dowding, 1979). It is shown that influences of natural earthquake on underground mining are limited, but these effects on surface operations are not ignored, and their resistance to earthquakes depends on the geomechanical properties of the ground, slope angle and water saturation (Lenhardt, 2009). Stevens supported this observation by stating that the effects of earthquake shaking are less in mines or caverns than at the surface due partially to the fact that many mines are located in solid rock, which is a good transmitter, and the wave energy is passed on through the rock with a minimum decrease in speed and the smallest displacement possible (Stevens, 1977).

A number of reports were cited by Tamura et al. to highlight further the reduced effects of earthquakes below the ground surface (Tamura et al., 1969). Dowding concluded from a number of observations in relation to tunnel damage as a result of earthquake shaking, that due to the same intensities, tunnels are much safer than surface structures. Also, in Modified Mercalli levels which little damage to tunnels is caused, the amount of destruction of surface structures is substantial (Dowding, 1979).

However, there are some examples of damage caused by the earthquake in tunnels such as the twin Bolu tunnels (Düzce ,Turkey), Wrights railway tunnel (California, United States), Kern County railway tunnel (California, United States) hit by the 1999 Düzce Mw=7.2, the 1906 San Francisco Mw=7.7 and the 1952 Kern County Mw=7.5 earthquakes, respectively (Kontogianni and Stiros, 2003). Thus, it is recommended that underground constructions within active earthquake areas should be at least 150 m below the surface.

2 CHARACTERISTICS OF THE STUDY AREA

TCM is the first fully mechanized coal mine in Iran that produces 1.1 million tonnes coal per annum. The mine is located in coal bearing basins of Parvadeh 1, which is in a remote rugged desert environment approximately 85 kilometers south of town of Tabas in Yazd province in mid Eastern Iran. North, south, east and west of the region is surrounded with quite smoothly desert plains, Triassic Jurassic heights, Shotori Mountains and Kalmard heights, respectively. Regional structure is almost uneven and its height from sea level is 800 to 1050. Parvadeh 1 anticline is limited to Rostam fault in north, boundary fault of Parvadeh 1 and 2 in south and southeast, sediments formation of Nayband in east and currently to a special North - South cross section in the west.

The study area is a desert region with a continental dry climate as previously mentioned, temperature fluctuations between -6.5°C and a maximum temperature of 49.5°C have been recorded at the meteorological station Parvadeh area. The humidity and rainfall of the area are low (IRITEC, 1992) .Location of TCM district is illustrated in Figure 3.

Figure 3. Location of TCM district in Iran

The Grid Reference location of the TCM that was used in the assessment of seismic impact on the TCM was:
Latitude: 33. 000°
Longitude: 56. 800°

To assess the hazard from seismic activity at the locality of the TCM it is first necessary to analyze past records of seismic activity for the region and determine what effects, they have had on the mine. This information can then be used to predict the hazard to the mine associated with future seismic activity and provide a basis of a seismic hazard assessment. Location of TCM district is illustrated in Figure 3.

3 DATA AND METHODS

The effects of seismic activity decrease with distance from the source of the earthquake due to attenuation of the wave energy as it passes through the ground. The effect of an earthquake for a specific locality is therefore, dependent both on the magnitude of the earthquake and the distance of the earthquake source from the locality. In general, the influence on underground structures not only depends on obvious distance of earthquake ground motions and the magnitude of the generating earthquake but also related to geomechanical properties of the surrounding rock mass, the overburden, the azimuth of the earthquake, its stress drop, rupture direction and seismic magnitude (Lenhardt, 2009).

In order to comment on the risk associated with seismic activity upon the stability of the Tabas coal mine, it is first necessary to establish the effects that would have been experienced at the locality of the mine of the previous earthquake activity. This information can then be used to predict the level of future risks associated with seismic activity.

3.1 Estimation of Earthquake Effect on Underground Structure

Sharma and Judd stated that the most significant parameters when determining the stability of an underground structure in a potentially active seismic area are depth, rock type, support type and earthquake parameters (Richter local magnitude and epicentral distance). The estimation of seismic risk is in general a difficult problem, for which important parameters are not always available (Sharma and judd, 1991).

Nieto-Obregon state that seismic risk may be evaluated in terms of three parameters of the probability of occurrence of a large earthquake, the vulnerability of structures likely to be affected by earthquake motions and The value of these structures from an environmental, economic and social perspective. The first of these is very difficult to estimate. In reality, the only imaginable way to estimate or predict the magnitude and intensity of the largest possible earthquake for any given region is to analyze past records (Nieto-Obregon, 1989).

Most tectonic earthquakes pass unnoticed underground but in few cases, little damage is experienced. Throughout the latter earthquake, only sudden dust was observed in the underground excavations, since on surface high level of damage was observed (Lenhardt, 2009). Based on experience, it is recognized that underground structures suffer damage only under exact situations.

Dowding and Rozen have correlated successfully the relationship between earthquake intensity and magnitude against underground structural damage. Although these studies were primarily centered on underground tunnel damage, these tunnels were located in rock environments; therefore, the applications of these results for this problem are valid (Dowding et al., 1978). Owen and scholl, Sharma and judd and Power et al. have updated Dowding and Rozen's work with 127, 192, 217 cases histories, respectively (Hashash et al., 2001).

A summary of Dowding and Rozen's work is given in the following Table 1 and Figure 4.

Table 1. Summary table relating peak ground acceleration to level of damage (Dowding and Rozen, 1978; Lenhardt, 2009)

Peak surface acceleration (g)	Peak surface acceleration (m/s^2)	Underground damage	Damage on surface to buildings	Macroseismic intensity
< 0.18	< 1.77	None (No damage)	frequent heavy damage	7
0.18 – 0.25	1.77 – 2.45	Few minor (Minor damage)	heavy damage to many buildings	8
0.25 – 0.5	2.45 – 4.9	Little (Minor damage)	massive	8-9
> 0.5	> 4.9	Larger (Damage/collapse)	major	10

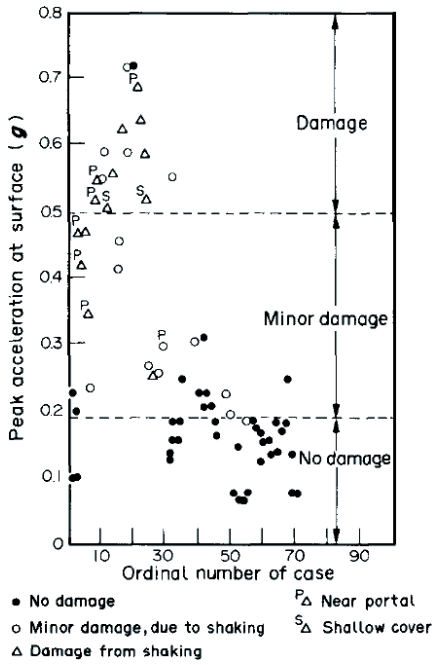

Figure 4. Calculated peak surface accelerations and related damage observations for earthquakes (Owen and Scholl, 1981; St John and Zahrah, 1987)

Dowding and Rozen state that "no damage" implied post shaking inspection revealed no apparent new cracking or falling of stones. "Minor damage" implicit fall of stones and formation of new cracks whilst "damage" implied major rock falls, severe cracking and closure (Dowding and Rozen, 1979). It has, however, been observed that severe local damage might occur if the mine intersects a fault, and if there is any displacement along this fault during the earthquake (Kaplanides and Fountoulis 1997). Bedding planes and other discontinuities may also serve as local faults within a mine structure.

3.2 Seismicity data for the Tabas region

Data in relation to previous seismic activity in the region of Iran where TCM is located was obtained from the British Geological Survey (BGS) and International Seismological Centre (ISC), Earthquake Information Services, which have compiled a World Seismicity Database (IRITEC, 2003; ISC, 2012). The database provides data relating to the location, magnitudes, epicentral depths, and intensities of earthquakes from 2500 BC onwards with increasing completeness and quality of solution with time. Prior to approximately 1900 the data was obtained mainly from historical sources whilst after that date, the data was derived from instrumental records. In this study, data was taken from International Seismological Centre (ISC) for the years after 1900, and before that date, data was obtained from the British Geological Survey (BGS).

The seismic data was obtained from the BGS and ISC for an area about 1000 kilometers by 1000 kilometers around and approximately centered on TCM, thus

approximating a 500 km radial area around the mine locality. This data forms the basis of this seismic assessment study. The seismic data for the 1000 km^2 region around the TCM indicates that the region has been an area of extensive seismic activity. The largest recorded earthquake is recorded to have occurred in 856 AD and had a surface wave magnitude (Ms) of 8.1. The level of seismic activity is illustrated in Figure 5, where the earthquake magnitudes are plotted against their date of occurrence for all recorded earthquakes since 800 ADs. Prior to this date only very few earthquakes have been recorded.

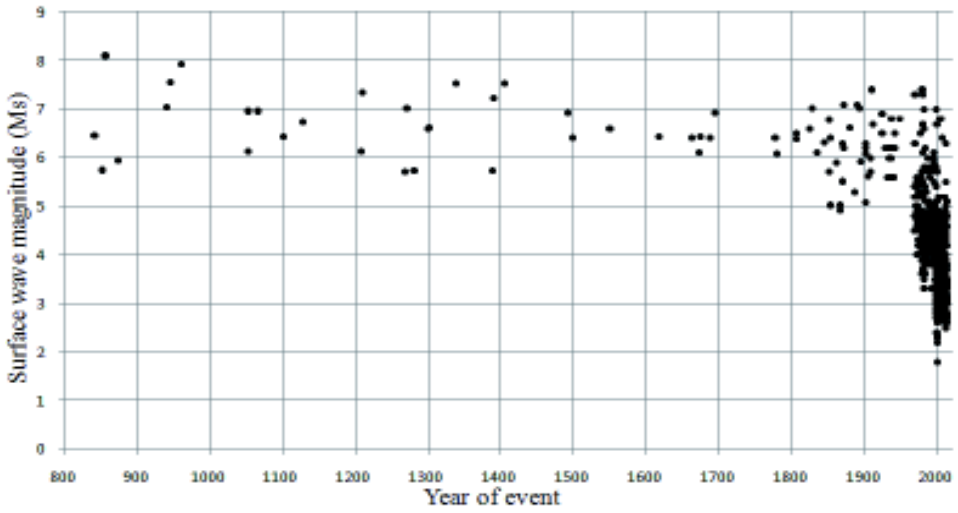

Figure 5. Surface wave magnitude (800 to 2012 AD) Tabas region

3.3 Seismic loads

There are two different methods to evaluate the seismic characteristics and predict earthquakes, empirical and physical modeling of the problem. Empirical modeling is a mathematical model based on regression techniques and varied data, which is important to have proper and adequate data for this approach. The other method is based on the stochastic modeling approach and random vibration theory, which is useful in the case of lack of certain data (Zafarani et al., 2008).

Iran is one of the world's most earthquake prone regions, which is located along the Alpine–Himalayan orogenic belt and there are more than 1000 stations in different active seismic regions (such as Tabas region) of Iran. As a result, there is sufficient and appropriate data then using of empirical approach is reasonable. To assess the effects that the ground motions would have on the mine stability, comparisons against Dowding and Rozen's limits on peak surface ground accelerations for underground tunnel damage have been made. The ground motion was determined as the peak horizontal ground acceleration (PHGA) expressed in different units like gravity (g, 981 cm/s^2), m/s^2 and cm/s^2 which was calculated using the attenuation laws, several empirical attenuation relationships are described below:

Fukushima and Tanaka, Ambraseys and Bommer, Ulatas and Firat Ozer, Ghodrati Amiri et al. and finally Bagheri et al. represent empirical attenuation relationships (equations 5-9) which are:

Fukushima and Tanaka's relation includes the Japanese region earthquakes:

$$\log(A) = [-\log_{10}(R + 0.032 \times 10^{0.41M_s})] + 0.217M_s + 0.41M_s - 0.0034R + 1.3 \quad (5)$$

Where A, M_s and R are PHGA (cm/s^2), surface wave magnitude and distance from the fault rupture zone, respectively (Fukushima and Tanaka, 1990).

Ambraseys and Bommer's relation includes the European region earthquakes:

$$\log_{10}(A) = -0.87 + 0.217M_s - \log_{10}\left((d^2+h^2)^{0.5}\right) - 0.00117\left(d^2+h^2\right)^{0.5} \quad (6)$$

Where A, M_s, d and h are PHGA (g), the surface wave magnitude, source distance (km) and the focal depth (km), respectively (Ambraseys and Bommer, 1991).

Ulatas and Firat Ozer's relation represents the Turkish region earthquakes (equation 8):

$$\log_{10}(A) = -\log_{10}\left(R + 0.0183\times10^{0.4537M_w}\right) - 0.0015R + 0.5344M_W - 2.7809 \quad (7)$$

Where A, M_w and R are PHGA (g), the moment magnitude and the closest distance from the fault rupture zone (km), respectively (Ulatas and Firat Ozer, 2010).

Ghodrati Amiri et al. and Bagheri et al. have provided two relations for Alborz and Central Iran with the assumption of rock condition (equations 9-10):

$$\ln A = 4.15 + 0.623M_s - 0.96\ln[R] \quad (8)$$

$$\log_{10}(A) = 2.173 + 0.185M_s + 0.006M_s^2 - 0.938\log_{10}\left((d^2+h^2)^{0.5}\right) \quad (9)$$

Where A, M_s, R, d and h are PHGA (cm/s^2), the surface wave magnitude and the distance of hypocenter to site (km) that is obtained by the S-P Method, source distance (km) and the focal depth (km), respectively (Ghodrati Amiri et al., 2007; Bagheri et al., 2011).

4 DISCUSSION AND RESULTS

4.1 Data Distribution

For this study, more than 750 data were applied within an approximate radius of 500 kilometers around the mine locality. The distributions of data are shown in the below histograms, which figure 6-7 indicate the number of records versus scope range of surface wave magnitude and ranges of distance (km), respectively.

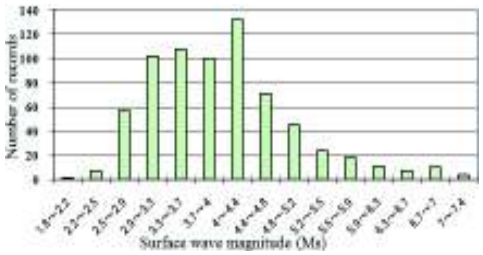

Figure 6. Histogram of surface wave magnitude (M_s)

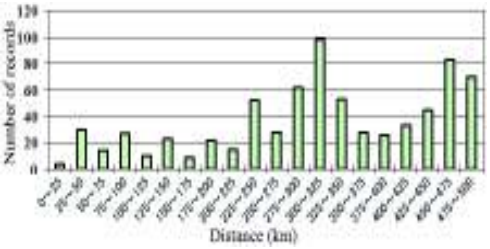

Figure 7. Histogram of distance (km)

4.2 Seismic Hazard Assessment

Figure 8 show plots of the calculated ground motions for TCM against dates of the seismic events with different empirical relations for the period 1900 to 2012 AD, these plots are related to the top 250 earthquakes, which produced much PHGA. It can be seen from the figure that all the earthquake events were calculated to have generated ground motions less than 1.8 g, and therefore, would be considered to have no effects on the stability of the TCM. The earthquake that was predicted to generate the greatest amount of ground motion at the site occurred in 1978 with a focus recorded to be approximately 75km to the west of the Tabas mine. This earthquake had the surface wave magnitude (M_s) of 7.4 and was predicted to have generated a PHGA up to 0.12 g. According to table 1, this degree of ground motion would be anticipated not to cause any damage in the mine. The available seismic data, therefore, indicates that past seismic activity would have caused little or no damage to the TCM.

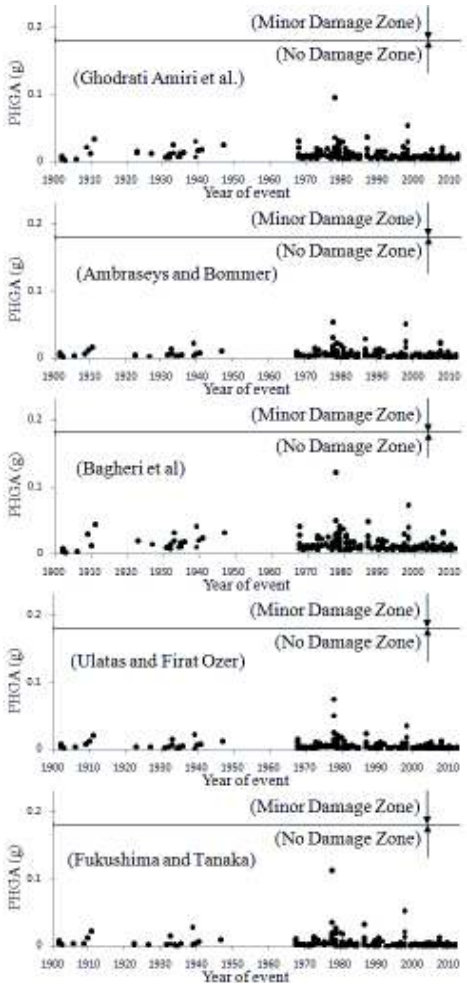

Figure 8. Peak acceleration predicted versus year of event for TCM locality (with different relations)

In appendix, each graph of different empirical relations of PHGA, based on changes in PHGA (g), surface wave magnitude (M_s), source distance (km) and focal depth (km) were plotted.

4.3 Affect of Earthquake on TCM

Although the Seismicity data indicates that no seismic event in the past would have caused damage to the Tabas coal mine, the data also indicates that the mine is within an area of active seismicity with eleven earthquakes of Ms magnitudes of greater than 7 occurring within the last eighty years. To illustrate the effect that the most well known recent earthquake would have on the Tabas coal mine at varying distance from the mine the peak ground accelerations were calculated for the Ms=7.4 earthquake with that occurred on 16 September 1978, and which had a devastating effect on the town of Tabas itself. Figure 9 plots the PHGA against distance between the mine site and earthquake focus with different empirical relations.

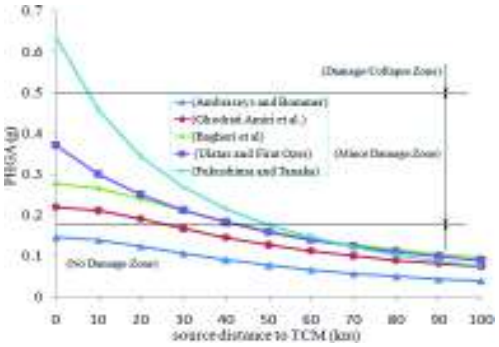

Figure 9. PHGA versus distance to TCM (M=7.4, focal depth = 34.1 km)

It can be seen according to different relations of PGHA, if this earthquake had occurred within nearly 9 km of the mine, then damage/collapse of the mine would be anticipated. With the focus between approximately between 9 and 50 km distance of the mine correspondingly minor damage would be anticipated. With the earthquake focus greater than 50 km from the mine then no damage would be expected.

According to Table 1, in the near ground portal area of drifts or adits the effects of ground shaking may be more damaging, and it is recommended that additional reinforcement use in these areas. It should be also being taken into consideration that tunnel displacement by fault movement usually results in serious damage. It is therefore recommended in areas of faulting, additional free standing steel supports be installed.

4.3.1 Affect of induced earthquakes

With mine advance, the possibility of induced earthquake in a radius of about 30 km of the large-scale mining increases. Magnitudes of these earthquakes directly depend on the tectonic stress regime (especially reverse fault regimes), magnitude of the mass shift and lateral distance that indicates an approximation of the rupture size (Klose, 2010, 2013).

According to table 2, the earthquakes within 30 km of TCM are observed, which occurred after the commencement of coal extraction. The seismic characteristics are quite similar to induced earthquakes. In Figure 10, the amount of acceleration due to earthquake induced by assuming of shallow depth (6 km) and medium-sized earthquake (M=6) is shown. In addition, the impacts of this type of human-made earthquakes on the surface facilities must also be considered.

Table 2 . Earthquakes within 30 km of TCM

DATE	LAT	LON	DEPTH	MAG
1/5/2008	33.042	56.541	4.3	3.2
7/24/2008	33.1	56.93	14	3.7
8/24/2008	32.9837	56.9207	10	3.7
6/11/2011	33.073	57.098	7	3

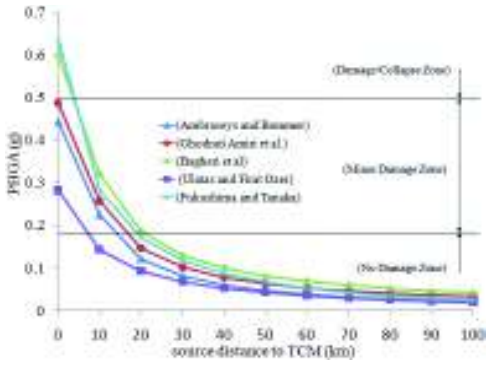

Figure 10: PHGA versus distance to TCM (M=6, focal depth = 6 km)

According to graph, if this earthquake had occurred within nearly 5 km of the mine, then damage/collapse of the mine would be anticipated. With the focus between approximately between 5 and 20 km distance of the mine correspondingly minor damage would be anticipated. With the earthquake focus greater than 20 km from the mine then no damage would be expected.

5 CONCLUSIONS

Tabas coal mine is in an active seismic area with eleven earthquakes of Ms magnitude of 7 or greater recorded to have occurred in the last 80 years within an approximate radius of 500 km around the mine locality. However, predictions of ground accelerations caused by the recorded seismic events indicates that the mine locality would have been unaffected by any of the events. These predictions are independent of the effects of seismic events on triggering reactivation movement on faults that may be present within the mine and which would depend on a variety of unknown factors.

The incompleteness of the seismic data, which may not include all earthquakes with a magnitude of greater than 7 prior to 1900, introduces a level of uncertainty into whether an earthquake may have occurred or may occur in the future within the influencing distance of the mine site. It is shown that if an earthquake of the same magnitude and focal depth of the Tabas earthquake of16 September 1978 occurred within approximately 9km of the mine site, then collapse of the mine or severe damage would be expected whilst with distances greater than 50 km no damage would be expected.

The earthquakes within 30 km of TCM which occurred after the commencement of coal extraction are quite similar to induced earthquakes. So, it is necessary to assess the behavior of this type of earthquake on TCM and especially, on the surface facilities. According to determining of impact of induced earthquake, it was shown that if it is occurred within approximately 5km of the mine site, then collapse of the mine or severe damage would be expected whilst with distances farther than 20 km no damage would be expected. However, induced earthquakes have an inverse relation between their distance and magnitude.

APPENDIX

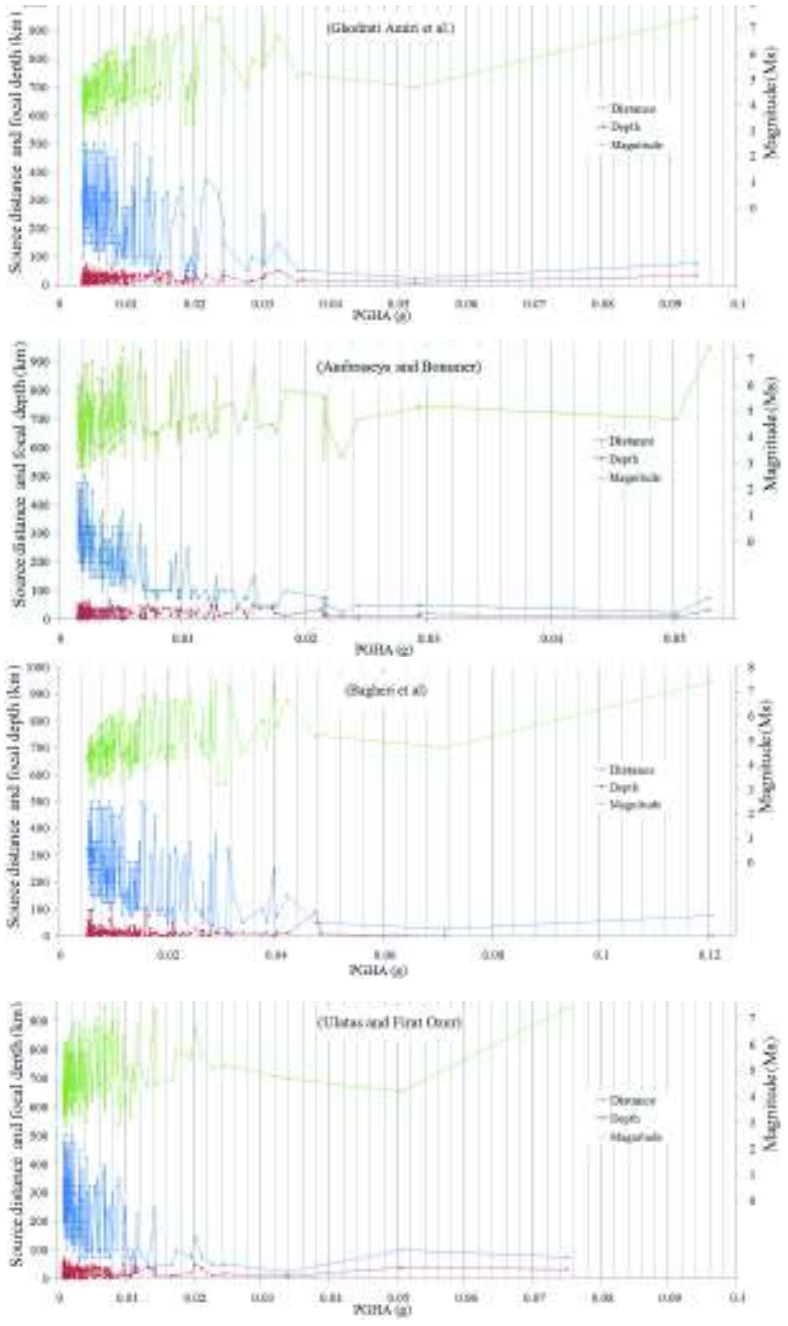
(Ghodrati Amiri et al.)
(Ambraseys and Bommer)
(Bagheri et al)
(Ulutas and First Ozer)
Source distance and focal depth (km)
Magnitude(Ms)
PGHA (g)
Distance
Depth
Magnitude

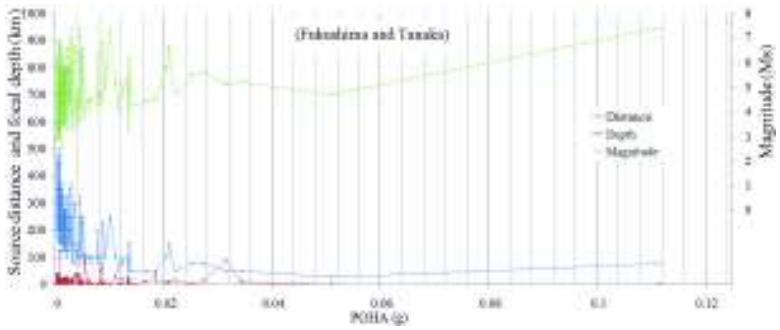

Figure 11. Graphs of different empirical relations of PHGA, based on changes in PHGA (g), surface wave magnitude (M_s), source distance (km) and focal depth (km)

REFERENCES

Ambraseys, N. N., Bommer, J. J., 1991. The Attenuation of Ground Accelerations in Europe, *Earthquake Engineering and Structural Dynamics*, 20, 12, pp.1179–1202.

Bagheri, A., Ghodrati Amiri, G., Khorasani, M., Haghdoust, J., 2011. Determination of attenuation relationships using an optimization problem, *International Journal of Optimization in Civil Engineering,* 4, 1, pp.597-607.

Brady, B.H.G., Brown E.T., (3th ed.), 2004. *Rock mechanics for underground mining*, Springer Science, New York, 626 p.

Dowding, C. H., 1979. *Site Characterization & Exploration,* American Society of Civil Engineers, New York, 395 p.

Dowding, C.H., Rozen, A., 1978. Damage to rock tunnels from earthquake shaking. J. Geotech. Eng. Div., ASCE 104 (GT2), 175_191.

Duke, C.M., Leeds, D.J., 1959. Effects of Earthquakes on Tunnels, Paper Presented at the RAND Second Protective Construction Symposium, March 24-26.

Fukushima, Y., Tanaka, T., 1990. A New Attenuation Relation for Peak Horizontal Acceleration of Strong Earthquake Ground Motion in Japan. *Bulletin of the Seismological Society of America*, 80, 4, pp.757–783.

Ghodrati Amiri, G., Mahdavian, A., Manouchehri Dana F., 2007. Attenuation Relationships for Iran. *Journal of Earthquake Engineering,* 11, 4, pp.469-492.

Hashash, Y.M.A., Hook, J.J., Schmidt, B., Yao, J.I.C., Seismic design and analysis of underground structures. *Tunnelling and Underground Space Technology,* 16, 4, pp.247-293.

Housner, G.W., Jennings, P.C., 1982. Earthquake design criteria, *Earthquake Engineering Research Institute*, Berkley, 140 p.

International Seismological Centre, 2012 *On-line Bulletin*, http://www.isc.ac.uk, Internatl. Seis. Cent., Thatcham, United Kingdom.

IRITEC, 1992. Internal Reports of Tabas coal mine, pp 17-60.

IRITEC, 2003. "Appendix A" of Final report of Tabas coal mine, pp.334-368.

Kanamori H., 1983. Magnitude scale and quantification of earthquakes. *Tectomophysics*, 93, pp.185-199.

Kaplanides A., Fountoulis D., 1997. Subsidence phenomena and ground fissures in Larissa, Karla basin, Greece: their results in urban and rural environment. *Proceeding of the International Symposium on the Engineering Geology and the Environment*, 1, pp. 729-735.

Klose, C.D., 2007. Geomechanical modeling of the nucleation process of Australia's 1989 Newcastle earthquake. *Earth and Planetary Science Letters,* 256, 3, pp.547-553.

Klose, C.D., 2007a. Mine water discharge and flooding: a cause of severe earthquakes. *Mine Water and the Environment,* 26, 3, pp.172-180.

Klose, C.D., Seeber, L., 2007. Shallow seismicity in stable continental regions. *Seismological Research Letters,* 78, 5, pp.554-562.

Klose, C.D., 2010. Human-triggered earthquakes and their impacts on human security. *Human and societal dynamics*, 69,1, pp.13-19.

Klose, C.D., 2013. Mechanical and statistical evidence of the causality of human-made mass shifts on the Earth's upper crust and the occurrence of earthquakes. *Journal of Seismology*, 17, 1, pp.109-135.

Kontogianni, V.A., Stiros, S. C., 2003. Earthquakes and Seismic Faulting: Effects on Tunnels. *Turkish Journal of Earth Sciences*, 12, pp.153-156.

Kuesel, T.R., 1969. Earthquake Design Criteria for Subways. *J. Struct. Div., ASCE ST6*, pp.1213-1231.

Lenhardt W.A., 2009. The Impact of Earthquakes on Mining Operations. *BHM Berg- und Hüttenmännische Monatshefte*, 154, 6, pp.249 254.

Nieto-obregon, I.J., Tectonic synthesis and seismic risk along the rio grande de santiago fault, in jalisco, mexico. *International Journal of Mining and Geological Engineering,*7,1, pp.37-51.

Owen, G.N., Scholl, R.E., 1981. Earthquake engineering of large underground structures. Report no. FHWA_RD-80_195. *Federal Highway Administration and National Science Foundation*.

Scordilis, E.M., 2006. Empirical global relations converting M_s and m_b to moment magnitude. *Journal of seismology*, 10, 2, pp.225-236.

Sharma, S., Judd, W.R., 1991. Underground opening damage from earthquakes. *Engineering Geology and the Environment*. 30, 263_276.

Stevens, P.R., 1977. A review of the effects of earthquakes on underground mines. *US Energy Research and Development Administration, Reston, VA, United States Geological Survey Open File Report,* pp.77-313.

St. John, C.M., Zahrah, T.F., 1987. Aseismic design of underground structures. *Tunneling Underground Space Technol*, 2 ,2, pp.165-197.

Tamura, T., Mizukoshi C., Ono T., 1969. Characteristics of earthquake motion at the Rocky Ground. *Proceeding of 4th World Conference on Earthquake Engineering*, Chile.

Ulutas, E., Fırat Ozer, M., 2010. Empirical attenuation relationship of peak ground acceleration for eastern marmara region in turkey. *The Arabian Journal for Science and Engineering*, 35, 1, pp.187-203.

Zafarani, H., Mousavi, M., Noorzad, As., Ansari, A., Calibration of the specific barrier model to Iranian plateau earthquakes and development of physically based attenuation relationships for Iran, *Soil Dynamics and Earthquake Engineering*. 28, 7, pp.550-576.

Design Method of Flexible Continuous Footings on Swelling Clay Soils

Med. Baheddi,
Dept of Civil Engineering, Batna University, 05000 Batna, Algeria.

M.D. Djafarov and A. Charif
Dept of Civil Engineering, Batna University, 05000 Batna, Algeria Laboratory of Soil Mechanics, Azerbaijan Civil Engineering University, Baku, Azerbaijan.
College of Engineering, King Saud University, P.O. Box 800 Riyadh 11421, Saudi Arabia.

ABSTRACT This paper analyses the behavior of swelling soils when they are moistened under buildings and structures. The methods and principles used currently for the design of structure foundations on swelling soils involve important problems due to non uniform deformations of these soils when subjected to the structure loads. In order to avoid the negative effects of swelling soils and to reach the desired performance on one hand, and the economical results on the other hand, the special computations of the foundations stiffness and deformability must take into consideration the prevention of the swelling soils feature and in some cases preserve it. The current study was conducted in order to design flexible continuous footings on swelling soils taking into account the water content change on one hand and the contact pressure distribution on the footing on the other hand.

1 INTRODUCTION

In any geotechnical study relative to a construction project, the swelling of a soil has a character as important as its settlement. The dimensional variations, which result from this phenomenon, constitute a permanent challenge for the design and geotechnical engineers. The durability of the structure constructed on the swelling soils depends on the good appreciation of the phenomenon.

The swelling of the clayey soils, containing smectites or illites in variable quantity, is at the origin of numerous distresses in buildings and large structures. These disturbances are frequent in the regions with dry climate as some Caucasian parts, in Kazakhstan, Algeria, Morocco, etc.
These soils, called "swelling", can provoke important material damages, or even partial to total rupture of the structure, when they are not taken into account in the design of projects. It is therefore important to foresee correctly the possible distortions of swelling soils, in amplitude and speed of evolution, and to analyze their influence on the serviceability or the stability of the structure.
The inflating soils have been a major concern for the designers for many years. Some construction procedures have been developed to limit the effects of inflation on the constructions and can be found notably in the classic works, of Mouroux and al. (1988) in French, Sorochan (1989) in Russian, and Chen (1988) in English.
Currently, an abundant documentation explains the mechanisms of the swelling of the clays, as much in the microscopic level as in test-tubes tested in laboratory or in-situ soil. Nevertheless, the survey of the behavior of the structures in contact with swelling soils constitutes a complex task and the existing methods contain some insufficiencies. Most of the research carried

out, is limited to the amplitudes of inflation of the clay soils in nature, under loads of superficial foundations. Little attention has been paid to the propagation of the inflation phenomena in the mass of the swelling soils as a function of time.

2 IDENTIFICATION OF THE MATERIAL

The studied swelling clay comes from the Urban District of Baku (Azerbaijan) where it has provoked many disturbances in the structures of a concrete channel. The survey has been achieved on test-tubes of undisturbed clayey soil samples, dated of the Pliocenes collected from the Shamour channel". Apcheron", (Baku, Azerbaijan) by the laboratory of soil mechanics of the Institute of civil engineering of Baku within a research program (Figure 1.).

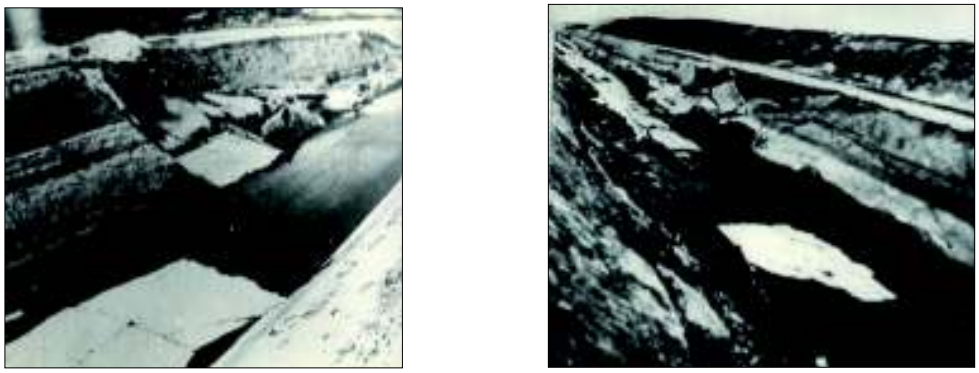

Figure 1. Example of disorders in the construction of « Samour –Apcheron » concrete channel.

2.1 Mineralogical Analysis

A diffractometry analysis by X-rays has been achieved to determine the mineralogy of the studied soils. The physical and mechanical properties are given in Table 1

Table 1. Physical and mechanical characteristics of the studied clay soils

Soil characteristics	Symbols	Unit	Values
Natural water content	W	%	10 -16
Degree of saturation	Sr	%	83 - 91
Wet Unit Weight	γ_h	kN / m^3	21.6 – 22.5
Dry Unit Weight	γ_d	kN / m^3	17.7 – 18.3
Specific Unit Weight	γ_s	kN / m^3	27.3 – 27.4
Voids Ratio	e	%	49.6 –54.2
Porosity	n	%	33 - 35
Liquid Limit	W_L	%	46 - 51
Plastic Limit	W_P	%	24 - 32
Plasticity Index	I_P	%	19 - 22
Liquidity Index	I_L	%	-41.0 to -74.0
Coefficient of compressibility	a_v	1/MPa	0.08
Modulus of distortion between 0.1 - 0.2MPa	E	MPa	
- At natural water content			7.0 – 7.8
- After saturation			6.0 – 7.2
Cohesion	C	MPa	
- At natural water content			0.2 – 0.58
- After saturation			0.08 – 0.14
Internal friction angle	φ	Degree	
- At natural water content			25 - 31
- After saturation			17 - 23
Grain size distribution			
0.5 - 0.25 mm	%		---
0.25 – 0.1 mm	%		---
0.1 – 0.05 mm	%		18.26
0.05 – 0.01 mm	%		23.58
0.01 – 0.005 mm	%		11.79
0,005 – 0.001 m	%		46.37

The chemical analysis of the samples of inflating clays gave the following composition:

SiO_2: 52.28 %	Al_2O_3: 15.27 %	Na_2O: 2.73 %
K_2O: 2.59 %	MgO: 2.45 %	CaO: 6.70 %
TiO2: 0.79 %	MnO_2: 0.10 %	Fe_2O_3: 6.77 %

The chemical analysis by the method of dosage of the elements composing the swelling clay has given the results of Table 2.

Table 2. Chemical composition of the studied clays

N° of the sample	Units	Denomination							
		Na+K	Ca^{++}	Mg^{++}	Cl	SO_4	HCO_3	CO_3	PH
1	%	13.88	1.49	0.33	7.3	6.59	1.19	0.63	7.5
2	%	12.18	1.69	0.33	7.30	5.42	0.89	0.59	7.8
3	%	13.88	1.29	0.25	7.30	6.84	0.89	0.39	7.8

3 EXPERIMENTAL ANALYSIS AND INTERPRETATION OF THE RESULTS

The rate of swelling, corresponds to the relative variation of volume (in %) of a sample subjected to a non-excitant overload or very low load (generally the weight of the piston in an oedometer) when it is put in contact with water with no pressure. The pressure of swelling is constituted of an "osmotic" component due to the difference of concentration in salts of the interstitial water and a "matrix" component governed by the initial negative interstitial pressure of the sample that plays, in most cases a major role.
Numerous methods have been proposed in the literature to evaluate the potential of a swelling soil from the measure of the parameters of plasticity and grading - for example Seed and al, 1962 (quoted by Didier, 1972) , Komornik and David, 1969, Vijayvergiya and Ghazzaly 1973, Dakshanamurphy and Raman, 1973 (Meisina in, 1996), Chen, 1988, and E.A.Sorochan, 1989 .

For these authors, a very high swelling potential corresponds to a free swelling (expressed in percentage) superior to 25%, an high potential, to an inflation between 5 and 20%, a medium potential, to an inflation between 1.5 and 5% and a low potential, to an inflation lower to 1.5%. For Komornik and David (1996), the corresponding pressures of swelling are, respectively, superior to 300 kPa (potential very elevated), varying between 200 and 300 kPa (elevated), between 100 and 200 kPa (medium) and lower to 100 kPa (weak).
Several methods also exist to measure the pressure of inflation in oedometer, among these methods we quote:
Method of Huder and Amberg (1970) .
Method of inflation with constant volume, according to the ASTM norm D 4546-90.
Method of inflation or settlement under constant load, which requires several identical samples.
Free swelling method followed by a reloading.
The experimental studies on the inflating soils (or expanding) show that the percentage of a soil inflation should increase proportionally with its density, its limit of liquidity, its contents clay, its indexes of plasticity and shrinkage, as well as its pressure of pre-consolidation (Seed and al, Ranganatham and Satyanarayana, 1965; Vijayvergiya and Gazzaly, 1973 and E.A.Sorochan, 1989). These same studies report that the pressure of inflation of an expanding soil should be inversely proportional to its natural water content.
The analysis of the experimental results, allowed us to draw the curves giving the variation of the swelling potential in function of time for different values of the compression stresses. It also allowed us to establish the dependence of the water content after inflation in function of the different values of the compression stresses, the distortion of soils after their inflation in function of the different

compression stresses as well as the variation of the inflation potential according to the water content in oedometer tests.

Figure 2. Test of inflation in a free cell oedometer (without piston)

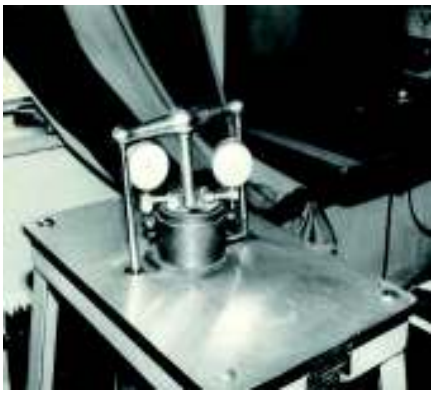

Figure 3. Swelling test in an oedometer under loading

The following section is relative to the mathematical description of the laws of behavior and inflation established from the oedometric testing of the samples.
The dependence of the water content inflating soil on the compression stresses after inflation has the shape of an exponential function, hence:

$$W_{SW} = W_{SW}^{0}\, e^{(-\bar{\gamma}P)} \quad (1)$$

With:

W_{SW}^{0} : The content in water of a sample after swelling without load (P = 0)
And

$$\bar{\gamma} = \left(\frac{1}{P}\right)\ln\left(\frac{W_{SW}^{0}}{W_{SW}}\right) \quad (2)$$

For the interval of the stresses, that is generally from 50 kPa to 400 kPa in civil and industrial constructions, the dependence between the water content of soil inflating and the compression stresses can be approximated by the relation.

$$\mathrm{W_{SW}} = \overline{\mathrm{W}}_{\mathrm{SW}} - \aleph P \quad (3)$$

With:

$\overline{W}_{SW}$: Initial value of content in water taken from the graph $W_{SW} = f(P)$ (Figure 5.).
$\aleph$: Depends directly on the slope $W_{SW} = f(P)$ and for the study of soil by the oedometer, we obtain:
$\overline{W}_{SW} = 0{,}24; \quad \aleph = 0{,}2\mathrm{MPa}^{-1}$

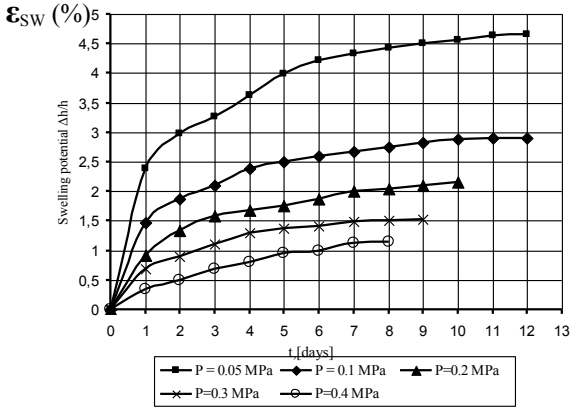

Figure 4. Variation of the swelling potential with time

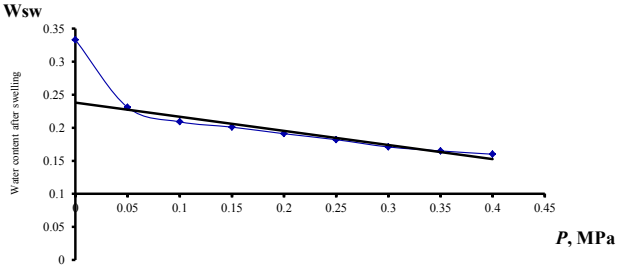

Figure 5. Variation of the water content with different load levels

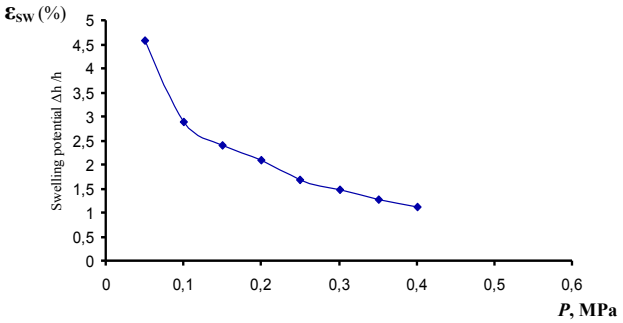

Figure 6. Variation of the inflation potential function of the different loads

The following section is relative to the mathematical model describing the expansion mechanism, established from the oedometric tests.

The dependence of the water content of an expansive soil, on the compression stresses (after swelling has taken place) can be expressed by an exponential function:

$$W_{SW} = W_{SW}^{0}\, e^{(-\bar{\gamma}P)} \quad (1)$$

with:

W_{SW}^{0}: Water content without loading (P = 0)

and $$\bar{\gamma} = \left(\frac{1}{P}\right) \ln\left(\frac{W_{SW}^{0}}{W_{SW}}\right) \quad (2)$$

For the interval of stresses, generally between 50 and 400 kPa in civil and industrial constructions, the dependence between the water content of the expansive soil and the compression stresses can be approximated by the relation.

$$W_{SW} = \overline{W}_{SW} - \aleph P \quad (3)$$

With:

$\overline{W}_{SW}$: Initial value of water content given by a straight line in Figure 5.

$\aleph$: Slope of the curve in Figure 5.

The obtained values are:

$\overline{W}_{SW} = 0{,}24; \quad \aleph = 0{,}2\text{MPa}^{-1}$

In this part, five models of inflation prediction according to the geotechnical properties of the inflating clays have been considered. Their formulations are given in Table 3.

Further review of the models indicates that:

Some models do not have as parameter the content in natural water of soil: models of Seed and al. first model of Vijayvergiya and Ghazzaly.

The limitation of the domain of application of these formulas between a lower boundary- of the inflation amplitude from which the soil is qualified as inflating (5%) and an upper boundary mark is equal to the greatest percentage of inflation having been observed (60%). This allows us to determine, from these models, a minimum water content comparable to the shrinkage limit of and content in maximal water comparable to liquid limit.

Mathematically, the models of prediction should constitute functional relations between a dependent variable, the percentage of inflation, and some independent explicative variables.

Table 3. Tested Models of prediction for the inflation of the clays.

Model	Reference	Mathematical expression
Seed and al.	Seed and al. (1962)	$\varepsilon_{sw} = 2{,}16.10^{-5} I_P^{2{,}44}$
Nayak and Christensen	Nayak and Christensen (1971)	$\varepsilon_{sw} = 2{,}29.10^{-2} I_P^{1.45} \frac{C_2}{W_0} + 6{,}38$
Vijayvergiya and Ghazaly-1	Vijayvergiya and Ghazzaly (1973)	$\lg(\varepsilon_{sw}) = \frac{62{,}42\gamma_d + 0{,}65W_L - 130{,}5}{19{,}5}$
Vijayvergiya and Ghazaly-2	Vijayvergiya and Ghazzaly (1973)	$\lg(\varepsilon_{sw}) = \frac{0{,}4W_L - W_0 + 5{,}5}{12}$
Johnson	Johnson (1978)	Pour I_P<40 $\varepsilon_{sw} = -9{,}18 + 1{,}5546\, I_P + 0{,}08424\, Z +$ $+ 0{,}1W_0 - 0{,}0432 W_0 I_P - 0{,}01215\, Z\, I_P$

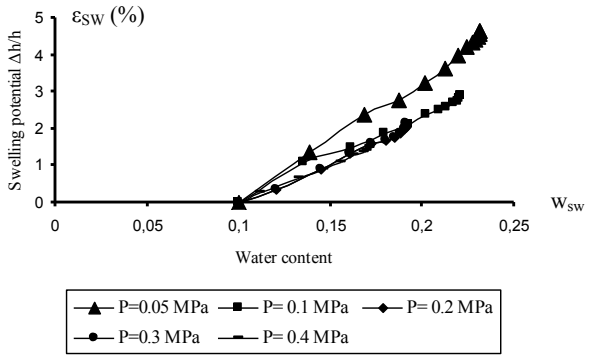

Figure 7. Variation of the swelling potential in function of the water content.

4 PROPOSITION OF A MODEL FOR THE SWELLING POTENTIAL OF THE STUDIED CLAYS

The analytical results obtained show that, the mechanism of variation of the potential of soil inflation, dependent on the values of compression stresses and the variations of the contents in water in the process of its swelling, is governed by:

$$\varepsilon_{SW} = \varepsilon_{SW}^{0}\left(1-\frac{P}{P_{SW}}\right)\left[(\overline{W}_{SW}-W_0)-\aleph P\right] \qquad (4)$$

As it was showed by the analysis, this analytical expression leads to determine with a good precision the value of the swelling potential of the clayey soils on the basis of their features obtained from the tests on samples of soil inflating in oedometer molds. This formula contains the specific features of the swelling soils:

ε_{sw} : Potential of swelling.

ε_{sw}^{0} : Potential of swelling without loading.

P_{sw} : Pressure of swelling.

$\overline{W}_{sw}$: Initial value of water content given by the graph $W_{sw}=f(P)$ (Figure 5.).

The expression of the inflation potential is different from the one found in the literature by a good approximation of the non-linearity of $\varepsilon_{sw}=f(P)$, so that the power of the P steers does not exceed 2

5 CALCULATION OF THE FLEXIBLE STRIP FOUNDATIONS UNDER THE ACTION OF THE SWELLING SOILS

The superficial foundations on swelling soils must be designed by taking into account the capacity of these soils to inflate when their content in water increases. The design of the foundations on swelling soils must take into account the various possible shapes of soil distortion at the time of the wetting such as:

- uplift of the foundation under the effect of the soil inflation;
- drop of the foundation in the layer of soil that inflated because of the deterioration of these physical and mechanical properties caused by the wetting;
- uplift of the foundation followed by its drop in the soil that inflated.

The swelling soils are characterized by a swelling pressure P_{sw} water content of inflation W_{sw}, and a value of the inflation distortion (ε_{sw} under the imposed pressure P). Given a flexible strip foundation of length L, with a constant bending rigidity on the whole length, the action of some outside loads $q(x)$, and the layer under the footing composed of one clayey inflating soil, the interaction of the foundation base with the surface of

inflating soil is determined according to the following proposed model :

$$R(x) = K_S\, b\left[y(x) - \bar{S}_{sw}(x)\right] \quad (5)$$

where:

$R(x)$: Reaction of the inflating soil pressure on the footing.

K_S : Coefficient of rigidity of the swelling soil.

b : The foundation width.

$y(x)$: The foundation strain.

The function $\bar{S}_{SW}(x)$ represents the variation in the vertical direction of the basis of the foundation to the upper surface of inflating soil, it is expressed as:

$$\bar{S}_{SW}(x) = S_{SW}^{\max} - S_{SW}(x) \quad (6)$$

In this last expression $S_{SW}^{\max}$ is the final distortion after stabilization of the phenomenon of inflation that is concomitant with the minimal value of the contact pressure. $S_{SW}(x)$ is the non uniform distortion induced by the swelling soil on the basis of the foundation in function of the variation of the water content The action of the contact pressure on the base of the footing is in conformity with experimental research [1]

$$S_{SW}(x) = S_{SW}^{0}\left\{\left[1 - \frac{P(x)}{P_{SW}}\right]\left[(\bar{W}_{SW} - W_0) - \aleph P(x)\right]\right\} \quad (7)$$

S_{SW}^{0} : Absolute amplitude of free swelling of soil, equal to: $S_{SW}^{0} = \varepsilon_{SW}^{0}.H_{SW}$ With

ε_{SW}^{0} : Free relative swelling,

H_{SW} : Thickness of the swelling soil layer.

P_{SW} : Pressure of swelling.

W_0 : Initial water content.

$\bar{W}_{SW}$: Initial value of the water content of the swelling soil, with P = 0

(Strait line that cuts the vertical axis taken from the diagram of the function $W_{sw} = f(P)$; (Figure. 5)

$\aleph$: Slope of the straight line representing the diagram of the contents in water according to the compression stresses.

$P(x)$: Distribution of the contact pressures under the base of the foundation, in correlation with the theoretical method of Simvoulidi concerning the calculation of a foundation on elastic soil.

$$P(x) = a_0 + \frac{2a_1}{L}(x - 0.5L) + \frac{4a_2}{L^2}(x - 0.5L)^2 + \frac{8a_3}{L^3}(x - 0.5L)^3 \quad (8)$$

where:

L : the length of the foundation

a_0, a_1, a_2, a_3 : known parameters depending on:

- the foundation rigidity.
- the foundation length.
- module of soil distortion.
- type and the location of the external load.

The indicative values of the parameters, in spite of their slight contribution facilitate the convenient calculations.

The differential equation of bending concerning the foundation will be written as follows:

$$EI\, y^{IV}(x) + K_S\, b\left[y(x) - \bar{S}_{sw}(x)\right] = q(x) \quad (9)$$

$$EI\, y^{IV}(x) + K_S\, b\, y(x) = q(x) + K_S\, b\, \bar{S}_{sw}(x) \quad (10)$$

Equation (10) can be used for bending of the footing on elastic soil, under the influence of an outside active load $q(x)$ and complementary loads.

$q_{eq}(x) = K_S\, b\, \bar{S}_{sw}(x)$: the equivalent load on the footing of a non-uniform distortion due to the contact of the surface of the footing with swelling soil after variation of its content in water.

Equation (10) can be written:

$$y^{IV}(x) + 4a^4 y(x) = \frac{1}{EI}\bar{q}(x) \quad (11)$$

where:

$$a = \left(\frac{K_S\, b}{4EI}\right)^{\frac{1}{4}}; \qquad \bar{q}(x) = q(x) + q_{eq}(x)$$

For computational convenience, let us consider the non-dimensional coordinates. $\eta = ax$. In these conditions the derived functions (x) with respect to x and η are given by.

$$y'(x)=\frac{dy(x)}{dx}=\frac{dy(x)}{d\eta}\frac{d\eta}{dx}=a\frac{dy(\eta)}{d(\eta)}$$

$$y''(x)=\frac{d^2y(x)}{dx^2}=\frac{d^2y(x)}{d\eta^2}a\frac{d\eta}{dx}=a^2\frac{dy(\eta)}{d\eta^2}$$

$$y'''(x)=\frac{d^3y(x)}{dx^3}=\frac{d^3y(x)}{d\eta^3}a^2\frac{d\eta}{dx}=a^3\frac{d^3y(\eta)}{d\eta^3}$$

$$y^{IV}(x)=\frac{d^4y(x)}{dx^4}=\frac{d^4y(x)}{d\eta^4}a^3\frac{d\eta}{dx}=a^4\frac{d^4y(\eta)}{d\eta^4}$$

Equation (11) with the non-dimensional coordinates takes the following form:

$$\frac{d^4y(\eta)}{d\eta^4}+4y(\eta)=\frac{4}{K_S\,b}\bar{q}(\eta) \qquad (12)$$

The boundary conditions of the problem are given by:

$$\left.\begin{array}{ll} y(0)=0 & ;\ y'(0)=\theta_0 \\ EI\,y''(0)=-M_0 & ;EI\,y'''(0)=-Q_0 \end{array}\right\} \qquad (13)$$

Where: y_0,θ_0,M_0,Q_0, are initial parameters of the problem:

y_0 : The strain of the footing.

θ_0 : the rotation angle .

M_0 : bending moment.

Q_0 : The shear in the beginning of the section of the footing (with η=0).

The mathematical formulation of the problem of the bending of strip foundation on a deformable basis due to inflation, leads to the resolution of the linear equation of the non-uniform distortion of the fourth degree (11) with constant coefficients. In general the resolution of this equation is based on the global resolution of an uniform equation.

$$\frac{d^4y(\eta)}{d\eta^4}+4a^4y(\eta)=0 \qquad (14)$$

(14) designates the particular solution of the heterogeneous equation (12).

The global resolution of the homogeneous equation (10), expressed with the help of the fundamental functions of Krylov $y_1(\eta);y_2(\eta);y_3(\eta);and\ y_4(\eta)$ is :

$$y(\eta)=A\,y_1(\eta)+B\,y_2(\eta)+C\,y_3(\eta)+D\,y_4(\eta) \qquad (15)$$

where:

$$y_1(\eta)=\cos\eta\,ch\eta$$

$$y_2(\eta)=\frac{1}{2}(\sin\eta\ ch\eta+\cos\eta\ sh\eta)$$

$$y_3(\eta)=\frac{1}{2}\sin\eta\ sh\eta$$

$$y_4(\eta)=\frac{1}{4}(\sin\eta\ ch\eta-\cos\eta\ sh\eta)$$

The function of Krylov satisfies the conditions of Cauchy and constitutes what is called the matrix unit:

$$\begin{array}{llll} y_1(0)=1\ ; & y_2(0)=0 & y_3(0)=0 & y_4(0)=0 \\ y_1'(0)=0 & y_2'(0)=1 & y_3'(0)=0 & y_4'(0)=0 \\ y_1''(0)=0 & y_2''(0)=0 & y_3''(0)=1 & y_4''(0)=0 \\ y_1'''(0)=0 & y_2'''(0)=0 & y_3'''(0)=0 & y_4'''(0)=1 \end{array}$$

While using the matrix of reduction and boundary conditions (13), the constants of integration, A, B, C and D are then given by.

$$A=y_0 \quad ; \quad B=\frac{1}{a}\theta_0 \quad ;$$

$$C=-\frac{1}{a^2EI}M_0 \quad ;D=-\frac{1}{a^3EI}Q_0 \ .$$

Considering the obtained expressions, the solution of the homogeneous equation (14) is written as:

$$y(\eta)=y_0y_1(\eta)+\frac{1}{a}\theta_0y_2(\eta)-\frac{M_0}{a^2EI}y_3(\eta)-\frac{Q_0}{a^3\ EI}y_4(\eta) \qquad (16)$$

The fundamental functions $y_i(\eta)$ (i = 1; 2; 3 and 4) possess remarkable properties; they express themselves by successive products

with precision until some constant coefficients repeat themselves, that is to say:

$$y_1'(\eta) = -4y_4(\eta); \quad y_1''(\eta) = -4y_3(\eta);$$
$$y_1'''(\eta) = -4y_2(\eta); \quad y_1^{IV}(\eta) = -4y_1(\eta).$$
$$y_2'(\eta) = y_1(\eta); \quad y_2''(\eta) = -4y_4(\eta);$$
$$y_2'''(\eta) = -4y_3(\eta); \quad y_2^{IV}(\eta) = -4y_2(\eta).$$
$$y_3'(\eta) = y_2(\eta); \quad y_3''(\eta) = y_1(\eta);$$
$$y_3'''(\eta) = -4y_4(\eta); \quad y_3^{IV}(\eta) = -4y_3(\eta).$$
$$y_4'(\eta) = y_3(\eta); \quad y_4''(\eta) = y_2(\eta);$$
$$y_4'''(\eta) = y_1(\eta); \quad y_4^{IV}(\eta) = -4y_4(\eta).$$

The features of the Krylov function lead to simplifications in the solution of the problem, as for example the non-necessity to express boundary conditions between separated sections of the foundation. This simplification leads to a unique solution of the shape equation (11). This solution permits to operate with any intermittent loads, with the exception of the one, where the unity matrix is reduced to zero with any type of anchorage of the foundations in the beginning of the section and when two out of the four unknown initial parameters are taken equal to zero.

The partial solution of the heterogeneous equation (12), considering the theory of Krylov takes the following shape:

$$\Phi(\eta) = \frac{4}{K_S\, b}\int_0^{\eta} y_4(\eta-\xi)\,\bar{q}(\xi)\,d\xi \qquad (17)$$

The global solution of the problem of flexible foundations, free and supported by elastic compressible soil, ($M_0 = Q_0 = 0$), has the following expression:

$$y(\eta) = y_0 y_1(\eta) + \frac{1}{a}\theta_0 y_2(\eta) + \frac{4}{k_S\, b}\int_0^{\eta} y_4(\eta-\xi)\,\bar{q}(\xi)\,d\xi \qquad (18)$$

The computation of the values of the reaction due to the pressure of soil, the bending moment and shear force, is carried out by means of expressions (19), (20) and (21):

$$P(\eta) = K_S\, b\left[y(\eta) - \bar{S}_{sw}(\eta)\right] \qquad (19)$$

$$M(\eta) = -a^2 EI\,\frac{d^2 y(\eta)}{d\eta^2} \qquad (20)$$

$$Q(\eta) = -a^3 EI\,\frac{d^3 y(\eta)}{d\eta^3} \qquad (21)$$

6 CONCLUSIONS

For expansive soils, the designers are only interested in the measurable quantities which are generally the pressure and the amplitude of expansion. These values influence the choice of the foundation system. On the basis of the non-linearity of the physical mechanism of distortion, the method developed in the present work, relates the phenomenon of expansion with the distribution of the contact pressure, the rigidity of the foundation and the soil properties, as well as the type and value of the external loading.

The proposed mathematical formulation includes the different parameters influencing the behavior of a flexible strip foundation in contact with an expansive soil and delivers the general solution.

The solution obtained in the studied real case corresponds to that of Krylov expressed by .

The obtained results open new perspectives for methods of conception of foundations on expansive clay soils

REFERENCES

Baheddi M. & Mustafaev A. A., (1990), Mechanism of distortion of the inflating clays under the effect of the centrifugal forces and the calculation of the seated foundation on these soils. Ph.D., thesis. Moscow, (in Russian).

Chen F.H., (1988), Foundations on expansive soils. Developments in Geotechnical Engineering, vol. 54, Elsevier publishing Co., Amsterdam, 464 p.

Didier G., (1972), Gonflement cristallin et macroscopique des montmorillonites, Thèse pour l'obtention du titre de Docteur Ingénieur, Université Claude Bernard, France.

Didier G., Laréal P., Gielly J., (1973), Prévision du potentiel de la pression de gonflement des sols, Comptes rendus du 8ème Congrès international de mécanique des sols et des travaux de fondations, Moscou, vol. 2.2, pp.67-72..

Huder J. Amberg G., (1970), Quellung in merged, opalinuston und anhydrite. Schweizerische Bauzeitung, n° 43, pp.975-980.

Johnson L.D, (1978), Predicting potential heave and heave with time in swelling foundation soils, Technical Report S-78-7, US Army Corps of Engineers, Waterways Experiment Station, Vicksburg, Miss.

Kabbaj M., (1989), Sols gonflants: mesure des propriétés en laboratoire. Revue marocaine du génie civil, n°26, p.17-27.

Komornik A., David D. (1969), Prediction of swelling pressure of clays. Journal of the Soil Mechanics and Foundations Engineering Division ASCE, vol.95 SM1, 209-225.

Krylov A. N. (1930); Calculation of beams on elastic soil. Moscow,135 p. (in Russian).

Magnan J.P., Shakhirev V., Ejjaouani, (1995), Etude expérimentale du comportement de pieux forés dans des sols gonflants, Bulletin de liaison des laboratoires des ponts et chaussées. N° 198, pp 29-38.

Meisina C., (1996), Critère et méthodes pour l'évaluation du gonflement de différents types de sols et terrains de la région de Pavie. Thèse de Doctorat, 281 p. (en italien).

Mouroux P., Margon. P., Pinte J.-C., (1988), La construction économique sur les sols gonflants, BRGM, Manuels et méthodes 14, 125 p,.

Mustafaev A. A., (1989), "Foundations on subsiding and swelling soils" (In Russian) Vysshaya shkola, Moscow, 592 pages.

Nayak N.V., Christensen R.W., (1971), Swelling characteristics of compacted expansive soils, Clays and Clay Minerals, vol. 19, 4, pp. 251-261.

Philipponnat G., (1991), Retrait gonflement des argiles, proposition de méthodologie. Revue Française de géotechnique, N° 57, pp.5-22.

Seed H.B.and al, (1962), Studies of swell pressure characteristics of compacted clays. "Highway research board". N° 113.

Shakhirev V., Magnan J.P., Ejjaaouani H. (1996), Etude expérimentale du comportement du sol lors du fonçage des pieux. *Bulletin de liaison des laboratoires des ponts et chaussées*, N° 206, pp. 99-116.

Ranganatam B.V., Santyanarayana B, (1965), A rational methods of predicting swelling potential for compacted expansive clays. *Proceedings of the 6th International Conference on Soil Mechanics and Foundations Engineering*, Montreal, vol. 1, pp. 92-96.

Simvoulidi A. A; (1987), *Calculation of constructions on elastic soil.* Moscow 375 p. (in Russian)

Sorochan E.A., (1989), Construction of works on the inflating soils. Strojizdat, Moscow 312 p. (in Russian).

Vijayvergiya V.N., Ghazzaly O.I., (1973), Prediction of swelling potential for natural clays, *3rd Int. Conf. on Expansive S*

Çimentosuz Macun Dolgu Uygulanabilirliği Üzerine Bir İnceleme ve Macun Dolgu Yerinde Dayanımının Laboratuvar Testleri ile Yanlış Tayininde Konsolidasyon Etkileri

An Investigation on Uncemented Paste Backfill Applicability and Consolidation Effects on Inaccuracy of Paste Backfill in situ Strength Estimation by Laboratory Tests

E. Kömürlü, A. Kesimal, B. Erçıkdı
Karadeniz Technical University Mining Engineering Department, Trabzon, Turkey

ABSTRACT In this study, it is aimed to point out the importance of consolidation condition differences between laboratory mixes and mine paste backfill for the responsibility of laboratory mix specimen tests. As another topic, strength of consolidated and drained uncemented paste backfill (UPF) was tested with Çayeli copper-zinc mine tailings. Necessary strength for paste fill is explained. Applicability of UPF is commented according to measured mechanical parameters. It is seemed that uncemented tailings can have enough strength to be durable under own weight of 5–7 meters height material. This height is up to tailings type and its consolidation. Even though it fails under its own weight, UPF can be applied as efficient reinforcement for some specific situations. Paste backfill consolidation ratio is different for laboratory mix specimens and in situ backfill material. Much more time is needed for in situ consolidation of backfill material. Cemented paste backfill can't complete consolidation in stopes. Its consolidation is stopped by hydration reactions. Consolidation ratio varies due to tailings type. Strength of paste backfill changes with void ratio of wet and granular media during hydration. This situation causes misleading laboratory results. When different material designs are compared, tailings that supply higher strength for laboratory specimens can be lower in situ strength one. Reasons are explained with consolidation theory.

Keywords: Paste Backfill, Consolidation, Uncemented mine fill, Sub-level Caving

1 INTRODUCTION

Paste backfill (PF) is a type of underground mine reinforcement and it generally contains tailings of mineral processing plant. Cemented wet tailings material is pumped to underground. Therefore, rheology of backfill is important. Water content has to supply applicable liquidity (Kesimal et al., 2004). Paste-backfill material is Non-Newtonian fluid; it doesn't flow without applying stress. Typical yield strength of fresh paste backfill is between 0.1 and 0.7 kPa (Yumlu, 2008).

Millions tons of waste is generated each months in the world. Deposition of waste is very important topic about environment. PF supplies advantage about disposing of mine waste material. With PF technology, underground stopes can be supported economically by using mineral processing plant tailings. Therefore, paste backfill will be standard application for many sub-level caving, cut-and-fill mines all over the world (Belem and Benzaazoua, 2004).

Generally, paste backfill is not used as main supporting material. Cemented rock backfill is main support that has higher strength. And, paste backfill reinforces the rock backfill, as it is schematically shown in Figure 1. Although strength increases for higher cemented PF, fluidity mustn't be as excessive as non-applicable level. Loaded rock fill (RF) tends to expand in horizontal direction, paste backfill reacts and causes to occur horizontal reinforcing pressure on RF.

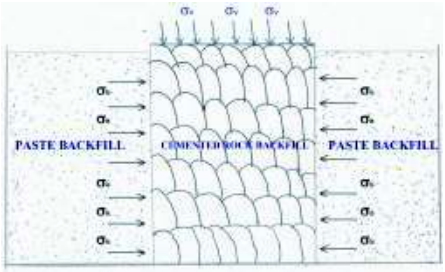

Figure 1. Interaction of rock and paste fills

The mission of paste backfill is not carry stope roof load. Because of its high water content, high rate settlement is actualized as a result of consolidation. Therefore, empty volume occurs between paste backfill and stope roof. If backfill is not drained, particles settle in wet media and moist backfill layer occurs on saturated backfill. Because of fine material content, consolidation time is long for paste backfill (PF). PF solidifies before consolidation ends. Strength is affected by excess water/cement ratio (Kömürlü and Kesimal, 2011). Draining decreases the PF consolidation time. Void ratio decreases more with more consolidation (Uzuner, 2007). Draining decreases the water content in PF. Strength is increased by draining PF (Ercikdi et al., 2008). Draining pipes can be used in stopes. Figure 2 shows usage of draining pipes, schematically.

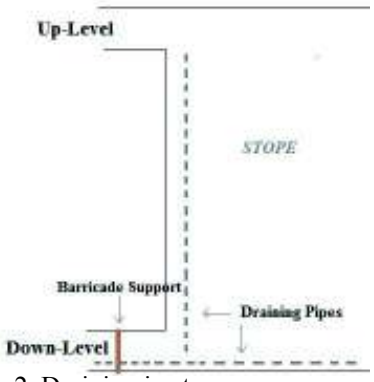

Figure 2. Draining in stope

When near stope is produced, paste backfill has to have enough strength to be durable under its self weight. Vertical stress due to PF self weight can be calculated as it is given in Equation 1 (Hudson and Harrison, 2000).

$$\sigma_v=\gamma.z \quad (1)$$

γ is unit volume weight of material (kN/m^3), z is the depth from the top of backfill (m). Uniaxial compressive strength has to be higher than stress due to weight. 1 MPa can be seen as widely aimed strength to reach for many paste backfill applications that have about 15 meters backfill height (Ercikdi, 2009). Even though 0.45 MPa is seemed as enough for 30 kN/m^3 unit volume weight. 1 MPa can be assumed as very typical desired strength for investigated conditions in mine. In addition to strength for static loads, reaction of backfill must be considered for dynamic loads since the stopes are opened by blasting. Ore dilution actualizes as a result of blasting (Ercikdi et al., 2003).

Draining also decreases the applied horizontal load on barricade. Horizontal stress of backfill material is applied on barricades (Kömürlü, 2012). Horizontal stress level is function of vertical stress and k ratio, as it is shown in Equation 2 (Gerçek, 2007).

$$\sigma_h=\sigma_v k \quad (2)$$

Where, σ_h is horizontal stress (MPa), σ_v is vertical stress (MPa). k ratio can be approximately calculated by using Mohr-Coulomb failure envelope. k ratio defines the slope of envelope. Therefore, it is up to internal friction angle (ϕ). k ratio can be divided into three: stable (normal) k ratio, active k ratio and passive k ratio. k ratio in Equation 3 is normal k ratio. In this situation, there is not un-stable form in material (Uzuner, 2007)

$$k=1-\sin\phi \quad (3)$$

Passive k (k_p) is the k ratio of material that is failed because of horizontal stress. Horizontal stress is major stress (σ_1) in passive failure. Passive k ratio is given in Equation 4 (Uzuner, 2007). Passive k ratio is not ratio of horizontal support pressure to vertical stress due to weight of material. It is about horizontal load and induced vertical stress due to horizontal load. k ratio is stress transportation parameter of material. Active k (k_a) is the ratio of horizontal stress to vertical stress when material is exposed to active failure. Vertical stress is major stress (σ_1) in actively failed material. Therefore, active k is smaller than 1. Failing because of material self weight is an example for active failure. If material's internal friction angle is zero, k ratios are 1 for both failed (actively

or passively) and stable forms. Active k ratio is given in Equation 5 (Uzuner, 2007)

$$k_p=(1+\sin\phi)/(1-\sin\phi)=\tan^2(45+\phi/2) \quad (4)$$

$$k_a=(1-\sin\phi)/(1+\sin\phi)=\tan^2(45-\phi/2)=1/k_p \quad (5)$$

k ratio is 1 in hydrostatic condition. Fresh cemented backfill material is not completely fluid. It behaves like a fluid when an external force is applied on it. It is non-Newtonian fluid. Internal friction angle of fresh cemented-backfill material is not zero, material is not hydrostatic and horizontal stress is not equal to vertical stress. However, measured horizontal stresses are similar with vertical stresses in fresh paste-backfill material (Karaoğlu et al., 2011). Some horizontal stress calculation models are suggested to use for backfill material. One of them is Marston's cohesionless model for 2D solution which is given in Equation 6 (Belem and Benzaazoua, 2004).

$$\sigma_h=\frac{\gamma B}{2\mu'}\left[1-\exp\left(\frac{2k_a\mu' H}{B}\right)\right] \quad (6)$$

Marton's modified model by Aubertin for 2D solution is given in Equation 7 (Belem and Benzaazoua, 2004).

$$\sigma_h=\frac{\gamma B}{2\tan\phi'}\left[1-\exp\left(-\frac{2k_a H\tan\phi'}{B}\right)\right] \quad (7)$$

Where B is width of stope (m), H is total height of filling material (m), μ' is sliding friction coefficent between filling material and sidewalls of stopes. μ' is tanδ. δ is wall friction angle, it can be assumed between 1/3 ϕ and 2/3 ϕ. Terzaghi's 2D model is a cohesive model that predicts horizontal stress as it is shown in Equation 8 (Kömürlü, 2012).

$$\sigma_h=\frac{(\gamma B-2c)}{2\tan\phi'}\left[1-\exp\left(-\frac{2k_t H\tan\phi'}{B}\right)\right] \quad (8)$$

$$k_t=1/(1+2\tan^2\phi) \quad (9)$$

Another cohesive model is Rankine's model. There are passive and active forms of Rankine model. Active model can predicts the horizontal stress of backfill material and it is given in Equation 10. Fresh backfill material tends to fail actively, barricade and stope walls are exposed to the actively distributed horizontal backfill stress (Li and Aubertin, 2009)

$$\sigma_h=k_a\sigma_v-2c\sqrt{k_a} \quad (10)$$

As it is seemed in Terzaghi's and Rankine's theorems, horizontal stress is decreased by increasing cohesion. Cohesion of fresh cemented tailings is not zero. If it was zero, there would be no need to act stress for its flowing. It has yield strength as a result of its cohesion. Therefore, horizontal pressure isn't equal to vertical pressures in backfill. Another model is 3D Belem model. It is given in Equation 11 and Equation 12 (Belem and Benzaazoua, 2004)

$$\sigma_h=\frac{\gamma H(H-z_e)}{3(B+L)}\left[1-\exp\left(-\frac{2(z_i-z_e)}{B}\right)\right] \quad (11)$$

$$\sigma_h=\frac{0.185\gamma H(H-z_e)}{B+L}\left[1-\exp\left(-\frac{2(z_i-z_e)}{B}\right)\right] \quad (12)$$

Where, L is strike length of stope (m), B is width of stope (m), z_e is measurement point elevation from floor of stope (m) and z_e is zero at the floor of stope, z_e can be minimum 0 and maximum H. H is total height of filled material ($z_e \leq z_i \leq H$). Equation 11 is used, if applying horizontal stress is longitudinal in stope. Equation 12 is used to calculate horizontal stress that is applied transversely.

Even though vertical stress is widely considered as it is shown in Equation 1, there is an approach for paste backfill material vertical stress distribution in stopes. It is given in Equation 13 (Li and Aubertin, 2009).

Li and Aubertin Model:

$$\sigma_v=\frac{\gamma_m}{2k_{am}\tan\delta_{sat}M}\left[1-\exp(-2H_m\tan\delta_m k_{am}M)\right]\exp\left(-2k_{as}(z-H_m)\tan\delta_{sat}M\right)+\frac{\gamma_{sat}}{2\tan\delta_{sat}k_{as}M}\left[1-\exp\left(-2k_{as}(z-H_m)\tan\delta_{sat}M\right)\right] \quad (13)$$

Where, δ_{sat} is wall friction angle for saturated fill, H_m is moist fill height, γ_m is unit volume weight of moist fill, γ_{sat} is unit volume weight of saturated fill, H_{sat} is saturated fill height that is under moist fill. Moist fill height can be negligible for well drained PF. z is the depth from the top of backfill. k_{am} is active k ratio of moist backfill

and k_{as} is active k ratio of saturated backfill. M is given in Equation 14.

$$M=B^{-1}+L^{-1} \quad (14)$$

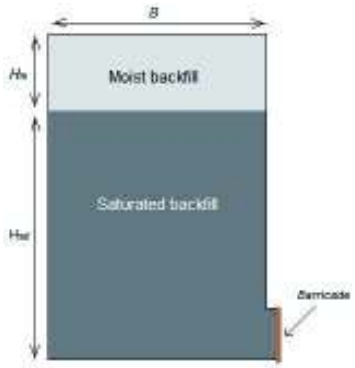

Figure 3. Moist and Saturated backfill layers for non-drained stopes (Kömürlü, 2012)

Aubertin suggests multiplying active k (k_a) ratio with vertical stress for calculating horizontal stress of fresh backfill. Fresh backfill is consolidated by its self weight. Consolidated material's void ratio decreases and internal friction angle increases. Increasing of internal friction angle causes to decrease k_a ratio, and lower k_a ratio decreases horizontal stress in backfill. Also, cohesion increases with consolidation.

If there is not water draining, total weight is same for same floor area, even if backfill is consolidated. Horizontal stress occurring due to vertical stress decreases with consolidation. If there is drainage, consolidation is faster, also k_a ratio decreases faster, horizontal stress decreases more until backfill solidifies. Weight of total material height decreases because of water loss, thus vertical stress decreases. Therefore, drainage provides lower applied horizontal stress on barricade.

Filling rate is another important factor for stress distribution in backfill material. Vertical and horizontal stresses increase with high filling rates (Li and Aubertin, 2009). Difference between vertical and horizontal stress increases with decreasing filling rates. Decreasing k_a by time is a reason for this situation. Drainage and low filling rates are advantages about preventing barricade failure. Excess pore water pressure occurring can be prevented by drainage. In addition to k_a decreasing by time, material becomes solid with hydration reactions. Stable k must be considered for solid hydrated backfill instead of k_a, if material has enough strength to be durable under its self weight. Direct horizontal stress doesn't apply on sidewalls from solid hydrated backfill. For example, barricades complete their mission, and there is no need to supply horizontal support pressure after backfill has enough uniaxial compressive strength to be durable under its self weight (Kömürlü, 2012). Stable k ratio can be used to calculate horizontal stress in backfill, not for reinforcing pressure to stope walls from backfill. Reinforcing pressure decreases with deformation of backfill. Cemented solid backfill expands horizontally until stress on surface vanishes when near stope is produced. This paste backfill becomes passive reinforcement. Because, it can supply horizontal confining pressure to rock backfill as a reaction for applied stress from RF that is filled in produced stope.

However, horizontal stress of unstable uncemented PF directly applies on stope wall. In this situation k_a ratio can be considered, and horizontal reinforcing stress doesn't change with sidewall reactions (SR) when k_a is valid. Reinforcing reaction (RR) is independent from sidewall stiffness and reactions. Ore or rockfill can be accepted as support. And, support stiffness doesn't affect the reinforcement pressure of uncemented PF that is higher than critical height (H_c).

Temperature increases because of hydration reactions. Heated backfill expands and it would cause bigger applied stresses on walls of stope and barricade. Temperature effect is neglected in schematically shown Figure 4. The reason for vertical stress decreasing at waiting time is water draining and dying down of inertial stresses. Inertial stresses on stope walls increase with increasing filling rate. Reason is absorbing more energy due to fluid paste fill motion in stopes.

More than one step backfilling can be applied to prevent barricade failure. Vertical stress and especially horizontal stress are decreased at waiting time between filling steps. Because, mechanical parameters improve, k_a parameter decreases as result of continuing hydration reactions at waiting time.

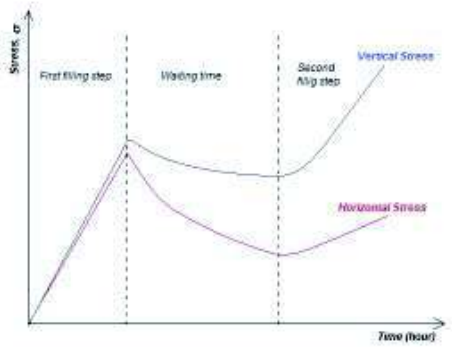

Figure 4. Vertical and horizontal stress changes in backfill by time (Kömürlü, 2012)

Factors that effect PF strength can be divided into two groups as internal and external (Benzaazoua et al., 2004). Internal effects deal with physical, chemical and mineralogical specifications of component materials of PF. Mechanical parameters of host rock or ore, interactions between stope wall and PF, consolidation, drainage, vibrations due to blastings, cure conditions like temperature or underground water can be considered as some examples for external effects (Ercikdi et al., 2008; Yilmaz et al., 2006).

Oxidizing of sulphuric minerals in tailings (like pyrite) causes occurring acid and sulfate that react with calcium hydroxide. Calcium hydroxide occurs as a result of hydration. Expansive gypsum and ettringite are formed by reactions between sulfate and calcium hydroxide (Annor, 1999; Santhanam et al., 2001; Yilmaz et al., 2003). Expansions of gypsum and ettringite cause to crack in PF material. Therefore, strength of PF is decreased by this effect (Ercikdi et al., 2008). This is an important internal effect on PF strength that becomes more dangerous for long curing times. A definite time for strength decreasing start of PF in stopes can't be reported according to laboratory specimens, because laboratory specimens and PF in stopes cure in different conditions.

For well referring in situ characteristics of PF, laboratory conditions aren't enough to consider some effects, accurately. Consolidation is another important effect that has to be considered when PF strength is estimated with laboratory specimens. For example, some misleading results can be obtained for comparing in situ strengths of PF of different tailings with lab specimens. In this study, reasons of misleading effects of neglecting in situ consolidation differences between different specimens are aimed to explain. Mineral processing plant tailings of Çayeli Copper Mine are used in experimental works.

Another question investigated in this study is how strength uncemented PF can reach due to consolidation under its self weight in stopes. Consolidation tests were applied on uncemented PF specimens for estimating in situ consolidation. Shear box tests are applied on different types of drained and consolidated uncemented Çayeli copper mine tailings.

2 EXPERIMENTAL STUDY AND DISCUSSIONS BY SEQUENCES

Two types of Çayeli copper mine tailings and their deslimed forms are investigated in experimental study. Spec tailings, Bornite tailings and their deslimed (classified) forms were tested. Important percentage of finer particles than 20 μm is deslimed for classified tailings preparation. For example, 44% of as-received Bornite tailings and 41% of as-received Spec tailings are finer than 20 μm, respectively. After desliming, 6% of C-Bornite and 12% of C-Spec tailings are finer than 20 μm, respectively.

Coefficient of curvature (C_c) and coefficient of uniformity (C_u) are important parameters to understand well-grading or poor-grading of granular materials. Well graded materials have higher strength (Kömürlü, 2012). If uncemented PF is aimed to fill in stopes, well graded material can supply higher strength. Uniformity and curvature coefficients can be calculated with Equation 15 and Equation 16 (Aytekin, 2000)

$$C_u = \frac{D_{60}}{D_{10}} \tag{15}$$

$$C_c = \frac{D_{30}{}^2}{D_{60} D_{10}} \tag{16}$$

More than 70% of both Bornite and Spec tailings (unclassified) have silt particle size material (2 - 63 μm). Approximately 10% of tailings have clay particle size (< 2 μm). Therefore, as-received (unclassified) tailings can be considered as sandy silt material. 75% of C-Spec (deslimed) is silt particle size material, 3% of C-spec is clay particle size. 65% of C-Bornite has silt particle size, and

2% of C-Bornite has clay particle size. Therefore, both of deslimed tailings are sandy silts, like as-received forms. Feret triangle can be used to classify granular material according to particle size distribution (Aytekin, 2000).

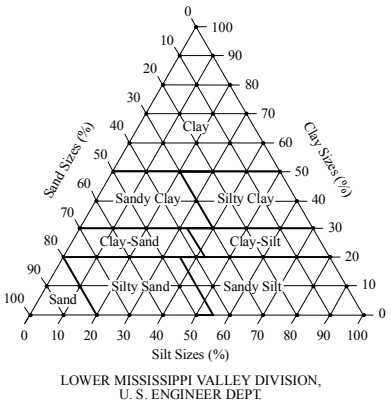

Figure 5. Feret Triangle

D_{10}, D_{30} and D_{60} are 10%, 30% and 60% passing particle sizes, respectively. C_c between 1-3 and higher C_u than 6 indicate well-grading material. However, if material is gravel higher C_u than 4 indicates well-grading (Aytekin, 2000).

Table 1. Uniformity and Curvature Coefficients

Type of Tailings	D_{10}	D_{30}	D_{60}	C_u	C_c
Bornite	2	7	26	13.0	0.94
Spec	2	8	26	13.0	1.23
C-Bornite	14	30	53	3.8	1.21
C-Spec	9	21	42	4.7	1.17

Deslimed tailings have preferable curvature coefficients, but they have non-desired uniformity coefficient. Particle size distribution is done with microsizer. Figure 6 shows particle size distributions of Cayeli copper mine tailings (Ercikdi et al., 2012).

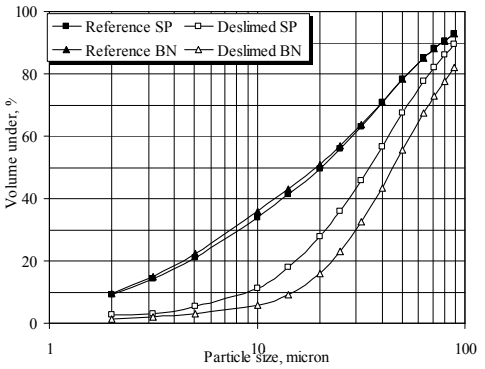

Figure 6. Particle size distribution of Bornite (BN) and Spec (SP) tailings (Ercikdi et al., 2012)

Surface area increases with decreasing particle size. And, permeability is low for fine particles. Consolidation completion time is longer for low permeable soils. Therefore, consolidation ratio (u) increases faster for highly permeable soils. Consolidation ratio depends on T_v unitless time factor, as it is shown in Equation 18 and Equation 19 (Kömürlü and Toptaş, 2012).

$$u = \frac{\Delta H}{\Delta H_\infty} \tag{17}$$

$$u = \sqrt{\frac{4Tv}{\pi}} \quad \text{, for } T_v<0.2 \tag{18}$$

$$u = 1 - \frac{8}{\pi^2} e^{-\pi^2 Tv/4} \quad \text{, for } T_v \geq 0{,}2 \tag{19}$$

ΔH is the settlement (mm) of material at the investigated time. ΔH at infinite time is ΔH_∞ (settlement at infinite time). T_v depends on consolidation coefficient (C_v), as it is shown in Equation 20 (Sarsby, 2000)

$$T_v = \frac{C_v t}{H^2} \tag{20}$$

$$C_v = \frac{K}{m_v \gamma_{wat}} \tag{21}$$

Where, t is time, H is height of soil. If soil can be drained from up and down level boundaries, H is considered as $H/2$ in Equation 20. K is permeability (m/sec), γ_{wat} is unit volume weight water (kN/m^3), m_v is the coefficient of volume compressibility (kPa^{-1}). It is given in Equation 22 (Ghosh, 2010).

$$m_v = \frac{\Delta V_\infty / V}{\Delta \sigma'} \tag{22}$$

Backfills in stopes consolidate in one dimension. Only, height of backfill changes due to consolidation. In this situation, volumetric change ratio is same with change ratio in height, and m_v becomes as follow:

$$m_v = \frac{\Delta H_\infty / H}{\Delta \sigma'} \tag{23}$$

$\Delta\sigma'$ is effective stress; settlement of completed consolidation (ΔH_∞) can be calculated with Equation 24 (Kömürlü and Toptaş, 2012):

$$\Delta H_\infty = \frac{H}{1+e_0} C_r \log \frac{\sigma_2}{\sigma_1} = \frac{H}{1+e_0} C_r \log \frac{\sigma_1 + \Delta\sigma}{\sigma_1} \tag{24}$$

e_0 is initial void ratio, σ_1 is initial stress, and σ_2 is final stress, C_r is compressibility index. Compressibility index can be divided into two groups. It can be primary compressibility index (C_c) or secondary compressibility index (C_r). C_c is signed as C_p in this paper, because coefficient of curvature is also signed as C_c. To prevent confusion, primary compressibility index is signed as C_p. C_p can be used instead of C_r in Equation 24. It is up to consolidation stress. Details will be given with experimental data, in further parts.

As it is seemed in Equation 21, consolidation coefficient increases with increasing permeability. T_v increases with increasing C_v. And, consolidation ratio (u) increases with increasing T_v. Therefore, it can be said that consolidation time is low for high permeable soils.

Permeability of soils can be measured with constant head or falling head permeability tests. Constant head permeability test is applied for high permeable gravels and sands. And, falling down permeability test can be applied for silts and clays (low permeable soils). 10^{-3} m/sec can be accepted as limit for changing permeability test method. If permeability of soil is higher than 10^{-3} m/sec constant head permeability test must be used, otherwise falling head method is suggested (Tiwari, 2008).

As it was mentioned before, mineral processing plant tailings of Cayeli copper mine is sandy silt particle size material. Therefore, falling head permeability test was applied. Permeability of material can be calculated with Equation 25 (Uzuner, 2007)

$$K = \frac{a.L}{A.\Delta T} . \ln \frac{H_0}{H_1} \tag{25}$$

where, A is cross-section area of specimen (m), L is length of specimen (m), a is cross-section area of burette (m). ΔT is time difference between two measurement points. H_0 is initial height of water in burette (m), and H_1 is final height of water in burette (m). Diameter of specimen is 0.1 m, length of specimen 0.14 m, internal diameter of burette is 0.012 m.

Table 2. Permeability test data

Type of Tailings	H_0 (m)	H_1 (m)	ΔT (sec)	K (m/sn)
Bornite	1.22	0.92	960	$5.9x10^{-7}$
Spec	1.20	0.84	960	$7.5x10^{-7}$
C-Bornirte	1.28	0.61	150	$9.2x10^{-6}$
C-Spec	1.29	0.78	150	$6.8x10^{-6}$

Figure 6 shows the falling head permeability test for tailings.

As it seemed in results, desliming increases the permeability. And, u increases with desliming. For example, permeability of Bornite tailings increases for 15.6 times after desliming. Permeability differences between tailings types change after desliming. Even though as-received (unclassified) spec tailings has 1.3 times higher permeability than as-received bornite tailings permeability, T_v of C-Bornite (classified) is nearly 1.5 times of T_v of C-Spec. This is an important difference. Not only particle size distribution affects the permeability. Also, mineralogy of tailings has an important role on permeability. Desliming changes the mineral percentages in tailings (Ercikdi et al., 2012).

Figure 6. Falling head permeability test

Material height is an important factor for consolidation time. As it is seemed in Equation 20, height of material affects the time factor and consolidation ratio. Consolidation completion time increases with increasing height. Hydration and solidification stop to consolidate. Consolidation time (t) of 15 meters height PF in stope is 22500 times of 10 cm height laboratory specimen PF. Consolidation ratio is same for same T_v. Therefore, time

difference between different heights of same material can be calculated for same consolidation ratio (u) as follow (Sarsby, 2000):

$$T_v = \frac{C_v t_l}{H_l^2} = \frac{C_v t_s}{H_s^2} \quad (26)$$

H_s and H_l are height of PF in stope and laboratory specimen PF height, respectively. t_s and t_l are in situ consolidation time and consolidation time for lab specimen.

When u is 0.9, 90% of consolidation is completed and T_v is equal to 0.848 for this situation. Consolidation coefficient must be known to calculate consolidation time. For calculating C_v, coefficient of volume compressibility (m_v) must be known.

Odometer test was applied on C-Bornite and C-Spec specimens. Initial void ratio of wet C-Bornite is 0.96 and it is 1.01 for wet C-Spec. Specimens are in liquefacted form. Load time should be higher than 90% consolidation time. Therefore, more than 90% of consolidation of specimen has to be completed under constant load. Loading time for consolidation is selected according to 90% of consolidation completion time (Kömürlü and Toptaş, 2012). Generally, 24 hours is enough time for clays. Even though less time is enough for tested material, load time was 24 hours for sandy silt type tailings. Normally, 7 or 8 hours are suitable load time for general of silts that have 2 cm thickness in mold. Consolidation test is applied in shear box, specimen thicknesses are 2 cm. Circular cutter sampler thickness of shear box is 2 cm. Most of soil test specimen has 2 cm thickness in this method. However, wet tailings are not sampled with circular cutter. Specimens were poured in mold. T_v and u relation is given in Figure 7. If linear part of graph is stretch out to x-axis, it intersects the axis at approximate value of original 0.9 u. T_v is infinite for 1.0 u value. Therefore, a time is considered for final settlement. 90% settlement time is considered to calculate ΔH_∞ as a result of linearization. As a matter of fact, settlement speed decreases with continuing time under constant load. Consolidation is higher for early times of loading (Uzuner, 2007). This situation is schematically shown in Figure 8.

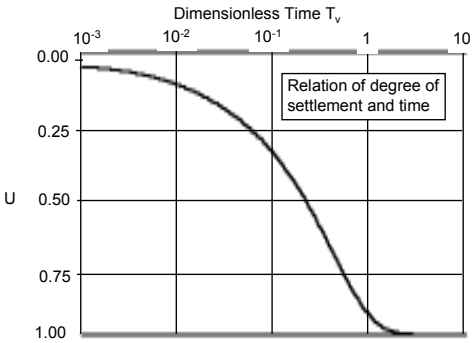

Figure 7. T_v and u relation (Cengiz, 2009)

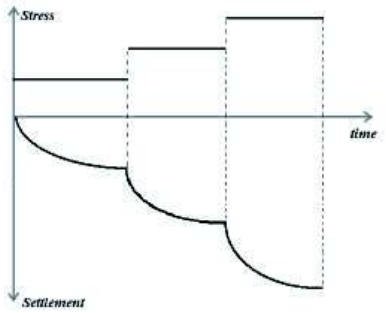

Figure 8. Time, settlement and stress relation

Desliming causes to increase the percentage of coarser particles, so permeability increases. As it is seemed in Figure 9 and Figure 10, consolidation is faster for deslimed tailings. Because, consolidation coefficient and T_v are higher for deslimed tailings. Same tailings in photos have same consolidation time.

Figure 9. Consolidations of classified and as-received Spec tailings under their self weights in molds (Ercikdi et al., 2013)

Figure 10. Consolidations of classified and as-received bornite tailings under their self weights in molds (Ercikdi et al., 2013)

Consolidation test data for C-Spec tailings specimen is given in Table 3. Specimen water content is enough to pump it to underground. 7 - 8 inches slump is typical slump level for applicable rheology. Water/(cement+tailings) ratio is 0.21 - 0.25 by weight for applicable rheology of cemented form of investigated C-Spec tailings when 5% - 7% of solid is cement (Ercikdi et al., 2013). In experimental study of this paper, cement wasn't used. Water/Tailings ratio is 0.23. Specific gravity of C-Spec is 4.16. Therefore, void ratio of wet saturated tailings is calculated as 0.96. Specimen thickness in consolidation test is 2 cm. Figure 12 shows consolidation test. Specimens are consolidated in water filled shear box test mechanism. Specimens are drained. Porous plates are used under and on specimens.

Table 3. Consolidation test data for C-Spec

σ (kPa)	log σ	e	Δe	ΔH (cm)
0	0	0.96	0	0
32.6	1.51	0.72	0.24	0.247
97.8	1.99	0.53	0.19	0.199
163.1	2.21	0.35	0.18	0.179
228.3	2.36	0.19	0.16	0.163

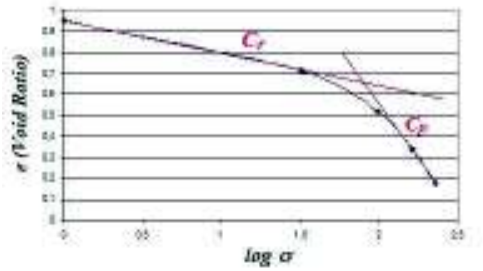

Figure 11. Void ratio changes with consolidation stress for C-Spec

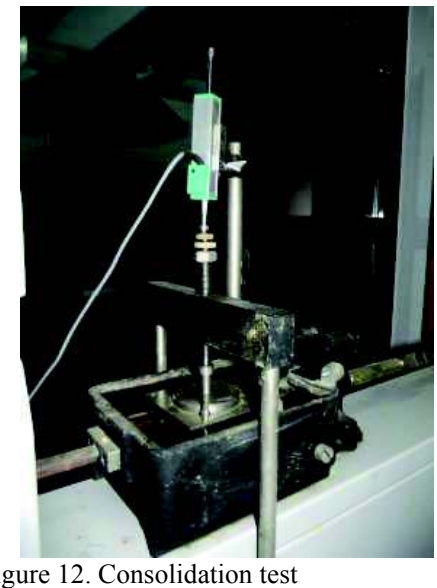

Figure 12. Consolidation test

C_r is 0.16 and C_p is calculated as 1.07 for C-Spec tailings. C_r and C_p are slopes of representative lines. Unit volume weight of PF material must be known for calculating ΔH_∞. Unit volume weight of tested saturated material can be calculated with Equation 27 (Cengiz, 2009).

$$\gamma_{sat} = \frac{\gamma_w (G_s + e)}{1 + e} \quad (27)$$

γ_w is unit volume weight of water, G_s is specific gravity. Unit volume weight of material is calculated as 25.7 kN/m^3. Let's investigate settlements in PF application that is done with two step filling. One step backfilling has risks about barricade failuring for investigated mine stopes. If total height is 14.5 meters and 7.5 meters height is filled in first step. 7 meters height material is filled in second step. ΔH_∞ for first step fill that is caused by weight of second step fill is calculated as 1.87 meters when consolidations due to self weight of first step fill before second step is neglected.

Mid depths of first filled material is considered for σ_1. σ_2 is sum of σ_1 and stress due to second step filled material. m_v is calculated as 1.39 Pa^{-1} ($\Delta\sigma$=179.9 kPa). Permeability of C-Spec was measured as 6.8x10^{-6}, and C_v is calculated as 0.5x10^{-9} m^2/sec. According to this data, 90% of consolidation (u=0.9) theoretically continues for more than 7 years. In situ consolidation is stopped by hydration reactions. And, few consolidation ratios can be actualizes in stopes. The most important reason is height of PF in stopes. If PF is drained from the floor H can be considered as H/2. Thus, consolidation time can be theoretically decreased for 4 times, as it is understood from Equation 20. Even though drainage decreases the consolidation time, in situ consolidations continue for years. Calculated consolidation is for drained stope, therefore H is considered as 3.75 meters (half height of first step fill).

However, lab casted specimens can have much more consolidation ratio until hydration, as a result of its low height. Especially, drained specimens consolidate fastly. C-Spec tailings in Figure 9 settled more than 3 cm in several hours. Its initial height was 20 cm. These types of $\Delta H/H$ ratios actualize in much longer time in stopes.

Especially, drained lab specimens can complete very important percentage of their consolidations until material solidifying. Sometimes specimens can practically complete their consolidations. Compared material designs can complete most part of their consolidations in lab molds and they can have similar u, but their in situ consolidation ratios (u) can be significantly different. Higher lab strength material design can be lower in situ strength one, as a result of less in situ consolidation.

Figure 13. Shear box test equipment

Consolidated specimens were sheared in shear box. And, strengths of uncemented PF were investigated. Consolidation test specimens are drained, shear strength test was applied as consolidated and drained (CD). Even though some small peaks were observed, shear strength magnitudes can be accepted as residually. Because, it is crushed and grinded material.

Table 4. Shear strength test (CD) data

σ (kPa)	τ (kPa)
32.6	54.4
97.8	105.1
163.1	126.3
228.3	149.5

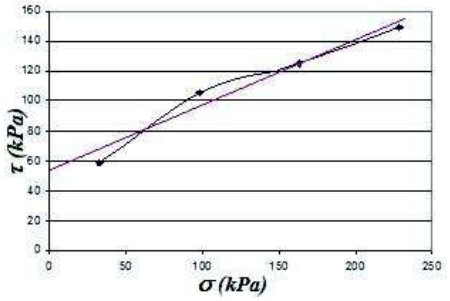

Figure 14. Failure envelope of uncemented PF

Cohesion (c) is considered as 53 kPa and internal friction angle (ϕ) is measured as 24°. If stress due to weight of material exceeds the strength of material, failure is actualized. According to Mohr-Coulomb failure envelope, critical height of material can be calculated with following equation (Kömürlü and Toptaş, 2012)

$$H_c = \frac{2c\sqrt{k_p}}{\gamma} \tag{28}$$

Critical height (H_c) is calculated as 6.3 meters. According to this result, investigated material is not durable under its own weight, if it is higher than 6.3 meters.

3 CONCLUSIONS

Near of UPF filled stope can't be excavated, if material has bigger height than critical height. In addition to stability under load of weight, UPF can't be applied because of blasting. If PF is not cemented, loosening can be easily actualized due to blasting. Therefore, UPF is not usable material for general backfill applications. However, it can be applied for some special situations. If near or down of stope won't be excavated, UPF can be applied. Even if material is failed due to its own weight, it can supply higher horizontal confining stress to rock fill support. Because, horizontal stress from failed UPF material actively apply on stope sidewalls. Reinforcing stress doesn't decrease with sidewall deformation as it is shown in Figure 15.

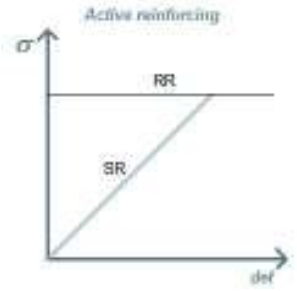

Figure 15. Active reinforcing reaction and support sidewall reaction

Solid cemented PF tends to expand horizontally as result of Poisson effect. If near wall is produced, PF expands until net stress becomes zero on open PF surface. Let's imagine removing sidewalls near solid cemented PF, and putting hands on solid PF surface after expansion end. Value of stress that acts on hand is acted stress on PF by hand, if PF is not failed. In this situation, major confining effect of PF is actualized when rock fill or ore support expand towards PF (For example, rock fill and ore tend to deform horizontally when they are exposed more load due to stope production). Therefore, it can be assumed that solid stable paste backfill passively reinforces support (rock fill and/or ore) as reaction of support loading. However, UPF horizontal stress at deeper points than H_c directly acts on sidewalls. Actively applied horizontal stress can be theoretically considered as k_a times of vertical stress.

Asymmetrical confining pressure due to different reinforcing reactions for sidewalls affect is negligible because of width/height ratio of backfills.

As conclusion words of consolidation effects on PF strength, it can be said that result of lab specimens are not accurate to compare in situ strengths of different designs.

REFERENCES

Annor, A.B., 1999. *A study of the characteristics and behaviour of composite backfill material*, PhD Thesis, McGill University, Montreal, 396 p.

Aytekin, M., 2000. *Deneysel zemin mekaniği*. Akademi Yayınevi, Trabzon, 264 p.

Belem, T., Benzaazoua, M., 2004. An overview on the use of paste backfill technology as a ground support method in cut-and-fill mines. Villaescusa & Potvin (eds.), *Proceedings of the 5th Int. Symp. on Ground support in Mining and Underground Construction*. 637 – 650, Perth, Western Australia, Australia

Benzaazoua, M., Fall, M., Belem, T., 2004. A Contribution to understanding the hardening process of cemented pastefill. *Min. Eng.*, 17,2, 141-152

Cengiz, K., 2009. Soil Mechanics lecture notes, Hacettepe University, Ankara

Erçıkdı, B., Cihangir, F., Kesimal, A., Deveci, H., Alp, İ., 2008. Effect of Drainage Conditions on the Strength of Paste Backfill. *Madencilik*, 47, 15-24.

Erçıkdı, B. 2009. *Effect of pozzolanic mineral and chemical admixtures on paste backfill performance*. PhD Thesis, Karadeniz Technical University, Trabzon, Turkey (In Turkish), 141 p.

Erçıkdı B., Baki, H., İzki, M., 2013. Effect of desliming of sulphide-rich mill tailings on the long-term strength of cemented paste backfill. *Journal of Environmental Management*, 115, 5-13.

Gercek, H., 2007. Poisson's ratio values for rocks. *International Journal of Rock Mechanics and Mining Science*, 44, 1–13.

Hudson, J.A., Harrison, J.P. 1997. *Engineering rock mechanics: an introduction to the principles*. Pergamon, Elsevier Science, Oxford.

Karaoglu, K., Kucukates, K., Thompson. B.D., 2011. Pastefill Pressure Monitoring at Inmet's Cayeli Underground Copper and Zinc Mine. Eskikaya Ş. in editor. *22th World Mining Congress & Expo.*, 325-334, Ankara, Turkey

Kesimal, A., Yilmaz, E., Erçıkdı, B., 2004. Evaluation of paste backfill mixtures consisting of sulphide-rich mill tailings and cement contents. *Cement and Concrete Research*, 34, 10, 1817-1822.

Kömürlü, E., 2012. *Effects of rock and granular material horizontal stresses on support design*, MSc thesis, Karadeniz Technical University Mining Engineering Department, Trabzon, Turkey (in Turkish), 180 p.

Kömürlü, E., Kesimal, A., 2011. Polymer fibre addition's effects for shotcrete tunnel support. *10th Regional Rock Mechanics Symposium*, 47-55, Ankara, Turkey

Kömürlü, E., Toptaş, S., 2012. Investigation about durability of steep excavated foundation in urban places. *Mining Turkey Scientific Journal of Underground Resources*, 1, 13-57.

Li, L., Aubertin, M., 2009. A three-dimensional analysis of the total and effective stresses in submerged backfilled stopes. *Geotechnical and Geological Engineering*, 27, 4, 559-569.

Li, L., Aubertin, M., 2009. Horizontal Pressure on Barricades for Backfilled Stopes. Part I: Fully Drained Conditions. *Canadian Geotechnical Journal*, 46, 1, 37-46.

Santhanam, M., Cohen, M.D., Olek, J., 2001. *Sulphate attack research - whither now?*. Cem. and Conc. Res., 31, 6, 845-851.

Sarsby, M., 2000. *Environmental geotechnics,* Thomas Telford, Bodwin, Cornwall, Great Britain, 587 p.

Tiwari, B., 2008. Soil Mechanics laboratory lecture notes, California State University Fullerton.

Uzuner, B,A., 2007. *Çözümlü problemlerle temel zemin mekaniği*. Derya Yayınevi, Trabzon, 377 p.

Yılmaz, E., El Aatar, O., Belem, T., Benzaazoua, M., Bussiere, B., 2006. Effect of consolidation on the performance of cemented paste backfill, *Proceedings of the 21st Annual Underground Mine Support Conference*, AMQ, Val d'Or, Quebec, Canada, 14 p.

Yılmaz, E., Kesimal, A., Erçıkdı, B., 2003. Macun dolgu dayanımı ve duraylılığını etkileyen faktörler. *Yerbilimleri, Hacettepe Üniversitesi Yer Bilimleri Uygulama ve Araştırma Merkezi Bülteni*, Hacettepe Üniversitesi, 28, 2, 155-169.

Yumlu, M., 2008. Barricade pressure monitoring in paste backfill. *Gospodarka Surowcami Mineralnymi*, 24, 233-244.

Evaluation of Hydrologic Conditions of Chaparabad Dam Foundation

M.A.Karbala
Head of Research and Technology Office, Higher Education and Research Complex of Khuzestan Water and Power Industry, (Affiliated with Ministry of Energy)

A.Aalianvari
Department of mining engineering,Faculty of engineering, University of Kashan, Kashan I.R.Iran

ABSTRACT In this research, after analyses of the field geotechnical data, hydrogeological conditions have briefly been studied and inspected. Fourteen boreholes were drilled in the dam axe area and they are considered as the major sources of data. As the results show, dam site chiefly consists of permeable quaternary alluvium. It seems likely that rock zones participate somewhat lower than soil parts in the effective seepage flows particularly at the centre of valley. Lithological structures and discontinuities such as joint sets and faults would cause to intensify seepage especially through both abutments. There is evidence of a steady groundwater regime. Groundwater flow is closely related to surface flow. It is highly probable that right abutment has spoiled by karstification. Left abutment is not expected to reach a sufficient groundwater level to preclude reverse flow at the reservoir toward left bank. Based on soil percolation and Lugeon test results and drilling cores logs, permeability of soil and rock sections was estimated and sketched by use of ordinary kriging method. Strata positions were also interpolated. The spatial distribution of permeability has been compared to strata conditions. The results have indicated that high permeable layers of sand and gravel are extended in the most part of dam foundation. At first, grouting works were set by designers in charge for sealing of all foundation regions. But according to considerable clay strata at the upper parts, very permeable sand and gravel layers at the middle and lower parts and weathered and fractured rock zones at the soil-rock contact area, cut-off wall and grouting have been respectively proposed for sealing of upper and lower parts of the foundation.

1 INTRODUCTION

The study of Permeability and other hydrogeologic features are most considerable parts of dam site investigations at the foundation and abutments. This reconnaissance tends to a suitable verification of hydrogeologic conditions respecting seepage and water escaping from reservoir. Poor hydrogeologic conditions cause momentous difficulties. Notwithstanding fair geomechanical conditions, these problems may finally result in relocation of dam axe (Iran Water and Power Resources Development Co., 1375). So this considerations and analyses of field data are obligatory for designers whilst the initial stages of the project are just commenced (Ewert, 1985; Kutzner, 1996; Shroff and Shah, 1999).

Generally, for this type of investigations, some technical and hydrological data such as height of reservoir water and river annual flow rate are reviewed. The stratigraphical and lithological situation of formations and the geotechnical data such as soil type classification and soil layer conditions are also determined. These data and engineering geological information such as joint study, Lugeon values, soil permeability values and

groundwater table values are assembled together. Then, data collection analyses are conducted to expose the hydrogeologic weakness zones. Data are usually obtained through drilling and superficial survey. The exploration area is emphasized to be sited around dam axe in the way that the exploration points must be particularly concentrate in the dam axes. This type of study are utilized widely around the world and ,for example, typically could be find in the research of Robinson and Robinson (1992), Al-Homoud et al (1995), Hutchinson (2001), Kiersch (2001), Turkmen et al (2002), Ghobadi et al (2005) and Hietfield and Krapp (2007).

In this research, the information was derived from superficial engineering geological survey and 14 exploration boreholes drilled in the Chaparabad dam site. Dam site was evaluated in order to discover the hydrogeological conditions and probable weakness points. Boreholes data are contained within a descriptive log of cores, permeability test results and water table positions. Superficial data includes geological map, inferred sections and joint sets condition in rock formations at site. The analyses and evaluations consist of bedrock topography map and bedding situation, joint sets orientation, alluvial deposits conditions, regional hydrogeologic regime and spatial distribution of permeability. In spite of grouting program proposed initially for full section of foundation, these results led into excavation of alluvium parts to set a cut-off wall without any grouting work in this area, but a grouting program is urged to seal rock zones.

2 CHAPARABAD DAM SITE AND PRELIMINARY INVESTIGATIONS

The Chaparabad earth dam is under construction on the Kanirash River and is intended for both gravity and under-pressure irrigation of 3600 hectares of Oshnavieh and Naghadeh farm lands. First study of this project started at 1994. Dam site is located in the South of West Azarbayejan province, Iran, 12 km of south of Oshnavieh city (Figure 1). Designed dam will be an earth dam with clay core and the height of 46 m from foundation.

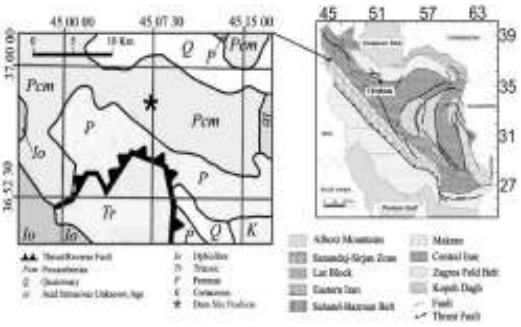

Figure 1. Dam site position in the regional geologic maps (after Hezarkhani 2006 and Pollastro et al. 1996).

The study area is located in Lesser Caucasus geologic province (Pollastro et al., 1996) and Sanandaj-Sirjan geologic zone in the Iran geologic map (Figure 1). In this area the broad trend of geological units are extended in NW-SE direction. Rock zones contain Precambrian and Cambrian sediments, including shale, slates, limestone, schist, and some weathered dolomite. Because of water penetration and freezing in shallow rocks, there are intensive developments of fractured and weathered zones. The geological map of the site area and geologic section of spillway is demonstrated in Figure 2. In this Figure, 14 boreholes positions that were the main source of data are also shown. The foundation area could actually be separated into two discrete but connected parts of alluvial and rock layers. Materials chiefly consist of alluvial and rock respectively in the central part of valley and both abutments. Figure 1 shows roughly the location of dam site in regional geologic map. Dam site is located in a mountainous area. Reservoir storage is provided by Kanirash River directly and Godar River by use of a small diversion dam. The Godar river basin area up to diversion dam and the Kanirash river basin area up to main dam are respectively 220 and 141 Km2. The annual flow volume brought by Kanirash and Godar river basin are respectively 289 Mm3 and 34 Mm3. The 50-year-average of annual precipitations of both basins is 500 mm.

Groundwater is briefly seeps through the carbonate fractured rocks and quaternary alluviums. There are evidences of two separate hydrogeologic media of rock and alluvium, which are supplied by precipitations and run-offs. Alluviums can be categorized into three groups as follows;

1. Impervious deposits, containing clay layers,
2. Quasi-permeable deposits, a combination of clay and sand, including debris of sedimentary and igneous formations, and
3. Permeable deposits, classified into recent alluvium deposits, coarse grain terrace and unconsolidated talus and debris.

Right abutment largely contains deposits considered as GP, GM, GC and GW. Indeed, these materials belong in brief range of GC-GW. Fewer parts of superficial alluvial materials are reckoned to be SC or SM. Fine grain soils of CL type are existed in the left abutment. Highest portion of central parts consist of sand especially SC and SM. Slender clay lenses are observed through the dam site.

Geomechanical properties of the bedrock improve toward depth, but mechanical strength of the rocks underneath the foundation is poor to very poor in general. Furthermore, the RQD values in this area are very low to mediocre.

3 EVALUATIONS AND ANALYSES OF DATA

All presented data are synopsis of surface and drilling records. Selection and classification of these data have been carried out in a way that the hydrogeologic features of the dam site is regarded and analyzed. Nevertheless, lack of data causes to increase uncertainty which could be diminished by the concentration of drilling network inside dam axe in further coming studies.

3.1 Strata Conditions

Figure 2 shows the inadequate conditions of layers with respect to seepage. Because of formations trend particularly in NW-SE direction as well as the valley situation extending in N-W direction, seepage through strata could be probably intensified. There are some washable sections such as gypsum and clay in the slate and schist layers, and then these layers are more likely to be washed out by piping and would increase seepage. These formations are more susceptible, and sealing works must be firmly done in their sections. Limestone layers have low potential of piping but they are probable to have karsts and cavities, and grouting strategy must be planned and equipped to fill and seal these probable great permeable zones.

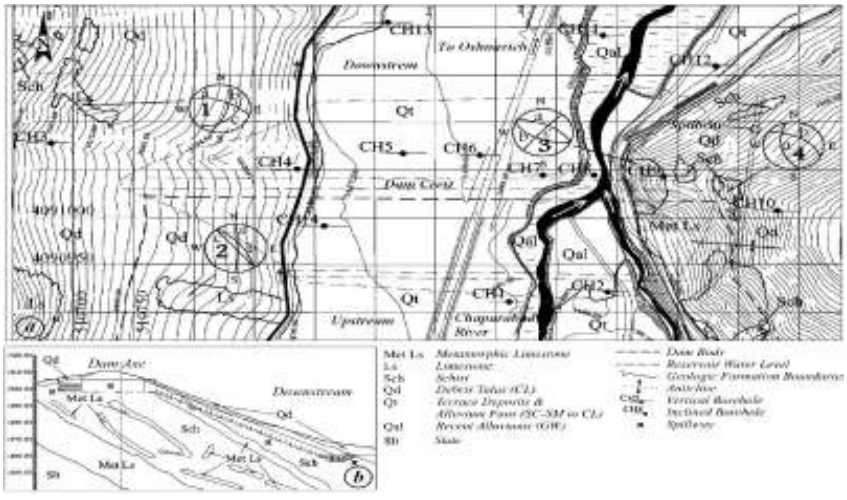

Figure 2. (a) Local geologic map and (b) geological section of dam axis. Coordination lines are set to UTM coordination system and elevation are set according to m in msal.

Crashed and faulted zones in the right abutment point out significance of strictly grouting works. Saline and sulfate materials in run-offs oblige to strengthen the grout that will be consumed in cut-off curtain and cut-off wall.

3.2 Hydrogeology

Fluctuations of water table in the boreholes through time are plotted as a hydrograph diagram in Figure 3. Apart from borehole CH10 that displayed unexpectedly falling of water table, fluctuation of water table in the other Boreholes is negligible. Tentatively, therefore, it may be concluded that a steady regime is more likely to prevail among the regional groundwater flows.

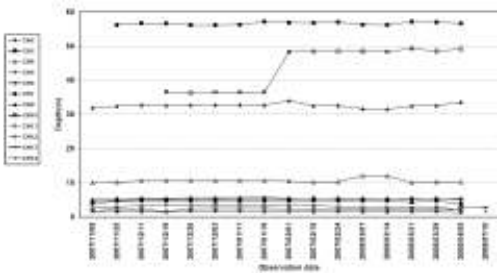

Figure 3. Groundwater Level Fluctuations observed in exploration boreholes since November 2007 till July 2008.

Groundwater head maps and section are sketched in Figure 4 based on the average of the boreholes water table level. It could be assumed that groundwater streamlines converge into nearby borehole CH9 (Figure 4.a). The convergence may be on account of a very permeable zone close to borehole CH9. This area of the right abutment involves particularly faulted and karstic zones amid limestone layers. Flows are expected to be conducted toward these highly permeable discontinuities. After eliminating the borehole CH9 data, headlines reshape to a typical one usually observed in dam sites (Figure 4.b). The groundwater gradient is generally coincided with river, and that could be interpreted as a close interaction between groundwater and river. Considering Darcy's equation with respect to Figure 4.c, left side is probable to have a negative impact on reservoir storage. Groundwater table is not seemingly inclined toward the reservoir in the left bank. The anticipated reservoir head will overcome the natural groundwater table. So, the reservoir would be evacuated by inverse flow into left abutment. Moreover, in a wide range of left abutment, the groundwater is not reached to a sufficient level. This problem must be regarded seriously since it is actually unfeasible to extend the cut-off farther than intersection point of reservoir level extension toward left side and groundwater table. Consequently, some underground parts of left abutment, which resemble as a highly permeable window, would remain unplugged.

3.3 Engineering Geology and Geotechnics

As mentioned above, dam foundation could be classified to two separate parts of soil and rock. So, sealing works must be considered for both soil and rock specifications.

In shallow zones the soil grain size distribution is erratic so that abrupt changes from a very permeable zone to an impervious clay zone or vice versa in alluvium strata may frequently be observed. The sealing method also must be altered when these variations are monitored. If grouting is opted as the sealing method, poor groutability conditions of clay layers raise the probability of washing-out, and finally may tend to cause permeable windows. As a result, construction of a curtain wall in preference to cut-off curtain is recommended in the shallow alluvial zones.

Grouting method could be preferably selected for remediation of bedrock against seepage flow. Because bedrock is extremely jointed and fractured especially in the upper parts, grouting in these parts are uniform and effortless. But regarding the high deformability and poor geomechanical conditions, grouting pressure should be kept under a low level and performed prudently.

3.3.1 Bedrock Conditions

Bedrock depth in the boreholes was recorded. Figure 5 shows bedrock elevation contours map. The valley morphology is nearly coincided with bedrock. A relatively deep valley in bedrock, especially in central part, could have an effect on growth of seepage and piping. This problem needs a denser network of drilling hole to investigate and explain the real circumstances as well as denser grouting holes.

3.3.2 Discontinuities situations

Dam axe is in E-W direction and hydraulic gradient is generally in south-to-north or upstream-to-downstream direction.

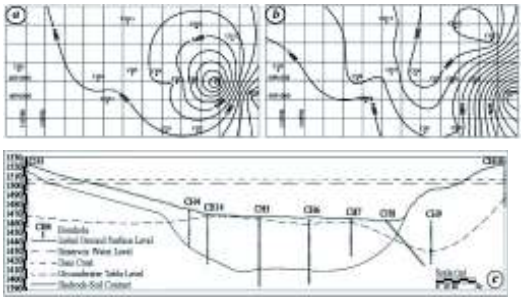

Figure 4. Groundwater hydrostatic contour maps (a) considering CH9 borehole, (b) after eliminating of CH9 borehole and (c) groundwater level section at the dam foundation. Coordination lines are set to UTM coordination system and elevation are set according to m in msal.

According to Figure 2, joint sets 1a, 3c and 4b in abutments are plunged down into downstream and joint sets 1b, 2a, 2b and 4b are perpendicular to the dam axe. As to dip and orientation, these entire joint sets have high potential of water escape from dam reservoir toward downstream. In comparison with other joint sets, grouting holes should preferably be oriented in directions that make an angle of 60 to 90 degree with the planes of these problematic joint sets to achieve sufficient penetration of grout.
Two identified minor fault have yielded wide crashed zones that may possibly cause to water escape from reservoir toward downstream. Accurate location of these hazardous zones should be determined where grout curtain plane intersects with them. Grouting in these zones would be executed more firmly.

4 PERMEABILITY AND STRATIGRAPHY OF DAM FOUNDATION

A simple classification of geological and permeability data obtained by boring, are done to enhance the assessment truthfulness.

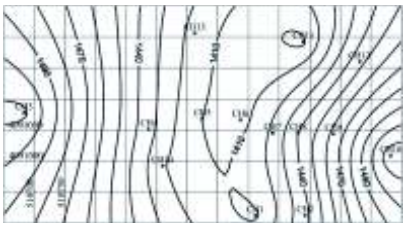

Figure 5. Foundation bedrock elevation contour map (coordination in UTM system and elevation in msal).

The soil classification was originally founded on Unified Classification (Das 2002), and then categorized in wide-ranging groups to simplify for sketching and comparing with permeability of sections. Percentage of fine grain (passing #200 sieves) is the main factor that discriminated the groups. It is known that fine grain contents of soil sample are contrarily related with permeability. Because of the important role of fine grain contents in the alluvial sediment permeability, percentage of passing #200 sieve, F200, have been considered as the main characteristic that differentiated the groups. At first, core contents classified in accordance with UC, and after that the results merged and reclassified according to F200 contents. The classification utilized here is presented in Table 1.

Geological section of foundation at dam axe is shown in Figure 6.a. This section is inferred and planned according to the above noted classification and rock type observed in drilling cores as well as some superficial surveys. Strata were interpolated and extrapolated between boreholes by Spline method.

Permeability data were achieved by Lugeon (water pressure) test and soil percolation test respectively in rock and soil stages. However all permeability data were expressed in cm/sec to be shown in a section coincided by aforementioned geological section (Figure 6). Permeability values were attributed to middle point of tested sections. Ordinary Kriging method (Journel 1990 and Deustch 1992) were applied to find spatial variation of permeability.

Regarding the information revealed in Fig. 6 and pervious results, some important features are described as follows;

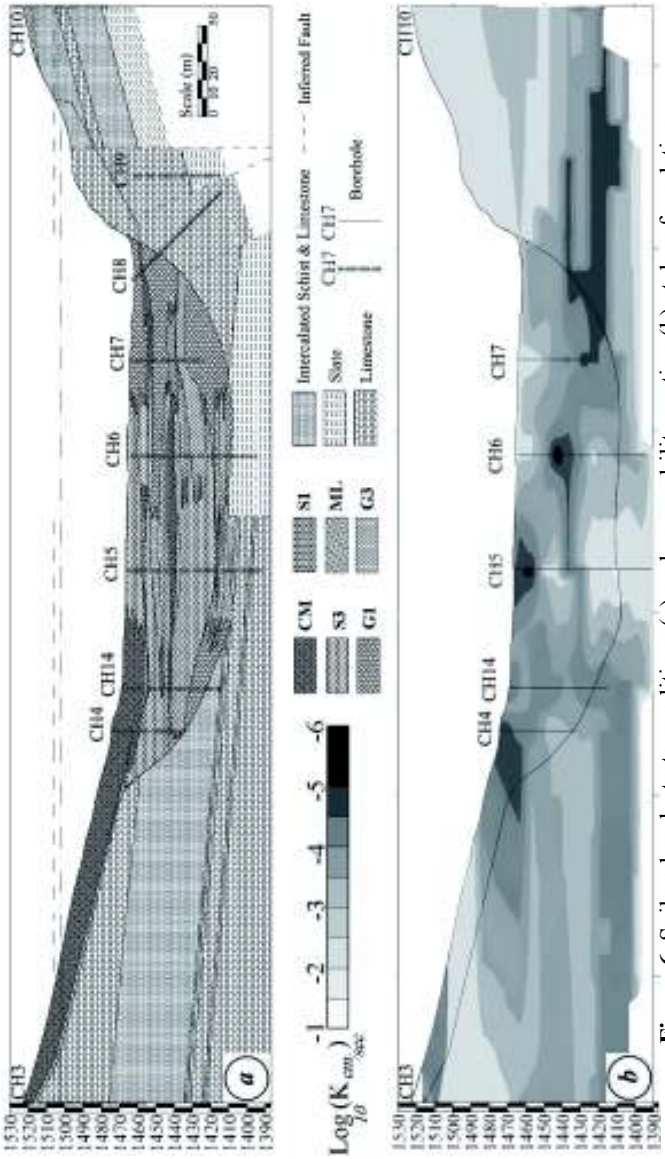

Figure 6. Soil and rock strata conditions (a) and permeability section (b) at dam foundation.

Elevation are set according to msal.

1. Despite of clay layers in the left abutment, alluviums in the other parts of foundation are high clayey sand and low clayey gravel.
2. Both S3 and G1 groups show a high permeability. Because of hard penetration of grout in these layers, grouting procedure will be hindered to stop seepage flow through foundation. Construction of a cut-off wall may be more suitable than grouting, at least in shallow parts of the foundation.

Table 1. Reclassification of main geotechnical groups of soil based on F_{200} (percentage of passing 200# Sieve).

Utilized Classification	Comparable Standard Classification	Specification
G1	GP, GW	$F_{200} < 5$
G2	GW-GM, GW-GC, GP-GM, GP-GC	$5 < F_{200} < 12$
G3	GM, GC, GM-GC	$F_{200} < 12$
S1	SW, SP	$F_{200} < 5$
S2	SM, SC, SM-SC	$5 < F_{200} < 12$
S3	SW-SM, SW-SC, SP-SM, SP-SC	$F_{200} < 12$
ML	Silt	-
CM	CL-ML	-

3. There is a high permeable zone in the contact of rock and soil layers. Also bedrock around this contact zone contains high permeable zones but reaches to impervious layer in depth. Grouting of this section may be the best way to prevent seepage flow. A grout curtain that sewed to deep and low permeable zone of bedrock, which have permeability less than 10-4 cm/sec (Figure 6) is a realistic way for sealing bed rock formations.
4. Permeable zones in the left bank around borehole CH3 is the main reason for low groundwater level and lack of adequate hydraulic gradient (Figure 4). This problem is discussed in the next section.

5 CONCLUSION

Considering aforementioned conditions and analysis, main results of this appraisal could be stated as follow;
1. Site area briefly is in poor hydrogeologic conditions and needs firm considerations for improvements.
2. Groundwater level is drastically low in the left abutment and does not be intersected by the line of reservoir water level. This area contains several high permeable zones that may be a good reason for low groundwater level and low hydraulic gradient. These problems must be noticed strongly, because as the reservoir fills up, flow may overturn to abutment and the reservoir may be discharged. Seepage is supposed to be analyzed and modeled in this area. A hanging curtain must be set in this abutment. It would be elongated so that the seepage through the left abutment reaches to a zone of acceptable limit.
3. In the right abutment there are overwhelming evidences of karstification. Since the karstic cavities can discharge reservoir in this area. A dense exploration drilling network as well as test grouting is recommended for disclosing these zone and remediation.
4. In the central part of valley, alluvium zones are extended deeply. Therefore soil grouting is needed in deeper parts of alluvium in addition to cut-off walls in shallow sections.
5. Deep alluvial in contact with rock demonstrates a piping and seepage hazardous zone. A concentrated grouting work may carry out in those sections.

REFERENCES

Belloni, L and Morris, D (1985) Grouting Efficiency in Soft Sedimentary Rocks, Proc of 15th ICOLD Congress, Q 58, R 75, p 1267-1297.

. Iran Water and Power Resources Development Co. (1996) Feasibility Study of Karun IV Dam and Hydropower (in Persian), Ministry of Energy, Iran.

Karbala, M (2004.a) Study of Chaparabad Dam Cut-off Curtain and Design Completion (in Persian), Technical Office, Sepano Cons Co, Tehran, Iran.

Karbala, M (2004.b) Design of Aghchai Dam Cut-off Curtain Based on Engineering Geological and Hydrogeological Data (MSc Thesis in Persian), Amirkabir Univ of Tech, Tehran, Iran.

Hietfield, KH and Krapp, L (2007) The problem of water permeability in dam geology, Bulletin of engineering geology and the environment, Spriger, p 79-83.

Study of Apatite-Nepheline Ores and Urtites Properties by Using Shear Test Device

A.A. Kozyrev, N.N. Kuznetsov
Mining institute KSC RAS, Apatity, Russia

E.V. Lodus
National Mineral Resources University

ABSTRACT Physical-mechanical properties of rocks are of great importance in the field of rock mechanics when estimating failure process in rock mass. Investigating them we can determine limit resistance of the rocks to various loads, their deformation behavior, conditions of elastic vibration transmission and etc. In turn, this information helps to determine if the rocks are prone to rockbursts and other kinds of rock pressure dynamic occurrence.

The article represents analyses and comparison of the test results obtained in determining the shear strength of the apatite-nepheline ore and urtite specimens of the Khibiny massif.

Tested specimens had parallelepiped and cylinder forms. These specimens were cut under various vertical loads with additional rupture energy (by installing the springs on the shear test device).

1 INTRODUCTION

The Khibiny massif includes varieties of rocks, such as apatite-nepheline ores, urtites, rischorrites, lyavochorrites, khibinites, and etc., and most of them are hard rocks. Large scale mining in the Khibiny deposits as well as high stress due to tectonic forces influence result in rock mass movement and cause different fractures. As is known, hard rocks are subjected to brittle fracture, which can cause a rockburst or induced earthquake. That's why it is very important to determine the value of strength limit for the Khibiny massif rocks under various loading conditions. Determination of other physical-mechanical properties is also of great importance.

The paper considers shear fracture in rock mass which usually occurs due to induced rockbursts and earthquakes when developing the Khibiny deposits. This process was modeled by shearing specimens on the shear test device. Shear strength, cohesion and coefficient of internal friction were the main investigated properties. Cohesion characterized shear strength of the rocks without outer loads. Coefficient of internal friction showed connection between changes of horizontal and vertical load values (Turchaninov et al., 1977). These parameters were needed to do accurate engineering calculations to determine the limit loads for rocks, stability of rock mass and pressure on the supports.

Apatite-nepheline ores and urtites have the greatest importance for our study, the first being the main object of mining in the Khibiny massif, and the latter being the host rocks. That's why these rocks specimens were used for testing. The specimens had parallelepiped and cylindrical shape. The total number of experiments accounted for 25 tests with different kinds of loadings.

2 TEST AND RESULT PROCESSING METODS

2.1 Shear test device

To determine the values of physical mechanical properties of apatite-nepheline ores and urtites we conducted experiments on the shear test device (Fig. 1) in the laboratory of the National Mineral Resources University.

Figure 1. Shear test device

The shear device consists of horizontal and vertical loading systems. The vertical loading system includes a hydraulic cylinder with a dynamometer attached to the end of its rod and a hydraulic compression unit mounted on the rigid frame. A compression force meter controls the vertical load values which are continuously transmitted from a strain gauge to the measuring unit.

The horizontal loading system doesn't essentially differ from the vertical one. The hydraulic shear unit is mounted on the rigid frame. A shear force meter controls the horizontal load values transmitted from the strain gauge to the measuring unit.

The additional equipment for the shear test device includes specimen grips with different cross-section. The upper grip is placed in a centralizer. The centralizer provides compression force transfer to the specimens, connects a specimen with the rigid frame; makes its axis perpendicular to the line of the horizontal load. The bottom part of the specimen is also placed in the grip fixed in the carriage. The movement of the carriage under the horizontal load is carried by a sliding unit and controlled by a displacement measurement unit. The values of displacement are continuously transmitted to the measuring unit.

The shear test device considered above allows conducting experiments on shearing specimens with varying vertical load values. Testing specimens without the vertical load helps to determine the values of cohesion. Applying the vertical load we can dispose of tensile stresses which dramatically reduce the shear strength (Citovich, 1983).

2.2 Software ACTest

Physical-mechanical properties of the specimens measured by the shear test device were determined on a basis of the processing data obtained as a result of loading process monitoring in the real time mode.

ACTest automatically reads values from the measuring units of the shear test device. This software is designed to automate the work on research, testing, technological and control-diagnostic devices. It operates on a PC-comparable computer fitted with a means of data collection. The software allows one to setup experiment conditions, storage and search for the appropriate case in the data base. Also, it makes possible to conduct measurements in real time with simultaneous archiving and visualization of experimental data, view and analyze results (from site).

ACTest consists of an experiment preparation and conduction module (Fig. 2) which receives signals from sensors in real time mode and performs primary mathematical data processing; and after session data processing module (Fig. 3) which allows analyzing the experiment results (in the form of stress-time relationship graphs).

3 RESULTS AND DISCUSSION

3.1 Shear tests without vertical load

Testing of the specimens was carried out at several stages: 1) shearing without vertical load; 2) shearing with gradual increase of vertical load from 50 to 150 at; 3) installation of 6 or 8 steel springs on the hydraulic shear unit. Each experiment was carried out on isolated specimens.

The specimens of lenticular-striped apatite-nehpeline ore were tested without vertical load. They had the shape of parallelepiped and cylinder. Shear strength for the first specimen was found as 7 MPa, and for the latter it was 16 MPa. The difference in the values meant that in the parallelepiped specimen shear stress concentration occurred in the edges. In turn, this resulted in decrease of the shear strength value.

Figures 4 and 5 present photos of the specimens before and after destruction. We can see that in the cases there was a pure shear. The lateral strain values of the specimens were near 9 mm. In general, the occurrence of tensile stresses wasn't observed in this test. The obtained values of the shear strength were used as the basic values of cohesion for lenticular-striped apatite-nehpeline ore specimens.

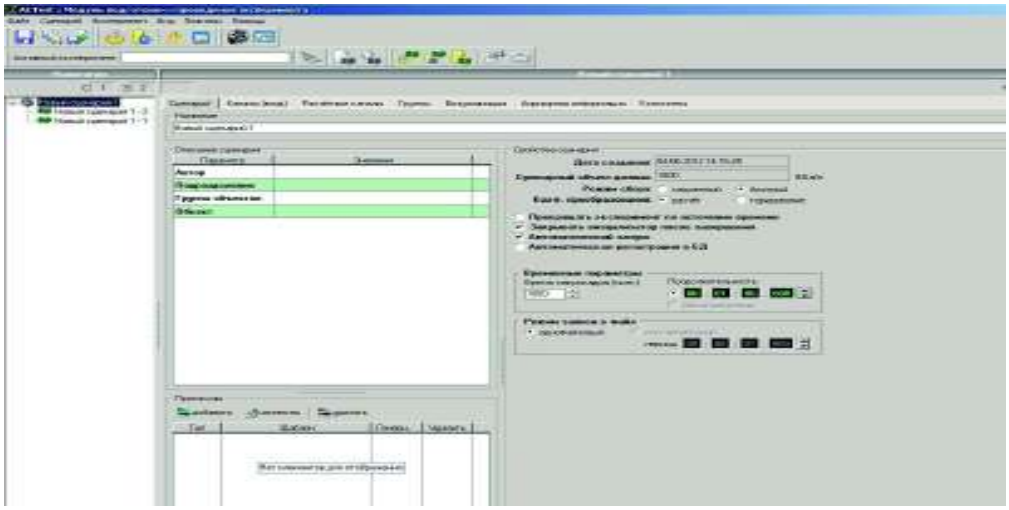

Figure 2. Interface of experiment preparation and conduction module

Figure 3. Interface of after-session data processing module

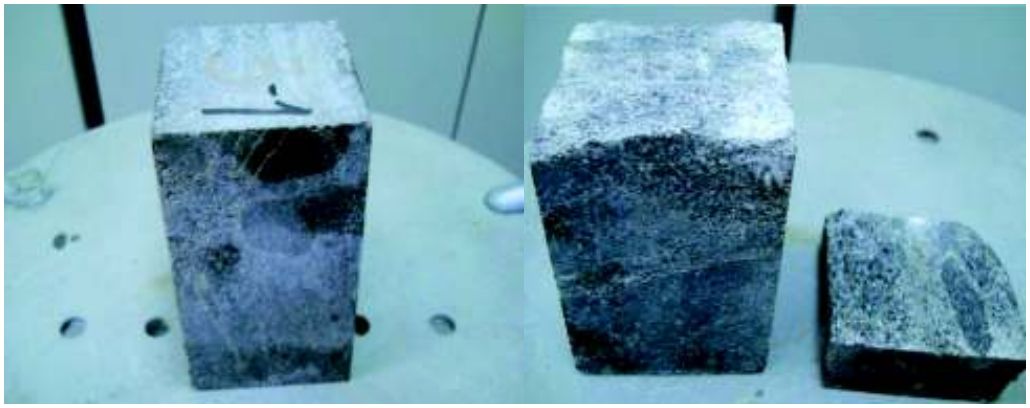

Figure 4. Parallelepiped specimens of the apatite-nepheline ore before and after destruction

Figure 5. Cylinder specimens of the apatite-nepheline ore before and after destruction

3.2 Shear tests with vertical load

The next stage included specimens testing when changing the values of the vertical load. It was established that increase of the vertical load value led to increase of the shear strength. This regularity was found for specimens of medium-granular massive feldspar urtite with sphen, fine-medium granular massive urtite and lenticular-striped apatite-nepheline ore. However, with increasing of the vertical load from 100 to 150 at we established two ways of the shear strength values changing: for medium granular massive and inequigranular massive feldspar urtites these values didn't change, while for apatite-nepheline ore they decreased. The first results were probably related to the fact that the specimens sufficiently consolidated under the influence of the vertical load. In the second case the fissuring in the weaker ore resulted in decreases of specimens shear strength.

Another characteristic feature of specimens testing under the vertical load was their stronger disturbance. The values of deformation under the vertical load at 50 at were significantly less than those obtained without it. However, increase of the load to 150 at led to gradual increase of the strain values. The values of the shear strength determined when testing specimens with applying the vertical load were used to create strength certificates.

3.3 Shear tests with steel springs

On the third stage the experiments were carried out on the specimens with installation of 6 or 8 steel springs on the hydraulic shear unit. These tests allowed effect of a rockburst occurred in the rock mass to be modeled on the specimens. The characteristic feature of the experiments was dynamic fracture with strong sound. This kind of fracture occurred due to decrease of load rigidness caused by adding the steel springs.

As is known, the Khibiny massif includes hard rocks. This fact means that failure occurs only under rigid conditions, i.e. when displacement is constrained. But if there is a possibility for displacement to occur then a shear resulted in rockburst is appeared.

The most significant disturbances of the specimens were observed during these tests in comparison with other experiments. In some cases the specimens were almost completely destroyed. Also, it was found that increasing of the number of the springs intensified the rockburst effect. This fact showed that loading speed influence on the specimens shear strength.

When testing specimens with installation of a steel spring on the hydraulic shear unit and changing the vertical load it was found that under the same load the increasing number of the springs led to increase of the shear strength values. This was typically for specimens of medium-granular massive urtite, medium-granular massive feldspar urtite with sphen, apatite-nehpeline ore and inequigranular massive feldspar urtite. For other tested rock specimens adding of the number of the springs didn't result in increase of the shear strength values.

By comparing tests with using of the steel springs and without them it can be said that for the tests with springs smaller values of the shear strength were observed. It was probably connected with the fact that when the springs were straightened, instantaneous transferred energy resulted in decrease of the specimen strength. Therefore such effect caused the reduction of the shear strength values.

3.4 Creation of the shear strength certificates

The final stage of the study consisted of creation of the strength certificates for all of the researched rocks. For this purpose the values of the shear strength and vertical loads were used. The certificates were built by using Mohr-Coulomb failure criterion, which is:

$\tau = c+\sigma*tg\varphi$,

where τ–horizontal stress (MPa), c–cohesion (MPa), σ–vertical stress (MPa), $tg\varphi$–coefficient of internal friction (Turchaninov et al., 1977).

The results were shown in the form of horizontal stress-vertical stress relationship graphs (Fig. 6) which allowed us to determine the values of cohesions and internal friction coefficients.

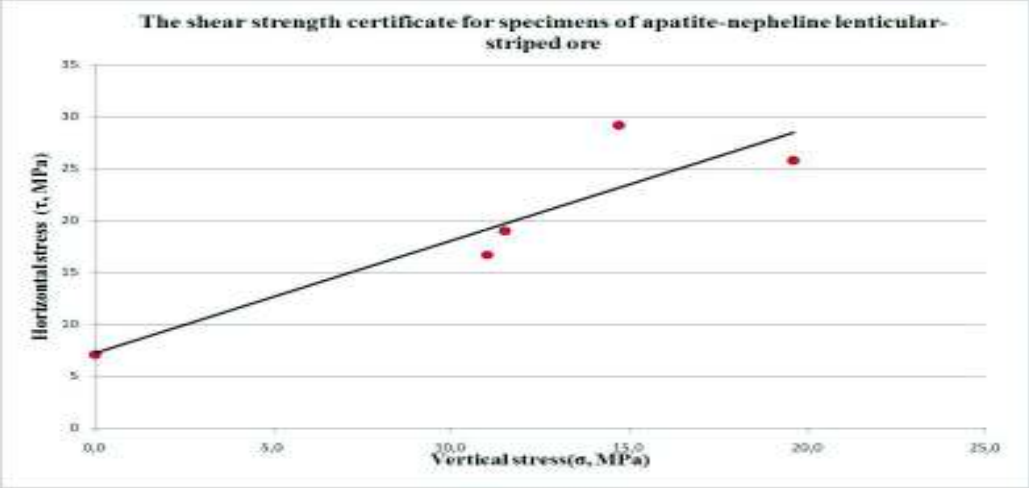

Figure 6. Strength certificate of the lenticular-striped apatite-nepheline ore

The Table 1 shows the results of specimens testing under the different vertical loads and data obtained on the basis of shear strength certificates. Their analysis was given above. It was established that specimens of inequigranular massive feldspar urtite had the greatest value of cohesion. Therefore this rock was the strongest one. The specimens of lenticular-striped apatite-nehpeline ore had the greatest value of the internal friction coefficient. And this rock was the weakest one.

Table 1. The results of shear tests

Rock	Horizontal stress (τ, MPa) without vertical load (0 at)	Horizontal stress (τ, MPa) under 50 at	Horizontal stress (τ, MPa) under 100 at	Horizontal stress (τ, MPa) under 150 at	Horizontal stress (τ, MPa) under 100 at with 4 springs	Horizontal stress (τ, MPa) under 100 at with 8 springs	Horizontal stress (τ, MPa) under 150 at with 4 springs	Horizontal stress (τ, MPa) under 150 at with 8 springs	Internal friction coefficient (tgφ)
Medium-granular massive urtite	11	-	19	24	-	-	23	27	0.6
Medium-granular massive feldspar urtite with spots	12	-	13	23	-	-	24	28	0.8
Lenticular striped apatite-nehpeline ore	7	17	20	28	19	20	22	23	1
Inequigranular massive feldspar urtite (cylinder)	20	-	28	28	24	25	-	-	0.5
Fine-medium-granular massive urtite (cylinder)	28	-	-	48	35	30	-	-	0.8

4 CONCLUSION

As the result the values of shear strength, cohesion and internal friction coefficient have been determined for all tested rock specimens. The fracture pattern of the specimens in each type of the experiments has been found. The analysis of obtained data has been carried out and some regularity patterns established. These data are essential in the development of recommendations on the selection and estimation of rational parameters for mine workings support, especially under conditions of dynamic rock pressure occurrence and unstable and oxidized rocks.

ACKNOWLEDGEMENT

The reported study was partially supported by RFBR, research project No. 12-05-00507.

REFERENCES

Citovich N.A., 1983, *Soil Mechanics*, "Vicshaya shkola", Moscow, 288 p.

Official site of ACTest developers: http://www.actech.ru/productions/serial/actest.shtml

Turchaninov, I.A., Iophis M.A., Kasparyan E 1977. *Foundations of Rock Mechanics*, "Nedra", Saint Petersburg, 507 p.

Rock Mechanics Monitoring of Hard Rock Massifs Using Space Geodesy Methods

A.A. Kozyrev, E.V. Kasparian, S.N. Savchenko, R.N. Dostovalov
Mining institute KSC RAS, Apatity, Russia

ABSTRACT The comparative analysis has been carried out of the results of optical distance and GPS-measurements in observation stations of the geodynamic testing site at the "Zentralny mine", "Apatit" JSC in the Khibiny rock massif. The results of GPS-measurements for 2007-2011 are presented. The values are determined of secondary stresses, deformations and rotations in the blocks under review with active response towards changes in the general geodynamic setting in the testing site.

1 INTRODUCTION

The methods of the space geodesy, particularly GPS-technologies are currently widely applied to define the absolute coordinates of the earth's surface points and the movement of different large geological objects, e.g., lithosphere plates in time and space [*Robert McCaffrey, 2005*].

But until recently the applying of these methods to study the deformation of relatively small-scaled rock masses located in the vicinity of the mining enterprises was restrained due to low accuracy of determination of movements and deformations [*Panzhin A.A., 2008*].

The geodynamical setting in the land allotment area of the Tsentralny mine is more difficult compare to other mines of "Apatit" JSC. This is caused by high rock mass intensity, large volumes of extracted and removed rock mass, developed underground vehicle excavations (deep orepasses and large sectional tunnels). The situation is additionally complicated by the underground mining operations at the Rasvumchorr mine, in the immediate proximity to an open-pit.

These factors cause higher geodynamical activity of the rock mass what is seen in periodical occurrence of large dynamical rock pressure in the vicinity of the Tsentralny mine.

2 PROBLEM STATEMENT

Natural stress-strain state of the rock mass at the Tsentralny mine is caused by simultaneous action of tectonic and gravity components. The tectonic component of the stress field acts along the ore body strike; the gravity component acts in the vertical plane and is determined by own weight of the rock mass and rocks removed into the dumps close to the open-pit wall. An initial task for the monitoring observations was to assess stability of the north-western pit wall which state was complicated by underworkings at the Rasvumchorr mine. Also there was a task to assess a large fault in the western part of the open-pit where large-scale works were carried out to form a waste rock dump. For these purposes special observations for rock mass deformations and displacements were organized by the survey agency of the

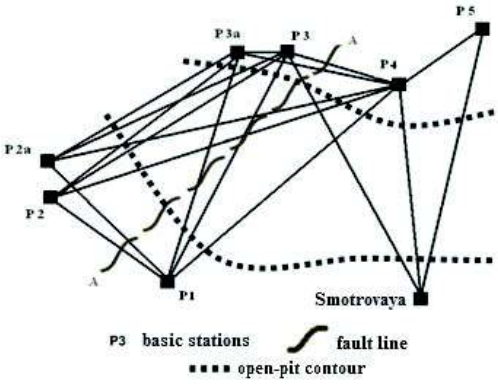

Figure 1. Geodynamic testing site

Tsentralny mine (1994) and the Mining Institute KSC RAS (1999) and are carried out to the present. The geodynamical testing site built in 1999 (fig.1) consists of eight basic stations, four of which are located from the same side of the monitored fault (A-A), and other four stations are located in the adjacent structural block.

The rock mechanics monitoring includes identification of displacements and deformations of basic and working testing site stations.

Both traditional geodesy (leveling, traverse survey, triangulation, trilateration survey) and space geodesy methods are likely to be applied for these purposes. The observations on the basic stations, the Tsentralny mine, are carried out by the complex method: optical distance measurements are made by an optical distance measuring device Mekometr-5000 (ME-5000), and the absolute coordinates of the stations are identified by the space geodesy methods (GPS-technologies).

3 MEASUREMENTS

The technique of the optical distance measurements was tested by long-term operations on geodynamical testing sites and consists of periodical measurements of inclined distances between basic and working stations. The optical distance measuring device and reflectors at the stations are installed out with forced centering, that's why installation errors are extremely negligible. This allows the measurements of distances between the stations in one-way movement only to reduce time and keep accuracy. Regular GPS-measurements have been carried out since 2007, GPS-satellites (USA) being used only.

To the date we have five sets of equipment, including JNS Lexon-GGD receiver and JNS Chock Ring CR3_GGD antenna designed and produced by "Javad Navigation System". During measurements the receivers are replaced in a certain order from the station to the station so that simultaneous equipment work time in each triangle is minimum 5 hours. Differential correction with a fixed GPS receiver located in the basic station with predetermined coordinate is applied to reduce measurement errors. During the whole measurement period the basic station accumulates data on coordinate determination errors which are taken into consideration by the specific software when processing data from mobile receivers installed in the monitored stations.

GPS-measurements register pseudo-distance to GPS NAVSTAR satellites on two frequencies of L1=1575,42 MHz and L2=1227,60 MHz with 30 sec interval. Signals registering and tracking are carried out automatically under control of firmware receivers.

The data obtained are treated by the software Pinnacle designed by the company producing the equipment applied. As a result we obtain the observation points coordinates in the international geodesic system WGS-84. Stations displacements are calculated by changing of the corresponding coordinate components from the cycle to the cycle. If GPS-measurements are applied to monitor the geodynamical state of the rock mass, one of the main issues is to provide the sufficient accuracy of the results obtained.

To solve this problem under the specific conditions of apatite-nepheline deposits the

GPS-measurement results, particularly, vectors lengths were compared to the results of optical distance measurements for the same distances. The data analysis indicates divergence between results of GPS and optical distance measurements from -3.5 to +32.9 mm, which is probably explained by significant systematic errors of both measurements. Other situation appears when comparing the stations displacement determined by results of optical distance and GPS-measurements. At that majority of comparison results are presented by considerably smaller values.

For the correct estimation of the distances measured and the rock mass displacements by results of optical distance and GPS-measurements we can calculate errors of results obtained.

Mekometr-5000 error equation (by results of the equipment calibration, October, 2006) can be determined as:

$m_{CB} = \pm(0.38 + .68 \cdot D)$ mm,

Where D – distance measured, km.

Displacements error by optical distance measurements can be expressed as:

$m_{\Delta L_{CB}} = m_{CB} \cdot \sqrt{2} = \pm\sqrt{2} \cdot (0.38 + 0.68 \cdot D)$ (1)

GPS-measurements error (at the average, by technical data of the equipment applied) is defined as:

$m_{GPS} = \pm(3 + 1ppm) = \pm(3 + 1мм$ for 1km). Then the displacements error by GPS-measurements is determined:

$m_{\Delta GPS} = m_{GPS} \cdot \sqrt{2} = \pm\sqrt{2} \cdot (3 + 1мм$ for 1km) (2)

Total error of displacements comparison is expressed as:

$M = \sqrt{2m_{CB}^2 + 2m_{GPS}^2}$ (3).

The calculation values of the errors for all the distances between the stations of the testing site are presented in the Table 1. The column 6 contains actual difference in movements identified by optical distance and GPS-measurements; values exceeding calculated errors are blue-colored.

According to the data given (Table 1) calculated values of mean-square errors are exceeded in 10 cases of 45 (22%). It is an evidence of some nonregistered local causes of inaccurate measurements. At that, maximum divergences from one cycle to another one are often observed for the same stations. This is an evidence of local causes, e.g., due to incorrect installation of antennas or some obstacles for satellite signals passing.

Table 1. Errors of optical distance and GPS-measurements results

Sites	Distance (km)	$m_{\Delta LCB}$, (mm)	$m_{\Delta GPS}$, (mm)	$M = \sqrt{2m_L^2 + 2m_{GPS}^2}$ (mm)	ΔME - ΔGPS, (mm)
1	2	3	4	5	6
Tsentralny mine, "Apatit" JSC					
P1–P2	0.8	±1.3	±5.3	±5.5	-1.5; -3.5; -0.7; -0.2; -0.9
P1–P3	1.8	±2.3	±6.8	±7.2	1.9; 2.9; 4.7; -1.9; -6.4
P1–P4	1.9	±2.3	±6.9	±7.3	***12.6;-21.3; 9.4***; -5.2;-6.9
P3–P2	1.7	±2.2	±6.6	±7.0	1.0; 1.1; 0.6; -2.4; -2.7
P4–P2	1.9	±2.4	±7.0	±7.4	4.2; ***-14.7***; 3.1; -0.9; -3.9
P4–P3	0.4	±1.0	±4.9	±5.0	***-6.2***; -3.4; 0.3; -0.3; -1.5
"Smotrovaya"–P3	2.1	±2.6	±7.2	±7.7	7.1; ***-9.5***; 4.1; ***-9.2***; 0.6
"Smotrovaya"–P4	1.8	±2.2	±6.7	±7.1	***26.8***; ***-27.5***; 5.2; ***-9.7***; 0.1
P1–P5	2.8	±3.2	±8.2	±8.8	4.1
"Smotrovaya"–P5	2.2	±2.7	±7.4	±7.8	-2.4
P2a–P1	0.9	±1.4	±5.5	±5.6	0.1
P2a–P3	1.7	±2.2	±6.7	±7.0	1.4
P2a–P4	2.0	±2.5	±6.9	±7.3	4.7

The data (Table 1) also demonstrate tendency to increase of difference between optical distance and GPS-measurements results with increasing of distances between the observation stations. Optimum distance between the basic stations is 1500 m. At that calculated value of distance determination error by optical distance measuring method is ±2.0 mm, and coordinates determination error by GPS-method is ±6.3 mm. The latter value should be taken as a limit error when monitoring stress-strain state of the rock mass.

4 TREATMENT OF MEASUREMENTS

The main aim of rock mechanics monitoring and, in particular, of GPS-measurements, is to identify space and time displacements of the basic stations due to large mining-induced impacts. Coordinates of all the stations in the geodynamical testing site vary under impact of the following causes:

- Global displacements of Euro-Asian lithospheric plate Δx_{global};
- Mining-induced displacements, $\Delta x_{techn.}$;
- Errors of GPS-measurements, Δx_{error}

In this case total displacements of basic stations can be determined by equation:

$$\Delta X = \Delta x_{global} + \Delta x_{techn.} + \Delta x_{error} \quad (4)$$

Coordinates of a basic station (Mining Institute) vary under impact of:

- Global displacements of Euro-Asian lithospheric plate $\Delta x_{MIglobal}$;
- Errors of GPS-measurements, Δx_{error}

$$\Delta X_{MI} = \Delta x_{MIglobal} + \Delta x_{MIerror} \quad (5)$$

It is suggested that:

$\Delta x_{global} = \Delta x_{MIglobal}$;

$\Delta x_{error} = \Delta x_{MIerror}$

Hence, to determine displacements of the stations from the geodynamical testing site due to mining-induced impacts only it's

necessary to deduct displacements of the basic station appropriate in time from the total displacements of each station. So, final mining-induced displacements of the stations can be determined by the formula:

$$\Delta x_{techn.} = \Delta X - \Delta x_{global} - \Delta x_{error} = \Delta X - \Delta x_{MIglobal} - \Delta x_{MIerror} = \Delta X - \Delta X_{MI}. \quad (6)$$

Table 2 presents "reduced" displacements of the stations, i.e., displacements calculated taking into account displacements of the basic station.

Table 2 Reduced displacements of basic stations

Year	ΔX, mm					ΔY, mm					ΔZ, mm				
	"Smotrovaya" site	P1	P2	P3	P4	"Smotrovaya" site	P1	P2	P3	P4	"Smotrovaya" site	P1	P2	P3	P4
2007	0,0	0,0	0,0	0,0	0,0	0,0	0,0	0,0	0,0	0,0	0,0	0,0	0,0	0,0	0,0
2008	0,0	0,4	-0,2	9,1	9,1	-0,4	-0,4	-0,5	9,5	18,6	-0,8	-2,8	-0,7	8,3	-37,3
2009	-261,0	-282,0	-275,0	-271,4	-272,0	-112,5	-126,0	-122,4	-128,6	-136,7	-633,1	-682,7	-655,5	-680,3	-655,4
2010	-20,9	-21,6	-17,1	-16,8	10,0	-12,0	-14,0	-11,7	-9,7	3,5	-46,5	-43,2	-44,9	-56,9	-9,3
2011	23,5	27,8	20,9	31,6	26,5	23,0	19,8	16,3	21,5	14,2	57,3	61,8	58,4	53,3	36,8
2012	6,9	10,1	4,7	38,0	27,9	-14,8	-18,9	-22,4	-0,2	-10,6	-2,2	-15,4	-36,9	35,3	2,9

By reduced displacements there were calculated values of secondary principal deformations and stresses, rotations and complementary specific deformation energy in structural elements of rock mass. The latter are triangles which apices are formed by the corresponding stations [*Savchenko, Kasparyan, 2007*]. The calculation results for the most typical structural blocks are presented in figure 2 and table 3.

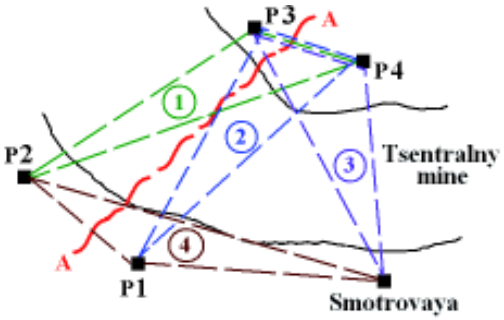

Figure. 2 Typical structural blocks of the testing site with estimated stress-strain state and energy-saturation

Table 3 Secondary stresses in the rock mass (σ_1, σ_2, σ_3), rotations and complementary specific deformation energy (w) in elementary volumes of structural blocks.

Block	Year	Secondary principal stresses, MPa			Rotation			Specific energy change, *w*, MJ/m^3	Notes
		σ_1	σ_2	σ_3	ω_1	ω_2	ω_3		
P2-P3-P4	2007-2008	0,6078	-0,0908	-0,3283	0,1 e-5	-0,9 e-5	5,4 e-5	3,28 e-05	
	2008-2009	0,1674	0,0014	-0,4111	-0,2 e-5	0,9 e-5	-3,1 e-5	1,36 e-05	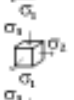
	2009-2010	0,7554	0,1328	-0,3892	3,1 e-5	1,7 e-5	-6,2 e-5	4,41 e-5	
	2010-2011	0,0914	-0,1061	-0,2878	-0,5 e-5	-0,3 e-5	2,2 e-5	0,53 e-5	
P1-P3-P4	2007-2008	0,5538	-0,0314	-0,2638	0,5 e-5	1,3 e-5	4,9 e-5	2,31 e-5	
	2008-2009	-3,6 e-5	-0,0824	-0,3617	-0,5 e-5	-1,1 e-5	-2,5 e-5	0,08 e-5	
	2009-2010	0,4237	-0,1211	-0,5795	3,4 e-5	-1,2 e-5	-5,2 e-5	3,22 e-5	
	2010-2011	0,1683	-0,0017	-0,1677	-0,8 e-5	0,7 e-5	1,8 e-5	0,38 e-5	
P3-P4- Smotrovaya	2007-2008	0,7553	0,1493	-0,5949	1,8 e-5	7,2 e-5	3,4 e-5	6,36 e-05	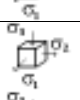
	2008-2009	0,3000	0,1062	-0,2970	-1,8 e-5	-2,4 e-5	-2,6 e-5	1,18 e-05	
	2009-2010	0,0161	-0,6860	-1,6177	3,9 e-5	-8,9 e-5	-2,4 e-5	14,03 e-5	
	2010-2011	0,4284	0,1866	-0,1336	-1,7 e-5	3,0 e-5	0,6 e-5	1,49 e-5	
P1-P2- Smotrovaya	2007-2008	0,3474	-0,044	-0,0144	0,3 e-6	-0,2 e-5	-0,1 e-5	0,01 e-5	
	2008-2009	0,1115	-0,3017	-0,7177	0,5 e-5	-4,8 e-5	1,8 e-5	3,36 e-5	
	2009-2010	-0,0241	-0,0358	-0,1381	0,1 e-6	0,1 e-5	0,4 e-6	0,08 e-5	
	2010-2011	0,2152	0,0992	0,0497	0,2 e-5	0,8 e-5	-0,3 e-5	0,20 e-5	

5 RESULTS ANALYSIS

The tensor of secondary stresses in all the calculated blocks for the period estimated (2007-2010) is caused by simultaneous action of compression and tension stresses, but for the "Smotrovaya P1-P2" block where change of stress state was caused by small compression stresses only (2009-2010), and by tension stresses only (2010-2011).

For the whole observation period (2007-2011) maximum tension stresses (σ_1=+0.75 MPa) were registered in «P2 – P3 – P4» block during 2009-2010, and maximum compression stresses σ_3=-1.62 MPa were registered in the "Smotrovaya-P3-P4" block. It's necessary to note that these stress values are realized stresses as a result of deformation for a time period from a previous observation period, i.e., from an initial state of the rock mass monitored. In general, the results obtained indicate that rocks intensity degree is characterized by rather low values of stresses changes for the period under review.

Value of complementary specific energy in all the blocks was varying during all the period under review. Maximum energy change (E=140.26 J/m^3) was registered in the "Smotrovaya-P3-P4" block for 2009-2010. This value was much smaller than a critical value of 0.25÷0.30 J/m^{3}determined by the samples destruction. During the subsequent cycle the energy value was reduced almost by an order.

Relatively large changes of energy magnitude correspond to the blocks containing P3 and P4 stations, which is evidence of larger activity into this part of A-A fault, and, into the hanging wall of the deposit, in general.

6 CONCLUSION

Monitoring of the geodynamical testing site located at the Tsentralny mine, "Apatit" JSC, indicates that the rock mass within an area observed noticeably responds on seismic events, and stress-strain state of structural blocks changes accordingly. The developed technique of measurements and results treatment allows tracking secondary deformations values, calculating angles of stress-strain state change, determining rotations and assessing a realized deformation energy magnitude for the structural blocks observed. The structural blocks the most actively reacting to change of a total geodynamical situation were selected. Continuing observations and further results accumulation must demonstrate how far these active blocks can indicate state of the whole rock mass. It is quite possible that these active blocks can demonstrate trends of change of the rock mechanics setting at the whole monitored rock mass.

ACKNOWLEDGEMENT

The reported study was partially supported by RFBR, research project No. 12-05-00507.

REFERENCES

Robert McCaffrey Block kinematics of the Pacific-North America plate boundary in the Southwestern United States from inversion of GPS, seismological and geologic data// Journal of Geophysical Research.-2005-V.110-BO7401-doi:10.1029/2004Jb003307.

Panzhin A.A. Practice of geodynamical GPS-monitoring on the objects of subsoil use / Geodynamics and stress state of the Earth's interiors: Proceedings of the scientific conference / Mining Institute of the Siberian Branch of RAS. Novosibirsk.-2008.

Savchenko S. Kasparyan E. The theoretical principles in geomechanical monitoring data processing for a block medium. Proceeding of the International Geomechanics Conference 11-15 June 2007, Nessebar, Bulgaria, V-1 – V-8.

Comparisons between Predicted and Observed Surface Settlement for Deep Excavation Adjacent to Building in Soft Ground

M. Akchiche, M. Kouici
Laboratory of Geotechnical Engineering, Infrastructure Development hydraulic, Faculty of Civil Engineering, USTHB, BP. 32 El Alia, Bab-Ezzouar, Algeria

ABSTRACT The development in urban areas typically requires the necessity of deep excavations near existing structures on the surface.

For reasons of space these excavations are near and structures in service area. The integrity and stability of these structures is a key issue during the different phases of new construction work (excavation, construction ...).

This problem represents a complex study of soil-structure interaction. In this paper, we present a numerical study of this interaction and we perform a comparison between the numerical results obtained in both two dimensional with CESAR-LCPC code.

Keywords Soil settlement, behavior, comperative study, measurement result, numerical code, foundation, deep excavation

1 INTRODUCTION

In dense urban environments where land is scarce and buildings are closely spaced, deep excavation for basement construction and other underground facilities such as mass rapid transit stations and cut-and-cover tunnels is unavoidable. As these excavations are usually carried out close to existing buildings, a major concern is to prevent or minimize damage to adjacent buildings and underground utilities. To date, most of the research has been on the prediction of ground settlement and the lateral movement of the retaining wall system Peck (1969); Clough and O'Rourke (1990); Ou et al. (1993).

Many studies on the performance of earth retention systems were done and reported since the past couple of decades. Lateral and vertical behavior of excavation, responses of adjacent structures, and performance of stiff support are referred to Finno and Harahap (1991), Finno and Bryson (2002), Son and Cording (2005, 2007). The effect of corners in strutted excavation in Singapore and performance of top-down excavation in Shanghai and Taiwan can be referred to Lee et al. (1998), Onishi and Sugawara (1999), Ou et al. (1998), and Kung (2008). Performance of permanent anchored wall and the stability issues are referred to Briaud et al. (2000) and Mueller et al. (1994).

Because of the great risk associated with the potential impact of construction deformations on adjacent structures. The designers of the design office undertook the responsibility of designing the excavation and shoring system to control ground deformations within specified limits.

The specified limits for deformations were developed based on detailed structural analyses that evaluated the response of each individual building to the estimated deformation profiles. In addition, specified requirements regarding the

excavation and shoring processes were developed to minimize the risk that ground deformations might exceed the tolerable limits determined from the structural analyses.

The philosophy and approach followed by The designers team was based on the premise that the designer is in the best position to specify the requirements for the various construction activities to achieve the intended results.

A monitoring program was implemented to measure ground and building deformations during construction. The ground deformations caused by the various construction activities were evaluated and compared with the estimates made during the design.

During construction in front of the buildings, the ground deformations as well as the performance of the buildings were monitored carefully and evaluated promptly, and they were compared with the results of the structural evaluation to verify that the existing buildings were not impacted adversely.

This study summarizes the geotechnical aspects of **airshafts** construction (PV1). It presents and discusses the subsurface conditions and the key elements of the excavation and shoring design, and summarizes the results of the measurements regarding the performance of the excavations and of the adjacent buildings (fig. 1). General conclusions from this case history are presented at the end of the paper.

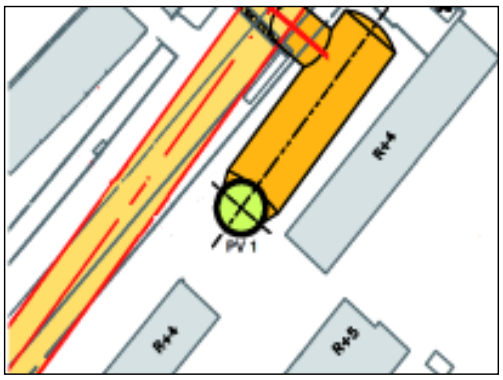

Figure 1: Map view of the part project area.

2 GEOLOGICAL AND GEOTECHNICAL CONDITIONS

Algiers region is constituted of three geomorphology types Sahel, lowland of Mitidja and Blideen Atlas. The recognition analysis of the geologic exploration showed that the basement is mainly made of a homogeneous structure. This structure is represented principally by four big distinct lithology types:

- The Plaisancien, formation of grey marl at grey greenish,
- The Astian formation, sandstone, fine at coarse sands,
- The Plio-quaternary formation, brown clay at blow,
- The Quaternary formation, colluviums, alluvial deposits.

The Algiers region is an active seismic zone, according to its geographical position on the verge of both tectonic plates, which are in continuous compression, Africa and Europe.

The medium geotechnical characteristics of the different skylines obtained at the geotechnical exploration are summarized in the tab. 1, and represented in figure 2. It has been observed following

- Embankment: Rx
- Quaternary clay: Q.A
- Tertiary clay: T.A
- Tertiary sandy: T.S

We note that the level of aquifer is below our buried structures

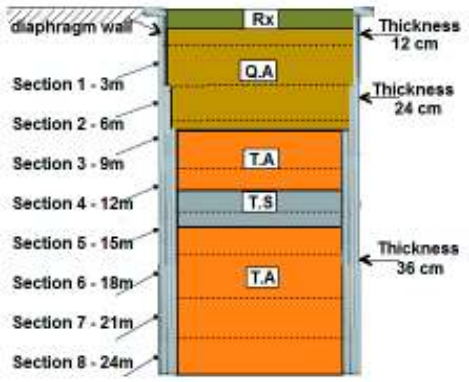

Figure 2: Calculating sections into the well.

Table 1: Commun physical and geotechnical properties of the soils

	Rx	Q.A	T.A	T.S
γ *(KN/m³)*	*19*	*20*	*22*	*21*
E (MN/m²)	*7*	*31*	*43*	*77*
C' *(kN/m²)*	*0*	*48*	*53*	*55*
C_u *(kN/m²)*	*5*	*72*	*89*	*76*
φ' *(°)*	*19*	*22*	*25*	*27*
φ_u	*19*	*16*	*17*	*21*
K (m/s)	-	10^{-5}	3.10^{-7}	10^{-4}
Ko	*0,6*	*0,6*	*0,6*	*0,6*

3 PROJECT DETAILS

At the completion of PV1, the digging was done with steps of progress whose value depended on the nature of the different strata of the ground to a depth of 24 m. Steps ranged from 0.5 meters to dig the most unstable layers, up to a pitch of 1.5m layers for more stable.

The support used is composed of Shotcrete more welded mesh. The well is applied compression; welded mesh is not involved in the resistance, but serves to keep up the shotcrete (table 2 and table 3).

Sections of calculation we have chosen correspond to the levels chosen by designers for measuring convergence in the well, and to be able to compare the results with actual measurements measured (figure 3).

Table 2: Propriety of projected concrete C25/30 (EC 2)

(γ) KN/m³	*σ_c MN/m²*	*σ_t MN/m².*	*E_b MN/m²*
25	*25*	*2,6*	*15.000*

Table 3 : Propriety of projected concrete C25/30 (EC 2) according to the depth

Depht	*Number of plies*	*Thicknesses corresponding [cm]*
3	*1*	*12*
6	*2*	*24*
9	*3*	*36*
12	*3*	*36*
15	*3*	*36*
18	*3*	*36*
21	*3*	*36*
24	*3*	*36*

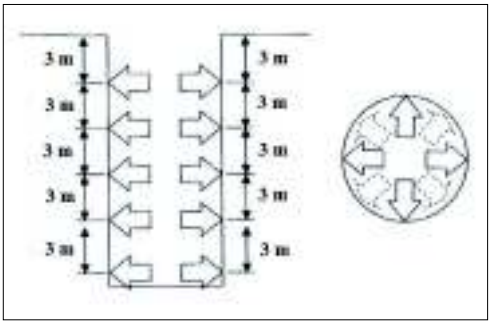

Figure 3 : Implementation targets in the well

4 FINITE ELEMENT ANALYSIS

A series of 2-D simulation using the finite element analysis were conducted by using CESAR-LCPC software. This program was designed to provide complex geotechnical structure analysis in two and three dimensions. Soils were modeled using the drained material properties with the linear elastic perfectly plastic "Mohr Coulomb" failure criteria.

Simulation of the TV 1 process was commenced with the selection of the PV 1 geometry and model geometry in two dimensions, the model takes advantage of the axisymmetrical of the problem.

The model was fixed in the horizontal direction at two vertical sides, which means that vertical movement was allowed, and the bottoms part of the boundary was fixed in the vertical movement. The vertical or horizontal movement was allowed at top surface the model, as can be seen in Fig. 6.

4.1 Sequential Excavation of Model.

In this analysis, excavation has been carried out in seventeen steps. The detail analysis procedures used during this sequential excavation model are as follows:
Step1. Constraint initialization (apply gravity forces),
Step2. Excavation 3m depth the representative elements of the lining are deactivated
Step3. The representative element of the lining support of the excavation is activating.
Step4. Excavation another 3m depth the representative elements of the lining are deactivated.
Step5. The representative element of the lining support of the excavation is activating (between 3 and 6 m),
Step 6. We redo steps 4 and 5 to step 17,

5 INTERPRETATION AND CONCLUSION

Figure 5 presents the comparison between the measured, analytical solution and numerical solution with Cesar-LCPC at PV 1.

After completion of the analyses, the measured indicated that at the completion of excavation, wall of excavation only developed 20 mm deflection to the excavation side at 16 m from the surface. This important deformation with respect to the value measured in the bottom of the excavation (3mm) and at the head of the excavation 4mm, is due to be possible errors in the measurements. Since displacements of the wall are important in design, it is desirable to obtain more accurate measurements. It is believed that since other measurements compare well with the predictions, the displacements from the finite element prediction can be considered to be reasonable.

In another time, the FEM modeling results indicated that at the completion of excavation, wall of excavation only developed 15 mm deflection to the excavation side. This small deflection can be attributed that Overload due to the building who did not have much im pact on the excavation of PV1.

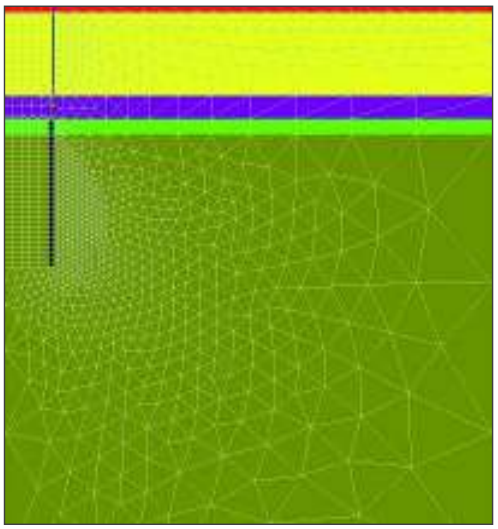

Figure 4: Finite element mesh for two dimensional models

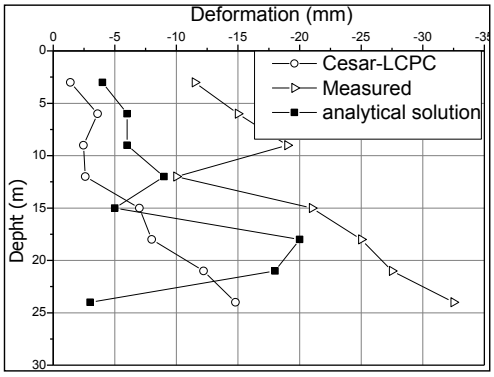

Figure 5: Results of deformation of the walls depending on the status of digging through the code Cesar-LCPC, analytical solution and measured.

In another time, the FEM modeling results indicated that at the completion of excavation, wall of excavation only developed 15 mm deflection to the excavation side. This small deflection can be attributed that Overload due to the building who did not have much impact on the excavation of PV1.

Finally the result of analytical solution given by the convergence confinement method is give 33 mm in the bottom of the excavation.

The observations of results of a deflection for differents analysis are:

- Deflection given by analytical solution is approximately twice the FEM.

- Deformation given by the FEM is less than that given by the measures. This is due, to our notice by the assumption made in axisymmetrical FEM, which involves; the loading is the same on the entire surface while our building is right in a part of the surface.

In conclusion, if appropriate soil parameters and construction conditions are used and assumed, continuous FEM modeling can predict performance of excavation of the well. Therefore, such analysis can serve as a reference for design or prediction on performance of retaining structures.

In addition, continuous FEM analysis is a powerful tool to understand soil–structure interaction mechanism under complex construction conditions.

REFERENCES

Boussinesq, J. (1885), *Application des potentiels a l'étude de l'équilibre et du mouvement des solides élastiques*, Gauthier-Villar, Paris.

Briaud, J. L., Nicholson, P., and Lee, J. S. (2000), Behavior of full-scale Vert wall in sand, *J. Geotech. Geoenv. Eng.*, 126(9), (pp.808–818).

Clough, G. W., and O'Rourke, T. D. (1990). Construction induced movements of in-situ walls, *Design and performance of an earth retaining structure, Geotech. Spec. No. 25,* ASCE, N.Y., (pp. 439-470).

Finno, R.J., and Harahap, I. S. (1991), Finite Element Analyses of the HDR-4 Excavation, J. of Geotech. Eng., ASCE, Vol. 117, (10),

Finno, R., & Bryson, L., (2002), Response of Building Adjacent to Stiff Excavation Support System in Soft Clay, J. Perf. Const. Facil., 16 (1); (pp. 10-20).

Kung, G. T. C. (2008), Procedure for evaluating excavation-induced damage of adjacent buildings, *Chinese Journal of Geotechnical Engineering*, Vol. 30, Supp., (pp. 138-143).

Lee, F. H., Yong, K. Y., Quan, K. C. N., and Chee, K. T. (1998), Effect of Corners in Strutted Excavations: Field Monitoring and Case Histories, *J. Geotech. Geoenviron. Eng.*, 124(4), (pp.339–349).

Mueller, C. G., Long, J. H., Cording, E. J., and Weatherby, D. E. (1994), Ground Movements From Model Tieback Wall Construction, *Geotech. Spec. Publ.*, 40, (pp.1337–1352).

Onishi, K., and Sugawara, T. (1999); Behavior of an Earth Retaining Wall During Deep Excavation in Shanghai Soft Ground, *Soils Found.*, 39(3), (pp.89–97).

Ou, C. Y., Hsien, P. G., and Chiou, D. C. (1993), Characteristics of Ground Surface Settlement During Excavation, Canad. Geotech. Jor., Ottawa, 30 (pp : 758-767).

Peck R. B. (1969), Deep Excavations and Tunneling in Soft Ground, Proc. 7 th ICSMFE, Mexico, State Of the Art. (pp. 225-290).

Son, M. & Cording E. (2005), Estimation of Building Damage Due To Excavation-Induced Ground Movements, J. Geotech. Geoenviron., Eng., 131 (2), (pp. 162-177).

Son, M. and Cording, E. (2007), Evaluation of Building Stiffness for Building Response Analysis to Excavation-Induced Ground Movements, J. Geotech. Geoenviron. Eng., 133(8), (pp. 995–1002).

Post-Peak Behavior of Geomaterials with Block-In-Matrix Texture

M. Afifipour, P. Moarefvand,
Amirkabir University of Tehran, Tehran, Iran

ABSTRACT Design and construction of engineering structures in geomaterials with block-in-matrix texture (referred as bimrock in literature) such as conglomerates, breccias and agglomerates are challenging task for engineers. When dealing with these materials in important structures such as open pits with high walls and pillars of deep underground mines, understanding the complete stress-strain behavior, including post-peak region, is a formidable yet crucial engineering practice. In this paper, to study the post-peak behavior of bimrocks, artificial specimens were fabricated. All the experiments were conducted under uniaxial compressive stress conditions using a servo-control compression testing machine. The results showed that, the highest block proportion specimens (around 90% by weight) showed a small decrease in stress with strain increment in post-peak part. The specimens with lower block proportion were characterized by an approximately steep fall in stress and following to residual stress. Based on the study it is inferred that all the artificial specimens undergo post-failure deformation and the type of post behavior depends on block proportions.
Keyword: bimrocks, uniaxial compression loading, servo-control, post-peak.

1 INTRODUCTION

In nature, there are a great number of geomaterials (rock or soil) with a texture of stiff rock blocks surrounded by weaker soil-like matrix. In the literature, these heterogeneous rock mixtures are commonly referred as block-in-matrix rock (bimrock) (Medley, 1994), soil-rock mixture (SRM) (Xu et al., 2008) or Stiff rock-soil mixture (SRSM) (Afifipour & Moarefvand, 2012).

The most widespread bimrocks are conglomerates, breccias in sedimentary rocks, agglomerates and pyroclastics in igneous rocks, tectonic mélanges and flysch in metamorphic rocks and in artificial forms, mine waste dumps, tailing dam materials and cemented rockfill as backfilling materials in underground mining (Medley 1994; Afifipour & Moarefvand, 2012).

Due to widely distribution of bimrocks in nature, mining engineers may encounter with such challenging materials during surface or underground mining projects. For example, conglomerate in Upper Witwatersrand basin in South African gold mines (Schweitzer & Johnson, 1997), coarse-grained cemented alluvium covered the host rocks and ore minerals in Gol-e-Gohar Iron mine(Iran) (Akbarijour et al., 2005), Shale-Limestone Chaotic Complex bimrock (SLCC) at the Santa Barbara disused open-pit mine (Italy) (Coli et al., 2011), soft conglomerates and claystones of Newcastle coalfiled (Australia) (Hutton, 2009) are some of bimrocks reported in mining activities. In artificial forms of bimrocks in mining projects, Cemented paste backfill is an illustrative example that increasingly used around the world as a structural component of

underground mine excavations. This artificial bimrocks is a mixture of total mill tailings generated during mineral processing, Portland cement or blended cement with supplementary cementitious material, and water (Hustrulid & Bolluck, 2001; Benzaazoua & Belem, 2008).

When dealing with bimrocks in mining engineering from geomechanic point of view, it is essential to understand their representative mechanical properties, in order that safe and economic mining operations can be achieved. In the mining activities especially underground mining, the stability control of surrounding rock mass is an important issue, which must be considered. The complete stress-strain curve of an intact rock specimen, whether tested in uniaxial compression or in a confined state, is useful in understanding the total process of specimen deformation, including pre and post-peak regions, can provide insight into potential in situ rock mass behavior (Fairhaust & Hudson, 2000).

The post-peak mechanical characteristic of rock mass plays a leading role in stability control of surrounding rock mass in engineering structures. For example in design of excavation in rocks, the information on the shape of the post-peak region of rock samples is an essential parameters in designing excavation in a rock mass (Fig. 1). Once the excavation area is completed, most of the rock material surrounding it is in pre-failure zone. To avoid failure the loading must be within the pre-peak region.

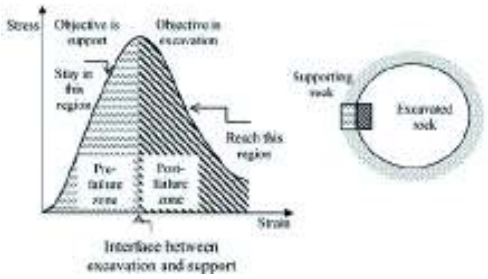

Figure 1. Relationship of complete stress-strain curve on rock excavation work (after Hudson, 1989)

Therefore, knowledge on the post failure phase would also help reducing any potential hazards that contribute to the economic advantages of construction (Abdullah & Amin, 2008). In regard to studying post-peak mechanical behavior of rocks, a lot of research has been carried out from different aspects of engineering practices (Hudson et al., 1972; Hallbauer et al., 1973; Chu et al., 1996; Xiurun, 1997; Hoek & Brown, 1997; Sterpi, 2000; Zhou, 2005; Liang et al. 2007, and Kumar et al. 2010). About bimrocks, there are few relevant studies in the literature. Many researchers (Medley, 1994, 2001, 2002; Medley & Goodman, 1994; Lindquist, 1994; Sonmez et al., 2004, 2006; Kahraman & Alber, 2006, 2008) have investigated the properties of different bimrocks. However, none of these studies specially investigated the post-peak behavior of bimrocks.

In this paper, to properly interpret the complete stress-strain behavior of bimrocks, especially with high rock block contents under uniaxial compression loading conditions, model bimrocks with rock block proportions more than 70 percent were fabricated. In more details, model bimrocks were fabricated for three high content of rock blocks including around 70, 80 and 90 percent. Uniaxial compression test on two sizes of cylindrical specimens were conducted. In the following, we first explain a little about common post failure response of rocks. After that, the experimental procedure including specimens preparation and testing are stated. Then, the

experimental results will be analyzed and discussed in details. Finally, we conclude with remarks about potential perspective of this work.

2 POST FAILURE RESPONSE OF ROCKS

In general, there are two main types of post-peak behavior of rocks as shown in Figure 2. The concept of Class-I and Class-II post-failure behavior was originally proposed by Wawersik and Fairhurst (1970), to classify the shape of the complete stress-strain curve for a particular rock according to its strain beyond the peak strength. If the strain increases monotonically throughout the failure process, the curve is designated as Class-I, and if the curve does not monotonically increase in axial strain, the behavior is Class-II. For Class II behavior, at the peak of the curve, the specimen contains more elastic energy than is necessary to continue failure and so some energy must be withdrawn, by reducing the axial strain, to continue non-violent progressive failure. Cylindrical specimens that exhibit Class I behavior tend to be somewhat ductile in nature when loaded axially; whereas specimens that exhibit Class II behavior tend to response in a brittle fashion to axial loading (Fairhurst & Hudson, 1999). Different controlling methods are necessary when testing specimens that exhibit Class II behavior.

Figure 2. Complete stress-strain curves of rocks under uniaxial compression illustrating the two main types of failure behavior.

Figure 3 schematically gives a set of common stress-strain curves, including post-peak region, observed in laboratory test of rock and soil specimen. They are typically classified as four types, i.e. perfectly brittle-plastic (curve I), strain-softening (curve II), perfectly plastic (curve III) and strain hardening (curve IV) (Zheng et al., 2005; Wang et al., 2011).

Concerning the rock mass scale, Hoek and Brown (1997) were among the earliest authors highlighting the significance of having an estimate of post-peak rock mass behavior (Alejano et al., 2010).

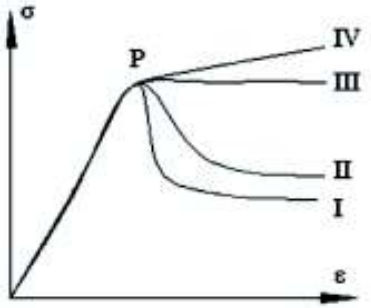

Figure 3. Stress-strain curves observed in laboratory test of rock and soil specimen focusing on post peak region (After Wang et al., 2011)

They categorized the rock mass responses according to the GSI value (Fig. 4). For massive brittle rock (70<GSI<90), Hoek and Brown (1997) reported high stress resulting in intact rock failure and practically all strength lost on failure. For heavily jointed rock (50<GSI<65), moderate stress levels result in a failure of joint systems and the rock becomes like gravel. For jointed intermediate rock (40<GSI<50), strain softening was assumed. Finally, for very weak rock (GSI<30), elastic–perfectly plastic behavior and no dilation was assumed; in other words, the failure criteria is already at the residual stage (Fig. 4). In the following the post-peak behavior of bimrocks specimens are discussed.

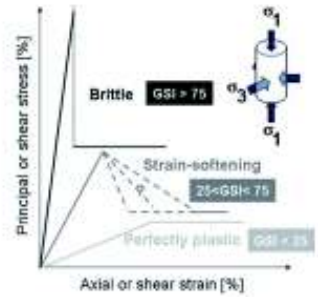

Figure 4. Different post-failure rock mass behavior modes for rock masses with different strength indexes (GSI) (Based on Hoek and Brown (1997))

3 ARTIFICIAL BIMROCKS FABRICATION AND TESTING

The main objective of this experimental study is to investigate the post-failure response of model bimrocks. In this research, three series of cylindrical specimens of sizes 150 *300 (mm) were fabricated. Artificial bimrock were prepared by mixing of rock particles and a cementing agent that in this research Portland cement was used.

For rock particles, river aggregates were chosen that the diameters range from 5 to 20 mm. The particles have a density of 2.53 gr/cm^3 with smooth surface and a good variability in spherity and almost normally distributed sizes. The compressive strength of the particles is around 25 MPa according to the correlation by point load test, so that they can break under moderate compressive loads.

For the matrix, Portland cement and water were mixed in the ratio of 0.3 (water/cement) to prepare mortar, which can be filled easily into the mold while embedding the rock blocks. Three artificial bimrock compositions were prepared with mixture ratio by weight of rock blocks range around 70, 80 and 90 percent. Three specimens of each proportion were created. The rock particles were mixed with desired amount of cement and water in a box at ambient temperature and carefully stirred manually until a homogeneous mixture was obtained. Then, the mixture was placed in the molds whose internal wall was covered by a greasy film, which had a weak adhesion with the cementing paste. The mixture compacted layer by layer in order to obtain a dense packing, which was unmolded after 24 hours. For curing the specimens, they were kept for 28 days in a wet environment at a temperature of around 25 and relative humidity of 95 percent. Three 150*300 (mm*mm) cylindrical specimens respect to their rock block proportion (RBP) by weight were fabricated, as shown in Figure 5.

The compression test was performed according to ASTM C 42(1995) which has several requirements regarding the shape of the test cylinders used for the compression test.

Figure 5. Fabricated model bimrocks with three different rock block proportion (RBP) in cylindrical mould of size 150*300 (mm*mm)

One of the main requirements is that, the ends of the specimens are required to be within 0.5 degree of perpendicular to the axis, and must be plane. Because of the high proportion of rock blocks in the model bimrocks, none of them met this requirement. Therefore capping the ends of the specimens is required. The cylinder specimens were capped at both ends with a gypsum capping compound following ASTM C617 (1995).

The servo-hydraulic testing machine frame used to perform uniaxial compression test, are shown in Figure 6. All the compression tests were carried out under displacement control at a rate of 0.03 mm/sec. In each test,

the loading was continued until full failure of the specimen occurs.

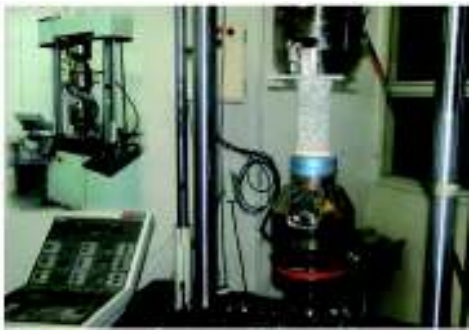

Figure 6. Servo hydraulic 8502 Instron instrument for compression testing containing model bimrocks

In the following section, we present and discus our main experimental results by focusing on the post-peak behavior of bimrocks as a function of high rock block proportions under uniaxial compression loading.

4 EXPERIMENTAL RESULTS

In Figure 7, a series of failed specimens with different RBP are illustrated. According to the figure, localized shear failure with tortuous shape were dominant failure modes for these specimens.

Complete stress-strain curves of two series of cylindrical samples are shown in Figure 8. Post peak behavior in all the uniaxial specimens was observed as strain softening and ductile.

Generally, softening is associated with a zone of localized microcracks that coalesece and propagate to form a fracture or shear band, depending upon loading condition.

Figure 7-A series of failed specimens with different RBP.

Inside the zone a decrease in stress is accompanies by an increase in strain, while outside the zone the strain decreases (Labuz et al., 1985; Labuz & Biolzi, 2007).

In all these curves, thickness of lines referred to the RBP of the specimen (Fig. 8). In pre-peak region, for all curves, the trend is more or less identical. In pre-peak region, first part is characterized by a non-linear concave upward section that is due to the porous texture of specimens and closure of voids and pre-existing fissures in the specimens. After this part an approximately linear part, exist that followed by a non-linear part up to the peak strength point. Of course, for the specimens a unique and sharp strength peak point could not considered. It may be due to the localized failure and rock block movement that lead to interlock with surrounding blocks.

The deformation patterns observed in the post-failure region can be broadly categorized in to three types. Of course, as a general result, increasing the RBP in the specimens change the deformation in post peak from “an approximate steep drop in stress” to “low decrease of strength with strain increment”.

1) 70 %RBP Specimen. After the peak stress, the stress drops steeply with continued deformation. The load bearing capacity of rock decreases very fast with a very small amount of deformation.

2) 80 % RBP Specimen. For this specimen, the stress drop rate decrease respect to the 70 RBP specimens and has a gentler trend.

3) 90% RBP specimen. In the post-peak region, the stress decreased gradually with significant deformation.

According to Figure 8, deformation modulus for the specimens has a special tread. Considering the tangent modulus (TM) for each stress point of the curves, for the first part, concave upward, the TM value increased gradually to reach a constant amount corresponding to the equivalent elastic modulus. After that, with strain increment, TM decreased gradually to zero at the peak zone.

Further, the modulus in the post peak zone is very important especially in both long wall mining and design of mine pillars (Bieniawski, 1984). In all these curves, the dotted line at the post-peak region shows the approximate slope of post-peak deformation (equivalent to the deformation modulus in post-peak region).

According to the figure 8, the negative slope of the stress-strain curves in post-peak part decreases with an increase in RBP of the specimens. For some specimens in post-peak region of stress-strain curves, the deformation changes locally from softening to hardening.

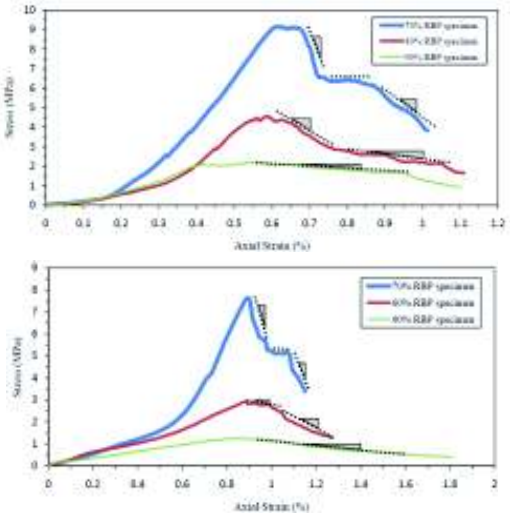

Figure 8- Two series of complete stress-strain curve for 150*300 (mm*mm) cylindrical specimen of artificial bimrocks with three high different RBP.

However, the dominant trend is softening for post-peak deformation. These locally hardening parts may be due to secondary interlocking during bond degradation between rock blocks and their resultant displacement.

The Class-II failure as reported in the literature was not observed in the specimens. Based on the study it is inferred that all the artificial specimens undergo post-failure deformation and the type of post behavior depends on specimens' RBP value.

5 CONCLUSION

Based on the laboratory tests on artificial bimrocks specimens with high RBP using a servo-controlled machine, stress-strain curves of bimrocks specially post peak behavior were investigated considering different RBP. Obviously, the stress-strain relation and deformation characteristic in post-peak region depend strongly on the RBP of the specimens. The specimen with the higher RBP has a gentler post-peak behavior. However, for the specimen with lower RBP the shape tends to become sharper.

REFERENCES

Abdullah, R.A., Amin, M.F.M., 2008. Verification of post failure behavior of rock using closed-circuit servo-controlled testing machine. *Geological Society of Malaysia, Bulletin* 54, PP 1-4.

Afifipour M, Moarefvand P., 2012. Numerical evaluation of failure pattern in stiff rock-soil mix media. *Eurock 2012*, Stockholm, Sweden.

Akbarijour, H., Rafizadeh, A., Najafabadi, M., Askari, A., Mansourpanahi, A.M. 2005. Slope stability analysis of Gol-e-Gohar iron ore mine area 3. *Iranian Mining Engineering Conference*, Tehran, Iran.

Alejano, L.R., Alonso, E., Rodrigues-Dono, A., Fernandez-Manin, G. 2010. Application of the convergence-confinement method to tunnels in rock masses exhibiting Hoek–Brown strain-softening behavior. *Int J Rock Mech Min Sci*. 47: 150-160.

American Society for Testing and Materials, ASTM C 617-94, 1995. Standard test method for capping cylindrical concrete specimens, Annual Book of

ASTM Standards 04.02, American Society for Testing and Materials, Philadelphia, PA, pp. 300-303.

American Society for Testing and Materials, ASTM C42-94(1995) Standard test method for compressive strength of cylindrical concrete specimens, Annual Book of ASTM Standards 04.02, American Society for Testing and Materials, Philadelphia, PA, pp. 24-27.

Benzaazoua, M., Fall, M., Belen, T., 2004. A contribution to understanding the hardening process of cemented pastefill. *Minerals Engineering*, Vol. 17, pp 141-152.

Bieniawski, Z.T., 1984. *Rock Mechanics Design in Mining and Tunneling.* A.A. Balkema Publications, Rotterdam, p. 271.

Chu J, Lo S.C.R.,Lee I.K., 1996. Strain softening and shear band formation of sand in multiaxial testing.*Geotechnique*;46(1):63–82.

Coli, N., Berry, D., Boldini, D., 2011. In situ non-conventional shear tests for the mechanical characterization of a bimrock. *Int J Rock Mech Min Sci*. Vol.48, pp 95-102.

Fairharst, C.E., Hudson, J.A., 1999. Draft ISRM suggested method for the complete stress-strain curve for intact rock in uniaxial compression. *Int J Rock Mech Min Sci*. Vol.36, pp 279-289.

Hallbauer D.K. ,Wagner, H, Cook, N.G.W. 1973. Some observations concerning the microscopic and mechanical behavior of quartzite specimens in stiff, triaxial compression tests. *Int J Rock Mech Min Sci. Geomech.Abst*.;10:713–26.

Hoek E, Brown E.T. 1997.Practical estimates of rock mass strength. *Int J Rock Mech Min Sci*; 34:1165–86.

Hudson J.A., Crouch S.L. ,Fairhurst C. 1972. Review-soft, stiff and servo-controlled testing machine: a review with reference to rock failure. *Engineering Geology*,;6: 155–89.

Hudson, J.A., 1989. *Rock mechanics principles in engineering practice*. London, Butterworths, 67p.

Hustrulid, W.A., Bullock R.L., 2001. *Underground Mining Methods: Engineering Fundamentals and International Case studies.* Society for Mining, Metallurgy, and Exploration, Inc. (SME), 8307 Shaffer Parkway Littleton, Colorado, USA.

Hutton, A.C.(2009). Geological setting of Australasian coal deposits. In R. Kininmonth & E. Baafi (Eds.), Australasian Coal Mining Practice (pp. 40-84). 15-31 Pelham Street, Carlton Victoria 3053: The Australasian Institute of Mining and Metallurgy.

Kahraman, S. and Alber, M. (2006). Estimating the unconfined compressive strength and elastic modulus of a fault breccia mixture of weak rocks and strong matrix, *Int. J. Rock Mech. Min. Sci*., 43, 1277-1287.

Kahraman, S., Alber, M., Fener, M. and Gunaydin, O. (2008). Evaluating the geomechanical properties of Misis Fault Breccia (Turkey) *Int. J. Rock Mech. Min. Sci*. 45, 1469-1479.

Kumar, R., Sharma, K.G., Varadarajan, A., 2010. Post-peak response of some metamorphic rocks of India under high confining pressures. *Int J Rock Mech Min Sci* ;44:400–11.

Labuz JF, Shah SP,Dowding CH. , (1985). Experimental analysis of crack propagation in granite. *Int J Rock Mech Min Sci Geomech Abstr*.;22:85–98.

Labuz, J.F. Biolzi, L., 2007. Experiments with rock: Remarks on strength and stability issues". *Int J Rock Mech Min Sci.* 44: 525-537.

Liang W., Yang C, ZhaoY. Dusseault MB,Liu J. , 2007. Experimental investigation of mechanical properties of bedded salt rock. *Int J Rock Mech Min Sci* ;44:400–11.

Lindquist ES (1994) The strength and deformation properties of mélange. PhD thesis, University of California at Berkeley.

Medley EW (1994) Engineering characterization of mélanges and similar block-in-matrix rocks. PhD thesis, University of California at Berkeley.

Medley EW, Goodman RE (1994) Estimating the block volumetric proportions of melanges and similar block-in-matrix rocks (bimrocks). In: Nelson PP, Laubach SE (eds) *Proceedings of the 1st North American rock mechanics symposium*. Balkema, Rotterdam, pp 851–858.

Medley EW (2001) Orderly characterization of chaotic Franciscan Mélanges. F*elsbau Rock Soil Eng* 19:20–33

Medley EW (2002) Estimating block size distribution of mélanges and similar block-in-matrix rocks (bimrocks). In: Hammah R, Bawden W, Curran J, Telesnicki M (eds) *Proceedings of the 5th North American rock mechanics symposium*. University of Toronto Press, Toronto, Canada, pp 509–516.

Schweitzer, J.K., Johnson R.A., 1997. Geotechnical classification of deep and ultra-deep Witwatersrand mining areas, South Africa. Miner. Dep. 32:335-348.

Sonmez, H., Tuncay, E. & Gokceoglu, C. 2004. Models to predict the uniaxial compressive strength and the modulus of elasticity for Ankara agglomerate. *Int J Rock Mech Min Sci*, 41: 717-729.

Sonmez, H. Gokceoglu C., Medley E.W., Tuncay E., Nefeslioglu H.A. 2006. Estimating the uniaxial compressive strength of a volcanic bimrock. *Int J Rock Mech Min Sci* 41: 554-561.

Sterpi D. 2000. Influence of kinematic testing conditions on the mechanical response of a sand. *Computers and Geotechnics*, Vol. 26: 23–41.

Wang, Sh., Zheng, H., Li, Ch. Ge, X. 2011. A finite element implementation of strain-softening rock mass. *Int J Rock Mech Min Sci*. 49: 67-76.

Wawersik W, Fairhurst C. 1997. A study of brittle rock fracture in laboratory compression experiments. *Int J Rock Mech Min Sci*;7:561–75.

Xiurun G. (1997). Post failure behavior and a brittle plastic model of brittle rock. In: Yuan JX, editor. *Proceedings of the ninth international conference on computer methods and advanced geomechanics*, Wuhan,China.

Xu WJ, Yue ZQ, Hu RL (2008) Study on the mesostructure and mesomechanical characteristics of the soil-rock mixture using digital image processing based finite element methods. *Int J Rock Mech Min Sci*, vol. 45, 749, 762.

Zheng H,Liu D.F,Lee C.F. ,Ge X.R 2005. Principle of analysis of brittle-plastic rock mass. *Int J Solids Struct*; Vol: 42, PP 139–58.

Zhou X.P. 2005. Localization of deformation and stress–strain relation for meso- scopic heterogeneous brittle rock materials under unloading.*Theor Appl Fract Mech*; vol. 44:27–43.

Mixed Mode I/II Stress Intensity Factors through the Thickness of Disc Type Specimens

A. A. Abd-Elhady
Mechanical Department, Faculty of Engineering, Jazan University, Jazan 706, Saudi Arabia; on sabbatical leave from Mechanical Design Department, Faculty of Engineering, Helwan University, Cairo 11718, Egypt

ABSTRACT Mode I and mode II stress intensity factors (SIFs) through the thickness of edge crack in semi circular bend (SCB) and center cracked circular disc (CCCD) specimens have been analyzed using three dimensional finite element analysis. The effect of the CCCD and SCB specimen thickness on the through-thickness variations of SIFs has been studied. For all mode of mixity, the peak value of mode I SIF is found at mid plane of SCB specimen and for thin CCCD specimen, while, this location is shifted to be near the free surface plane in thick CCCD specimen. The variation of mode II SIF in CCCD and SCB specimens has a similar trend.

Keywords: Stress intensity factor; Mixed mode I/II; SCB specimen; CCCD specimen; three dimension finite element.

1 INTRODUCTION

Cracks experience a combination of two major modes of loading: mode I and mode II due to arbitrary orientation of flaws relative to the overall applied loads. Two frequently employed disc type specimens are the centre cracked circular disc (CCCD), subjected to diametral compression, often called the Brazilian disc, and the edge cracked semi circular bend (SCB) specimen subjected to three-point bend loading. The major advantages in using these two specimens are that specimens can be easily extracted from the cores of rocks materials; they have a simple geometry and simple loading configuration. In addition, the test procedure is straightforward, there are few machining operations and different mode of mixities may be introduced from pure mode I to pure mode II. Hence these test specimens have been used frequently to investigate mixed mode crack growth of rock materials, concrete, biomaterials, and other material (Sallam, and Abd-Elhady, 2012), (Chen, et al. 1998), (Ouinas, et al. 2009). Ayatollahi and Aliha (Ayatollahi, and Aliha, 2008) depicted that the normalized mode I and mode II stress intensity factor are functions of the crack length ratio *a/R* and crack angle β only for CCCD specimen and crack length ratio *a/R*, crack angle β and *S/R* for SCB specimen as shown in Figure 1.

The stress state near an actual crack tip is always three-dimensional and can significantly influence crack growth. Hutar et al. (Hutar et al. 2010) show that, the stress singularity exponent is not constant along the crack front and the stress field around the crack tip is usually based on stress intensity factors. Garcia-Manrique et al. (Garcia-Manrique et al. 2013) use Al 2024-T35 compact tension specimen under mode I nominal loading to evaluate the SIFs distribution along the thickness. They concluded that, a smaller SIFs value is present near the surface than in the interior causing a smaller plastic zone than the expected value with plane stress condition. Kwon and Sun (Kwon and Sun, 2000) concluded that, except for plates with very large thicknesses, the 2-D SIFs is quite different from the 3-D SIFs at the mid-plane. Furthermore, the profile of stress intensity along the thickness direction is still in question. Kown and Sun (Kwon and Sun,

2000) stated that, SIFs should drop to zero at the plate free surface due to the weaker singularity than square root, but this is difficult to obtain by the finite element method

Accurate stress analyses of these through-cracks components are needed for reliable prediction of their crack-growth and fracture strengths. However, because of the complexities of such problems, exact solutions are not available. To the best knowledge of the author, SIFs through the thickness of edge crack in SCB and CCCD specimens is still not fully studied. Therefore, this paper concentrated on computation the SIFs through the thickness of CCCD and of SCB specimens for different specimen thicknesses and mode of mixities using 3D FEA.

2 FINITE ELEMENT ANALYSIS

Figure 1 shows the geometry and loading condition of the CCCD and SCB specimens used for mixed mode I/II fracture tests.

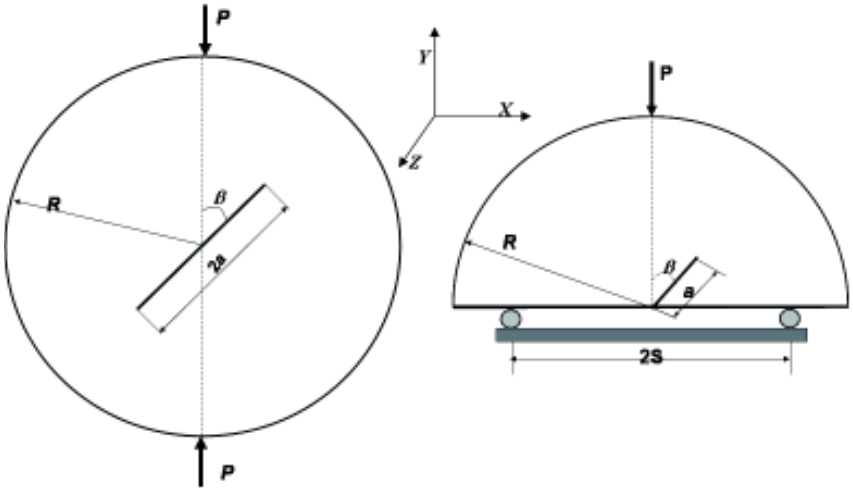

Figure 1. Geometry and loading conditions of CCCD and SCB specimens subjected to mixed mode I/II loading

In the CCCD specimen, the orientation of the centre crack of length 2*a* relative to the applied load *P* is defined by the angle β and varies the state of crack deformation, giving different combinations of modes I and II. Similarly for the SCB specimen, by changing the inclination angle β of the edge crack of length *a* with respect to the applied load *P*, various mode of mixities can be achieved. For both specimen shapes, $\beta = 0^o$ corresponds to pure mode I (opening mode) loading. By increasing the loading angle □ from zero, mode II is introduced.

To study the effect of mode of mixity and the effect of specimen thickness, *B*, on through-thickness stress intensity factor, several CCCD and SCB specimens with different crack angles were simulated. The geometry and dimensions of the CCCD and SCB specimens are listed in Table 1. For the sake of comparison, the basic dimensions of CCCD and SCB specimens *R* (specimen radius), 2*t* or *B* (specimen thickness), and *a* were considered to be the same for each two corresponding specimen sizes (see Table 1). SCB specimen is placed on two bottom supports of distance 2*S*. Thus, the ratio of *a/R* was equal to 0.3 and the ratio of *S/R* was 0.43 in the SCB specimens. Mixity parameter, M^e, is defined as (Aliha et al. 2008):

$$M^e = \frac{2}{\pi}\arctan\left(\frac{K_I}{K_{II}}\right) \quad (1)$$

Where K_I and K_{II} are mode I and mode II stress intensity factors, respectively. In the present analysis, the values of M^e varied through 1 (pure mode I), 0.75, 0.5, 0.25 and 0 for pure mode II.

The general-purpose finite element program ABAQUS was used (ABAQUS, 2002). A three-dimensional finite element model has been developed to account for geometric and material behavior of isotropic material. In the present work the domain integral method used to extract stress intensity factors (SIFs). The domain integral method has proven useful for both two and three-dimensional crack problems. In the domain integral method, a crack-tip contour integral is expressed as an equivalent domain/volume integral over a finite domain surrounding the crack tip. A domain integral method commonly used to extract stress intensity factors (SIFs) (Nakamura, and Parks 1989), (Nakamura, 1991), (Gosz, et al. 1998), (Gosz, and Moran, 2002). The finite element meshes constructed with hexagonal structural mesh, C3D8 (8-node linear brick) elements, are used under Standard/static analysis. Around from 32 planar layers are divided through the thickness of the specimen varying with the plate thickness. Within each layer, the size of element decreases gradually with distance from the crack tip decreasing. The finite element meshes in the neighborhood of the crack tip are much denser. The values of mode I and II stress intensity factor were traced over the crack front of the specimen from the mid plane of specimen where $z = 0$ to the specimen surface where $z = t$. In the present analysis, the mode I and mode II normalized stress intensity factors are denoted as Y_I and Y_{II}, respectively, and it can be deduced from Ref. (Hutar et al. 2010), (Lim, et al. 1993) the general formula for normalized stress intensity factor Y_i, which is defined as:

$$Y_i = \frac{4RtK_i}{P\sqrt{a\pi}} \qquad i = I, II \qquad \text{for SCB specimen} \quad (2)$$

$$Y_i = \frac{2RtK_i}{P}\sqrt{\frac{\pi}{a}} \qquad i = I, II \qquad \text{for CCCD specimen} \quad (3)$$

Where:

K_I = mode I stress intensity factor
K_{II} = mode II stress intensity factor
$t = B/2$ half specimen thickness
P = applied load
R = radius of specimen
a = crack length

The normalized mode *I* and mode *II* stress intensity factors at the midpoint of the specimen (at $z = 0$) are Y_{Imp} and Y_{IImp}, respectively, and at surface point of specimen (at $z = t$) are Y_{Isurf} and Y_{IIsurf}.

Table 1 Specimen geometries and crack inclination angles in the tested CCCD and SCB specimen

	R (mm)	$2t$ (mm) $= B$	a (mm)	β (°)				
				M^e = 1	M^e = 0.75	M^e = 0.5	M^e = 0.25	M^e = 0
CCCD	75	15	22.5	0	5	10.5	18	27
	75	30	22.5	0	5	10.5	18	27
	75	45	22.5	0	5	10.5	18	27
	75	60	22.5	0	5	10.5	18	27
SCB	75	15	22.5	0	18.5	33	42.5	50
	75	30	22.5	0	18.5	33	42.5	50
	75	45	22.5	0	18.5	33	42.5	50
	75	60	22.5	0	18.5	33	42.5	50

3 RESULTS AND DISCUSSION

To verify the accuracy of the present result for SIFs evaluation, the values of various normalized mode I and mode II stress intensity factors at the surface of CCCD and SCB specimens ($Z = t$), for R = 75 mm, B = 7.5 mm, a/R = 0.3 and S/R = 0.43 are compared with the previous numerical results using 2-D analysis found in the literature, R = 50 mm, B = 5 mm, a/R = 0.3 and S/R = 0.43, (Aliha et al. 2010), (Ayatollahi and Aliha, 2007), as shown in Figures 2 and 3. Figures 2 and 3 show a good agreement between the present results for normalized mode I and mode II stress intensity factors and those obtained by Aliha at el (Aliha et al. 2010), (Ayatollahi and Aliha, 2007). The values of normalized mode I and mode II stress intensity factors at the mid plane (at $z = 0$) and at free surface ($z = t$) of CCCD and SCB specimens are tabulated in tables 2 and 3 respectively. The value of Y_{Imp} of CCCD specimen decreases by increasing B/R, while, Y_{Isurf} increases. The value of Y_{Isurf} of SCB decreases by increasing B/R. Y_{Isurf} and Y_{Imp} of CCCD and SCB specimens decrease by decreasing the value of mixity parameter.

Figure 4 shows the variation of Y_I normalized by Y_{Imp}, Y_I/Y_{Imp}, through the crack front of CCCD and SCB specimens for different M^e and different B/R. For thin specimen, i.e. B/R = 0.2, value of Y_I/Y_{Imp} decreases gradually with increasing z/t up to z/t equals about 0.8 then the rate of decreasing change from gradually to sharply decrease for both specimens and all mode of mixities. For $B/R > 0.2$ the distribution of Y_I/Y_{Imp} is not the same for both specimens. In the case of CCCD specimen, the value of Y_I/Y_{Imp} increases gradually to its peak value Y_{Imax}, then decreases sharply up to the specimen surface, i.e. bell shape.

It is worth to note that, SIFs at the specimen surface should be equal zero, but it is difficult to get it by using FEM as mentioned by Kown and Sun (KWON, and SUN, 2000). The site of peak value of the Y_I/Y_{Imp} is near the specimen surface. The peak value of Y_I/Y_{Imp} of CCCD specimen increases by increasing B/R. This finding is in agreement with Zhixue (Zhixue, 2006).

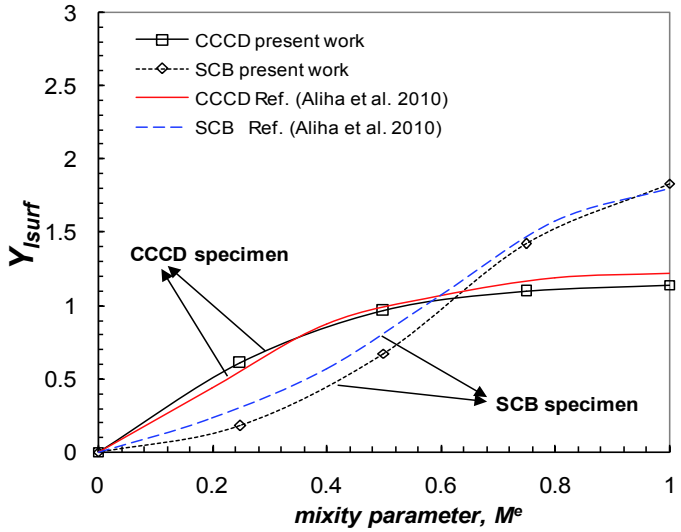

Figure 2. Comparison between the present normalized Y_I at the free surface of the specimen and those found in the literature using 2-D analysis (Aliha et al. 2010).

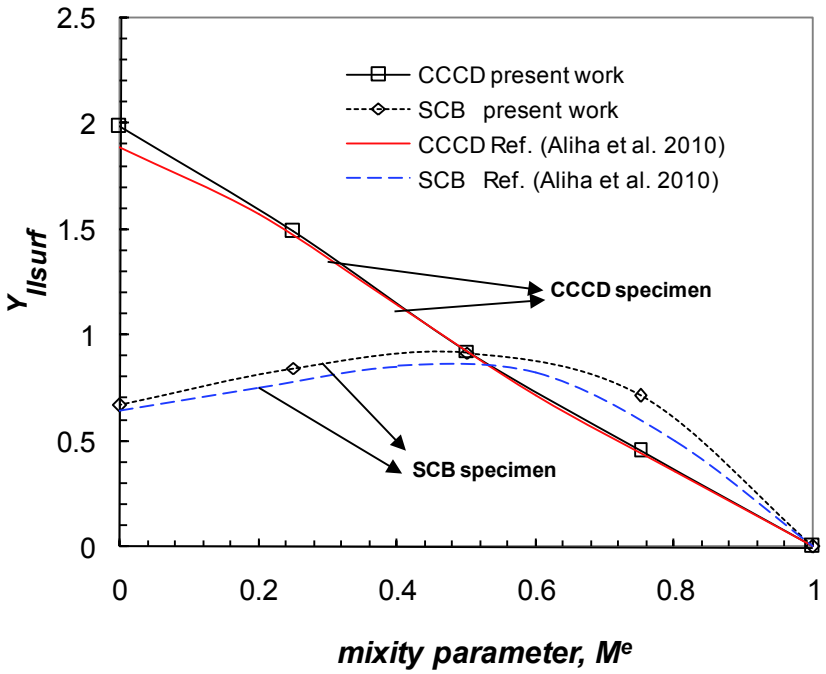

Figure 3. Comparison between the present normalized Y_{II} at the free surface of the specimen and those found in the literature using 2-D analysis (Aliha et al. 2010)

Table 2 The values of normalized mode I stress intensity factor Y_I at mid point (z/t = 0) and at surface (z/t = 1) for the CCCD and SCB specimens for different values of M^e and different specimen thickness ratios.

Specimen	B/R		$M^e = 1$	$M^e = 0.75$	$M^e = 0.5$	$M^e = 0.25$	$M^e = 0$
CCCD	0.2	Y_{Imp}	1.17474	1.12806	0.97819	0.62394	0
		Y_{Isur}	1.10662	1.05881	0.92223	0.58257	0
	0.4	Y_{Imp}	1.15584	1.10799	0.96398	0.60951	0
		Y_{Isur}	1.12696	1.07748	0.93850	0.58931	0
	0.6	Y_{Imp}	1.13433	1.08638	0.95097	0.60126	0
		Y_{Isur}	1.14119	1.09197	0.96065	0.60402	0
	0.8	Y_{Imp}	1.10684	1.06073	0.92154	0.57824	0
		Y_{Isur}	1.18888	1.13710	0.99391	0.63199	0
SCB	0.2	Y_{Imp}	2.09601	1.65985	0.85306	0.32454	0
		Y_{Isur}	1.83337	1.42287	0.67280	0.17889	0
	0.4	Y_{Imp}	2.10187	1.67603	0.87104	0.35329	0
		Y_{Isur}	1.77569	1.36208	0.60562	0.12369	0
	0.6	Y_{Imp}	2.10794	1.65012	0.86398	0.33354	0
		Y_{Isur}	1.73930	1.29862	0.55021	0.07408	0
	0.8	Y_{Imp}	2.07458	1.64056	0.82505	0.31634	0
		Y_{Isur}	1.71102	1.28638	0.51505	0.05856	0

Table 3. The values of normalized mode II stress intensity factor Y_{II} at mid point (z/t = 0) and at surface (z/t = 1) for the CCCD and SCB specimens for different values of M^e and different specimen thickness ratios.

Specimen	B/R		$M^e = 1$	$M^e = 0.75$	$M^e = 0.5$	$M^e = 0.25$	$M^e = 0$
CCCD	0.2	Y_{IImp}	0	0.4295	0.8890	1.4035	1.8699
		Y_{IIsur}	0	0.4470	0.9262	1.4643	1.9630
	0.4	Y_{IImp}	0	0.4304	0.8826	1.4140	1.8711
		Y_{IIsur}	0	0.4463	0.9143	1.4656	1.9421
	0.6	Y_{IImp}	0	0.4268	0.8765	1.4049	1.8713
		Y_{IIsur}	0	0.4529	0.9294	1.4916	1.9859
	0.8	Y_{IImp}	0	0.4250	0.8719	1.3979	1.8505
		Y_{IIsur}	0	0.4511	0.9242	1.4807	1.9594
SCB	0.2	Y_{IImp}	0	0.6592	0.8604	0.7937	0.6118
		Y_{IIsur}	0	0.6865	0.9090	0.8299	0.6318
	0.4	Y_{IImp}	0	0.6676	0.8601	0.7753	0.6131
		Y_{IIsur}	0	0.7012	0.9055	0.8150	0.6446
	0.6	Y_{IImp}	0	0.6728	0.8611	0.7889	0.6164
		Y_{IIsur}	0	0.7139	0.9191	0.8470	0.6686
	0.8	Y_{IImp}	0	0.6527	0.8578	0.7796	0.6142
		Y_{IIsur}	0	0.7051	0.9282	0.8502	0.6753

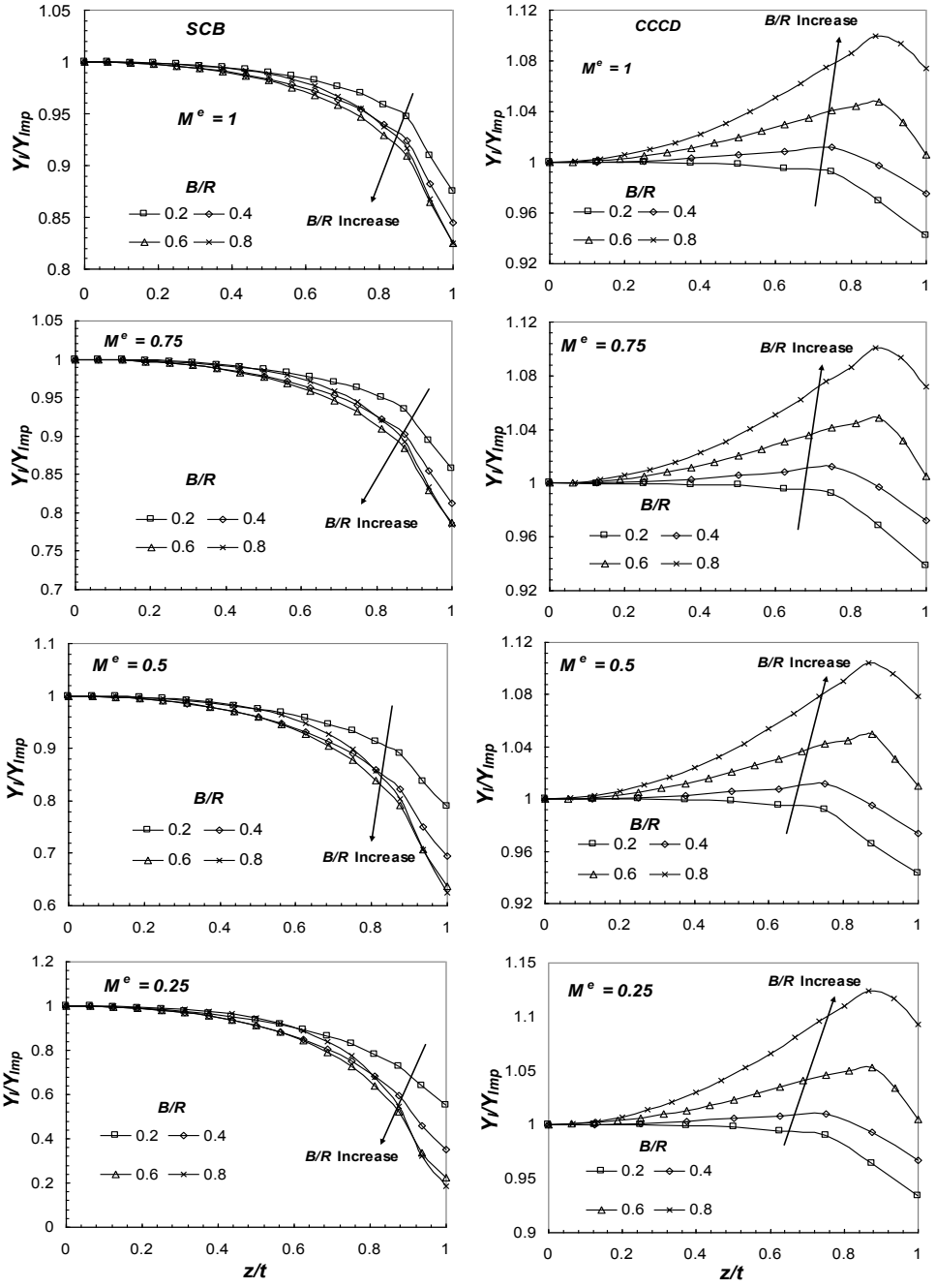

(a)SCB specimen (b) CCCD specimen

Figure 4 The through-thickness distributions of the normalized mode I stress intensity factor along crack front of (a) CCCD and (b) SCB specimens, for different M^e .

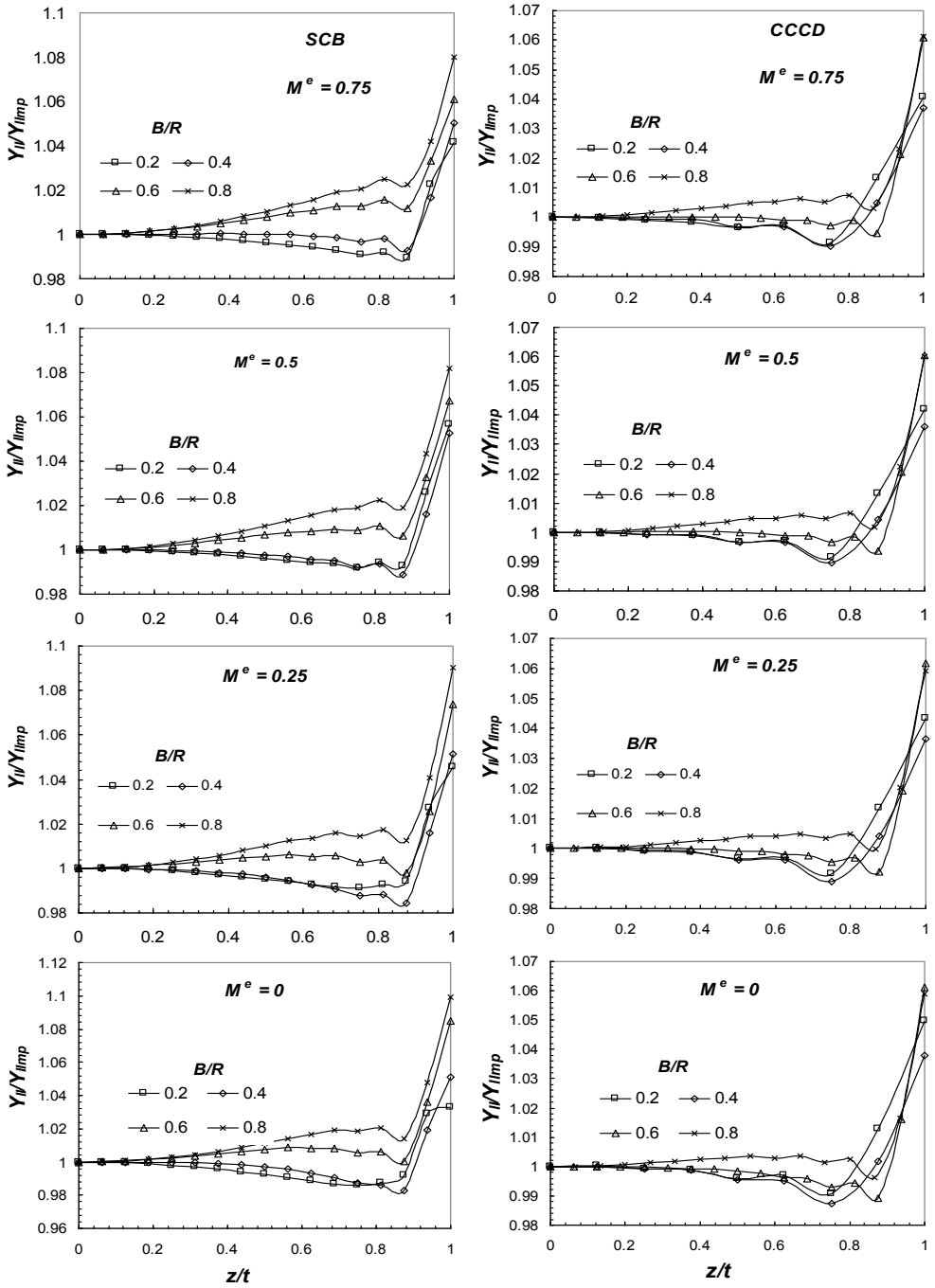

(a) SCB specimen (b) CCCD specimen

Figure 5 The through-thickness distributions of the normalized mode II stress intensity facto along crack front of (a) CCCD and (b) SCB specimens, for different M^e

However, in the case of SCB specimen the shape of Y_I/Y_{Imp}–z/t curve is not affected by B/R or mode of mixity, i.e. the peak value of Y_I/Y_{Imp} is at the mid plane. This peak value of Y_I/Y_{Imp} decreased by increasing *B/R*, i.e. opposite trend of CCCD specimen with B/R > 0.2. Therefore it can be concluded that, the shape of Y_I/Y_{Imp}–z/t curve is similar for all mode of mixities and B/R for SCB specimen and the peak value is found at the mid plane. In the case of CCCD specimen, the shape of Y_I/Y_{Imp}–z/t curve depends on the specimen thickness. For thin specimen (B/R= 0.2), the shape is similar to that in SCB specimen, while, the bell shape is found for B/R > 0.2 and the peak value is near the specimen surface. In these cases, the normalized mode I stress intensity factor is not only function of *a/R*, as concluded by Aliha and Ayatollahi (Ayatollahi, Aliha, 2008) but also function of *z/t.*

Figure 5 depicted the through-thickness variation of Y_{II}/Y_{IImp} along the crack front of CCCD and SCB specimens for different M^e and *B/R*. The normalized mode II SIF through the crack front of SCB specimen has the similar trend from it exited in CCCD specimen as shown in the figure. For both specimens, the variation of Y_{II}/Y_{IImp} through the specimen thickness is small and not exceed 10%. The maximum value of Y_{II} for both specimens located at the specimen surface.

4 CONCLUSIONS

The 3D FEA of mode I and mode II SIF through the crack front in SCB and CCCD specimens reveals the following conclusions:

1- The normalized mode I stress intensity factor (Y_I/Y_{Imp}) is not only function of *a/R*, but also function of *z/t*.
2- The shape of Y_I/Y_{Imp}–z/t curve is similar for all mode of mixities and B/R for SCB specimen and the peak value is found at the mid plane.
3- In the case of CCCD specimen, the shape of Y_I/Y_{Imp}–z/t curve depends on the specimen thickness. For thin specimen (B/R= 0.2), the shape is similar to that in SCB specimen, while, the bell shape is found for B/R > 0.2 and the peak value is near the specimen surface.
4- For both specimens, the maximum value of normalized mode II stress intensity factor located at the specimen surface.

5 REFERENCES

Sallam, H.E.M. and Abd-Elhady, A.A. 2012. Mixed Mode Crack Initiation and Growth in Notched Semi-Circular Specimens-Three Dimensional Finite Element Analysis, Asian Journal of Material Science, 4(2), 34-44.

Chen, C.S., Pan, E. and Amadei, B. 1998. Fracture mechanics analysis of cracked discs of anisotropic rock using the boundary element method, Int J Rock Mech Min Sci; 35(2): 195–218.

Ouinas, D., Bachir Bouiadjra, B. Serier, B. Benderdouche, N. and Ouinas, A. 2009. Numerical analysis of Brazilian bioceramic discs under diametrical compression loading, Computational Mat. Sci., 45: 443–448.

Ayatollahi, M.R., Aliha, M.R.M. 2008. On the use of Brazilian disc specimen for calculating mixed mode I–II fracture toughness of rock materials, Eng. Fract. Mech., 75, 4631–4641.

Hutar, P., Nahlik, L., Knesl, Z., 2010. The effect of a free surface on fatigue crack behaviour", International Journal of Fatigue, 32; 1265–1269.

Garcia-Manrique, J., Camas, D., Lopez-Crespo, P., Gonzalez-Herrera, A., 2013. Stress intensity factor analysis of through thickness effects, International Journal of Fatigue, 46; 58-66.

KWON, S.W. and SUN, C.T., 2000. Characteristics of three-dimensional stress fields in plates with a through-the-thickness crack, International Journal of Fracture, 104: 291–315.

Aliha, M.R.M., Ayatollahi,M.R., Smith,D.J., Pavier, M.J., 2010. Geometry and size effects on fracture trajectory in a limestone rock under mixed mode loading, Eng. Fract. Mech., 77: 2200–2212.

ABAQUS, 2002., user's manual version 6.9. Pawtucket, RI: Hibbitt, Karlsson and Sorensen Inc.

Nakamura, T., and Parks, D.M., 1989. Antisymmetrical 3-D stress field near the crack

front of a thin elastic plate, International Journal of Solids and Structures, 25: 1411-26.
Nakamura, T. 1991. Three-dimensional stress fields of elastic interface cracks, Journal of Applied Mechanics, 58: 939-46.
Gosz, M., Dolbow J., Moran, B., 1998. Domain integral formulation for stress intensity factor computation along curved three-dimensional interface cracks, International Journal of Solids and Structures, 35: 1763-83.
Gosz, M. and Moran B., 2002. An interaction energy integral method for the computation of mixed-mode stress intensity factors along non-planar crack fronts in three dimensions, Eng. Fract. Mech., 69: 299-319.
Lim, I. L., Johnston, I. W., Choi, S. K., 1993. Stress intensity factors for semi-circular Specimens under three-point bending, Eng. Fract. Mech., 44, 3, 363-382.
Ayatollahi, M.R., Aliha, M.R.M., 2007. Wide range data for crack tip parameters in two disc-type specimens under mixed mode loading, Comput Mater Sci, 38(4):660–70.
Zhixue, Wu, 2006. On the through-thickness crack with a curve front in center-cracked tension specimens", Eng. Fract. Mech., 73: 2600–2613.

Kayaçların Delinebilirlik ve Aşındırıcılık Özelliklerinin Karşılaştırılması

Comparison of Drillability and Abrasivity Properties of Rocks

M. Çapik, A. O. Yılmaz, S. Yaşar
Karadeniz Teknik Üniversitesi, Mühendislik Fakültesi, Maden Mühendisliği Bölümü, Trabzon

O. Yaralı
Bülent Ecevit Üniversitesi, Mühendislik Fakültesi, Maden Mühendisliği Bölümü, Zonguldak

İ. Çavuşoğlu
Gümüşhane Üniversitesi, Maden Mühendisliği Bölümü, Gümüşhane

ÖZET Delinebilirlik, bir delici matkabın kayaç içinde ilerleme yapabilme oranı olarak tanımlanmaktadır. Aşınma ise kazı sırasında keskilerin kayaçlar tarafından koparılmasıdır. Farklı formasyonların sahip olduğu, farklı aşındırıcılık ve sertlik özellikleri mekanize kazı sistemlerinde kazılabilirlik ve delinebilirliği önemli oranda etkilemektedir. Çünkü aşındırıcı ve sert kayaçlar, kısa zamanda keskilerin körelmesi nedeniyle ilerleme oranın düşmesine ve kazı maliyetinin artmasına yol açmaktadır.

Bu çalışma Hopa-Borçka (Artvin) Cankurtaran Karayolu Tünelinde gerçekleştirilmiştir. Laboratuvar çalışmaları için Cankurtaran tünelinde farklı kayaç formasyonlarından örnekler alınmıştır. Uygun boyutlarda ve miktarda deney örnekleri hazırlanmıştır. Kayaçların delinebilirlik özelliğini belirlemek için kırılganlık ve Sievers minyatür delme deneyleri gerçekleştirilmiştir. Kayaçların aşındırıcılık özelliğini belirlemek için Cerchar Aşınma İndeksi (CAI), Norveç Aşınma deneyi (AV), Böhme aşınma Deneyleri gerçekleştirilmiştir. Ayrıca kayaçların mekanik özelliği belirlemek için tek eksenli basınç dayanımı, nokta yük dayanımı ve Brazilian dolaylı çekme dayanımı deneyleri gerçekleştirilmiştir.

ABSTRACT Drillability is defined as the penetration rate of a drill bit into the rock. Abrasion is broken off by the tools during the excavation of rocks. Different types of rock formations have different abrasiveness and hardness properties and that is significantly affected excavatability and drillability in the mechanical excavation systems. Because, abrasive rocks and hard rocks lead to an increase of the cost excavation, decrease of the penetration rate and atrophy of the cutter in a short time.

This study was carried out in Hopa-Borcka (Artvin) Cankurtaran Highway Tunnel. Rock samples were obtained from Cankurtaran Tunnel at the changing rock formations for the laboratory studies. The test samples were prepared at the appropriate size and quantity. Sievers J-miniature drill test (SJ) and the brittleness tests were carried out and for the drilling rate index values were calculated. Cerchar Abrasivity Index (CAI), Norway Abrasion Value (AV) and Bohme abrasion tests were carried out and for abrasiveness of rock properties. Uniaxial compressive strength, point load strength and Brazilian tensile strength tests were determined for the calculations mechanical properties of rock.

1 GİRİŞ

Geçmişten günümüze yeraltında ve yerüstünde yapılan kazılarda, gerek madencilik alanında gerekse inşaat alanında değişik metotlar uygulanmıştır. Ülkemizde özellikle son yıllarda teknolojinin gelişimiyle birlikte mekanize kazı yöntemleri tünel metro, ve madencilik sektöründe yaygın

olarak kullanılmaya başlanmıştır. Bunların yanında su tünelleri, demiryolu tünelleri, karayolu tünelleri, sığınak ve depolama projelerinde de mekanize kazı yöntemleri yaygın olarak kullanılmaya başlanmıştır.

Doğu Karadeniz Bölgesinde HES (Hidroelektrik Santrali) projeleri kapsamında yapılan su tünelleri, arazi şartları nedeniyle sahil yolu yapımında açılan tüneller ve iç kesimlerdeki ağır hava şartlarına bağlı olarak imal edilen tünellerin sayısı her geçen gün artmaktadır. Doğu Karadeniz Bölgesindeki bu tünellerin kazı çalışmalarında genellikle delme patlatma yöntemi kullanılmaktadır. Delme patlatma yönteminde jumbo delici makinaları kullanılmaktadır.

Bu yöntemde önemli olan kriterlerin başında, deliklerin hızlı ve ekonomik olarak delinmesi gelmektedir ki bu da işletme maliyeti açısından büyük önem taşımaktadır. İşletmenin bu kriterleri sağlaması için delinecek kayacın fiziksel-mekanik özellikleri, mineralojik ve petrografik yapısının yanında, kayacın delinebilirliği ve kazılabilirlik özelliklerinin de bilmesi gerekmektedir.

2 KAYAÇLARIN DELİNEBİLİRLİK VE AŞINDIRICILIK ÖZELLİĞİ

Kayacın delinebilirliği; bir delici matkabın kayaç içinde ilerleme yapabilme oranı olarak tanımlanmaktadır (Tamrock, 1987). Bir başka ifadeyle delinebilirlik; makinanın belli güç harcayarak dönerli veya darbeli olarak delici uçların kayaç içinde makinanın tipine, hızına, kuvvetine ve kayacın sertliğine bağlı olarak belirli bir süre içinde kayacı delerek ilerlemesidir.

Aşınma, kazı esnasında keskilerin kayaçlar tarafından koparılmasıdır. Yüksek aşındırıcı özelliğine sahip kayaçlar, kısa zamanda keskilerin körelmesine neden olabilmektedir. Bu durum, bir yandan keski tüketimini artırmakta, diğer yandan kazı verimini düşürmekte ve dolayısı ile kazı maliyetinin artmasına yol açmaktadır.

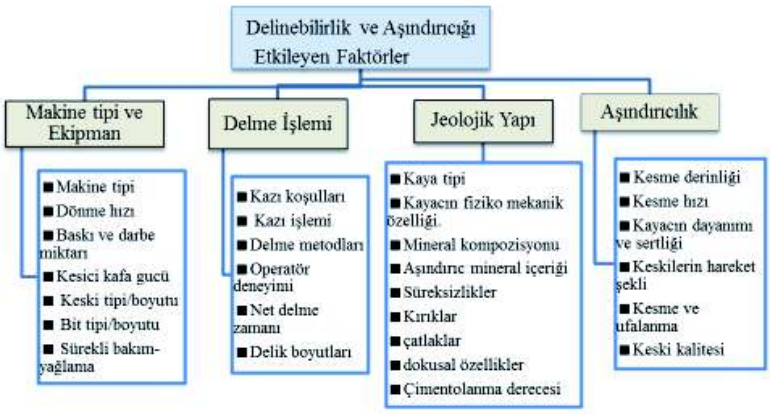

Şekil 1. Delinebilirlik ve aşındırıcığı etkileyen faktörler (Kahraman, 1999; Thuro vd, 2002)

Delinebilirlik tahmininde doğru ekipmanın seçilmesi büyük önem kazanmaktadır. Delmede kullanılacak makinenin tipi, basma gücü, matkabın darbesi ve dönme hızı, keski ve bitlerin tipi ve makinenin düzenli bakımı delinebilirlik için çok önemlidir. Delinebilirliği ve aşınmayı etkileyen pek çok faktör vardır, ancak bunların çoğu ampirik yaklaşımlara dayanmasına rağmen temel de üç faktör vardır. Bunlar; makine tipi ve ekipman delme işlemi ve jeolojik yapıya bağlı faktörlerdir. Bu faktörler kontrol edilebilen ve edilemeyenler olarak sınıflandırılabilir. Makine tipi, ekipman ve delme işlemi kontrol edilebilir parametrelerdir. Ancak jeolojik özelliklere bağlı parametreler arazi yapısıyla ilgili olduğundan kontrol edilemeyen parametrelerdir (Şek. 1). (Tamrock, 1987), (Thuro and Spaun, 1996), (Thuro, 1997a), (Thuro, 1997b), (Kahraman, 1999), (Plinninger, vd., 2002). Bu faktörler dışında delinebilirliği ve aşındırıcılığı etkileyen başka faktörlerde vardır. Başlıca faktörler

olarak Mohs sertliği, kaya dokusu ve yapısı, porozite, yoğunluk, sertlik, P-dalga hızı, elastisite ve plastisite, tek eksenli basınç dayanımı, nokta yük indeksi ve Schmidt değeri, çekme dayanımı, Cerhar aşınma indeksi, delinebilirlik indeksi, Norveç aşınma indeksi, Schimazek aşınma indeksi ve koni delici değeri sayılabilir (Jimeno, vd, 1995), (Ersoy ve Waller, 1995), (Osanloo, 1998), (Kahraman, vd., 2000), (Kahraman, vd., 2003), (Alber, 2008), (Hoseinie, vd., 2008) (Dahl, vd., 2012).

3 YAPILAN ÇALIŞMALAR

3.1 Çalışma Alanı

Çalışma alanı, Doğu Karadeniz Bölgesi ile Doğu Anadolu Bölgesini birbirine bağlayacak olan Hopa-Borçka Cankurtaran Tünelidir. Hopa-Borçka karayolu tüneli 7+980-13+208 km'leri arasında çift tüp olarak inşa edilmektedir Yapımı tamamlamasıyla birlikte 5 bin 288 metre uzunluğu ile Türkiye'nin en uzun tüneli olma özelliğini taşıyacaktır (Şekil 2). Cankurtaran tünel hattı boyunca 4 adet litolojik birim geçilmektedir. Bunlar Subaşı Sırtı Formasyonu, Cankurtaran Formasyonu, Şenkaya Sırtı Formasyonu ve Kabaköy Formasyondur.

Şekil 2. Çalışma alanına ait yer bulduru haritası (Kaya, 2012)

Subaşı Sırtı Formasyonuna ait volkano-tortul kayaçlar bu litolojik birimden oluşur. Cankurtaran formasyonuna ait marn ara katkılı kireçtaşları bu litolojik birimimde oluşur. Şenkaya Sırtı Formasyonunda yer yer kil taşı ara katkılı marnlardan oluşmaktadır. Son olarak tünelin çıkış bölümünde yer alan Kabaköy Formasyonu bazaltlardan oluşan bir litolojik birimden oluşmaktadır (Şekil 3).

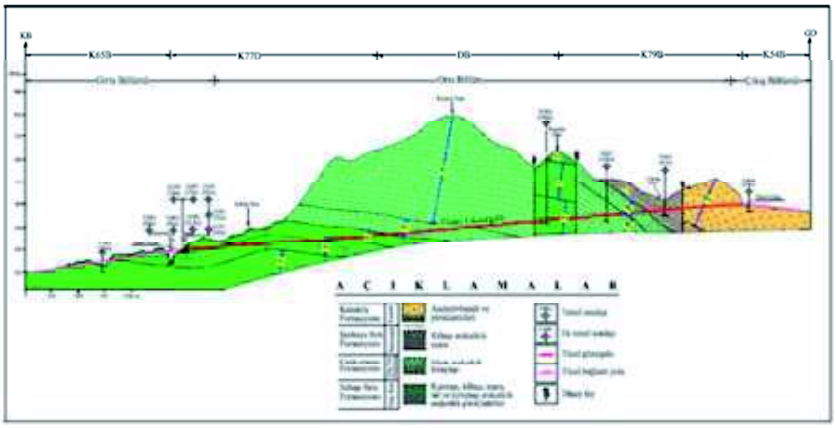

Şekil 3. Cankurtaran tünelinin jeolojik haritası (Kaya, 2012)

3.2 Materyal ve Metot

Laboratuarda yapılacak deneyler için örnekler, iki tüpten oluşan Hopa-Borçka Cankurtaran tünelinin hem giriş hem de çıkış tüplerinden belli aralıklarla ve değişen kayaç formasyonlarında sağlam, çatlaksız süreksizlik içermemesine dikkat edilen kaya bloklarından alınmıştır. Alınan bu bloklardan deney standartlarına göre uygun boyutta ve miktarda karot numunesi hazırlanmıştır. Hazırlanan karotlar üzerinde delinebilirlik deneyleri, aşınma deneyleri, dayanım ve çekme deneyleri gerçekleştirilmiştir.

Delinebilirlik ve aşınma deneylerinin bir kısmı Bülent Ecevit Üniversitesi (Zonguldak) Maden Mühendisliği Bölümü Maden Mekanizasyonu Laboratuvarı'nda gerçekleştirilmiştir. Dayanım deneyleri ve Böhme aşınma deneyi Karadeniz Teknik Üniversitesi Maden Mühendisliği Bölümü Laboratuvarı'nda gerçekleştirilmiştir.

3.2.1 Delinebilirlik Deneyleri

Delinebilirlik deneyi için (DRI) iki temel deney gerçekleştirilmiştir. Kırılganlık deneyi (brittleness test), S_{20} ve Sievers minyatür delme deneyi (Sievers miniature drill-test value), SJ dir.

Kırılganlık deneyi (brittleness test), $S_{20;}$ Darbe sonucu kayacın kırılmaya karşı gösterdiği direncin dolaylı ölçülmesini belirleyen bir deney yöntemidir (Yaralı ve Kahraman, 2011). Deney düzeneği Şekil 4'de gösterilmiştir.

Sievers Minyatür delme testi; kayacın yüzey sertliğinin veya delmeye karşı direncinin ölçülmesinde kullanılmaktadır. Sievers minyatür deney düzeneği Şekil 5'de gösterilmiştir Deney 30 mm boyunda ve 54 mm çapında kayaç numuneleri üzerinde gerçekleştirilmiştir.

Şekil 4. Kırılganlık deney düzeneği (Dahl vd, 2012)

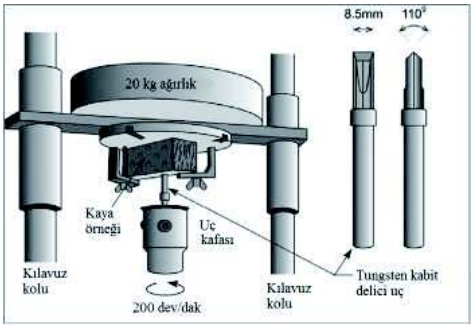

Şekil 5. Sievers minyatür delme deney düzeneği (Dahl vd., 2012)

3.2.2 Aşındırıcılık Deneyleri

Kayaçların aşındırıcılık özelliklerinin belirlenmesi için gerçekleştirilecek deneyler; Cerchar Aşınma indeksi (CAI), Norveç aşınma deneyi (AV) ve Böhme aşınma deneyi

Cerchar Aşınma indeksi (CAI), deney yöntemi keski aşınımı, keski değişim maliyeti ve kayaç dayanımı gibi önemli parametreleri doğru tahmin edilmesinden ve kayaç aşınımını belirlenmesinde yaygın kullanılan bir deney yöntemidir. Deneyde Rockwell sertliği 54/56 olan uçlar kullanılmış ve deneyler West (1986)'ya göre yapılmıştır. Deney 30 mm boyunda, 54 mm çapında örnekler üzerinde gerçekleştirilmiştir. Uçlarda oluşan aşınma 25X büyütmeli mikroskop yardımıyla üsten ve yandan ölçülmüştür. Kayaçlara ait Cerchar aşınma indeks değeri 5 çizimin

aritmetik ortalaması alınarak bulunmuştur. Deney aleti ve aşınma sonrası aşınan deney numuneleri Şekil 6'da verilmiştir.

Şekil 6. Cerchar aşınma aleti ve deney sonrası uç görünümü

Norveç aşınma deneyi (AV), Deney özellikle 1980'li yılların ilk yarısından itibaren klasik delme patlatma yöntemiyle ve tam cepheli tünel açma makinalarında (TBM) keski tüketiminin ve performanslarının önceden belirlenmesinde kullanılmaktadır (Johannessen 1998). Norveç Aşınma düzeneği ve deney aleti Şekil 7'de gösterilmiştir

Böhme aşınma deneyi, sürtünmeden kaynaklanan aşınma kayıpları, genellikle karbonatlı kayaçlarda yüksek, mineral içeriği ve içerdiği minerallerin özellikleri nedeniyle magmatik kökenli kayaçlarda ise düşüktür. Sürtünme ile aşınma kaybının belirlenmesi her kayaç türünde 7 cm boyutunda dörder adet karot numunesi kullanılmıştır. Numunelerin alt ve üst yüzeylerinin birbirine paralel olmasına dikkat edilmiştir. Deneylerde aşındırıcı malzeme olarak zımpara tozu kullanılmıştır.

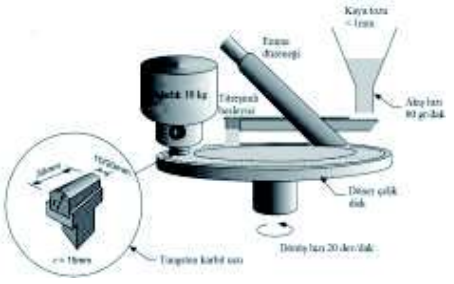

Şekil 7. Norveç aşınma aleti deney düzeneği (Dahl vd, 2012)

Böhme aşınma deneyi, sürtünmeden kaynaklanan aşınma kayıpları, genellikle karbonatlı kayaçlarda yüksek, mineral içeriği ve içerdiği minerallerin özellikleri nedeniyle magmatik kökenli kayaçlarda ise düşüktür. Sürtünme ile aşınma kaybının belirlenmesi her kayaç türünde 7 cm boyutunda dörder adet karot numunesi kullanılmıştır. Numunelerin alt ve üst yüzeylerinin birbirine paralel olmasına dikkat edilmiştir. Deneylerde aşındırıcı malzeme olarak zımpara tozu kullanılmıştır.

3.2.3 Mekanik Deneyler

Laboratuarda kayaçların mekanik özelliklerini incelemek için Cankurtaran Tüneli'nden alınan bloklardan NX boyutunda (54 mm çapında) karot alınmıştır. Hazırlanan karot örnekler üzerinde kayaçların mekanik özellikleri belirlemek için. Tek eksenli basınç dayanımı, dolaylı çekme dayanımı ve nokta yük dayanım deneyleri gerçekleştirmiştir.

Tek eksenli basınç dayanımı, kayacın dayanımının delinebilirlik, uç tüketimi ve aşındırıcılık deneyleri ile arasındaki ilişkilerini araştırılmasında kullanılmaktadır (Plinninger vd., 2004). Tek eksenli basınç dayanımı deneyi için boy/çap oranı 2.0 - 2.5 olacak şekilde örnekler hazırlanmıştır. Her kaya numunesi için en az 5 örnek hazırlanmıştır (ISRM 1981).

Dolaylı çekme dayanımı deneyinin yapılmasındaki amaç kayaç örneklerinin çapsal yükleme altında çekilme dayanımlarının dolaylı yoldan tayinidir. Kayacın dolaylı çekme dayanımı deneyi ISRM (1981)'e göre yapılmıştır. Deneyler,

her kayaç örneği için kalınlığı yarıçapıyla eşit olan (2,7 cm) boyunda yaklaşık 10'ar adet örnek üzerinde gerçekleştirilmiştir.

Nokta yük dayanımı, kayaçların dolaylı basınç dayanımlarını bulmak amacıyla yaygın olarak kullanılmaktadır. Nokta yük dayanım deneyi ($I_{S(50)}$) ISRM (1985)'e göre yapılmıştır. Deney eksenel olarak, boy/ çap oranı 0,3-1 arasında olacak şekilde yaklaşık 10'ar adet örnek üzerinde gerçekleştirmiştir.

4 LABORATUAR ÇALIŞMALARI

4.1 Delme Hızı İndeksinin Değerlendirilmesi

Delme hızı indeksi Şekil 8'de verilen grafik yardımıyla bulunur. Grafiğin altındaki kırılganlık (S_{20}) değeri ile Sievers minyatür delme (SJ) deneyinden elde edilen sonuçlarla DRI değeri bulunur. Laboratuvarda gerçekleştirilen kırılganlık (S_{20}) ve Sievers minyatür delme (SJ) deney sonuçları Çizelge 1'de verilmiştir. Bulunan sonuçlar Çizelge 2'de verilen DRI kayaç sınıflandırılması göre sınıflandırılmıştır. Sievers minyatür delme deneyinde kullanılan deney örnekleri Şekil 9'da verilmiştir.

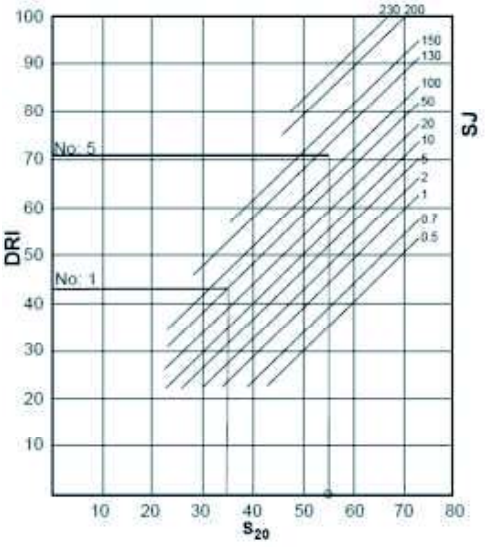

Şekil 8. Delme hızı indeksi belirleme diyagramı (Dahl 2003)

Çizelge 1. Delme oranı indeks deney sonuçları ve sınıflandırılması

No	Can Kurtaran Tüneli	Kayaç tanımı	SJ_{ort}	SJ, Sınıfı	S_{20ort} (%)	$S_{20,}$ Sınıfı	DRI	DRI, Sınıfı
1	Sağ çıkış	Andezit	50,00 ± 0,05	Orta	35,15	Düşük	43	Çok düşük
2	Sağ çıkış	Marn	82,70 ± 2,96	Yüksek	55,93	Orta	66	Yüksek
3	Sağ giriş	Bazaltik-andezit	140,00 ± 1,69	Oldukça yüksek	43,47	Orta	64	Yüksek
4	Sol çıkış	Kumtaşı	73,40 ± 0,38	Yüksek	34,44	Düşük	44	Düşük-orta
5	Sol giriş	Kireçtaşı	113,60 ± 1,89	Oldukça Yüksek	56,58	Yüksek	71	Çok yüksek

Çizelge 2. DRI, SJ ve S_{20} deneylerinin sınıflaması (Dahl 2003)

Sınıf	DRI sınıflaması	(SJ) sınıflaması	(S_{20}) sınıflaması
Oldukça düşük	≤25	<2	<30
Çok düşük	26-32	2-3	31-34
Düşük	33-42	4-6	35-41
Orta	43-57	7-18	42-50
Yüksek	58-69	19-55	51-59
Çok yüksek	70-82	56-86	52-67
Oldukça yüksek	≥83	>86	>67

Şekil 9. Sievers minyatür delme deneyinde kullanılan deney örnekleri

4.2 Kayaçların Aşındırıcılık Özellikleri

Kayaçlarının aşındırıcılık özelliğini belirlemek için gerçekleştirilen deney sonuçları Çizelge 3'de gösterilmiştir. Çizelge 3'ü incelediğimizde en fazla Cerchar aşınma indeksi 2,16 değerinde sağ çıkış tüpten alınan andezit örneğinde görülmektedir. Andezit örneğine ait Cerchar aşınma uçlarının üsten ve yandan ölçüm sonuçları Şekil 10'da verilmiştir. Ayrıca aşındırıcılık deneyi için gerçekleştirilen diğer aşınma Böhme aşınma deneyidir. Bu aşınma deneyi sürtünmeden kaynaklanan aşınma kayıplarını vermektedir. Kalınlık ve ağırlık kaybına göre gerçekleştirilen Böhme aşınma deney sonuçları Çizelge 4'de verilmiştir.

Çizelge 3. Cerchar aşınma indeks ve Norveç aşınma indeksi deney sonuçları ve aşındırıcılık sınıflaması

No	Can Kurtaran Tüneli	Kayaç tanımı	CAI_{ort}	CAI sınıfı	AV_{ort}	AV sınıfı
1	Sağ çıkış	Andezit	2,16±0,73	Aşındırıcı Çok aşındırıcı	1	Çok düşük
2	Sağ çıkış	Marn	0,70±0,13	Hafif aşındırıcı	-	-
3	Sağ giriş	Bazaltik-andezit	1,87±0,54	Aşındırıcı	0,5	Oldukça düşük
4	Sol çıkış	Kumtaşı	2,01±0,16	Aşındırıcı	1	Çok düşük
5	Sol giriş	Kireçtaşı	0,54±0,18	Hafif aşındırıcı	0,5	Oldukça düşük

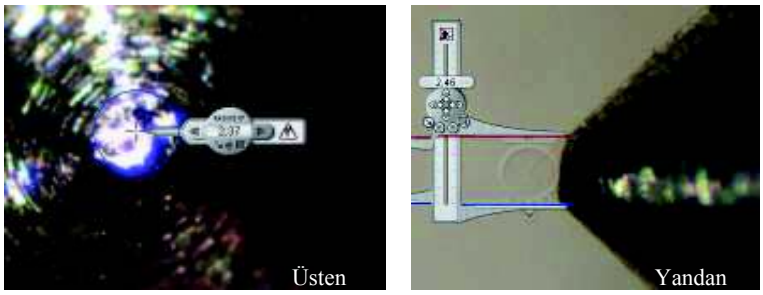

Şekil 10. Andezit örneğine ait Cerchar aşınma uçlarının üsten ve yandan ölçülmesi

Çizelge 4. Böhme aşındırma deney sonuçları

No	Can Kurtaran Tüneli	Kayaç tanımı	Ağırlık kaybı ($gr/23cm^2$)	Kalınlık kaybı ($cm/23\ cm^2$)
1	Sağ çıkış	Andezit	11,7	1,9
2	Sağ çıkış	Marn	18,8	3,0
3	Sağ giriş	Bazaltik-andezit	14,5	2,4
4	Sol çıkış	Kumtaşı	17,0	2,7
5	Sol giriş	Kireçtaşı	16,7	2,8

4.3 Kayaçların Mekanik Özellikleri

Kayaçlar üzerinde gerçekleştirilen tek eksenli basınç dayanım sonuçları ve Deere ve Miller (1966) göre kaya dayanımın sınıflandırması Çizelge 5'de verilmiştir. Nokta yük dayanımı deney sonuçları ve Bieniawski (1975) göre nokta yük dayanımım sınıflandırması Çizelge 6'da verilmiştir. Dolaylı çekme dayanımı ait deney sonuçları Çizelge 7'de gösterilmiştir.

Çizelge 5. Tek eksenli basınç dayanımı deney sonuçları ve kaya sınıflandırılması

No	Can Kurtaran Tüneli	Kayaç tanımı	Örnek sayısı	Çap (mm)	Boy (mm)	Doğal ağırlığı (gr)	Tane hacmi (cm^3)	Birim hacim ağırlık (gr/cm^3)	Tek eksenli basınç dayanımı σ_c (MPa)	Kaya sınıfı
1	Sağ çıkış	Andezit	5	53,8	109,0	661,5	248,0	2,7	163,4	Yüksek dayanımlı
2	Sağ çıkış	Marn	6	54,3	120,2	736,2	277,9	2,6	19,3	Çok düşük dayanımlı
3	Sağ giriş	Bazaltik-andezit	7	53,5	109,4	663,0	246,0	2,7	37,4	Düşük dayanımlı
4	Sol çıkış	Kumtaşı	5	54,4	117,9	741,0	274,1	2,7	101,0	Yüksek dayanımlı
5	Sol giriş	Kireçtaşı	5	53,6	112,9	670,3	254,2	2,6	29,9	Düşük dayanımlı

Çizelge 6. Nokta yükleme deneyi sonuçları ve kaya sınıflandırılması

No	Can Kurtaran Tüneli	Kayaç tanımı	Örnek sayısı	Çap (mm)	Boy (mm)	$Is_{(50)}$ MPa	Kaya sınıfı
1	Sağ çıkış 2	Andezit	7	53,7	38,8	8,9	Çok yüksek dayanım
2	Sağ çıkış 4	Marn	9	54,1	43,7	1,8	Düşük dayanım
3	Sağ giriş 5	Bazaltik-andezit	10	53,6	33,6	2,0	Orta dayanım
4	Sol çıkış 1	Kumtaşı	8	54,3	35,7	5,2	Yüksek dayanım
5	Sol giriş 5	Kireçtaşı	10	53,5	36,6	2,5	Orta dayanım

Çizelge 7. Dolaylı çekme dayanımı (Brazilian) deney sonuçları

No	Can Kurtaran Tüneli	Kayaç tanımı	Örnek sayısı	Çap (mm)	Boy (mm)	Çekme dayanımı σt (MPa)
1	Sağ çıkış	Andezit	10	53,9	29,9	17,5
2	Sağ çıkış	Marn	8	54,1	31,2	7,5
3	Sağ giriş	Bazaltik-andezit	13	53,5	29,6	8,1
4	Sol çıkış	Kumtaşı	7	54,3	30,5	13,7
5	Sol giriş	Kireçtaşı	6	53,5	28,4	5,4

5 VERİLERİN DEĞERLENDİRİLMESİ

Çalışma kapsamında Cankurtaran Tünelinde alınan kayaçlar üzerinde delinebilirlik, aşındırıcılık ve mekanik deneyleri gerçekleştirilmiş. Elde edilen aşındırıcılık ve mekanik deney sonuçları delme oranı indeksi verileri ile basit regresyon analizleri kurarak istatiksel olarak değerlendirilmiştir.

Kayaçların mekanik özelliklerinden olan tek eksenli basınç dayanımı, nokta yük dayanımı, dolaylı çekme dayanımı ve Cerchar aşınma indeksi değerlerinin DRI ile ilişkilerine bakıldığında yüksek korelasyonun olduğu görülmüştür. Bu ilişkiler Şekil 11 ve Şekil 12'de sırasıyla gösterilmiştir.

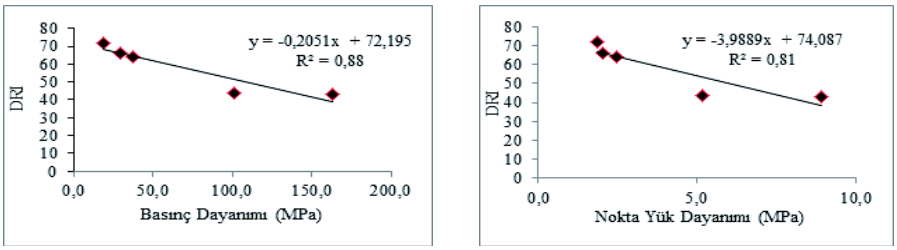

Şekil 11.Tek eksenli basınç dayanımı ile nokta yük dayanım sonuçlarının DRI ile ilişkisi

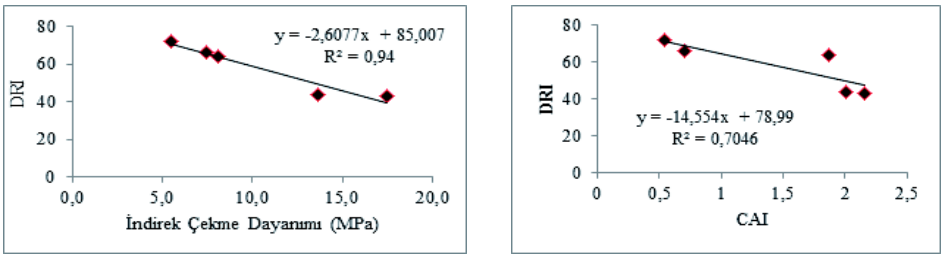

Şekil 12. Çekme dayanımı ile CAI sonuçlarının DRI ile ilişkisi

DRI ile bu parametreler arasında yüksek korelasyonlu ters bir lineer ilişkinin olduğu görülmüştür. Diğer bir ifadeyle kayaçların mekanik ve aşındırıcılık özelliklerinin artması delme hızı indeksinin azalmasına neden olmaktadır

Ayrıca kayaçların diğer aşındırıcılık özelliklerinden olan Böhme aşınma indeksi değerlerinin DRI ile ilişkilerine bakıldığında yüksek korelasyonun olduğu görülmüştür (Şek 13). DRI ile bu parametreler arasında anlamlılık düzeyi yüksek korelasyonlu bir lineer ilişkinin olduğu görülmüştür. Diğer bir ifadeyle ağırlık ve hacim bakımında aşınma kayıplarının artması kayaçlar üzerinde delme oranı indeksinin arttığını göstermektedir. Delme oranı indeksi yüksek olduğu için ağırlık ve hacim kaybı yüksek olur.

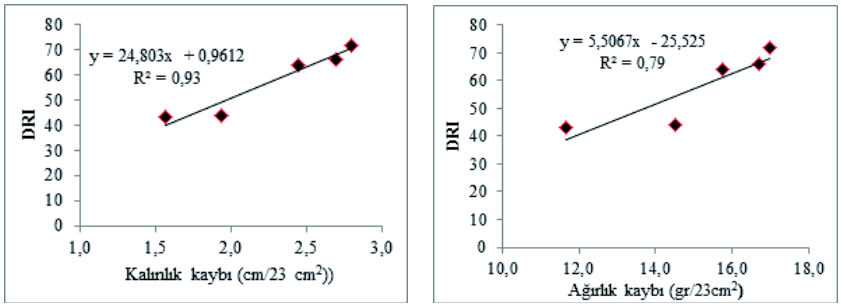

Şekil 13. Böhme aşınma dayanımının kalınlık ve ağırlık kaybının DRI arasındaki ilişki

6 SONUÇLAR

Çalışma alanı yapımı tamamlanmasıyla 5.288m uzunluğu ile Türkiye'nin en uzun karayolu tüneli özelliğini taşıyacak olan Hopa-Borçka Cankurtaran Tüneli'dir. Çift

tüp olarak inşa edilmekte olan tünelin giriş ve çıkışında farklı kayaç formasyonlarından alınan örnekler üzerinde gerçekleştirilmiştir.

Cankurtaran Tüneli'nden alınan andezit, bazaltik andezit, marn, kireçtaşı ve kumtaşı kayaçları üzerinde delinebilirlik, aşındırıcılık ve mekanik deneyler gerçekleştirilmiştir. Delme oranı indeksi ile tek eksenli basınç dayanımı, nokta yük dayanımı, dolaylı çekme dayanımı ve CAI değerleri ile arasındaki ilişkileri incelediğimizde kayaçların dayanım ve aşınma değerleri arttıkça delmeye karşı gösterdikleri direnç artmaktadır. Ayrıca Böhme aşınma indeksi değerleri arasında ilişkiyi incelediğimizde kayaç aşınımı artıkça delme oranı indeksinin artığını göstermektedir.

Sonuç olarak, laboratuvar ve arazi çalışmaları sonucunda elde edilen veriler, araştırmalar, analizler ve deneyimler değerlendirildiğinde kayaçların mekanik ve aşınma özellikleri DRI değerleri arasında belirgin bir ilişkinin olduğu ortaya çıkmıştır.

TEŞEKKÜR

Bu çalışma, K.T.Ü. Bilimsel Araştırma Projeleri Fonu tarafından desteklenen 8683 nolu proje kapsamında gerçekleştirilmiştir. Sağlanan destek için K.T.Ü. Bilimsel Araştırma Projeleri Fonuna teşekkürü bir borç biliriz.

Arazi çalışmaların yapılması için, Hopa – Borçka Cankurtaran Tünelini yürüten NAS-YSE Ortak girişim yetkililerine ve taşeron Jumbo İnşaat ve Kartaş İnşaat yetkilerine teşekkürü bir borç biliriz.

KAYNAKLAR

Alber, M., 2008. Stress dependency of the Cerchar abrasivity index (CAI) and its effects on wear of selected rock cutting tools, *Tunnelling and Underground Space Technology*, 23, 351–359.

Dahl, F., Bruland, A., Jakobsen, PD., Nilsen, B. and Grøv, E., 2012. Classifications of properties influencing the drillability of rocks, based on the NTNU/SINTEF test method, *Tunnelling and Underground Space Technology* 28: 150–158.

Ersoy A, Waller MD., 1995, Prediction of drill-bit performance using multivariable linear regression analysis. *Trans Inst Mining Metall* A;104:101–14.

Filip Dahl, F., Bruland, A., Jakobsen, P.D., Nilsen, B., Grøv E., 2012. Classifications of properties influencing the drillability of rocks, based on the NTNU/SINTEF test method *Tunnelling and Underground Space Technology 28,* p 150–158.

Hoseinie, S.H,. Aghababaeib, H., Pourrahimian, Y,. 2008. Development of a new assification system for assessing of rock mass drillability index (RDi), *International Journal of Rock Mechanics & Mining Sciences* 45, p 1–10.

ISRM, 1981. Rock Characterization, Testing and Monitoring –ISRM Suggested Methods. Brown, E.T. (ed), Pergamon Pres, 211p.

ISRM, 1985. Suggested Method for Determining Point Load Strength. Int. J. Rock Mech. Min. Sci. And Geomech., 22 (2), 51-60.

Jimeno CL, Jimeno EL, Carcedo FJA., 1995, Drilling and blasting of rocks. Rotterdam: Balkema.

Johannessen, O., 1998. Hard Rock Tunnel Boring,Advence Rate And Cutter Wear, Project Report, IB-98, NTNU,Trondheim,Norwegian, 54.

Kahraman S, Balci C, Yazici S, Bilgin N., 2000, Prediction of the penetration rate of rotary blast hole drilling using a new drillability index. *International Journal of Rock Mechanics & Mining Sciences*;37:729–43.

Kahraman, S., 1999. Rotary and percussive drilling prediction using regression analysis, *International Journal of Rock Mechanics and Mining Sciences*, 36, 981-989. (Technical note).

Kahraman, S., Bilgin, N., Feridunoglu, C., 2003. Dominant rock properties affecting the penetration rate of percussive drills*, International Journal of Rock Mechanics & Mining Sciences*, 40, p, 711–723.

Kaya, A., 2012, Cankurtaran (Hopa-Artvin) Tünel Güzergahının ve Çevresinin Jeoteknik Açıdan İncelenmesi, Doktora Tezi, Karadeniz Teknik Üniversitesi, Fen Bilimleri Enstitüsü, Trabzon. s, 35-40.

Nilsen, B, 2003. Investigation and testing for Norwegian hard rock TBM performance prediction, *Türkiye Yeraltı Kaynaklarının Bugünü ve Geleceği, İTÜ Maden Fakültesi 50. Yıl Sempozyumu Kitab*ı, pp. 89-96, İstanbul.

Osanloo M., 1998, Drilling methods. Teheran: Sadra Published.

Plinninger, R.J., and Thuro, K., 2004, Wear Prediction in Hardrock Excavation Using the Cerchar Abrasiveness Index (CAI) Eurorock *53rd Geomechanics Colloquium. p 599-604.*

Plinninger, R.J., Spaun.G., and Thuro, K.**,** 2002. Prediciton and classification of tool wear in drill and blast tunnelling, *Engineering Geology for Developing Countries - Proceedings of 9th Congress of the International Association for Engineering Geology and the Environment*. Durban, South Africa, P 2226-2236.

Tamrock, 1999. Rock Excavation Handbook, Sandvik Tamrock Corp., 305 p. USBR. 1998. Engineering geology field manual. Field index tests. Vol. 1,. pp. 111– 112.

Tamrock. 1987, Handbook of Underground drilling, Tamrock Drills SF-33310 Tampere,Finland, p327

Thuro, K,. Plinninger, R.J,.Spaun, G,. 2002. Drilling, Blasting and Cutting- is it possible to quantify geological parameters relating to excavatability?, Proceedings of 9th Congress of the International Association for Engineering Geology and the Environment. Durban, South Africa, 2853-2862.

Thuro, K. and Spaun., G., 1996. Drillability in hard rock drill and blast *Tunnelling,Geomechanics*1-11

Thuro,. K., 1997a, Drillability prediction: geological influences in hard rock drill and blast tunnelling, *Geol Rundsch* 86: 426-438.

Thuro,. K., 1997b, Prediction of drillability in hard rock tunnelling by drilling and blasting, *Balkema, Rotterdam.* p.103-108

Yaralı, O,. 2010. Zonguldak Bölgesi Kayaçlarının Aşındırıcılık Özelliklerinin Belirlenmesi, *Türkiye 17. Kömür Kongresi Bildiriler Kitabı*, TMMOB Maden Mühendisleri Odası Yayını, Zonguldak.

Yaralı, O., ve Kahraman, S,. 2011. The drillability assessment of rocks using the different brittleness values, Tunnelling and Underground Space Technology, 26 406–414.

Experimental and Statistical Investigation on Noise Level of Diamond Sawblades in Granitic Rock Sawing

I. Karakurt, G. Aydın, K. Aydıner

Karadeniz Technical University, Department of Mining Engineering, Trabzon-Turkey

ABSTRACT This paper presents an experimental and statistical study on noise level generated during of rock sawing by circular diamond sawblades. Influences of the operating variables on the noise level were investigated. Statistical analyses were then employed and models were built for the prediction of noise levels depending on the operating variables. The derived models are validated through some statistical tests. It was determined that increasing of peripheral speed, traverse speed and cutting depth result in an increase in noise levels. On the other hand; a decreasing trend for noise levels is initially observed with the increasing of flow rate of cooling fluid. It was concluded that the peripheral and traverse speed are the significant operating variables affecting the noise level.

1 INTRODUCTION

Circular diamond sawblades are one of the most used cutting tools that have been widely used in sawing of natural stones throughout the world (Atıcı and Ersoy, 2009; Rojek et al., 2011). Sawing performance and life of a circular sawblade are affected by many factors including diamond and matrix properties, operating variables, sawing modes (up-cutting, down-cutting), physico-mechanical and mineralogical properties of the rock to be cut, condition of the sawing machine and the skills of the operator (Fener et al., 2007; Buyuksagis, 2007). Basically, the parameters affecting the performance and life of the sawblades indicate the complexity of these tools. In spite of the complexity of the system, a considerable amount of work has been conducted and published by many researchers in the relevant literature to understand the cutting tool itself and mechanism behind the phenomena. In recent years, due to the importance in cost estimation and planning of the plants, the prediction of the cutting performance of circular diamond sawblades in sawing of natural stones has been the subject of considerable research. Kahraman et al. (2004), Ersoy and Atıcı (2004), Buyuksagis (2007), Yılmaz et al. (2011), Yurdakul and Akdaş (2012), and Ataei et al. (2012) are among the known attempts studying the prediction of cutting performance of circular diamond sawblades in sawing of rocks.

Noise is an effect arising in the rock cutting process as well as in other industries where machining and/or processing of materials is conducted. High noise levels not only affect the workers' life, but also contribute rather serious problems to the working environment. Additionally, noise level may be a good indicator for tool performance against the cutting. Therefore, alternative designs aiming at minimizing the noise generated during the sawing of rocks have recently gained attention. Furthermore, from the relevant literature, it can be clearly concluded that although there are many studies focusing on the investigation of the sawing performance and life of a circular sawblade including the prediction studies, almost none of them has investigated the influences of the operating variables on the noise level generated during the sawing of rocks. Therefore, the lack of investigation on the noise level has attracted the authors to

conduct the current study. Effects of the operating variables on the noise level were investigated. Predictive models were then developed by SPSS regression analysis to estimate the noise level from the operating variables. Contribution of each operating variable on the noise level was also determined. Finally, the derived models were validated through some statistical tests.

2 MATERIAL AND METHOD

Three granitic rocks having different percentages of minerals and grain size distributions were selected from a stone processing plant. The selected rocks are known Giallo Fiorito, Nero Zimbabwe and Star Galaxy as commercial names. The granite samples have a length of 30 cm and 10 cm × 3 cm section. Some physico-mechanical properties of the selected granites are given in Table 1. It may be important to note that in practice, there are serious difficulties of preparing and testing hard rocks including granites for their mechanical properties such as uniaxial compressive and bending strength. For these reasons, the uniaxial compressive and flexural strengths of the tested rocks were provided by the stone processing company where the selected rocks were provided. Density (kN/m^3), water absorption by volume (%), porosity (%), ultrasonic velocity (m/s), Schmidt hammer hardness, shore hardness were determined according to related ISRM (1981) suggested methods.

The microhardnesses of samples were measured by a Vickers Microhardness meter. In the microhardness measurements, it was observed that it is difficult to identify indention diagonal of various hard brittle minerals due to the fractures around the indentation, thus a load of 100 g was chosen as recommended by Xie and Tamaki (2007). An average of 3-5 points was quoted as a value of microhardness of a mineral forming the rock. Then, the microhardness value of the mineral was multiplied with the proportion of the mineral forming the rock. The same procedure was followed for other minerals and finally, the microhardness of each rock was determined as a total of these calculations. Similar procedure was applied for the determination of Mohs' hardness of each rock sample.

For Cerchar abrasiveness index testing, a pointed steel pin which has 610±5 Vickers hardness, 200 kg/mm^2 tensile strength, and a cone angle of 90° was applied to the surface of the rock samples for approximately one second under a static load of 68.646 N to scratch a 10 mm long groove. This procedure was repeated five times in various directions using a fresh pin for each repetition. The abrasiveness of the rock was determined by the resultant wear flat generated at the point of the stylus, which was measured in 0.1 mm units under a microscope. The unit of abrasiveness was defined as a wear flat of 0.1 mm which is equal to 1 Cerchar abrasivity index, ranging from 0 to 6 (Valantin 1974; Yarali and Kahraman 2011).

Table 1. Mechanical and intact properties of rocks used in the sawing tests

Rock Properties	*Giallo Fiorito*	*Nero Zimbabwe*	*Star Galaxy*
Uniaxial strength (MPa)	167.65	242.6	201.47
Density (kN/m^3)	26.60	30.30	28.40
Bending strength (MPa)	22.06	24.02	19.61
Water absorption by volume (%)	0.28	0.14	0.10
Porosity (%)	0.80	0.30	1.00
Ultrasonic Velocity (m/s)	3917	6054	6863
Cerchar abrasion Index	4.166	3.412	4.29
Schmidt hammer hardness	48	64	65
Microhardness (HV)	543.47	501.84	463.18
Shore hardness	73.55	71.9	60.8
Mohs hardness	5.7	6.2	5.8

Sawing experiments were conducted on a fully-instrumented cutting machine (see Fig. 1). The diamond sawblade used in the tests was of 40 cm diameter, having 28 impregnated diamond segments (circumferential length 40 mm, width 3.5 mm and height 10 mm). The diamonds were sized at 40/50 US mesh with a concentration of 30 which is recommended for the sawing of hard materials.

Figure 1. Experimental set-up

Disc movements forward-backward in the horizontal plane and up-down in the vertical plane were driven with two 0.75 kW ac motors, while the turn of the disc were driven with 4 kW ac motor. Moreover, 0.75 kW ac motor was used to move the wagon in the cutting line. Vertical, horizontal, axial forces were measured using sensors, load cells, transducers and an encoder in the monitoring system. All movements of the cutting machine were controlled by a computer.

In order to determine the levels of operating variables for the study, some preliminary cutting tests were conducted by considering instructions of diamond disc manufacturers and the relevant studies in the literature. Consequently, valid for all types of tested rocks, the operating variables was selected as given in Table 2 and varied at the levels presented in Table 3. Rock samples were sawn through their lengths and all sawing experiments were performed by the same cutting mode (down-cutting mode).

A noise level meter modeled as "DT-8852" (Fig. 2) was used to measure the noise level during the cutting process. The main specifications of the noise level meter are given in Table 4. The equipment has a screen showing the noise level values and the max, min and instantaneous noise levels during the cutting can be seen on this screen. The data obtained was transported to a PC and the average noise level for every cutting was reported through a software interface.

Figure 2. Noise level meter used for the measurements

Table 2. Levels of operating variables

Operating Variables	***Levels***				
Peripheral Speed (m/s)	25	30	35	40	45
Traverse Speed (cm/min)	40	50	60	70	80
Cutting Depth (cm)	0.5	1.0	1.5	2.0	2.5
Flow Rate of Cooling Fluid (ml/s)	50	100	150	200	250

Table 3. Experimental layout

Number of Experiment	*Peripheral Speed (m/s)*	*Traverse Speed (cm/min)*	*Cutting Depth (cm)*	*Flow Rate of Cooling Fluid (ml/s)*
1	**25**	60	2.0	150
2	**30**	60	2.0	150
3	**35**	60	2.0	150
4	**40**	60	2.0	150
5	**45**	60	2.0	150
6	35	**40**	2.0	150
7	35	**50**	2.0	150
8	35	**60**	2.0	150
9	35	**70**	2.0	150
10	35	**80**	2.0	150
11	35	60	**0.5**	150
12	35	60	**1.0**	150
13	35	60	**1.5**	150
14	35	60	**2.0**	150
15	35	60	**2.5**	150
16	35	60	2.0	**50**
17	35	60	2.0	**100**
18	35	60	2.0	**150**
19	35	60	2.0	**200**
20	35	60	2.0	**250**

Table 4. Specifications of the sound level meter used in the study

Standard applied	IEC61672-1 Type 2,ANSI S1.4 Type2
Accuracy	±1.4dB
Frequency range	31.5HZ ~ 8KHZ
Dynamic range	50dB
Level ranges	LO:30dB~80dB Med:50dB~100dB Hi:80dB~130dB Auto:30dB~130dB
Time weighting	FAST (125mS), SLOW (1s)
Microphone	1/2 inch electret condenser microphone
Resolution	0.1dB
Display Update	2 times/sec
Analog output	AC/DC outputs, AC=1Vrms,DC=10mV/dB

3 RESULTS AND DISCUSSIONS

Influences of the operating variables on the noise level were depicted in Figures 3-6. It can be stated that increasing of peripheral speed, traverse speed and cutting depth resulted in an increase in noise levels recorded for all rocks. Unlike the behavior of other operating variables, a decreasing trend for noise levels reported for all rocks was initially observed with the increasing of flow rate of cooling fluid. It can be also stated that the noise levels increased as a result of the increase in specific removal rate that is the quantity of the material sawn in unit time or the area cut per unit time as shown in Figure 7.

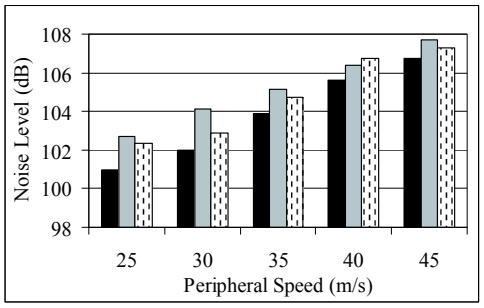

Figure 3. Peripheral speed versus noise level

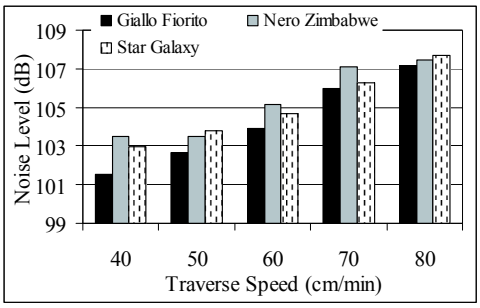

Figure 4. Traverse speed versus noise level

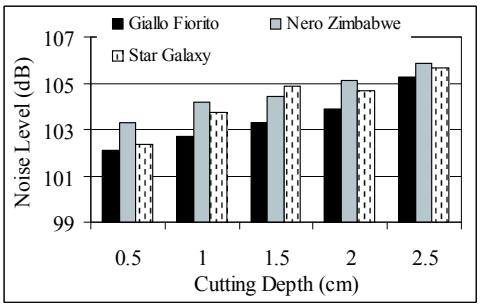

Figure 5. Cutting depth versus noise level

To build models for prediction of noise level from operating variables, multiple regression analysis was performed using the dependent (noise level) and independent variables (operating variables). Contribution of each operating variable on the noise level was also determined. Results of the multiple linear regression analysis were presented in Table 5. The dependent and independent variables are denoted as following; NL: noise level, A: peripheral speed, B: traverse speed, C: cutting depth, D: flow rate of cooling fluid. The models developed for the estimation of noise level from operating variables for each rock are presented together with the contribution rates (CRs) of each operating variable (Eqs. 1-3).

NL_{GF} (dB) = 82.8019 + 0.3040 A + 0.1461 B + 1.4743 C - 0.0067 D
CR (%): A: 36.44, B: 35.02, C: 20.55, D: 7.98 (1)

NL_{NZ} (dB) = 88.0695 + 0.2470 A + 0.1157 B + 1.3030 C - 0.0061 D
CR (%): A: 35.74, B: 33.48, C: 21.93, D: 8.85 (2)

NL_{SG} (dB) = 86.9416 + 0.2738 A + 0.1200 B + 1.5088 C - 0.0115 D
CR (%): A: 34.04, B: 29.84, C: 21.82, D: 14.30 (3)

The peripheral speed was determined as the most significant operating variables affecting the noise level. The peripheral speed was followed by traverse speed, cutting depth and flow rate of cooling fluid respectively. It can be also concluded that among the operating variables, the flow rate of cooling fluid was the operating variables that has less effect on the noise level.

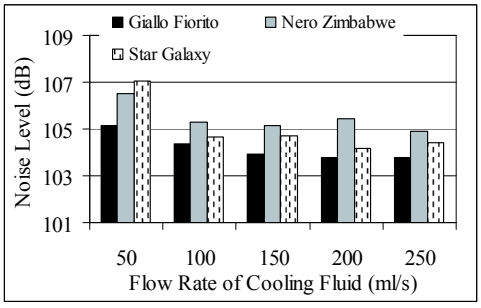

Figure 6. Flow rate of cooling fluid versus noise level

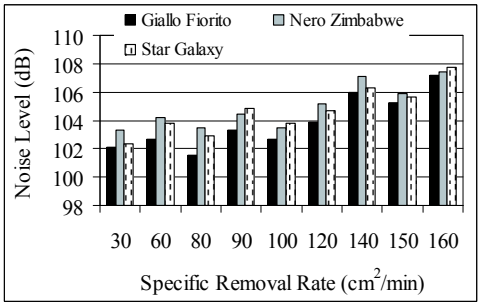

Figure 7. Specific removal rate versus noise level

From Table 5, it was seen that the R^2 of the models are greater than 0.90. These values indicate that there is a high degree of

relationship between the predicted and observed noise levels. The prediction capability and/or verification of the derived models were tested by the F-test, while each operating variable involved in the models was verified by the t-test. In verification tests, a 95% level of confidence was chosen.

Table 5. Results of the multiple linear regression analysis

Rock type	*Independent variables*	*Coefficient*	*Standard error*	*Standard error of estimate*	*Determination coefficient (R^2)*
Giallo Fiorito	S	88.0695	1.332	0.411	0.9456
	A	0.2470	0.026		
	B	0.1157	0.013		
	C	1.3030	0.224		
	D	- 0.0061	0.003		
Nero Zimbabwe	S	82.9560	0.734	0.227	0.9880
	A	0.2734	0.014		
	B	0.1545	0.007		
	C	1.4859	0.123		
	D	- 0.0056	0.001		
Star Galaxy	S	82.8019	1.069	0.330	0.9759
	A	0.3040	0.021		
	B	0.1461	0.010		
	C	1.4743	0.180		
	D	- 0.0067	0.002		

If the calculated F-and t-values are greater than those of tabulated, it confirms that the related models and each operating variable involved in the models are statistically significant. In other words, it can be concluded that the derived models are valid. As can be seen in Table 6, all calculated F- and t-values are greater than those of tabulated values suggesting that the derived models are statistically valid.

Table 6. F-test and t-test results for regression analysis

Rock Type	*t-value*	*Tabulated t-value*	*F-ratio*	*Tabulated F-ratio*
Giallo Fiorito	66.135 9.491 8.892 5.824 -2.352	1.729	52.151	3.13
Nero Zimbabwe	113.015 19.059 21.541 12.049 -3.932	1.729	246.980	3.13
Star Galaxy	77.482 14.557 13.992 8.211 -3.189	1.729	121.312	3.13

4 CONCLUSIONS

It was concluded that increasing of peripheral speed, traverse speed and cutting depth resulted in an increase in noise levels recorded for all rocks. Unlike the behavior of other operating variables, a decreasing trend for noise levels was initially observed

with the increasing of flow rate of cooling fluid. Modeling results revealed that the noise level can be effectively predicted from the operating variables. Peripheral speed and traverse speed were determined as important operating variables in term of noise level. The verification methods confirm the correctness of the developed models.

ACKNOWLEDGEMENTS

The authors would like to thank to the Scientific Research Fund of Karadeniz Technical University for the financial support of this work (No. 2009.112.008.3). Additionally, the authors are most grateful to Granitaş A.Ş. stone processing company for supporting this research by providing dimensioned rock samples for the sawing experiments.

REFERENCES

Ataei, M., Mikaeil, R., Hoseinie, H.S., Hosseini, M.S., 2012. Fuzzy analytical hierarchy process approach for ranking the sawability of carbonate rock. International Journal of Rock Mechanics and Mining Sciences 50, 83–93.

Atici, U., Ersoy, A., 2009. Correlation of specific energy of cutting saws and drilling bits with rock brittleness and destruction energy. Journal of Materials Processing Technology 209, 2602–2612.

Buyuksagis,S.I., 2007. Effect of cutting mode on the sawability of granites using segmented circular diamond sawblade. Journal of Materials Processing Technology 183, 399–406.

Ersoy, A., Atıcı, U., 2004. Performance characteristics of circular diamond saws in cutting different types of rocks. Diamond Related Materials 13, 22–37.

Fener, M., Kahraman, S., Ozder, O.M., 2007. Performance prediction of circular diamond saws from mechanical rock properties in cutting carbonate rocks. Rock Mechanics and Rock Engineering 40(5), 505–517.

ISRM, 1981.Rock Characterization Testing and Monitoring, Suggested Methods, in: E.T. Brown (Ed.), Pergamon Press, 211 p.

Kahraman, S., Fener, M., Gunaydin, O., 2004. Predicting the sawability of carbonate rocks using multiple curvilinear regression analysis. International Journal of Rock Mechanics and Mining Sciences 41(7), 123–1131.

Rojek, J., Onate, E., Labra, C., Kargl, H., 2011. Discrete element simulation of rock cutting. International Journal of Rock Mechanics and Mining Sciences 48: 996–1010.

Valantin, A., 1974. Examen des différent procèdes classiques de la nocivité des roches vis-à-vis de l'abatage mécanique. Industrie Minérale Mine 133–140.

Xie, J., Tamaki, J., 2007. Parameterization of micro-hardness distribution in granite related to abrasive machining performance. Journal of Materials Processing Technology 186, 253–258.

Yarali, O., Kahraman, S., 2011. The drillability assessment of rocks using the different brittleness values. Tunneling and Underground Space Technology 26, 406–414.

Yılmaz, G.N., Goktan, M.R., Kibici, Y., 2011. An investigation of the petrographic and physico-mechanical properties of true granites influencing diamond tool wear performance, and development of a new wear index. Wear 271, 960– 969.

Yurdakul, M., Akdas, H., 2012. Prediction of specific cutting energy for large diameter circular saws during natural stone cutting. International Journal of Rock Mechanics and Mining Sciences 53, 38–44.